THE UNIVERSITY OF ASTON IN BIRMINGHAM

THE WEAR OF STEEL/NON STEEL SYSTEMS IN THE PRESENCE OF
AVIATION KEROSENE

Thesis Submitted for the Degree of
Doctor of Philosophy

by

LI FAH WONG, B.Sc.(Hons),M.Tech.,Tech.(CEI)

Supervisor: Mr. J.L. Sullivan

Department of Physics   August 1982

THE UNIVERSITY OF ASTON IN BIRMINGHAM

THE WEAR OF STEEL/NON STEEL SYSTEMS IN THE PRESENCE OF
AVIATION KEROSENE - by LI FAH WONG

Submitted for the Degree of Doctor of Philosophy - August 1982

SUMMARY

The introduction of new refining techniques designed to
improve thermal stability of modern jet aircraft fuel has resulted
in the removal of hetrocyclic compounds and other polar impurities.
This leads to a reduction in the fuels lubricating ability and
hence premature failure can result in aircraft fuel systems.
Failures may be alleviated by the use of corrosion inhibitors
which also act as boundary lubricating additives.

In this investigation, a Denison pin-on-disc machine was
used to measure friction and wear for aluminium-bronze sliding
against steel in the presence of fuel alone and with the addition
of one of the new generation of additives. The experiments were
conducted in the load range from 24N to 200N inclusive at sliding
speeds of 0.6, 2 and 4 ms^{-1} respectively and wear rates of between
10^{-15} and 10^{-13} $m^3 m^{-1}$ were found. Compared with experiments conducted
when using fuel alone as a lubricant, the presence of the additive
produced an increase in wear rates under mild boundary condition.
As the condition became more severe, however, the wear rates were
lower than with fuel alone and the system showed a reduced tendency
to seize.

Metallographic techniques of taper sectioning and etching
were employed to give a better understanding of the structural
changes involved at the sub-surface layer of the worn pins. The
results obtained showed that at least five different structures of
aluminium-bronze have been used by various investigators. On the
sub-surface layer of worn pins, aluminium-bronze was found to
undergo superplastic deformation, with the formation of cavities
and this was related to the enhanced strain-rate sensitivity of
the material at elevated temperatures. The superplasticity of
aluminium-bronze material has an effect of reducing wear.

Based on the results of analyses using Auner Electron Spec-
troscopy(AES), Electron Probe Microanalysis(EPMA), Scanning Elec-
tron Microscopy(SEM) and X-ray Powder Diffraction, possible wear
mechanisms are suggested to explain the wear of this material
combination in the presence of fuel alone and of fuel with additive.

Finally, a new theory of oxidational wear under boundary
lubricated condition has been proposed to predict wear rates.

WEAR/ADDITIVE/BRONZE/PHYSICAL TECHNIQUES/SUPERPLASTICITY/

ACKNOWLEDGMENTS

CONTENTS

Page

LIST OF FIGURES

LIST OF TABLES

CHAPTER 1

INTRODUCTION

The very rapid expansion of the aviation industry in the last thirty years due to significant developments of the jet engine has enabled the operator to get more power from a given weight of equipment. This trend still applies and is coupled with the aim of extending the life of the equipment resulting in the production of turbine fuel specification which are more restrictive, in particular with respect to thermal stability and cleanliness. As turbine fuel production has increased and its specifications become more restrictive, new processes have been introduced to satisfy both demand and quality. One result of this was that problems arose in the aircraft fuel system, where components are fuel lubricated, for example the fuel pump in particular. This was attributed to the poor lubricating properties of fuel. The latter problem is the subject studied for this dissertation.

In order to understand the relationship between the fuel characteristics and its lubrication capability, it is interesting to recall briefly the priciples of the aircraft fuel system, its background problems, the lubrication mechanisms, its bearing metallurgy and the fuel lubricity.

1.1 Aircraft Fuel Systems

A jet aircraft fuel system consists basically of the pumping element, a control unit to regulate the fuel supply, and a method of injection into the combustion chambers. A high pressure fuel pump is used in the system in order to obtain correct atomisation of the fuel passing into the combustion chambers. There are basically two types of pump, one is a rotor pump and the other is a piston pump of the type manufactured by Lucas Aerospace. Since the latter type was the one in which the initial problems experienced gave rise to this study we shall consider this. This type of pump is a positive displacement piston type driven by the engine gear train. The fuel pump consists of a rotor assembly fitted with seven pistons, the ends of which project from their bores, and carry slipper pads which bear on a non-rotating camplate set at a variable angle (Figure 1.1). The inclination of this camplate imparts a reciprocating motion to the pistons, thus producing a pumping action. The camplate angle can be varied to alter the stroke of the pistons. The pump output depends upon its rotational speed, and the stroke of the pistons. Pistons are manufactured from KE961 steel which is a high carbon (1.45 - 1.65%), 13% chromium steel. The pistons run in aluminium-bronze bores with a thin cadmium plating. The bronze (DTD 197A aluminium-bronze) consists of 10% aluminium , 5% nickel, 5% iron with the remainder copper. A single fuel pump can deliver fuel at the rate of 455 - 2273 litres per hour at a maximum pressure of about 14 MNm^{-2}.

As the rotor is rotated the pistons are successively driven down into the cadmium plated aluminium-bronze bores. On the return stroke the pistons are forced back against the swash plate by a spring and the pressure of the incoming fuel. The surfaces between the pistons and bores are in relative motion and, during this motion, they are lubricated by the fuel which is being pumped. A simple harmonic motion is performed by the pistons relative to the bores while the pump is running. The pistons reach a maximum velocity when travel half way through the stroke and will be instantaneously at zero velocity at each end of the stroke. This range of speeds can produce various lubrication conditions between the pistons and bores.

-4-
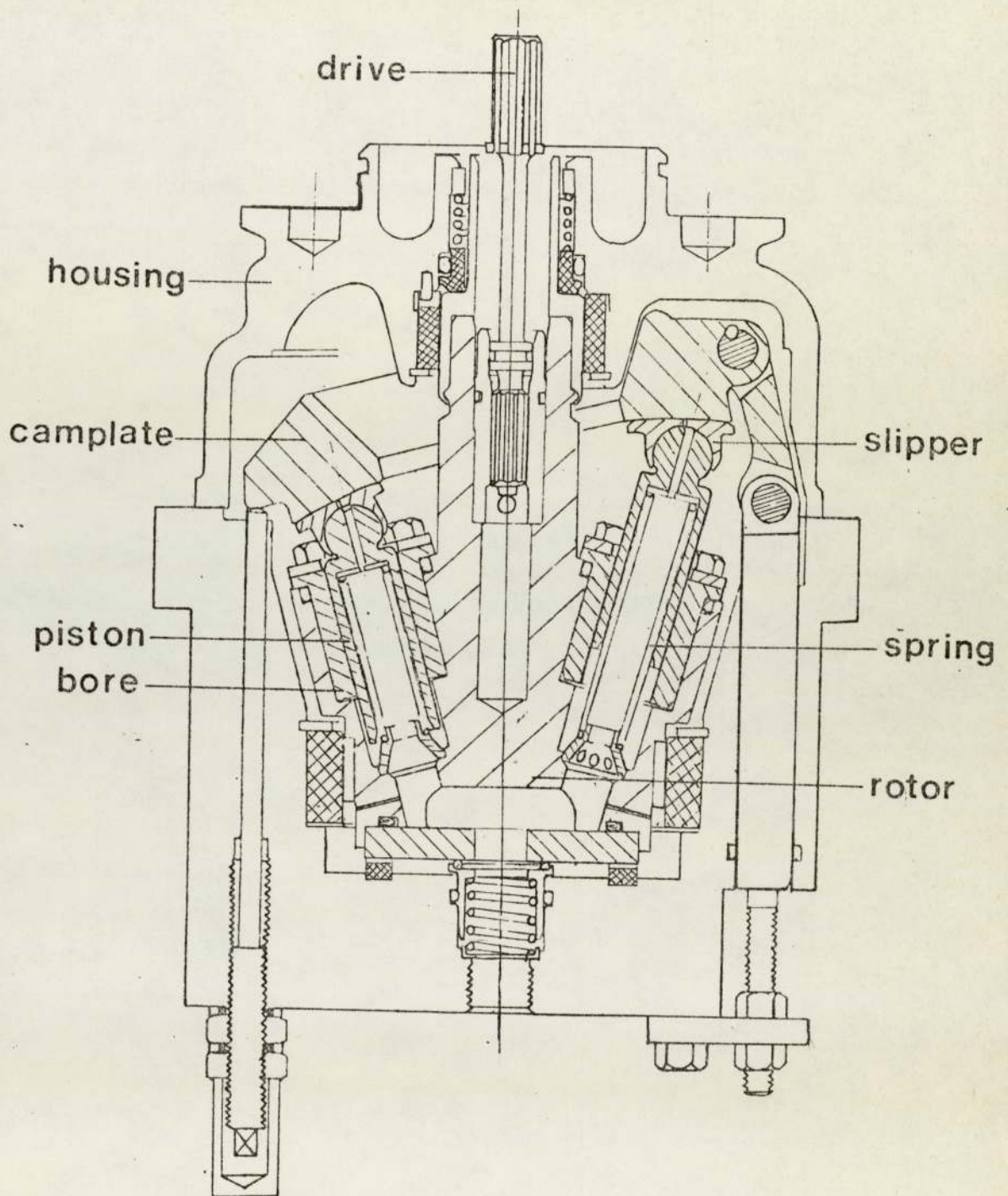
Figure 1.1 Lucas Two-Piston Rig.
Courtesy-Lucas Aerospace

1.2 Background to the Problem

During recent years a major problem has been experienced in Europe with the failure of jet engine piston type fuel pumps due to operation on fuel having inadequate lubricity characteristics. Lubricity was defined as the non-viscosity part of lubrication, that is, if two liquids have the same absolute viscosity but one gives lower wear, or lower friction, or a lower tendency to scuff, it will be considered to have better lubricity. However, modern jet engines such as a turbojet (1) require fuel of high thermal stability. Fuel becomes increasingly warmer as it successively receives heat input through engine fuel pumping, oil cooling and distribution to the spray nozzles. The lack of thermal stability under such usage results in the formation of deposits which plate-out on critical surfaces or otherwise plug vital strainers and passages of fuel system components. The refinement of the turbojet into a higher performance machine has required that jet fuels have better resistance to degradation by heating. Hence, the introduction of hydrotreated fuel, replacing the traditional chemically treated fuel, is necessary to achieve the fuel requirements for supersonic transport. Although hydrotreating has some beneficial effects, it removes many of the polar impurities present in fuels refined using traditional techniques(2). Hence, it leads to a reduction of some highly active polar compounds in the fuel required for the boundary film lubrication.

In normal operation many additives are introduced into aviation fuel, for example, anti-oxidants, metal deactivators and corrosion inhibitors. Aird and Forgham (3) report that many incidents involving pump failure had occurred between 1965 and 1969. The majority of the pump failures was attributable to the use of hydrogen treated fuels apart from one occasion in 1969 when an acid treated fuel was involved. Vere (4) also found that when a severely hydrotreated fuel was used, it had a greater wear effect than either production hydrotreated fuel or chemically treated fuel. When only a 10% copper sweetened fuel was added to the severely hydrotreated fuel, the wear rate was reduced to that experienced with a copper sweetened fuel. The use of additives to overcome the lack of lubricity in the severely hydrotreated fuel was also investigated. Neither the anti-oxidant nor the metal deactivator had the effect on lubricity, but corrosion inhibitor had been proved to be significant in reducing wear rate as well as friction.

Why has the copper sweetened aviation jet fuel better lubricity than the severely hydrotreated fuel? In order to answer this, Vere (4) carried out an investigation using a thin layer chromatography and mass spectrometry to isolate and identify lubricity agents of these two fuels. Polynuclear aromatics and fully saturated sulphur compounds were extracted and identified. Vere concluded that the latter seemed to be more active lubricity agents when adding 150 p.p.m. to the hydrotreated fuel.

There is little agreement among investigators as to

which fuel properties are important. Among the properties
claimed to reduce friction and wear are viscosity (5),
pressure-viscosity (6), volatility (7), aromatics (8),
sulfur (9), oxygenated compounds (10), and dissolved
oxygen (11, 12). Many attempts have also been made by the
operating companies to alleviate the pump failure, but there
has been no general acceptance of any particular solution.
Some operators modified fuel pumps using carbon faces on the
sliding surfaces and these have proved satisfactory. However,
the conversion of all pumps to this metallurgy is not feasible.
Up to the present, corrosion inhibitors have solved the problem
but the mechanisms of protection are not understood. Hence,
this leads to the present project in determining the mechanism
of protection afforded by the additive.

1.3 Characterization of Wear

Wear has been defined as "the progressive loss of subs-
tance from the operating surface of a body occurring as a
result of relative motion at the surface" (13). Loss of
material can be the result of a variety of mechanisms such
as adhesion, abrasion, corrosion, erosion and surface fatigue.
In any particular instance of wear one may have any of these
mechanisms operating either singly or combined. They may
operate completely independently of each other or they may
interact and the situation can become extremely complicated.
For instance, the initial wear debris formed in sliding may
become oxidised by frictional heating and the hard oxide may
then act as a fine abrasive to the surfaces.

Wear behaviour will be more complicated under lubricated conditions. The interaction of lubricated surfaces is a complex subject involving changes in the surfaces, their substrates, and the lubricating film between the surfaces. The effects of speed, load and ambient temperature are manifested as chemical changes in both the surfaces and the lubricating film, and dependant on the lubricating system, corresponding changes in friction and wear.

In general, it is accepted that wear can be classified as either "Mild" or "Severe" as proposed by Archard and Hirst (14). In a mild wear situation, the contact resistance is high, analysis of wear debris shows small, i.e. about 100 nm diameter particles which are produced by reaction with the ambient atmosphere or fluid, and the microscopic examination of the surface is extremely smooth. In a severe wear situation, it is characterised by low contact resistance, wear debris normally consists of large, i.e. about 10^{-2} mm diameter, metallic particles, and produces rough, deeply torn surface. Let us now consider the classifications of wear in details as follows.

1.3.1 Adhesive Wear

If friction is high, adhesive junctions may form (cold welding) and material may be torn out and transferred from one surface to the other. Whether or not this occurs depends not only on the magnitude of the interatomic forces, but also on the mode of junction rupture on shear straining, as

determined by the mechanical properties of the interface and the parent metals (15).

The existence of this adhesive metal transfer can be demonstrated in a number of ways; probably the most convincing is by means of radioactive traces (16).

In theory it would appear that all the wear transfer will be from the softer material. In practice most of the wear does come from it but by no means all. This suggests that in the hard material there are some regions of low strength balanced by regions of high strength in the softer material.

The amount of adhesive transfer is profoundly affected by the nature of the surfaces and the ambient conditions. Cleanliness of the surfaces greatly facilitates adhesive wear. In a vacuum, especially if the surfaces have been heated to drive off any adsorbed films and oxide, they will adhere strongly under the slightest pressure. Any oxide or adsorbed film, such as water vapour, oxygen etc., reduces this tendency. High temperatures also favour adhesive wear.

In general, transfer of material from one surface to the other is not the same as wear. A transferred particle may remain attached to the acceptor surface for an indefinite period of time or transferred particles may travel back and forth repeatedly from one surface to the other, without the formation of loose wear debris. Even if adhesive material transfer does not lead to severe volume wear, considerable roughening of the contacting surfaces usually results. In lubricated systems this seriously impedes the continuity of liquid lubricant films.

1.3.2 <u>Abrasive Wear</u>

In abrasive wear, hard asperities or particles form grooves in the softer material. The primary requirement for the occurrence of abrasive wear is that there must be a great dissimilarity in hardness between the sliding surfaces. The work of Krushchov (17), Wellinger et al (18), and Mulhearn and co-workers (19, 20) has shown that in severe abrasive wear and for technically pure metals the wear resistance (i.e. 1/wear) is proportional to the hardness in the fully cold-worked condition. Hardening by heat treatment may further improve the abrasion resistance.

Abrasion produces a marked change in the structure and orientation of the surface layers of metals. Wilman (21) has shown that the abrasion texture is similar to that produced when the metal is deformed between hard rollers.

The case of abrasion caused by loose particles between the two sliding surfaces is very important and is probably responsible for the largest amount of wear in industrial machinery. This is because of the general prevalence of airborne dust and grit in most industrial environments. The external environment is not the only source either; hard particles, such as iron oxide which is very abrasive, may be present as a result of the wear process.

Whilst lubrication was stated to be the most effective method of reducing adhesive wear, this is not so with abrasive wear. The lubricant may introduce loose particles between sliding surfaces or it may tend to hold debris there. The only effective way of controlling abrasive wear is to

use hard and tough materials and to exclude all foreign
matter from the sliding surfaces.

1.3.3 Surface Fatigue Wear

This occurs primarily when surfaces are in contact
with rolling motion, such as ball and roller bearings and
gears. The cyclic stress involved in such situations can
cause fatigue of the rolling surfaces which is characterised
by local pitting or flaking of the surfaces and occurs
rather suddenly without any prior visible signs after a
relatively long life. In some cases, failure is initiated
at a surface flaw or crack, possibly formed during the first
few cycles in the life of the component. More often, however,
since the maximum shear stress occurs below the surface, the
failure will be initiated below the surface, particularly
if there is some inhomogeneity in the structure of the
surface material.

Davies (22) in studying the contact conditions between
a loaded sphere and a flat plate mapped the distribution of
stress in the plate and found that the shear stress reached
a maximum value at a point slightly below the centre of the
area of contact. That the maximum shear stress occurs at
a point below the surface would explain the occurrence of
sub-surface cracks in the tracks of rolling bearings and
in the faces of gear teeth subject to surface fatigue.

Lubrication as such does not influence fatigue greatly
since it is caused by stress x cycles. However, it can
help indirectly by keeping the surfaces clean and smooth,
by eliminating all adhesive wear and by preventing corrosion

of the surfaces which accelerates fatigue by increasing the
load stress concentration.

Surface fatigue on a micro-scale could also be respon-
sible for many other types of wear, e.g. oxidational wear
of steel (23) where oxide builds to a critical thickness
before being removed. The removal could be due to continual
asperity contact and hence fatigue since adhesion is not
likely to be responsible.

1.3.4 Corrosive Wear

Corrosive wear is a form of chemical wear which results
from the interaction of the environment with sliding surfaces,
followed by the rubbing off of the products of the reaction.
The most usual environments causing corrosion are moisture,
elevated temperature and the lubricant. In the presence of
water, hydroxides may result, whereas oxides are produced
in dry air at elevated temperatures. The presence of a
lubricant can exert a marked effect on corrosive wear. It
may protect the surfaces by reducing frictional heating and
the lubricant itself may react chemically with the surface
thus promoting a different form of reaction compound on the
surface. However, it is not uncommon for corrosive elements
to be dissolved in lubricants, such as water in oil, and
also lubricants can be degraded in time and become progress-
ively more corrosive.

The control of corrosive wear depends primarily on
control of the atmosphere surrounding the sliding parts and
the greatest offender in this is moisture, particularly if

either or both surfaces are ferrous base materials.

Corrosion is not necessary a bad thing, for example, oxidation of a surface in general reduces adhesive severe wear and protects the surface leading to lower wear rates. Similarly the addition of such additives as Tricresyl phosphate to oils produces phosphoric acid which interacts with surfaces forming complex corrosion products and affording good anti-wear action.

1.3.5 Erosive Wear

Erosive wear is caused by high velocity impact of particles. A popular example of errosion by solid particles is sand-blasting. Other examples of erosive wear are those of nozzles and blades of gas turbines due to solid particles in the products of combustion. Fluid erosion results from the repeated impact of drops of fluid and shows itself in the form of roughening of the surface under impact and pitting. The coating of a carbon-fibre reinforced plastic on turbine blades has been introduced to increase erosion resistance.

1.4 Lubrication Regimes and Lubricity

1.4.1 Hydrodynamic Lubrication

In hydrodynamic lubrication, the moving surfaces are completely separated by a continuous film of lubricant and the resistance to motion arises solely from the viscosity of the lubricant itself (figure 1.2(a)). This condition

can only happen when the sliding velocity is relatively
high and the load relatively light. The great advantages
of hydrodynamic lubrication are that there is, in the ideal
case, no wear of the moving parts and the friction coefficient
is extremely low - typically of the order of 0.001 - 0.01.

In practical situations, hydrodynamic lubrication
cannot be maintained throughout the process of operation of
the moving components. For instance, fluid film breaks down
during each end of the piston stroke in the fuel pump system.
The precise conditions under which fluid film conditions
occur will also depend on temperature and pressure, because
of the change of the physical properties of an oil, on the
geometry of the sliding system and on surface roughness.
The minimum film thickness normally exceeds 2×10^{-7} m which
is many times thicker than the surface roughness.

The three parameters (viscosity (ζ), speed (u) and
load per unit area (p)) are sometimes combined to form the
dimensionless bearing-number, C, defined as:-

$$C = \frac{\text{viscosity x speed}}{\text{unit load}}$$

By plotting the variation of coefficient of friction with
a dimensionless bearing-number, sometimes called Stribeck
Curve, the various lubrication regimes can then be identi-
fied as shown in the diagram (figure 1.3) and given by
Dowson (24).

1.4.2 Elastohydrodynamic Lubrication (e.h.l.)

This occurs for higher loads and the resulting high
pressures increase the viscosity of the fluid and the surfaces
undergo elastic deformation in the contact zone (figure 1.2(b)).
These effects drastically change the geometry of the lubri-
cating film which in turn alters the pressure distribution
at the contacts. However, very little wear takes place
since the thickness of the film is usually greater than the
roughness of the surfaces. Elastohydrodynamic analysis has
predicted that lubricant films may be 10 or 100 times greater
than those estimated by conventional hydrodynamic lubrication
theory. For normal engineering contacts, the film thickness
is of the order 2.5×10^{-8}m to 2.5×10^{-6}m.

1.4.3 Mixed Lubrication

Mixed lubrication takes place in a region where the
transition from elastohydrodynamic to boundary lubrication
occurs. There are some intermittent contacts between the
sliding surfaces and this results in wear (figure 1.2(c)).
The behaviour of the contact is governed by a mixture of
"boundary" and "elastohydrodynamic" effects. The surfaces
are separated by films of molecular proportions and the
film thickness ratio is normally between 1 and 5, defined
as (25):-

$$\text{Film thickness ratio} = \frac{\text{equivalent film thickness}}{\text{surface roughness}}$$

1.4.4 Boundary Lubrication

Boundary lubrication occurs only if a surface active agent is present. Boundary lubrication is defined as a condition of lubrication in which the friction between two surfaces in relative motion is determined by the properties of the surfaces and by the surfactant properties of the lubricant (figure 1.2(d)). This type of lubrication occurs under some combination of high load and small apparent area of contact, low sliding speed and rough surfaces. These conditions are found in journal bearings during starting and stopping, in rolling contact bearings cages, in gears, and in numerous sliding mechanisms in reciprocating engines - at the top and bottom of the stroke in the piston pump.

Since fluid properties play no part in boundary lubrication, a successful lubricant has to rely on properties other than viscosity for its operation. These are the physical and chemical properties of the boundary lubricants and the surfaces to be lubricated.

In general, two forms of boundary lubricating activity may be distinguished, operating under different conditions and having different effects. These may be termed "anti-wear" and "extreme pressure" (E.P.) activity. Anti-wear is essentially a low temperature property, having adsorption of very thin films on metal surfaces preventing excessive metal-metal contact. Some typical anti-wear additives are long chain acids, amines and esters which are frequently added to commercial oils to improve their low temperature boundary lubricating properties.   E.P. additives, which are

designed to operate at temperatures above which anti-wear
additives become ineffective. Such organic compounds
containing a reactive group are sulphur, chlorine, phospho-
rous or zinc, which can combine chemically with the surface
to give a film of low shear properties.
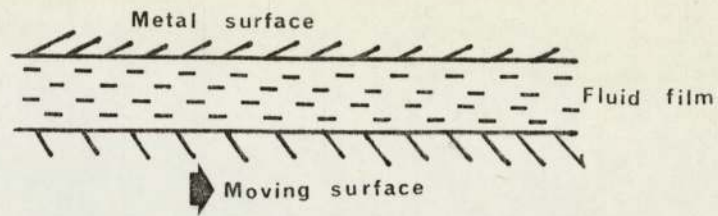
a. Hydrodynamic lubrication
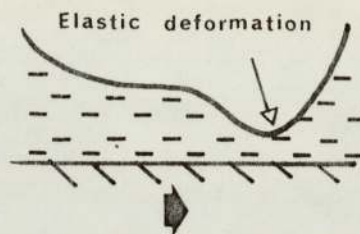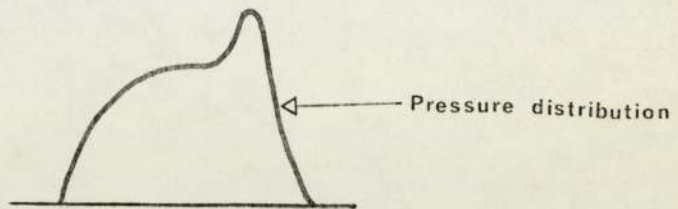
b. Elastohydrodynamic lubrication
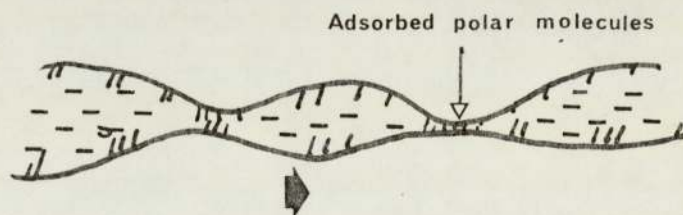
c. Mixed lubrication

d. Boundary lubrication

Figure 1.2. Lubrication Regimes
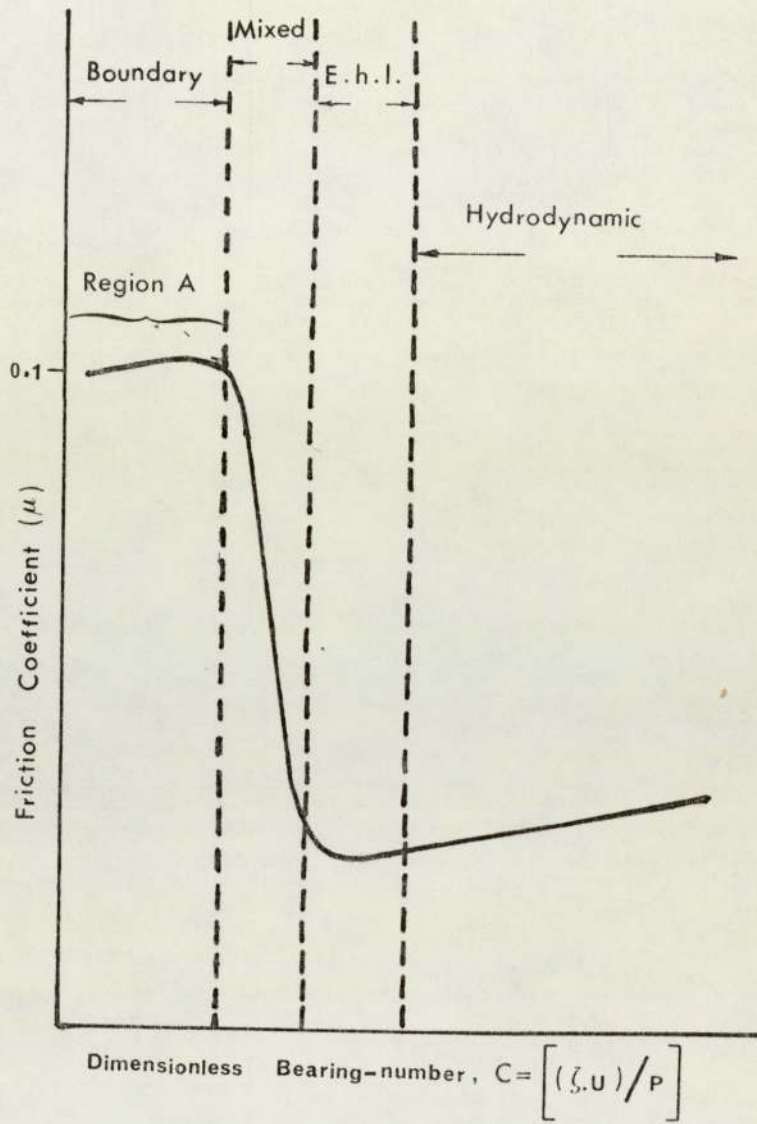
Figure 1.3. Classical Stribeck Curve

1.4.5 Lubricity

Experience has indicated that certain animal and vegetable oils keep smooth surfaces slippery compared with mineral oils of the same viscosity. This ability has been defined by Dukek and Vere (2, 4) in which if two liquids have the same viscosity, and one gives lower friction, wear, or scuffing, it is said to have better lubricity.

In order to understand the changes in fuel lubricity, it is necessary to recall the possible influence of the refining process on fuel lubricity. Originally fuels were produced by acid treating and by copper sweetening. The above two methods will, in one or the other way, remove the mercaptan sulfur by chemical reaction or convert the mercaptan sulfur into disulfides. In order to meet the high thermal stability requirements of modern fuel specifications and also in view of the tightening up of regulations governing environmental pollution, hydrotreating was introduced which is generally a cleaner process than the long established chemical methods (26).

Since hydrotreatment breaks down the sulfur, nitrogen and oxygen compounds present in the fuel, this process is in theory responsible for removing polar compounds from the fuel and consequently is said to be responsible for decreasing the boundary layer lubricity of the aviation fuel. The removal of chemically active species, such as mercaptans and aromatics, is invariably associated with poor lubricity (2). The use of additives to overcome a lack of lubricity in a fuel was obviously a possibility. The addition of

about 15 parts per million (p.p.m.) by volume of polar
compounds has been found sufficient to restore lubricity
to fuels (5). The blending of 10-20% of a conventional
treated fuel to a highly refined fuel has also been found
to improve lubricity to the level of the conventional
fuel. Hitec E515 is often added to middle distillate
fuels in order to inhibit or retard the corrosion of pipe-
lines and tankage. Aird and Forgham (3) have shown that
as little as 12 p.p.m. of Hitec E515 was of benefit in
reducing fuel pump wear. The introduction of a new corro-
sion inhibitor Hitec E580 is the main subject of the present
investigations.

1.5 Additives

The lubricity of today's jet fuels has been a matter
of concern, because there is an ever-increasing demand for
higher engine temperatures and accompanied with fuels of
better thermal stability. Fuel supplies can now furnish
fuels so highly refined they have essentially no lubricity
at all. In pumps and fuel control, these fuels can cause
sticking, wear, or catastrophic failure. The introduction
of a certain type of compound to jet fuel is one of the
possible solutions to the lubricity problem. These additives
not only have an effect of reducing friction and wear, they
also have characteristic functions of anti-oxidation, anti-
sludging, and anti-icing (27, 28).

Of the many additives approved for use in jet fuels,
corrosion inhibitors are the most surface active and remain

widely in use in the aviation industry. The corrosion
inhibitor Hitec E515 was manufactured by Edwin Cooper
Chemicals and the molecular structure of this product
consists of dimers of poly-ethenoid mono-carboxylic
acids (29). Work on the effect on additive response at
elevated temperatures was carried out by Smith on a two disc
machine (26). The result showed that Hitec E515 was still
effective at 100°C but less so than at ambient and its
effectiveness had gone at 150°C. Dacre et al (30) deter-
mined the effectiveness of various components of Hitec E515
in improving lubricity, using radioactive tracer techniques,
and found that dimer acid is the most important component
forming   strong adsorbed multilayers onto the surfaces,
even at high temperature (80°C and 100°C).

The additive behaviour depends upon additive concent-
ration, additive combinations and the nature of the base
fluids. Zinc dialkyl dithiophosphate and formulated polymer
and complex ester combinations produced synergistic effects
in paraffinic base oils and adverse effects in cyclic hydro-
carbon base fluids (31).

Recent work carried out by Poole and Sullivan (32, 33)
studied   the effects of Hitec E515, containing phosphate
ester and dimer acid, on the wear of aluminium-bronze on
steel on the presence of aviation fuel . They proposed that
the   additive had an effect of preventing transfer of
aluminium to the steel by removing it from the bronze
surface through preferential corrosion, thus giving initial
pro-wear effect, but it had an extreme-pressure effect at
high loads. The above example shows the complexity of

additive behaviour in different base fluids.

A new additive, Hitec E580, has been recently intro-
duced in which there is no phosphate ester component. The
concentrate of Hitec E580 was formed from the following
ingredients in the stated proportions by weight (29):-

Dimer Acid (Empol 1022)	45%
Sterox ND	15%
Process Oil	10%
Kerosene	30%

The above mixture comprises (a)from 1.8 to 25 parts by weight
dimerised unsaturated fatty acid, said fatty acid containing
from 8 to 20 carbon atoms and (b)1 part by weight of an
ethoxylated alkyl phenol, said phenol having an average of
3-4 ethylene oxide units per molecule and said phenol having
one or more alkyl substituents which contain a total of from
4 to 16 carbon atoms and which mixture provides a Water
Separation Index, Modified (WSIM) number of at least 60.
The WSIM number is a numerical rating indicating the ease
of separating water from a hydrocarbon liquid by coalescence.

The role of the new additive, Hitec E580 contains no
phosphate ester, was not known. It appears to be as effective
as Hitec E515. Hence, it leads to the present work on how
Hitec E580 behaves in the presence of hydrotreated fuels.

1.6 Metallurgical Considerations

The aluminium-bronzes are a group of copper alloys containing aluminium as the principal alloying element, the properties of which depend on both composition and microstructure.

Referring to the binary phase diagram (34) shown in Figure 1.4, under equilibrium conditions up to 9% aluminium can be accommodated in the terminal alpha(α) solid solution. The commercial single phase alloy (BS 2871, CA 102), however, also contains up to 3% iron to give grain refinement. Under equilibrium conditions, the solubility of iron in this type of alloy below 550°C is less than 1%, but the precipitation reaction of δ iron begins when the temperature drops below 1000°C (35).

Binary alloys containing more than about 8% aluminium are no longer single phase and in general exhibit a duplex alpha-beta structure. However, as shown in Figure 1.4 the body-centred cubic beta phase is metastable and will decompose eutectoidally during slow cooling or annealing below 565°C to form α and γ_2. The γ_2 phase is an intermetallic compound of approximate composition Cu_9Al_4 and has a $D8_3$ crystal structure (36).

A further important group of alloys is the complex aluminium-bronzes, containing additions of nickel, iron and manganese. A pseudoquaternary phase diagram (37) of a complex aluminium-bronze (BS 2872, CA 104) is shown in Figure 1.5. Manganese has equivalent effects to aluminium in that it stabilises the beta(β) phase (38). Nickel is

rarely added to binary alloys to the exclusion of other elements, but it has been shown (39) that at addition levels below 2% this element remains essentially in solid solution, further additions promoting the formation of a Ni-Al precipitate.

In the cast Ni-Al bronze alloy 958 (ASTM B148 or MIL-B-24480), a rather unique situation exists whereby the composition range of 8.5-9.5 wt.% Al, 3.5-4.5 wt.% Fe and 4.0-5.0 wt.% Ni allow as-cast microstructural and property variations (40-45). For example, in compositions containing ~4 wt.% Ni, increasing the Al content from 8.5 to 9.5 wt.% alters the cast structure from one comprised only of α+Fe/Ni/Al intermetallics, to one which includes the chemically active $Cu_2Al(\gamma_2)$ phase (42,43). At a fixed Al level, on the other hand, changing the relative amounts of Fe and Ni affects the cast microstructure by altering the character- istic of the Fe/Ni/Al phases. When the Ni:Fe ratio exceeds unity, the globular dispersed form of intermetallic, commonly referred to as Fe-K, is replaced by a continuous inter- granular lamellar phase, Ni-K, i.e., the cast microstructure changes from α+Fe-K to α+Ni-K. The net effect of such phase boundaries, one relating to the γ_2 phase, and the other to the Fe/Ni/Al intermetallic compounds, is that different within-specification compositions offer different compromises between the good corrosion resistance associated with high Ni levels, due to the suppression of the γ_2 phase and the superior toughness of alloys containing α+Fe-K (45). These relationships between structure and composition are made even more complex by the susceptibility of the cast

alloy to microsegregation which may, for instance, result
in local concentrations of Al or a local deficiency of Ni,
giving rise to the appearance of the corrosion-prone γ_2
phase. Although such microstructural anomalies may be
modified by heat treatment (43), in the case of large cast-
ings it is clearly more feasible to rely on compositional
control of the structure.

The complex aluminium-bronzes used in this work con-
tained compositional variations of 9-11 wt.% Al, 3.5-6
wt.% Fe, 3-6 wt.% Ni and ~1 wt.% Mn (table 3.2), it is
essential to see how these variations influence the
microstructure and mechanical properties.

Figure 1.4. Copper-Aluminium Phase Diagram
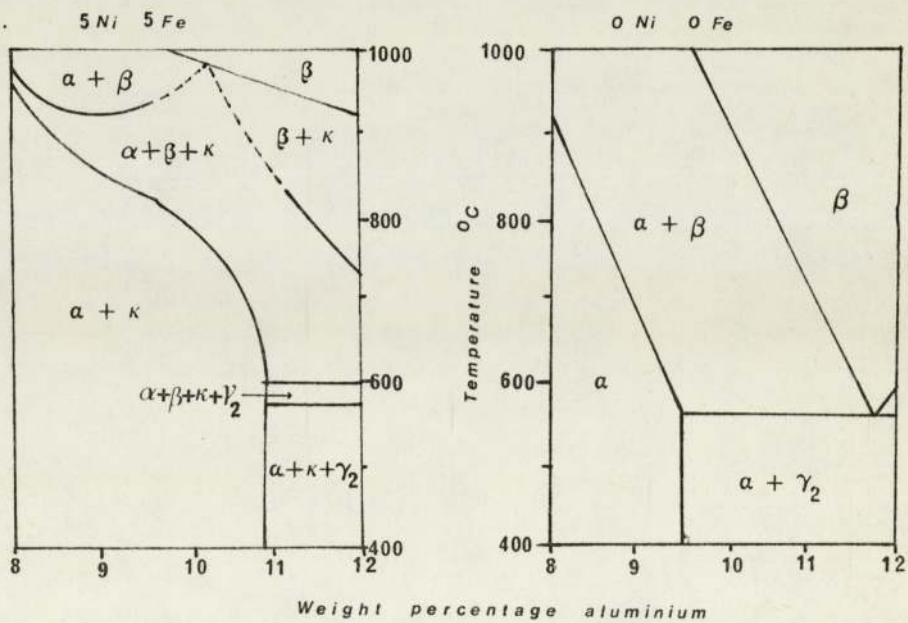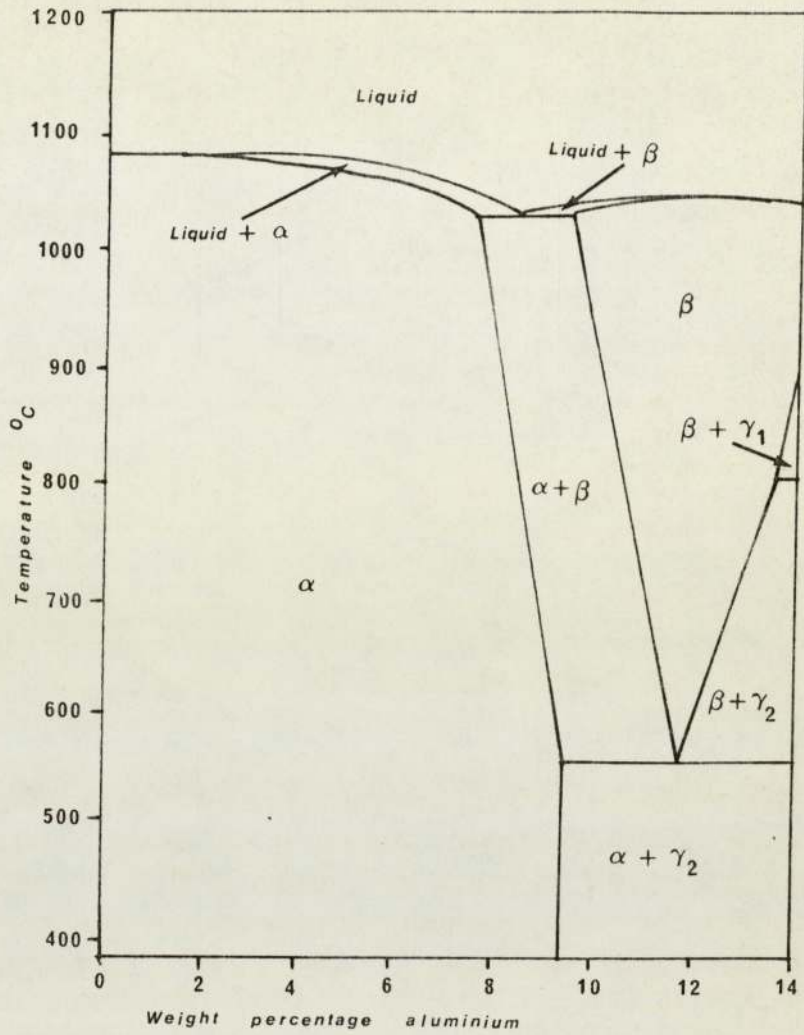
Figure 1.5. Showing effect of 5% Ni and 5% Fe addition on Cu-Al Phase Diagram

1.6.1 Mechanical Properties

The effects of Fe, Ni and Al on the tensile properties of Ni-Al bronze of composition range of 8.5-9.5 Al, 1.3-3.0 Mn, 3-6 Fe and 3-6 Ni had been reported by Crofts and Thomson (41,46). Higher nickel contents than iron in the alloys increase yield strength in the expense of elongation. If the Ni-Fe ratio exceeds 1.8, the UTS is drastically reduced.

The effect of temperature upon the mechanical properties of complex aluminium-bronze (specification D.T.D. 197) has also been reported (47). It has been shown that the ductility of the alloys increases markedly in the temperature range between 300-450°C, followed by a decline to a minimum at 600°C, and a further increase at temperatures above 600°C. The high ductility arises because of an increase in the stacking-fault energy of the α matrix, while the subsequent decrease in ductility in the range 400-600°C is due to the increased width of precipitate-free zones adjacent to the α grain boundaries. At higher temperature the reversion of the precipitates aids the recovery processes leading to an increase in the overall ductility of the alloys. Cottrell (48) has reported that metals and alloys may fail prematurely at temperatures approaching 0.6 T_m (541°C for copper, where T_m is the absolute melting temperature) owing to a weakening of the grain boundaries, even though the grains themselves may still be strong.

Cook et al (49) observed the structure and properties of complex aluminium-bronzes containing 8-12% aluminium and 4-6% each of nickel and iron. Structurally, the alloys they

were classified as follows:-

    (1)   alloys containing 8-9% aluminium, consisting of α and β at 1000°C, change to α and K at lower temperatures;

    (2)   alloys containing 10% aluminium, consisting of β at 1000°C, α , β , and K between 800° and 900°C, and α and K at lower temperatures; and

    (3)   alloys containing 11-12% aluminium, consisting of β at 1000°C, changing from β+K to α+ β +K over the range 800°-600°C, and finally changing to α+K+γ_2.

The mechanical properties of alloys containing 8, 10 and 12% aluminium with 5% each of nickel and iron had been determined in the quenched, quenched and tempered, hot-rolled, and hot-rolled and annealed conditions. They found that the optimum properties were obtained from the 10/5/5 alloy.

The impact resistance of sand cast aluminium-bronze (BS 1400:AB2) has been investigated by Sarkar and Bates (50). Increasing the aluminium content from 8.5 to 10.5% increased the tensile strength of the alloys from 602 to 710 MNm^{-2} and the 0.1% proof stress from 200 to 278 MNm^{-2} at the expense of ductility which fell from 26 to 13% and impact resistance 54 to 14J. The best combination of properties in alloys containing $\sim$ 5% iron with $\sim$ 5% nickel was obtained at 9.5-9.7% aluminium. Alloys in this composition range should meet minimum property requirements of 649 MNm^{-2} tensile strength, 239 MNm^{-2} 0.1% proof stress, 18% elongation and 20J impact value. Decreasing the iron content to $\sim$ 3.5% reduced the tensile strength by $\sim$ 62 MNm^{-2} and the proof stress by $\sim$ 31 MNm^{-2} without significantly

improving ductility or impact resistance. Increasing the
nickel content to ~ 6.5% severely reduced both ductility
(by 8%) and impact resistance (by 14J), but there was no
useful improvement in strength. By raising the iron content
to the maximum (5½%) and reducing the nickel content to tne
minimum (4½%) allowed in B.S. 1400:AB2, the impact resist-
ance was increased by 3-4J above that of a 5% iron-5%nickel
alloy of similar aluminium content. Hence, the best com-
bination of properties would be obtained in alloys containing
5-5½% iron and 4½-5% nickel with 1% manganese.

The present investigated aluminium-bronze (DTD 197A-
Delta bronze) was a drawn rod, obtained from Delta (Manganese
Bronze) Limited, which has a mechanical properties of 400-
440 MNm^{-2} 0.2% proof stress, 740-800 MNm^{-2} tensile strength,
20-25% elongation, 210-300 VPN hardness and 460-520 MNm^{-2}
shear strength (51).

1.6.2 Corrosion Performance

The aluminium-bronzes have been employed to great
advantage in many applications in marine conditions and in
corrosive environments involving contact with many acids
and salt solutions. They have been found suitable, for
instance, for parts such as pickling crates, chains, hooks,
pump bodies, impeller blades, etc., which come into direct
contact with acids such as HCl, H_2SO_4 and HNO_3.

A wide range of aluminium-bronze alloys is available
in both wrought and cast forms, the good resistance to
corrosion depending basically on the formation of protective

surface films. Additions of a number of other elements (including Fe, Ni, Mn, As, Sn, Si, Cr, Co) are made to aluminium-bronzes to improve mechanical properties and/or corrosion resistance.

The corrosion resistance of aluminium-bronzes largely depends upon the microstructure (52). It has been reported that the eutectoid decomposition of the β phase to $\alpha + \gamma_2$ is accompanied by a fall in corrosion resistance. Microstructure is affected by cooling rates, and by additions of alloying elements such as manganese, nickel and iron which help the retention of the β phase in these alloys (53).

The single phase alloy is considered to have good general corrosion resistance, and although stress corrosion failures have been reported (54), additions of 0.5% tin or silver have been shown to be beneficial in conferring immunity to intergranular failure. It is suggested that this mode of cracking is related to segregation of atoms at grain boundaries, and to a lesser extent within the crystal lattice. Such concentrations allow selective corrosion to occur. It is considered that aluminium segregates in this manner in the alpha aluminium-bronze alloy, but that the additions of tin or silver, because of their atomic diameter, accumulate preferentially in these sites, and by their more noble nature inhibit intergranular corrosion.

The duplex alpha-beta aluminium-bronze is considered to have better corrosion resistance than high tensile brass. However, corrosion trials (53) have shown that the γ_2 phase

which may form in this alloy is susceptible to selective attack. The anodic nature of this phase has been confirmed by open circuit equilibrium potential measurements in seawater (55).

Although iron additions, present in the commercial alloy (BS 2874, CA 103) as a grain refining agent, modify the binary equilibrium diagram (35), additions up to 3% have no effect on the susceptibility to selective phase corrosion. However, it has been demonstrated that an improvement in corrosion performance of the basic 90%Cu-10%Al alloy can be achieved by control of composition (53). In particular, restriction of the aluminium content to 9% produces the γ_2 in an isolated form on slow cooling. This will prevent the continuous selective network of corrosion, although pitting attack may still occur. Additions of manganese to inhibit the eutectoid reaction, however, result in increased rates of corrosion of retained beta phase compared with the manganese-free alloy. This is particularly so under deaerated crevice conditions when fairly rapid beta corrosion can occur (55).

In complex aluminium-bronzes containing iron and nickel, the corrosion performance is very sensitive to the presence of the anodic γ_2 phase in the microstructure and is therefore a function of its thermal history and Al, Ni, and Fe contents (56,57). In its most insidious form, the reactivity of γ_2 can produce serious corrosion penetration by de-aluminization in alloys having a continuous network of intergranular $\alpha+\gamma_2$ eutectoid, i.e., in compositions having a combination of high Al (>9.5 wt.%) and very low

Ni:Fe ratio (< 0.5) (42). A good corrosion resistance can
be obtained if the Ni:Fe ratios > 1.2 with relatively low
Al levels (< 9.2 wt.%), as β decomposes entirely to α+Ni-K
and no residue of γ_2 is formed.

1.6.3 Dealuminization of Aluminium-bronzes

Aluminium-bronzes have been observed to undergo five
forms of local accelerated attack, namely - pitting corrosion,
crevice corrosion, galvanic corrosion, impingement attack
and dealuminization (58). The latter form, which is of
particular interest in the current project, is analogous
to dezincification of brasses (59). Classically, dealumi-
nization is attributed to the difference in electrochemical
characteristics between the copper-rich alpha and aluminium-
rich $gamma_2$ phases (60). In the presence of sea-water, an
electrolytic cell is set up at the interface of the alpha
and $gamma_2$ phases. The latter, being less noble than the
alpha phase, will corrode preferentially, accompanied by
a severe loss in aluminium. If the anodic constituent is
present in the microstructure as an inter-connected secondary
phase, it will provide an easy path for dealuminization to
follow. A dealuminized area can sometimes be recognized
by its distinct copper colour.

To date, it appears that there are two practical
means of combating dealuminization: (a) Modification of
Composition and (b) Heat Treatment. Additions of iron and
nickel to the basic Cu-Al alloy system have been effective
in reducing or eliminating the amount of $gamma_2$ produced,

thereby improving resistance to dealuminization. Iron
acts as a refiner (59) but more significantly, it forms
an iron-rich phase in combination with Al which appears
as small globules and/or rosettes in the microstructure.
In this manner, the addition of iron reduces the amount
of aluminium available to form gamma$_2$.

Similarly, nickel combines with aluminium in the
Cu-Al solid solution to form a new "kappa" phase believed
to be Ni-Al (37). This phase takes with the form of
elongated rods, often in a lamellar array with alpha.
Thus it has been reported that nickel improves dealumini-
zation resistance by forming a "pearlite" boundary layer
between the aluminium-rich and copper-rich phases (61).
In addition, the formation of nickel-rich kappa reduces
the amount of Al available to form gamma$_2$ and results in
an apparent shift of the alpha/alpha+gamma$_2$ phase boundary
to higher Al contents.

In the case of heat treatments for aluminium-bronze, much
depends on whether mechanical or corrosion properties
are to be optimized. For optimum tensile properties the
recommended heat treatment is (1)water quench from about
850°C, (2)reheat to about 720°C for 2 hours and (3)air
cool. The air cooling is used to reduce residual stresses
which result from quenching in water (62). A modification
in the post-quench treatment is also suggested (59) -
(1)quench from about 850°C and reheat to between 570 to
650°C; or (2)heat to 850°C; slowly cool to between 550 to
600°C and quench.

The heat treatment recommended for grade 2, 3 and 4

of MIL-B-16033 to minimize corrosion is (1)water quench from between 870 to 900°C and (2)reheat to between 540 to 650°C and quench. The improvement over other methods is considered to be associated with elimination of eutectoid structure (57).

While a majority of the basic research on dealloying corrosion has centered on the dezincification of brass, the mechanisms proposed for dezincification have been success-fully used to explain dealloying in other alloy systems. In this connection, the following factors which have been observed to influence dezincification (63) are considered pertinent to the dealloying of Aluminium-bronze.

    (1)   a restricted oxygen supply favours dealloying, particularly stagnant water, crevices and porous surface films

    (2)   chlorides, especially in salt water, cause dealloying

    (3)   dealloying appears favoured by acidity, although it can also occur in alkaline situations

    (4)   environments which favour the presence of Cu ions may induce dealloying

    (5)   surface residual stresses, differential aeration or contact with more noble metals may cause anodic behaviour and accelerate dealloying corrosion

    (6)   dealloying reactions increase with temperature

The above factors are particularly relevant to the boundary lubricated conditions of aluminium-bronze sliding on steel.

The presence of fuel supply into the system restricts free oxygen from the surroundings to come into contact to the sliding surfaces. The shear stresses induced on the

sliding surfaces together with the increase in surface temperatures due to frictional heating may induce dealuminization. The presence of additive containing dimerised unsaturated fatty acid coupled with the high concentration of copper ions on bronze surfaces may further increase susceptibility to dealuminization.

1.6.4 Cavity Growth in Aluminium-Bronzes

The effect of cavity formation on creep ductility at high temperatures has been the subject of much research during the past decade. Hull and Rimmer (64) illustrated the importance of diffusion-controlled cavity growth. Hancock (65), and Beere and Speight (66) have recently developed the concept of plasticity-controlled cavity growth. An important difference between diffusion-controlled and plasticity-controlled cavity growth is that the former mechanism predicts the rate of change of cavity volume with time to be almost independent of current volume, whereas in the latter mechanism these two parameters are proportional.

Many superplastic alloys, such as Al-bronzes, can achieve a total elongation exceeding several hundreds percent under an optimum superplastic strain rate conditions at high temperature (67,68,69). Dunlop et al (67) investigated the anisotropic ductility of a superplastic aluminium-bronze (CDA 619 containing Cu-9.5%Al-4%Fe). A marked anisotropic ductility was observed at the intermediate strain rates with maximum elongation occurring as high as 700% when the tensile axis was at 90 degree to the rolling direction at testing temperature 800°C in air. Cavities found at the interfaces between phases were rounded and equiaxed in shape. In this alloy fracture occurs by the formation and slow interlinkage of cavities. Shapiro et al (68) carried out the investigation of this alloy further and found that a significant cavitation occurs only in material strained at rates higher than that corresponding to maximum m (m is

a strain-rate sensitivity determined by the slope of flow
stress versus strain rate). The extent of cavitation
increased with increasing strain-rate. Electron shadow-
graphic technique showed that the shape of these cavities
are bulbous, suggesting that nucleation and growth occurred
along $\alpha-\beta$ interfaces. Fracture was resulted from the con-
tinued nucleation, growth, and interlinkage of cavities.

In this current project, cavities have also been
found in the lubricated wear of aluminium-bronze. The
mechanism of cavity growth and formation is very much
related to the mechanism of diffusion-plasticity cavity
growth as in the creep process. The influence of segrega-
tion also contributes to the acceleration on creep cavitation.

1.7 Theoretical Considerations

Metals wear by different mechanisms which are dependent
on the environment and loading conditions. Wear can be
caused by such mechanisms as abrasion, adhesion and corrosion
as well as by fatigue. In a given situation more than one
mechanism may be operating simultaneously but often the wear
rate is controlled by a single dominant mechanism.

Of the various type of wear processes, the most diffi-
cult to overcome is adhesive wear. The adhesive wear process
takes place in the metal-metal contact area. If it is not
controlled, adhesion between surfaces can lead to galling
and eventually to machine failure. An expression for adhe-
sive wear under dry conditions has been developed by a
number of researchers. Holm (70) determined that the real

area of contact is formed by the plastic deformation of
contacting asperities and considered wear as an atomic
process. Burwell and Strang (71), in their practical ex-
periments, verified that wear rate is dependent on load
and is independent of the apparent area of contact. The
Archard wear law (72) expresses wear rate in terms of the
real area of contact, namely $\omega = KA$. Archard (73) interprets
K as the probability of producing a wear particle at any
given asperity encounter. If K is independent of load,
then one could say that wear equation ($\omega = KA$) leads to the
Wear Laws, since $A = W/P_m$ (where W is normal applied load
and P_m is normally taken to be the hardness of the bulk of
the material beneath the areas of contact and is, of course,
independent of the load). Using this value for A, Archard
(74) showed that K can vary from 10^{-2} down to 10^{-5} dependent
on the material combinations being used. It is this wide
variation of K-factors which makes wear results more diffi-
cult to analyse than friction results.

Kingsbury (75,76) introduced the concept of the frac-
tional film defect to take into account the introduction of a lubricant.
The factors that influence wear are the boundary molecular
size, the fundamental time of vibration of the boundary
molecule and the thermal adsorption-desorption of the
particular type of boundary molecule.

Rowe (77), Thompson and Bocchi (78) tried to adapt
Archard's theory to lubricated sliding contacts. Rowe
introduced the concept of the fractional film defect into
Archard's equation and this allowed the wear to be correlated
with the effectiveness of the lubricant. Unfortunately,

Rowe's model does not take into account the fact that the total load is supported by the lubricating film as well as by the contacting asperities. The approach of Thompson and Bocchi does not include the role of the lubricant in the mitigation of adhesive wear. To remove these limitations, Stolarski (79,80) proposed a model which incorporates the concept of the fractional film defect (75) and the solution proposed by Johnson et al (81) which deals with the division of the total load between the lubricating film and the contacting asperities. However, considerable experimental evidence (82) suggests that the adhesive mode of wear is not the sole wear mechanism operating in lubricated sliding contacts and the fatigue mechanism of wear must be taken into account.

The most comprehensive review of boundary lubrication is that of Beerbower (83), who classified the regimes and modes of lubrication and wear according to the severity of damage as a function of the normal load. At low loads (at a given speed) the conditions of hydrodynamic, elastohydrodynamic and quasi-hydrodynamic lubrication exist. Under these situations wear is either minimal or absent. At intermediate loads, under boundary lubricated conditions, the wear regime is classified as mild wear. The wear modes are taken as sliding fatigue, adhesive wear, corrosive wear, mixed corrosive-adhesive wear and mixed corrosion fatigue. At a specific load a transition from mild wear to severe wear is caused by scuffing and scoring. As the load is increased above the transition load, seizure can occur

caused by welding.

Metals will undergo oxidation due to the generation
of frictional heat between the two sliding surfaces. Oxi-
dation can occur in dry sliding as well as in boundary
lubricated conditions. Quinn (84) developed an oxidational
wear expression for the K-factor in terms of oxidational
parameters in a form of Archard's wear equation. Sullivan,
Quinn and Rowson (85) developed the oxidational theory of
mild wear even further. They suggested that it is possible
to use the oxidational theory of the mild wear of metals,
together with measurements of heat flow and analysis of
wear debris structures, to obtain otherwise unobtainable
information about the number of asperities, the size of
these asperities, the thickness of the critical oxide film
formed on those asperities, the temperature at which the
oxide is formed on the asperities and the oxidational
constants appropriate to the conditions of oxidation
during wear. Poole (86) tried to adapt Sullivan's concept
to develop the oxidational wear theory of aluminium-bronze,
since oxidation has been found to occur between bronze-steel
interfaces under boundary lubricated wear conditions. Unfor-
tunately, Poole failed to mature the theory due to the pre-
sence of large numbers of undeterminable parameters which
make the wear equation unmanageable. The later Sullivan's
concept in developing an oxidational theory of the aluminium-
bronze on steel system under boundary lubricated wear is
of particular interest to the present investigation.

1.8   Outline of the Research Carried Out in this Investigation

Work carried out by the oil companies and fuel-pump manufacturing companies has been directly concerned with finding a quick solution to the original problem. The role played by the corrosion inhibitors in reducing pump wear has been investigated extensively. The effect of zinc dithiophosphates (87) has been shown to provide anti-wear protection on axial piston pump performance. More recent investigation (32,33) has shown that the commercial corrosion inhibitor containing phosphate ester eliminated pump wear. The presence of a corrosion inhibitor (Hitec E515) changes the wear to a corrosive mechanism in which aluminium transfer is prevented by the action of the additive, but provides extreme-pressure effect and reduces wear when the surface conditions become severe. A new additive, Hitec E580, has been recently introduced in which there is no phosphate ester component. Little is yet known about this additive which leads to the present investigation in finding the role of Hitec E580 on the boundary lubricated wear of aluminium-bronze on steel system.

The aims of the present study were thus: (1)to obtain wear rate against load curves for percolated hydrotreated fuel with and without Hitec E515; (2)to repeat the above procedure with additive Hitec E580 which contains no phosphate ester; (3)to run the tests for a sufficient duration in order to establish wear under conditions of boundary lubrication; (4)to record the coefficient of friction as it is one of the important parameters contributing to wear;

(5) to analyse the worn surfaces and sub-surface deformation by taper sectioning; (6) to analyse the wear debris.

The usefulness of new surface analysis instruments in understanding boundary lubrication has been reviewed by Godfrey (88). X-ray diffraction (XRD) reveals the structure of crystalline material from which compounds can be identified, for instance, wear debris. Scanning electron microscopy (SEM) permits significant advances in understanding fatigue and delamination wear, diffusion of alloying elements and the nature of corrosive wear. Electron probe microanalysis (EPMA) and Auger electron spectroscopy (AES) reveal the concentration and distribution of elements and fragments of compounds from lubricating oil additives in boundary lubrication films on metal surfaces. So by using the above analytical techniques in this present investigation, it was the hope that an understanding of the mechanism of fuel pump failure would be gained. This could eventually, aid the development of theoretical prediction of the wear of aluminium-bronze on steel system in the presence of aviation fuels under boundary lubricated conditions.

CHAPTER 2

EXPERIMENTAL APPARATUS AND PROCEDURE

2.1 Introduction

Using a conventional pin-on-disc machine, a study
of boundary lubricated wear of aluminium-bronze sliding
on steel system can be divided into three major sections.
Experiments were conducted to measure friction and wear
rate under sliding wear conditions in the presence of
aviation fuel, both with and without additives. The wear
experiments were conducted in two locations — Thornton
Research Centre and Aston Tribology Laboratory. Tests
carried out at Thornton Research Centre were operated under
fuel supply of flooded conditions, whereas, the other set
of tests conducted at Aston Tribology Laboratory were
operated under starved conditions, mainly because of using
different structural bronzes of different strength and
toughness. These will be discussed in detail later.

The second stage of investigation was carried out to
examine metallographic structures of aluminium-bronze and
this included taper sectioning on worn pin surfaces to
reveal any structural change after wear.

Finally, the investigation was carried out to analyse
the worn surfaces, the wear debris and the effects of addi-
tive on wear. The techniques used for the sample analysis
consist of Optical Microscopy, Scanning Electron Microscopy,
Electron Probe Microanalysis, Auger Electron Spectroscopy,
Leitz Wetzlar Microhardness Machine and X-ray Power Diffrac-
tion.

2.2   The Thornton Wear Machine

The layout of the Rotating Cylinder Friction and
Wear Tester is shown in Figure 2.1.

The pin-on-disc machine is a modified version of an
Amsler Wear Tester. A 3.7 KW electric motor drives the
disc via a hydraulic variable speed drive unit, 3 vee-
belts and shaft. The pin was mounted on a 3:1 lever arm,
the weight of which was counter-balanced by a light spring.
The height of the spring was adjusted until the pin just
balanced on the disc. An eccentric rod was fixed trans-
versely to support this lever arm which controlled the pin
in 'Loaded' or 'Unloaded' position on the disc. The loads
were applied to the end of this lever, so putting pressure
on the pin when the eccentric rod was in 'Loaded' position.
A capacitance transducer probe was mounted under this lever
arm to trace continuously the wear of the pin on the wear
recorder. Friction was monitored by means of a torque-
transducer with a digital readout, to the output of which
was connected a potentiometric recorder. This gave a conti-
nuous trace of the torque.

The flow rate of fuel was 20 ml min^{-1} (2 lb/hr) to
the conjunction of the pin and disc in a single pass
flooded heat-sink.
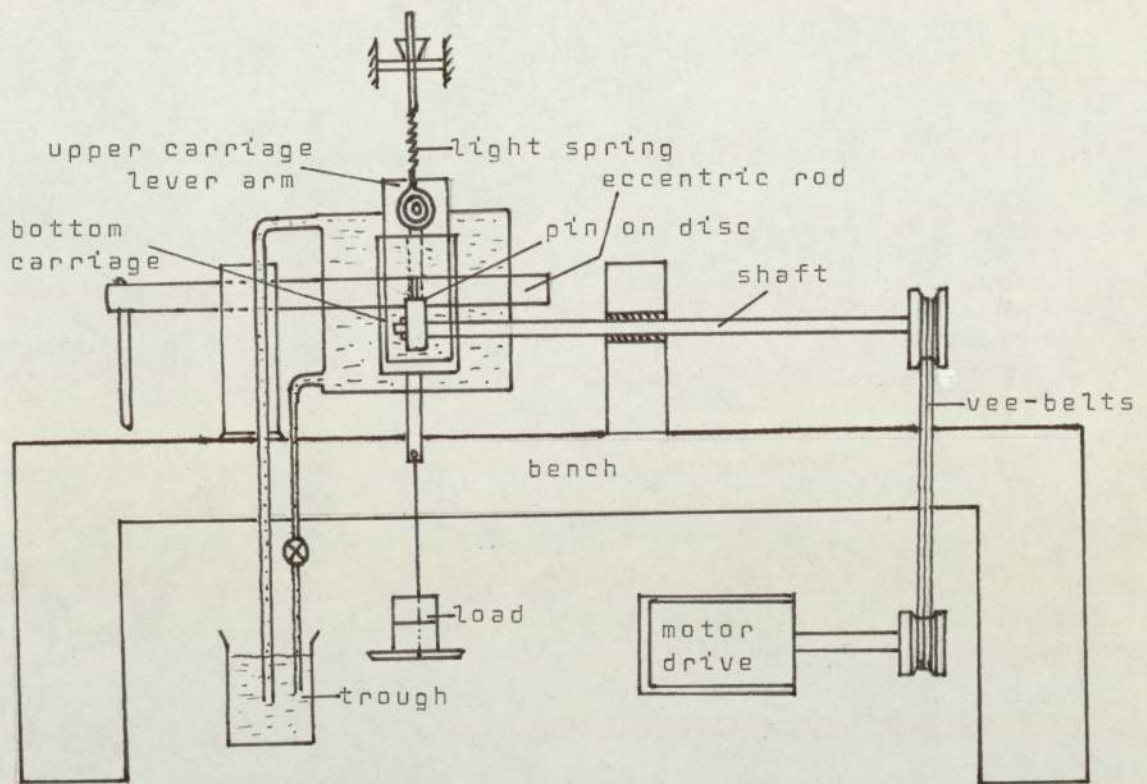
Figure 2.1   Schematic layout of Thornton's rotating
cylinder friction and wear tester

2.3 The Denison Wear Machine

A Denison Model T62 Tribotester was used in the
Aston Tribology Laboratory for wear experiments (figure
2.2(a) and 2.2(b)). This tribotester consists princi-
pally of a pin which is able to be loaded against the
flat surface of a rotating disc in the presence of a
lubricant. The disc is driven by a servo controlled
motor, with speeds in the range of 100 to 600 r.p.m.
Speed is indicated on the servo motor control panel and
a vernier gauge on the machine measures the radius of
the running track. When this radius is changed to give
a new disc wear track, the motor speed can be varied to
maintain the same relative velocity at the pin/disc con-
tact point. The calculations of a required speed relative
to the change of a new disc wear track were shown in
Appendix 1. The gimbal mounting can be adjusted to enable
the pin to be positioned at different radii on the disc,
so giving maximum utilisation of the disc's surface. A
device was fitted for raising or lowering the loading lever,
so that the proportional weights could be added or removed
from the weight pan, with the pin held clear of the moving
surface. The wear pin was held in a brass holder and the
maximum force between the pin and the disc was 200 N.

A single pass system was used to supply fuel to the
disc to avoid any debris being carried back to the system.
Glassware was used for the majority of the system except
that where flexible connections were required. The Vinescol
23 type with 6 mm diameter rubber tubing was used. This

type of tubing was selected because it does not contain
plasticisors. A peristaltic pump was used to circulate
the fuel in the single pass system. The flow rate of the
fuel was adjusted to give a boundary lubricated condition.
For a constant flow rate of 1.7 ml min^{-1}, a one hour test
run would require about 0.15 litre for the fuel to circu-
late once in the system.

Figure **2.2** {a} Complete View of Denison Model
T62 Tribotester
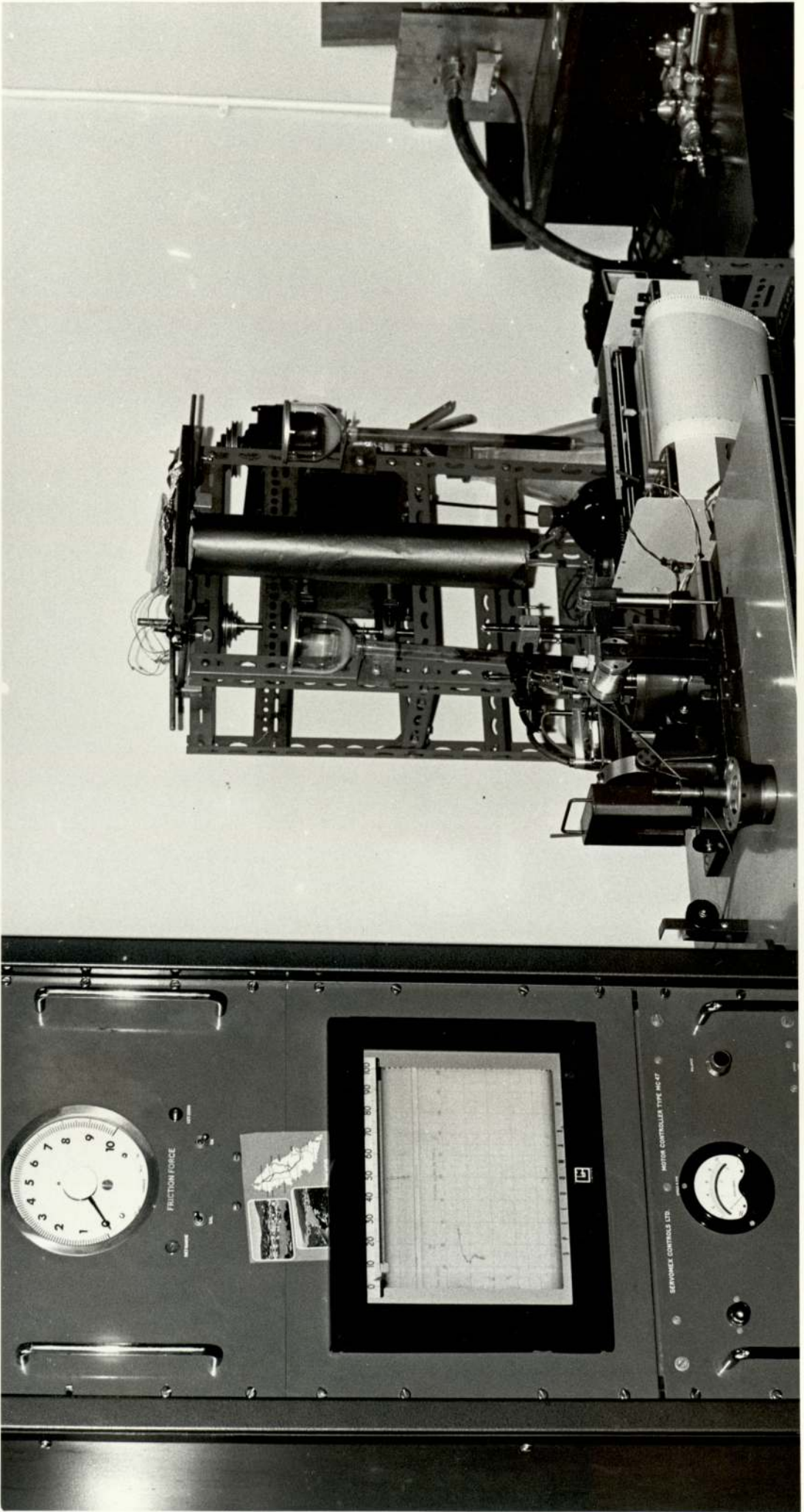
Figure 2.2 {b}   Detail of Denison Wear Test
Rig Showing the   Al–Bronze Pin
Running on KE 180 Steel–Disc in
the Presence of Aviation Fuel
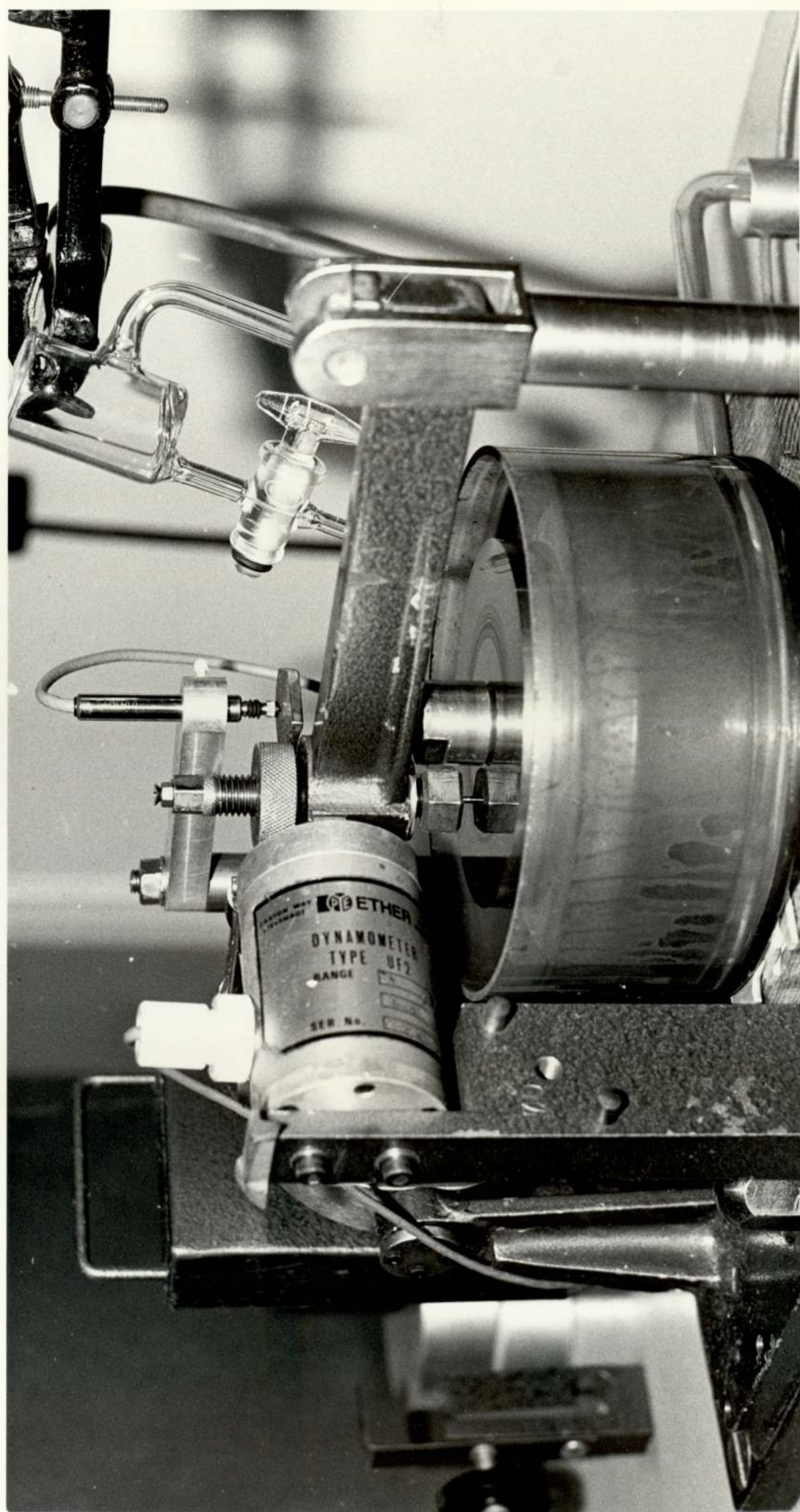
2.4　The Disc Specimens

　　　The disc specimens were made of KE 961 and KE 180
steel, the composition of which is given in Table 2.1.
The only difference between these two steel materials is
that KE 180 does not contain the 0.5 to 0.75% tungsten
that KE 961 contains.　The disc surfaces were flatly
ground to give a surface finish of approximately 0.025 μ.m.
centre-line-average(C.L.A.) , the measurements being made
on a Talysurf 4/Talynova System.　A sand-blasted disc was
used to achieve conformity on pin surface.　The sand-blasted
disc had a surface finish of approximately 1.00 μ.m.
centre-line-average (figure 2.3).

　　　For use with the Thornton Wear Machine, the dimen-
sions of the discs were 50×10^{-3} m in diameter and
10×10^{-3} m in thickness.　Since the thickness of disc is
10×10^{-3} m, two tests can be done on the disc surface
periphery rubbed by 3×10^{-3} m diameter pin.　In the first
test, the pin is rubbed close to one edge of the disc.
After completing the test, the disc is removed and turned
over so presenting a new track to the new pin, i.e., the
second test now uses the other edge of disc surface peri-
phery.　The KE 961 steel disc had an indentation hardness
of 779 VPN.

　　　For use with the Denison Wear Machine, the discs were
100×10^{-3} m in diameter and 10×10^{-3} m in thickness.　The
KE 180 steel disc had a hardness value of 674 VPN.　A pre-
wear disc was sectioned and examined in a scanning electron
microscope which was linked to a X-ray fluorescence spec-
trometer.　Figure 2.4(a) is the electron micrographs of

pre-wear KE 180 disc surface and Figures 2.4(b)-(f) show
the iron, chromium, aluminium, silicon and sulphur X-ray
distributions respectively. The presence of chromium in
steel is non-uniformly distributed. The aluminium distri-
bution was shown so that comparison could be made in the
latter stage when the disc surface had been worn by Al-
bronze pin so as to determine the level of aluminium trans-
ferred towards the worn track disc surface. Figure 2.5
is the energy dispersive spectrum on a pre-wear disc
surface showing principally two elements of iron and chro-
mium present.

TABLE 2.1   MATERIALS SPECIFICATION

DTD 197A (Aluminium-bronze)		KE 961 Steel		KE 180 Steel	
Copper	Rem.	Iron	Rem.	Iron	Rem.
Aluminium	8-11%	Chromium	12.5-13.5%	Chromium	12.5-13.5%
Iron	4- 6%	Carbon	1.45-1.65%	Carbon	1.45-1.65%
Nickel	4- 6%	Tungsten	0.50-0.75%	Tungsten	NIL
Manganese	2.5% Max.	Manganese	0.30-0.50%	Manganese	0.30-0.50%
Silicon	0.25% Max.	Silicon	0.40-0.65%	Silicon	0.40-0.65%
Zinc	0.50% Max.	Sulphur	0.04% Max.	Sulphur	0.04% Max.
		Phosphorous	0.03% Max.	Phosphorous	0.03% Max.

Figure 2.3. Talysurfs of Disc surfaces
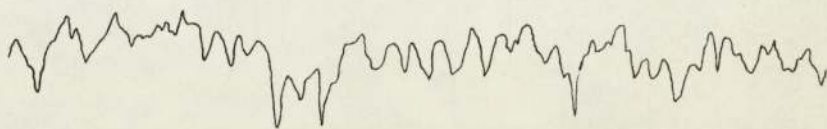
Sand-blast disc for running-in

Vertical magnification   X 1000

Linear   magnification   X 100

C.L.A.   1 μm

Wear disc

Vertical magnifical   X 50,000

Linear   magnification   X 100

C.L.A.   0.0253 μm

Figure 2.4. Scanning Electron Micrographs of Pre-wear Disc Surface

a. Pre-wear disc surface
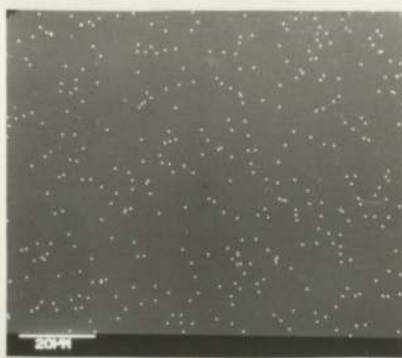
d. Aluminium X-ray distribution

b. Iron X-ray distribution
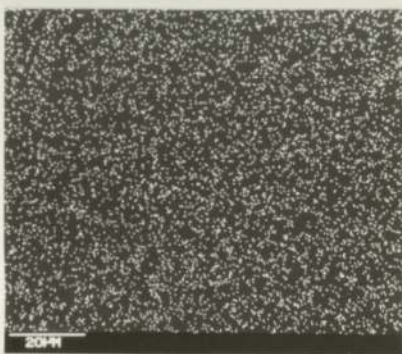
e. Silicon X-ray distribution
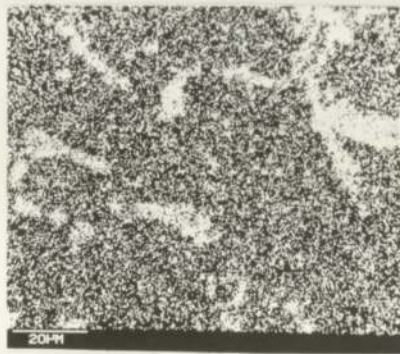
c. Chromium X-ray distribution
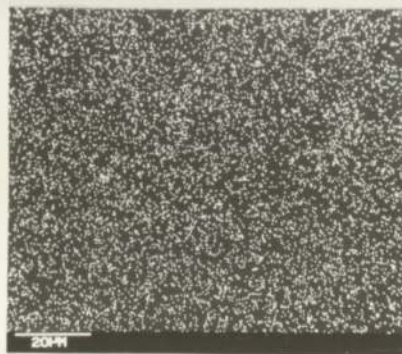
f. Sulphur X-ray distribution
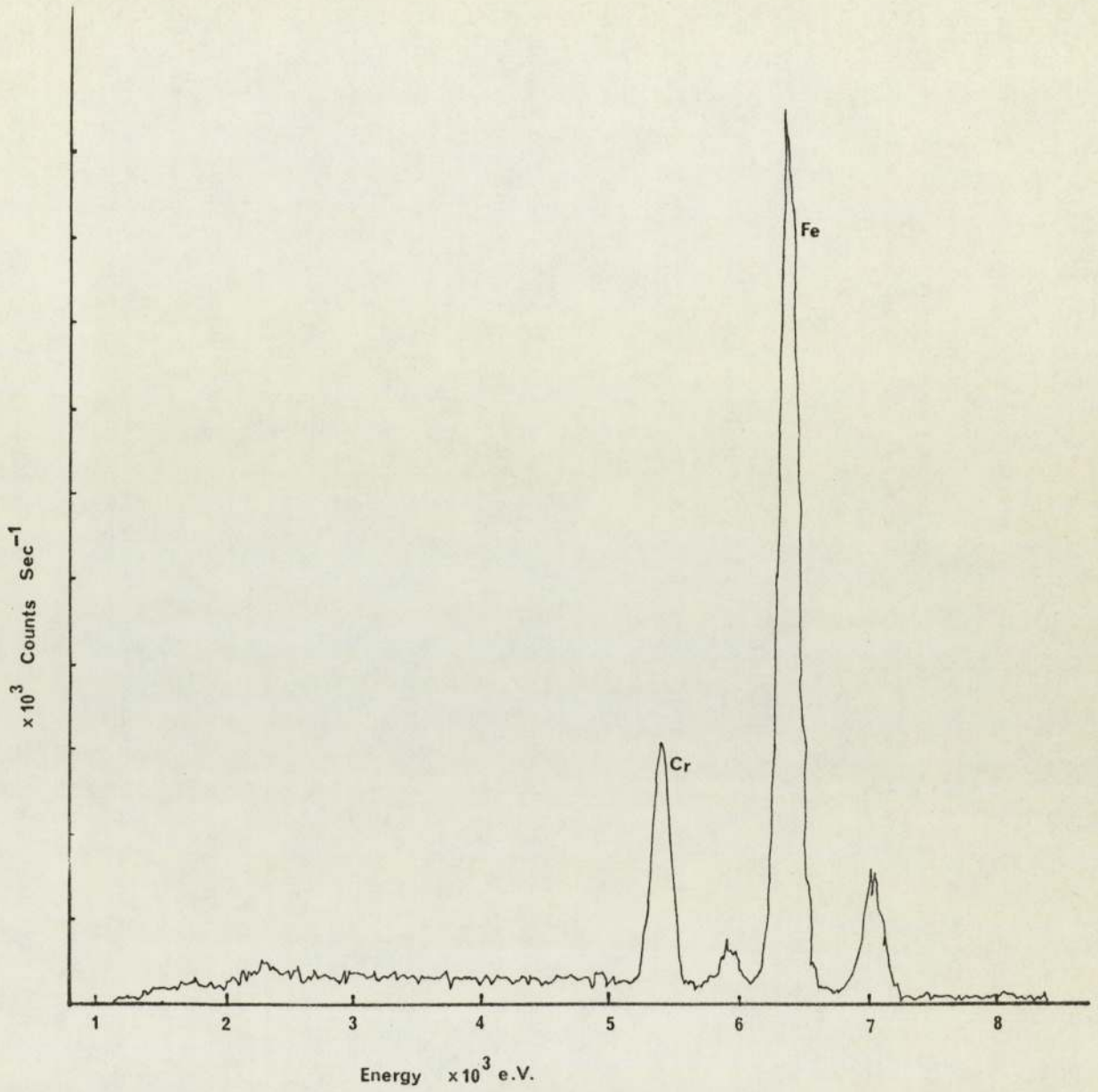
Figure 2.5. Energy dispersive spectrum of elements present on a pre-wear disc surface

2.5   The Aluminium-Bronze Wear Pin Specimens

The wear pin specimens were made of DTD 197A Aluminium-bronze, the composition of which has been shown in Table 2.1.   The details of the dimensions and tolerances for the pins are shown in Figure 2.6.

It was found that there were at least five micro-structural differences used in the wear tests though they all belong to the same category of Al-bronze material. The five microstructural differences of aluminium-bronzes were designated as Bronze A(IMI), Bronze B(Poole Type I), Bronze C(Poole Type II), Bronze D(Original Fuel Pump) and finally, Bronze E(Delta).   Most of the wear experiments were conducted at Aston Tribology Laboratory, using Bronze E(Delta) pins with 2 mm diameter contact areas.

2.6   The Aviation Test Fuel

The basic lubricant used in this work was a hydro-treated aviation kerosene in which the lubricity agents had been removed.   Hence one would expect that this fuel had a low lubricity.

Firstly, the tests were carried out using fuels with-out additives and later containing additives of 12 p.p.m. Hitec E515 and Hitec E580 respectively.   The test fuels containing additives were prepared in the laboratory by mixing 12 p.p.m. of Hitec, by weight, with alumina-catalyst-filtered, hydrotreated kerosene.

The molecular structure of Hitec E515 consists of

dimers of poly-ethenoid mono-carboxylic acids. The low
percentage of phosphorous (about 0.35%) probably indicates
the presence of acid-phosphate esters. The structure of
Hitec E515 may be represented as (32):-

$$CH_3(CH_2)_5\!\!-\!\!-\!\!-CH\!\!-\!\!CH\!\!-\!\!-\!\!-CH\!\!-\!\!-\!\!-CH(CH_2)_7\!\!-\!\!-\!\!-\!\!COOH$$

$$CH_3(CH_2)_5\!\!-\!\!CH \qquad CH\!\!-\!\!(CH_2)_7\!\!-\!\!-\!\!COOH$$

$$CH\!\!-\!\!-\!\!CH$$
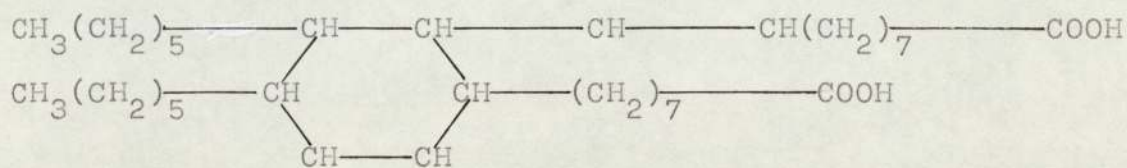
The additive Hitec E580 contains no phosphate ester compo-
nent and its molecular structure consists of dimers of
ethoxylated alkyl phenol acids. Details of the chemical
compositions of Hitec E515 have been given in Section 1.5.
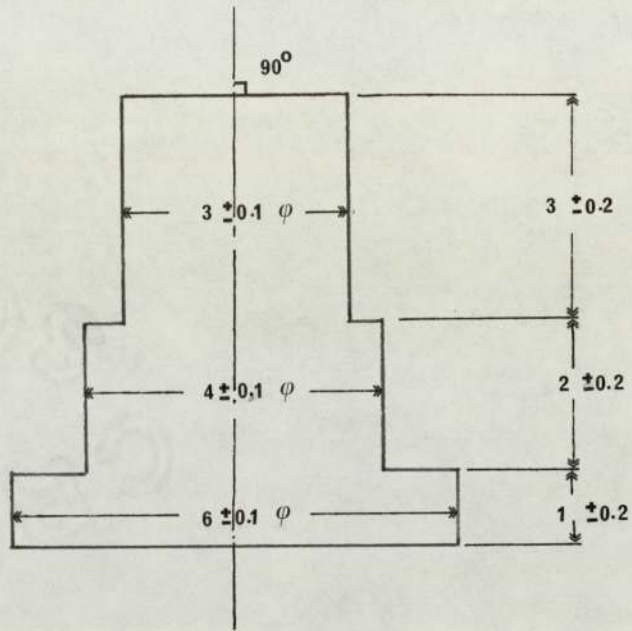
All dimensions in mm
φ - diameter

Figure 2-6   DTD 197A Aluminium-Bronze Wear Pin

2.7 Viscosity Measurement

Suspended-level Viscometer was used to measure the viscosity of the fuel. Fuel was fed into the glass capillary tube of Suspended-level Viscometer. The time was then taken for the fuel to drain from the upper-marked level to the lower-marked level. The value of viscosity was calculated based on the manufacturer's formula. That is,

Viscosity (centistokes) = Time (sec.) x Constant,
(where Constant equals 0.0013365).

The results of three measuring times were obtained and an average time was taken to calculate the viscosity of fuel. The viscosity measurement was found to be equal to 1.57 centistokes or 1.2246×10^{-3} Nsm^{-2}.

2.8 The Wear Test Procedure

Before each wear test, it was important to ensure that the wearing components, such as wear pin and disc, and all other parts which came into contact with the test fluid were thoroughly cleaned. The pins and discs were initially washed in a vapour bath using Shell SBP2 petroleum ether for half an hour, followed by 2 minutes ultrasonic cleaning with petroleum ether. A disposable glove was used at all times to handle all wearing components so as to prevent any contaminant transferred from the fingers.

When using Thornton Wear Machine, the wear tests consisted of two stages. The first stage was a running-in to conformity of the pin using sand-blasted disc and the second stage involved the actual wear test replacing with a 0.025

μ.m. C.L.A. surface finished new disc. In the first stage, the pin was fixed on the upper carriage lever arm with the sand-blasted disc locked in position on the shaft. The upper carriage arm was lowered to the bottom carriage and at the same time the upper carriage lever arm was balanced by adjusting the tension of spring until the pin just cleared the disc surface periphery. The eccentric rod was swung upwards to offset the pin into coming contact on disc surface so   allowing 19.6N load to be applied on load-carrier without putting pressure on the pin. The flow rate was about 20 ml min^{-1} whilst the speed required for pin conformity was about 0.5 ms^{-1} (200 r.p.m.). After swinging the eccentric rod downwards, the conformity on pin was achieved after running for about 3 minutes. In the second stage, the pin and disc assembly and setting procedure were same as the first stage. Wear measurements were made by using a Wayne-Kerr Capacitance Transducer probe set parallel to the under surface of the upper carriage lever arm with clearance about 0.025 mm. Friction was monitored by means of a torque transducer with a digital readout, to the output of which was connected a potentiometric recorder. Each test run lasted for about one hour.

In the case of the Denison Wear Machine, the change in length of the wear pin during a wear test was measured using a linear displacement transducer attached to a flat plate of the load arm (figure 2.2(b)). As the pin wore, the load arm moved downwards hence giving a continuous measurement of pin displacement on the chart recorder. The continuous measurement of specimen length provided information

which was subsequently used to produce wear versus time and wear versus load curves.

A resistance bridge type strain gauge load cell (Pye-Ether Dynamometer type UF2) was used to measure frictional force. Frictional forces were calibrated on the chart recorder by applying static loads against the load cell connected with a pulley and weights. A full scale deflection of 24.5N on friction-indicator was sufficient to measure the coefficient of friction in a boundary lubricated condition. Figure 2.7 shows a plot of friction-indicator readings versus frictional force. Drift characteristics were plotted for the friction and wear transducers. As shown in Figure 2.8, a negligible drift was recorded on the chart recorder after 3 hours running, starting from cold.

In order to achieve the best operating conditions for boundary lubrication, wear tests were carried out for loads of 24.5N to 196N, in steps of 24.5N, at a constant speed. For these tests one pin was used on one wear track with the load being periodically increased. It was found that if a Bronze E(Delta) type of pin was used, the boundary lubricated condition could only be achieved by reducing the flow rate from 20 ml min^{-1} to 1.7 ml min^{-1} maximum and also the contact area of the pin had to be reduced from 3 mm to 2 mm diameter. Having established the operating conditions, each test was run with a new pin on a new track on the disc. The operating wear velocities were 0.6, 2.0 and 4.0 ms^{-1} respectively with applied loads of 24.5N up to maximum 196N. The wear tests lasted for about 90 minutes or more depending

upon the amount of wear occurring.

For a 2mm diameter pin, the wear rate was calculated from the equation as follows:-

$$\text{Wear Rate} = \frac{4.3354 \ \Delta x}{U \ \Delta t} \ \times \ 10^{-9} \ m^3 \ m^{-1}$$

where Δx is the displacement in mm, measured directly from the chart recorder output of the displacement transducer; U, the wear velocity in ms^{-1} and Δt the duration of the experiment in seconds.
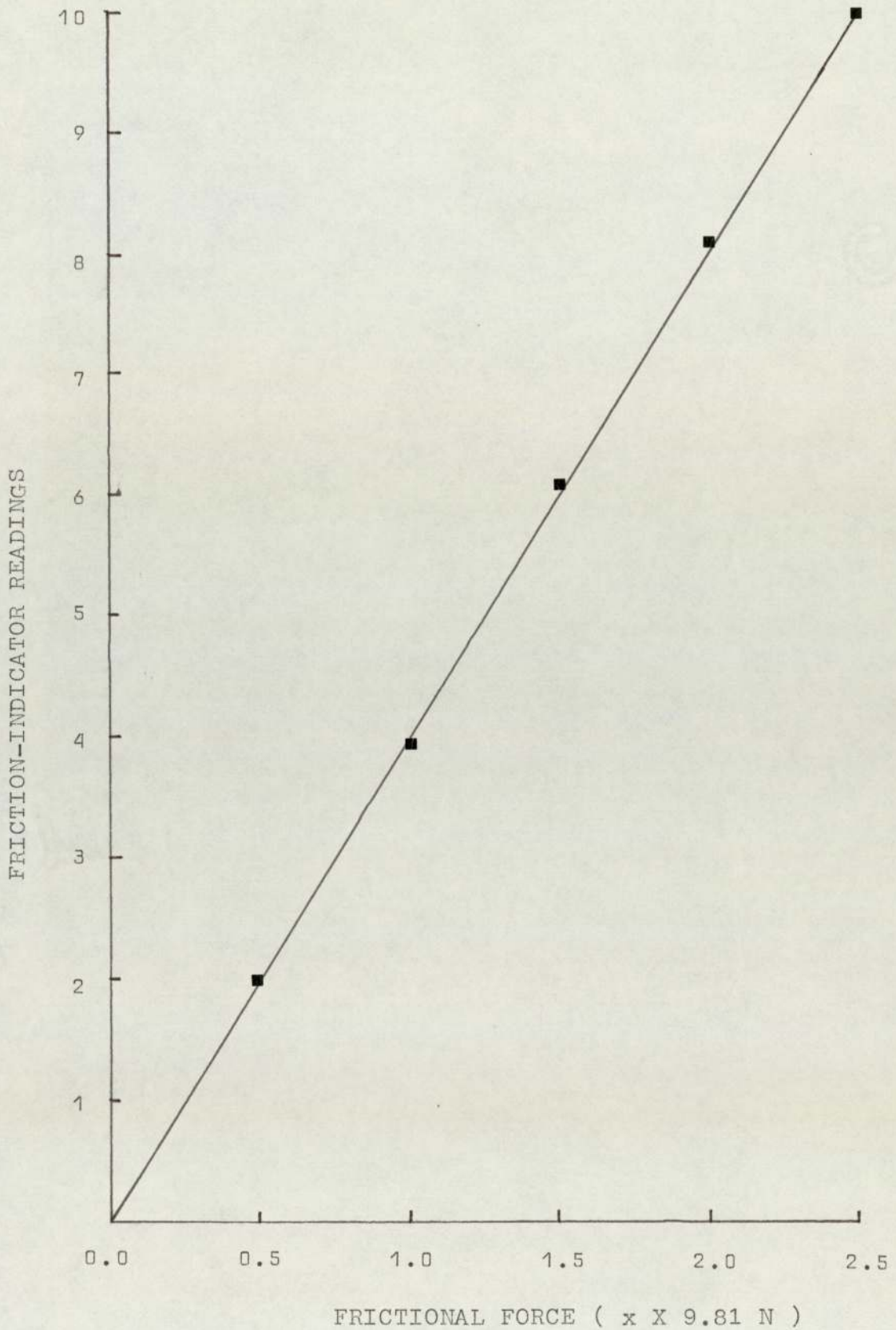
Figure 2.7   Friction-indicator readings
versus frictional force
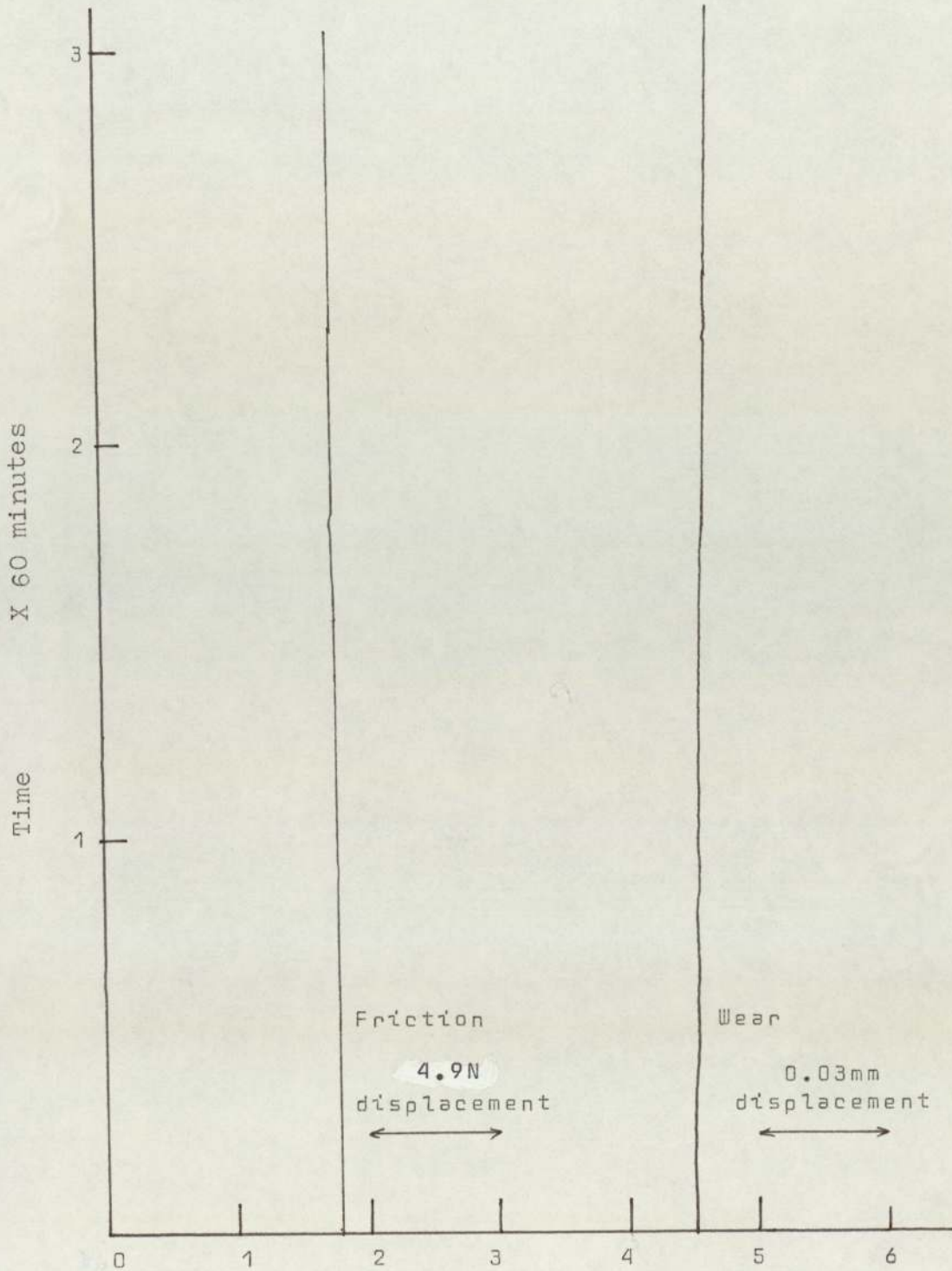
Figure 2.8 Drift characteristics

2.9 Hardness Test

The hardness test specimens of Al-bronzes and steels were prepared having been metallurgically polished to a 1 μ.m.. finish.   The hardness values were obtained, using a diamond indenter at a load of 294N for Al-bronzes and 490N for steels. The avarage Vicker's Hardness Number of each specimen was obtained from three indentations. Table 2.2 is the results of Vicker's Pyramid Numerals (VPN) for Al-bronzes and steels.

It has been claimed that when a metal is strained or work hardened, it has the effect of strengthening the metals (89). The wear process due to high load and speed was suffi-cient to stress the rubbing surfaces beyond its elastic limit, causing work or strain hardening. Hence, tapered sections of worn pin surface and microhardness tests were employed here to obtain some knowledge of the sub-surface properties as affected by wear compared to its bulk region.

2.10 Design of Steel-Jig for Edge Preparation and Taper Sectioning

A steel-jig was designed to accommodate the standard size of bakelite mounted specimen. The steel-jig was made from a 50 mm diameter steel rod with its dimensions shown in Figure 2.9. A $11\frac{1}{2}^{\circ}$ tapered section was chosen on steel-jig so that a larger and shallower area would be obtained on a deformed layer of the worn pin. Care should be taken not to over polish the worn pin surface during taper sect-ioning.

TABLE 2.2 HARDNESS TEST ON AL-BRONZES AND STEELS

Materials Specification	Vicker's Pyramid Numerals (VPN)
Bronze A(IMI)	226
Bronze B(Poole Type I)	233
Bronze C(Poole Type II)	226
Bronze D(Original Fuel Pump)	237
Bronze E(Delta)	239
KE 180 Steel	674
KE 961 Steel	780
Original Fuel Pump Piston (steel)	720

The procedure for edge preparation and taper sec-
tioning on a worn pin is shown in Figure 2.10. A thin film
of Araldite was used to apply on the worn pin surface. It
was essential because any deposit or transferred material
on the worn surface would be protected during polishing
stages. The coated specimen was heated at about $50^{\circ}C$ on
the surface of a hot-plate to increase the fluidity of the
Araldite. After the Araldite had been completely cured, a
slight flat polish was required on the surface of Araldite
so that it allowed the worn pin to stand upright while
mounting the specimen. After mounting the worn pin, the
mounted specimen was gripped on the steel-jig to obtain $11\frac{1}{2}^{\circ}$
tapered section after grinding from coarse to fine grinding
stages. The polished specimen had a final surface finish
of 1 μ.m. which was ready for optical examination or used
for microhardness test.

In the case of 2 mm diameter worn pin, Araldite coat-
ing was discarded as the small end of the pin would not be
able to stand upright during bakelite mounting. Instead
the large end of the worn pin sat upright while mounting
and the remaining tapered section procedure was same as
before.
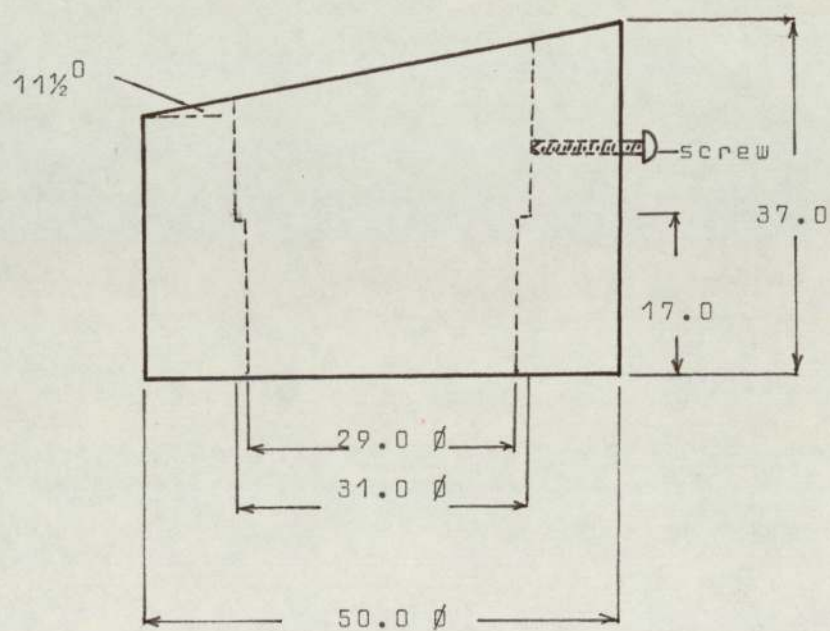
All dimensions in mm

Figure 2.9 Steel-jig for tapered section

araldite

worn pin

(a)

upper ram

prestopress mounting press

bakelite

trimmed araldite surface

lower ram

(b)

$11\frac{1}{2}^0$

screw

steel-jig

(c)

plasticine

glass-slide
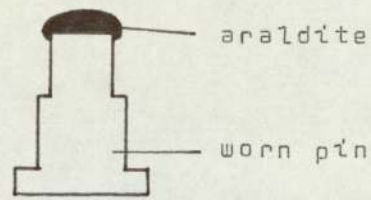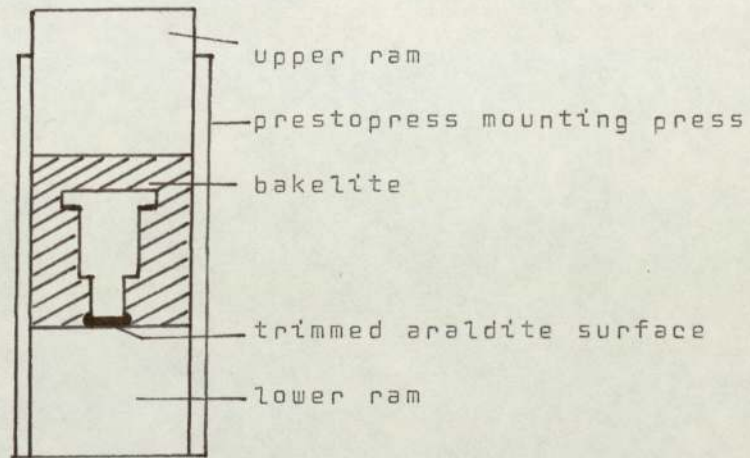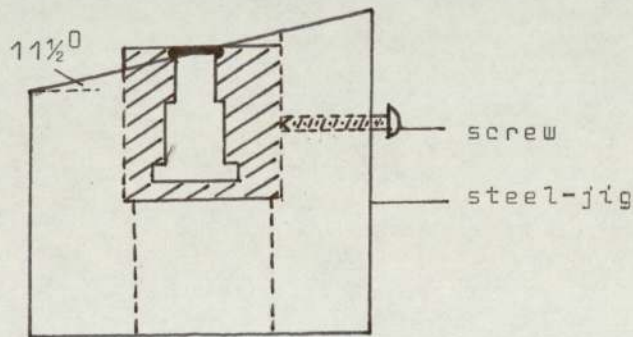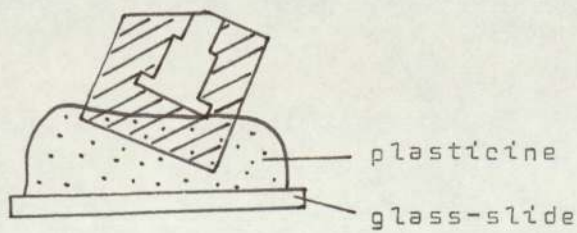
(d)

Figure 2.10 Tapered section procedure

2.11 Microscopy

The optical reflection microscope and scanning electron microscope have been used to monitor the surface topography of wear samples.

Most of the wear pins were analysed under an optical reflection microscope as soon as the wear test was completed. Some selective worn pins were examined in conjunction with the worn tracks to reveal their mating surfaces. The appearance and colour of the pins and worn tracks were noted.

The scanning electron microscope (88) has a large depth of field and is, therefore, ideal for the examination of wear surfaces. In this investigation, a Cambridge Stereoscan SEM, shown in Figure 2.11, was used extensively to examine wear surfaces produced in the pin-on-disc machine experiments. A selective samples of worn surfaces were examined to study the mechanism of its wear. Tapered sections were also performed in certain worn pins to study the sub-surface metallurgical changes as affected by wear, these pins being metallurgically polished to 1 μ.m. and etched with ferric chloride in alcohol. Wear debris and sectioned disc were also analysed under a SEM to detect the presence of aluminium and transfer of aluminium to the steel surface. Note that all the samples prepared for the analysis were obtained from the tests with percolated hydro-treated fuel and fuel with additives. The operating conditions for the scanning electron microscope were carried out using a 20 KeV beam and emission current of about 1 A for an 70 $\overset{o}{A}$ spot size. This microscope had a solid state

detector for X-ray analysis. X-ray distribution photo-
graphs, of selected elements, could be obtained along with
an energy scan to determine the elements present on the
surfaces.

Figure **2.11**   The Cambridge Stereoscan SEM used
in the investigation of worn surfaces
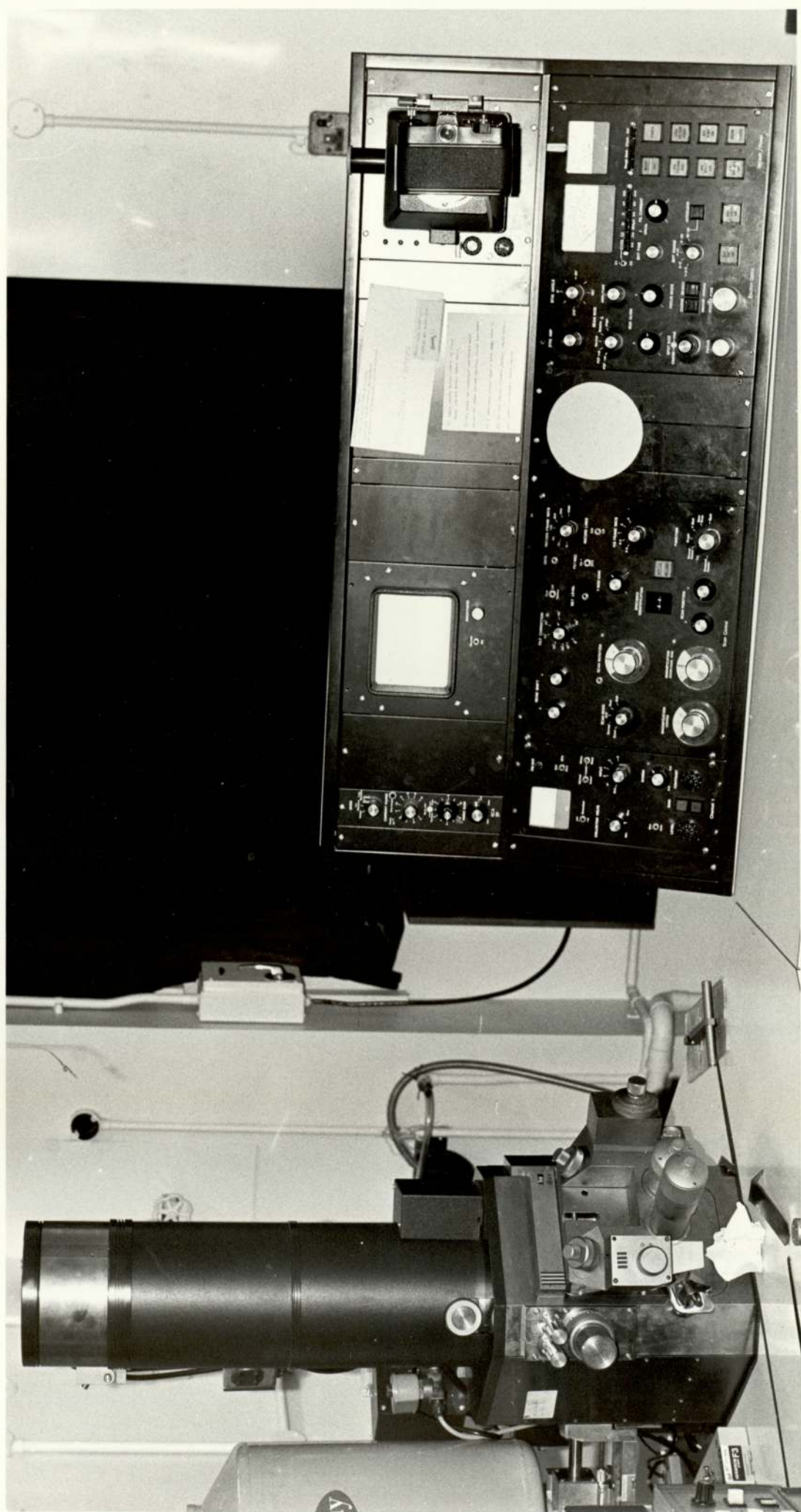
2.12   Electron Probe Microanalysis (E.P.M.A.)

The use of electron probe microanalyser gives us an
important scientific research tool in analysing accurately
the chemical analysis of inclusions, distribution of various
elements present in a surface, phases or precipitates,
study of grain-boundary depletion and enrichment, analysis
of thin surface layers and the quantitative investigation
of microsegregation (88,90,91).   Table 2.3 gives typical
examples of crystals and the ranges of elements for which
they are effective (92).   Hence, for the elemental identi-
fications of Al-bronze, the RAP crystal was used to detect
aluminium whilst the LIF crystal was used for the detection
of copper, iron, nickel and manganese, after the correct
settings of their respective Bragg angles.   The present
application of E.P.M.A. was carried out to analyse mainly
the depletion of aluminium on wear pin surfaces,
transfer of aluminium to steel counterpart and finally the
phases and compositions of various designations of Al-
bronze, such as Bronze A(IMI), Bronze B(Poole Type I),
Bronze C(Poole Type II), Bronze D(Original Fuel Pump), and
Bronze E(Delta).   The microscan V E.P.M.A. (figure 2.12)
was operated at a beam energy of 15 KeV with 80 μA beam
current for an 3000 $\overset{\circ}{A}$ spot size.   A special holder was
made to accommodate four wear pins to analyse at one time
as shown in Figure 2.13.   The samples were degreased in
petroleum ether before mounting in the instrument.   The
probe was positioned by means of the electron image for
spot analysis.   Each sample was analysed with a total of

ten spots on random areas. The composition of each element

was calculated as follows:-

Proportion of Element =

$$\frac{\text{Element Count} - \text{Background Count} + \text{Dead Time (sample)}}{\text{Element Count} - \text{Background Count} + \text{Dead Time (pure)}}$$

The result of the proportion of element was further computed

and corrected due to the inherent effects of atomic number

effect, absorption and fluorescence present in the system (92).

Table 2.3 Typical examples of crystals and ranges of elements for which they are effective

ATOMIC NUMBER / ANALYSING CRYSTAL	10	20	30	40	50	60	70	80	90	100
LIF		Ca	Kα Si	Sb		La			U	
QUARTZ	S		Cu Nb				W Hg		U	
PET	Si		Fe Rb			Dy Hf	Hg		U	
RAP	F P Cr		Nb	La			Hg			
MYRISTATE	B F Cl	Fe								
STEARATE	B O S	V								
LIGNOCERATE	B N P	Ti								
CEROTATE	Be N Si	Sc								
MELISSATE	Be C Si	K								

Figure 2.12 The Microscan V EPMA used in this
investigation
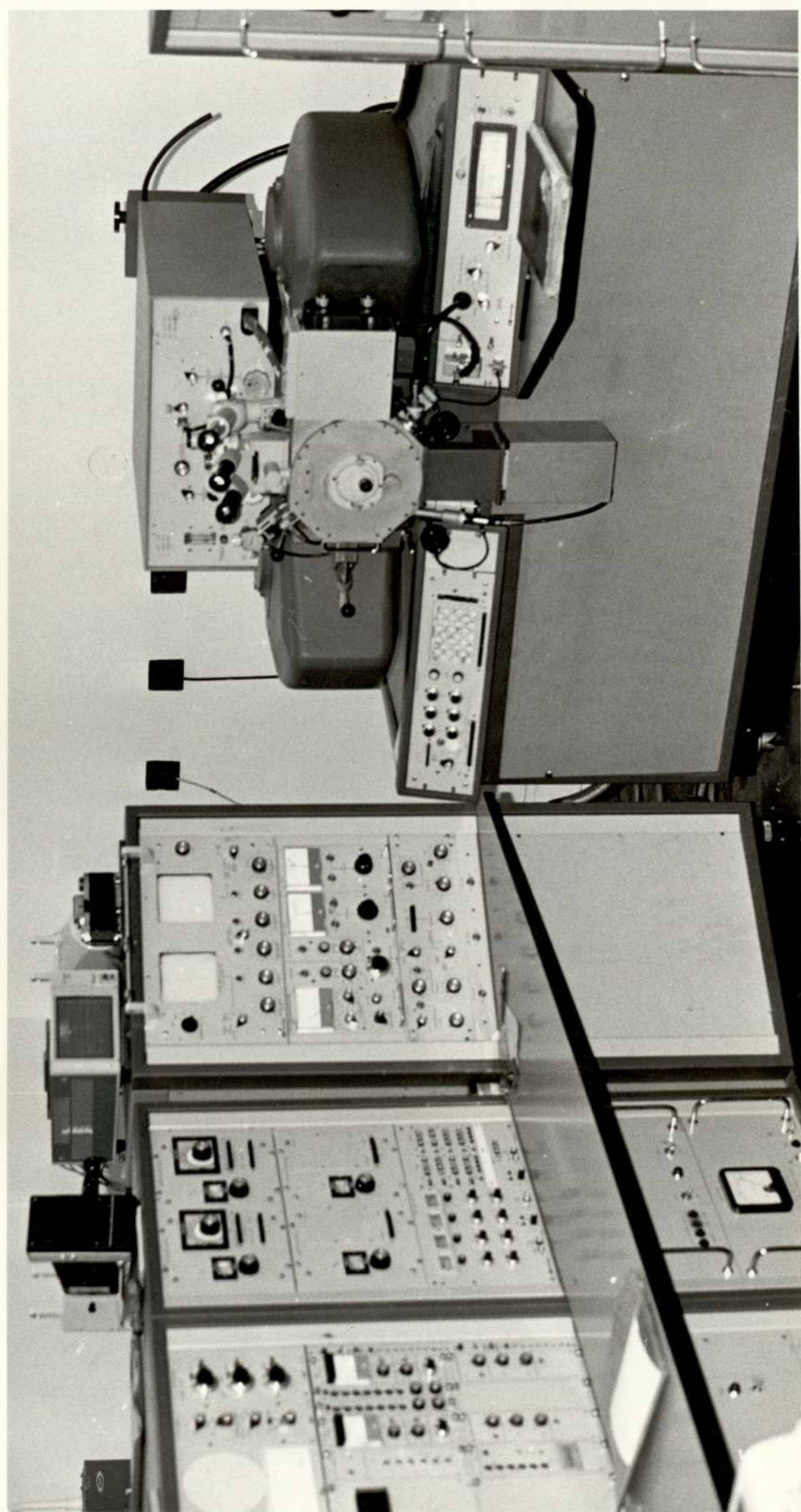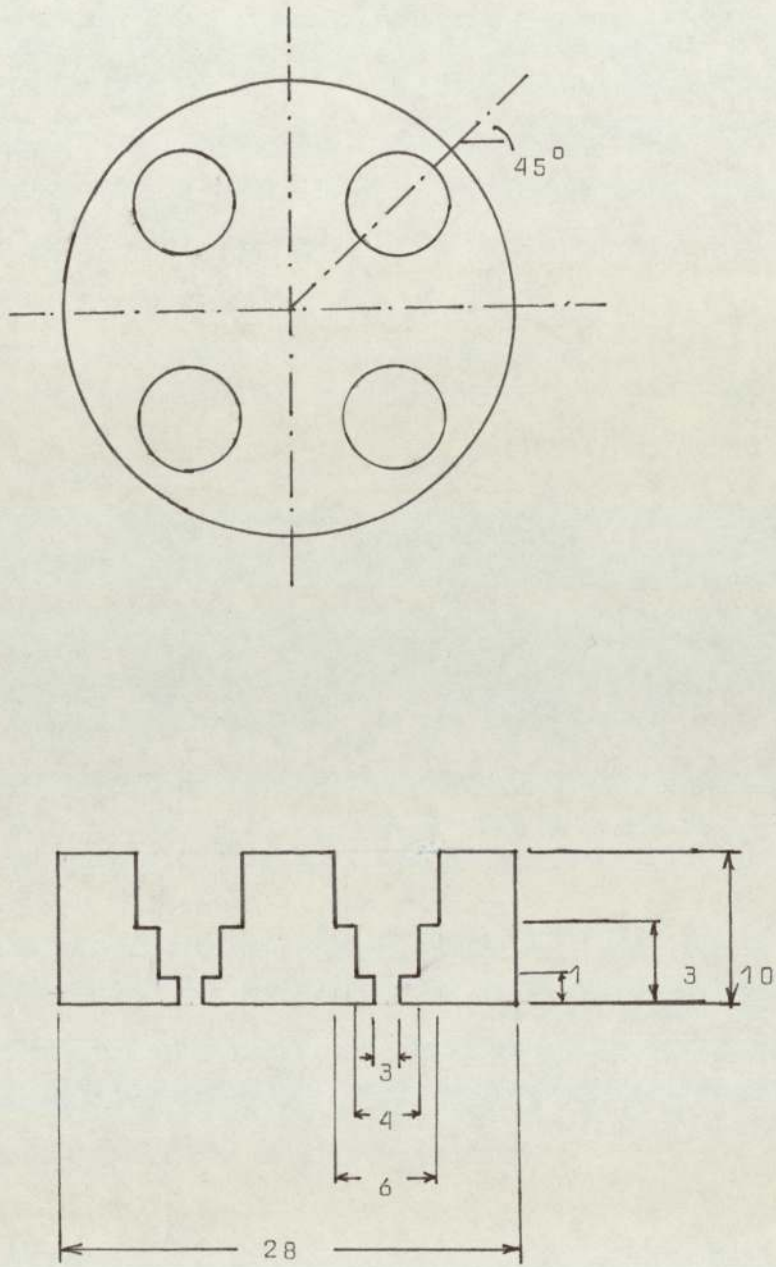
All dimensions in mm

Figure 2.13 Wear pin holder used in EPMA

2.13 Auger Electron Spectroscopy (AES)

Two techniques that have been used in the past for
the analysis of surface films formed by surface-active
lubricating additives are Glancing Angle X-ray Diffraction
and Electron Probe Microanalysis (93). The diffraction
technique provides information on surface compounds present,
providing the material is crystalline and of sufficient
thickness to give an observable diffraction pattern.
Electron Probe Microanalysis only provides information about
the elements present, with a decreasing sensitivity with
decreasing atomic number. However, both techniques show a
lack of surface sensitivity in that their sampling depth is
quite large.

Auger Electron Spectroscopy (AES) has developed
rapidly over the past fifteen years into a powerful technique
for surface analysis. In boundary lubrication, it is parti-
cularly useful for detecting the important elements —— carbon,
sulfur, nitrogen, phosphorus, and oxygen (88). AES is accom-
plished by irradiating the surface of a solid with a primary
electron beam while energy analysis is performed on the
resultant secondary electrons. Differentiation of the second-
ary electron spectrum enables the Auger Peaks to be resolved.
By plotting the differential function $dN(E)/dE$ against elec-
tron energy (eV), the peak-peak amplitudes of Auger peaks
give a measure of element concentration.

A typical Auger process that may occur when the inci-
dent radiation ionizes a surface atom by creating a vacancy
in the K-level is depicted in Figure 2.14 (94). The excited

atom can decay to its ground state by having an electron
from a higher level (L_1) drop into the vacancy. The energy
released by this transition is either emitted as a photon
or given to another electron. If this energy is sufficient,
an electron can be ejected from the atom, as illustrated for
another electron at $L_{2,3}$. This process is called the $KL_1L_{2,3}$
Auger transition. The energy released is $E_K-E_{L_1}$, but the
ejected electron must expend the energy ($E'_{L_{2,3}} + \Phi$) to escape
the atom, where Φ is the work function and $E'_{L_{2,3}} \neq E_{L_{2,3}}$
due to the extra positive charge of the atom. Because of
this positive charge, $E'_{L_{2,3}}$ should be approximately equal to
the $L_{2,3}$ ionization energy of the next heavier element, or
$E'_{L_{2,3}}(Z) = E_{L_{2,3}}(Z+\Delta)$, where Z is the atomic number and $\Delta \approx 1$
to account for the extra charge. This gives

$$E(Z) = E_K(Z) - E_{L_1}(Z) - E_{L_{2,3}}(Z+\Delta) - \Phi \qquad \ldots\ldots(1)$$

The above equation is useful because E is expressed in terms
of single ionization energy levels which can be found in the
X-ray and photoelectron energy tables (95).

In AES, the range of useful electron energies is 50-
2500 eV. Auger electrons with their characteristic energies
can only be detected when they are emitted from the top few
atomic layers of a solid surface. Auger electrons emitted
from a greater depth within a solid surface suffer inelastic
collisions and, therefore, lose energy and are no longer
useful for element identification. Also, to preserve the
energy with which the Auger electrons are emitted from the
surface, the analysis must be performed in an ultra-high

vacuum environment (10^{-8} torr or better).

In this investigation, samples of the pin surfaces were analysed after wear by using Scanning Auger Microprobe (SAM) which were done in Thornton Research Centre. The purpose of the analysis was to observe changes in the relative concentration of elements, in particularly C, S, O, Fe, Cu and Al, which occurred through the outermost layers of the worn surfaces. Each sample was mounted and introduced into the spectrometer in such a position that its worn surface was aligned with both the cylindrical mirror analyser (CMA) and the ion beam used for the depth profile procedure. Each sample was introduced separately in order to avoid cross contamination in the spectrometer during the ion sputtering procedure. The primary electron beam (E_p) energy was 3 KeV giving 2 μA current in an approximately 20 μ.m. diameter spot at the sample. With the primary electron beam located approximately in the centre of the pin, depth profile analyses were carried out in each sample, by sputtering their surface with 0.5 KeV Argon ions whilst monitoring the peak intensities of the elements of interest. Spectra were recorded before and after depth profiling.

ENERGY-LOSS
ELECTRONS

AUGER
ELECTRON

VACUUM

E_c

E_f

VALENCE
BAND

PRIMARY
ELECTRON

$L_{2,3}$

L_1

K
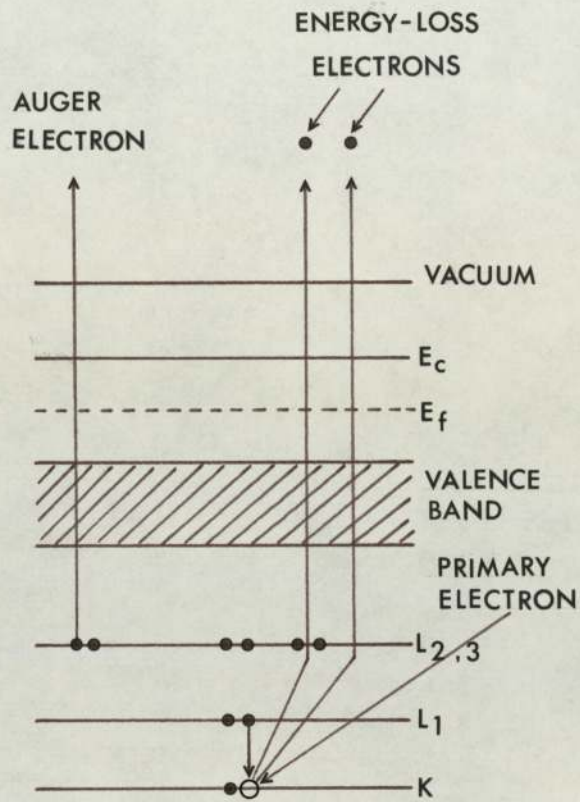
Figure 2.14   The $KL_1L_{2,3}$ Auger Process for a

singly ionized atom. E_f is the

Fermi level with zero energy;

E_c is the bottom of the conduction

band.

2.14 Wear Debris Analysis

X-ray diffraction is the most useful technique in identifying the structures present in wear debris and worn surfaces. Hence, an X-ray powder camera was employed to obtain information about the types of elements or compounds present in the wear debris.

The wear debris was collected from the pin-on-disc system and centrifugally washed with petroleum ether. It was then packed into a 0.3 mm diameter capillary tube and mounted at the centre of a 114.6 mm diameter powder camera. Cobalt radiation with an iron filter was used for analysis with the X-ray beam being operated at 35 KeV and 34 m A for about 40 minutes. Finally, the measured interplanar spacings were compared to the interplanar spacings listed in the X-ray Powder Data File published by the American Society for Testing and Materials.

CHAPTER 3

EXPERIMENTAL RESULTS

3.1 Introduction

The experimental results presented here will be
divided into sections similar to those used for the descrip-
tion of the experiments. The initial operating conditions
for boundary lubricated wear were established using the
Thornton Wear Machine to develop a Stribeck curve which was
subsequently used as a guide for boundary wear investiga-
tions. The boundary lubricated wear modes, using Thornton
Wear Machine and Denison Wear Machine, will be fully des-
cribed followed by the samples analyses. The results of
the optical microscopy on worn surfaces will also be
commented on from selected samples. Finally, more sensitive
analytical techniques, such as Scanning Electron Microscopy
(SEM), Electron Probe Microanalysis (EPMA) and Auger Electron
Spectroscopy (AES) were used to quantify the hypothesis of
the wear mechanism of the aluminium-bronze sliding on steel
in the presence of aviation fuel.

3.2 Thornton Wear Mode

In order to study the types of boundary regimes under
a constant load with increasing speed, a plot of Stribeck
curve may give a useful means of determining conditions for
boundary lubrication. Figure 3.1 shows a plot of the
coefficient of friction(μ) versus (speed(U) x viscosity(ζ))/
pressure(p) (sometimes called dimensionless bearing-number C)

for three constant loads, assuming constant absolute viscosity.
Consider only curve A of Figure 3.1 for a 49N load, three
regions of lubrication are shown. They are classified as
fluid film(Region 1), mixed(Region 2), and boundary(Region 3)
lubrications respectively. In Region 1, the surfaces of pin
and disc were completely separated by the fluid film. In
this region friction was due to viscous losses in the lubri-
cant, which caused μ to decrease with decreasing value of C
(where C is the dimensionless bearing-number). This decrease
in friction continued until, at critical value of C, the
fuel film became so thin that the tops of the highest asperi-
ties of pin and disc surface touched each other. The system
then entered the region of mixed lubrication (Region 2) and
a further decrease in C was accompanied by an increase in
friction towards a value characteristic of a boundary-
lubricated system (Region 3). In Region 3, the surfaces of
pin and disc were separated merely by adsorbed films. Curves
B and C are similar to curve A, but are shifted towards lower
bearing-number due to the higher loads. This then limits the
useful speed range if boundary lubrication is to be maintained.
The above Stribeck plots are presented as an aid to understand
and estimate the regimes of lubrication but they are by no means
universally applicable, since they do not take into account
many parameters which will affect the transitions from hydro-
dynamic to boundary lubrication, for example, increase in
surface temperatures, variation of viscosity with temperature,

dissolved oxygen in the fuel, the properties of the bearing metal and the chemical nature of the lubricant.

Figure 3.2 shows a plot of wear rate versus speed. The wear rates were negligible for 49N and 98N loads while sliding at 5 ms^{-1}. The negligible wear was mainly due the fact that a largely hydrodynamic film separated the surfaces while operating at high speeds and low loads. At low speeds, wear could be observed on both 49N and 98N loads. They were both regarded as mild wear as no scuffing marks were observed on wear pin surfaces. For a 245N load, the wear pin failed after sliding for about 6 minutes at 5 ms^{-1}. It was very obvious that the wear suddenly increased disproportionately on the chart recorder. On removing the pin and disc for visual examination, many scuffing marks were apparent on the wear surfaces and a lump of bronze metal transferred to the disc surface was also observed. In this case, the effect of adsorbed films in this boundary lubricated system was negligible, it was likely to be purely metal to metal contact. On reducing speeds, the wear rates were gradually decreased with no metal transferred to the disc surface. The wear pin surface was relatively smooth with only one striated mark present on the worn surface.

Figure 3.3 shows the wear rate against load curve for six velocities. The values imprinted on the curves are the coefficients of friction. Some of these values indicated that the operating conditions were in the regions of fluid film or mixed lubrications, in particular when the operating linear velocities exceeded 2 ms^{-1}.

The corrosion inhibitor Hitec E515 is used to improve

the lubricity of fuels so that reduced wear might be
expected. Figure 3.4 shows the Stribeck curves for fuel
with Hitec E515 which followed the same general pattern
as those sliding without additive (figure 3.1). The
difference between these two Stribeck curves was that the
coefficient of friction fell quite significantly,
especially in the region of boundary lubrication (i.e.
Region 3), for the fuel with Hitec E515. It appears that
the additive has the effect of reducing metal to metal
contacts and hence the coefficient of friction. From the
graph shown in Figure 3.5, there seemed to be no significant
difference between the wear rates with additive to those of
purely percolated hydrotreated fuel shown in Figure 3.2.
The same conclusion had been revealed by Simm (96) that at
ambient temperature no beneficial effect is obtained from
adding 14 p.p.m. Hitec E515 to the fuel. In fact, it has
quite often been found to have a pro-wear effect in the
presence of additives (31,32,33). The graph of wear rate
versus load (figure 3.6) also shows that the operating
system was in mixed and fluid film lubrication, for fuel
with additive, when the sliding speed exceeded 2 ms^{-1}.

Figure 3.1. Stribeck Curves Showing Three Constant Loads — 3 mm diameter Bronze A pins — Fuel alone
(Thornton Wear Rig)
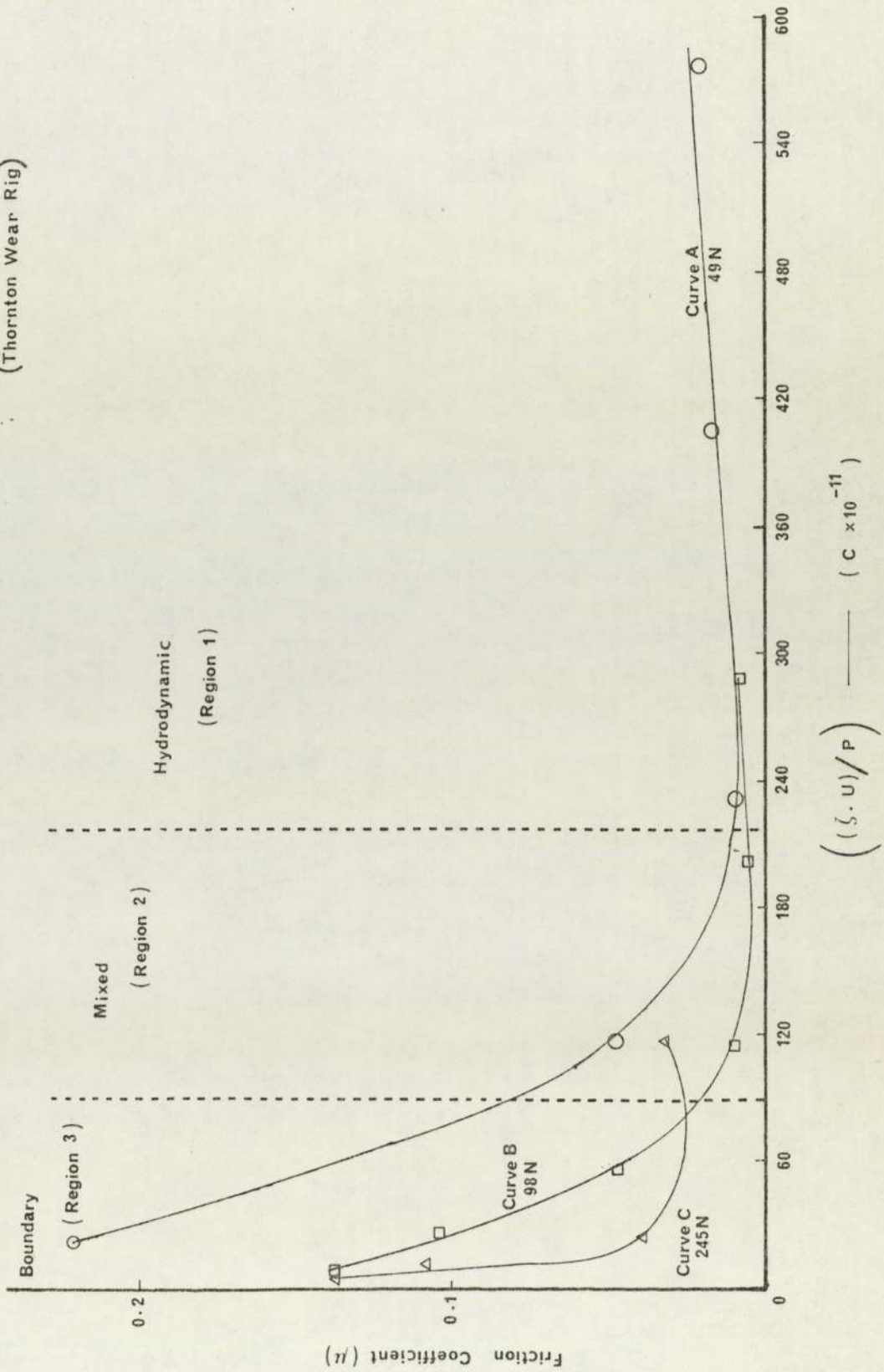
Figure 3.2. Wear Rate Versus Speed ÷3mm φ Bronze A Pins with Fuel Alone (Thornton Wear Rig)
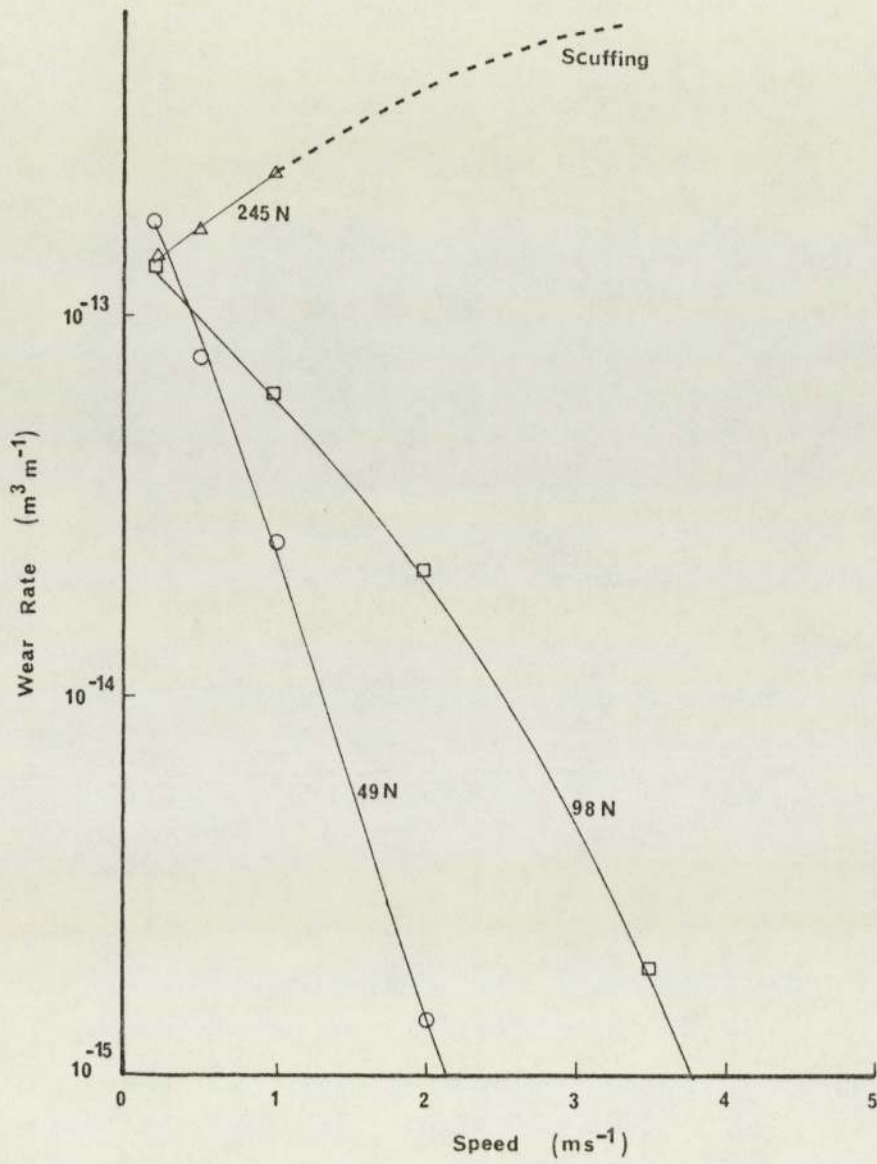
Figure 3.3. Wear Rate Versus Load *for* Different Velocities — 3 mm diameter Bronze A pins (Thornton Wear Rig)
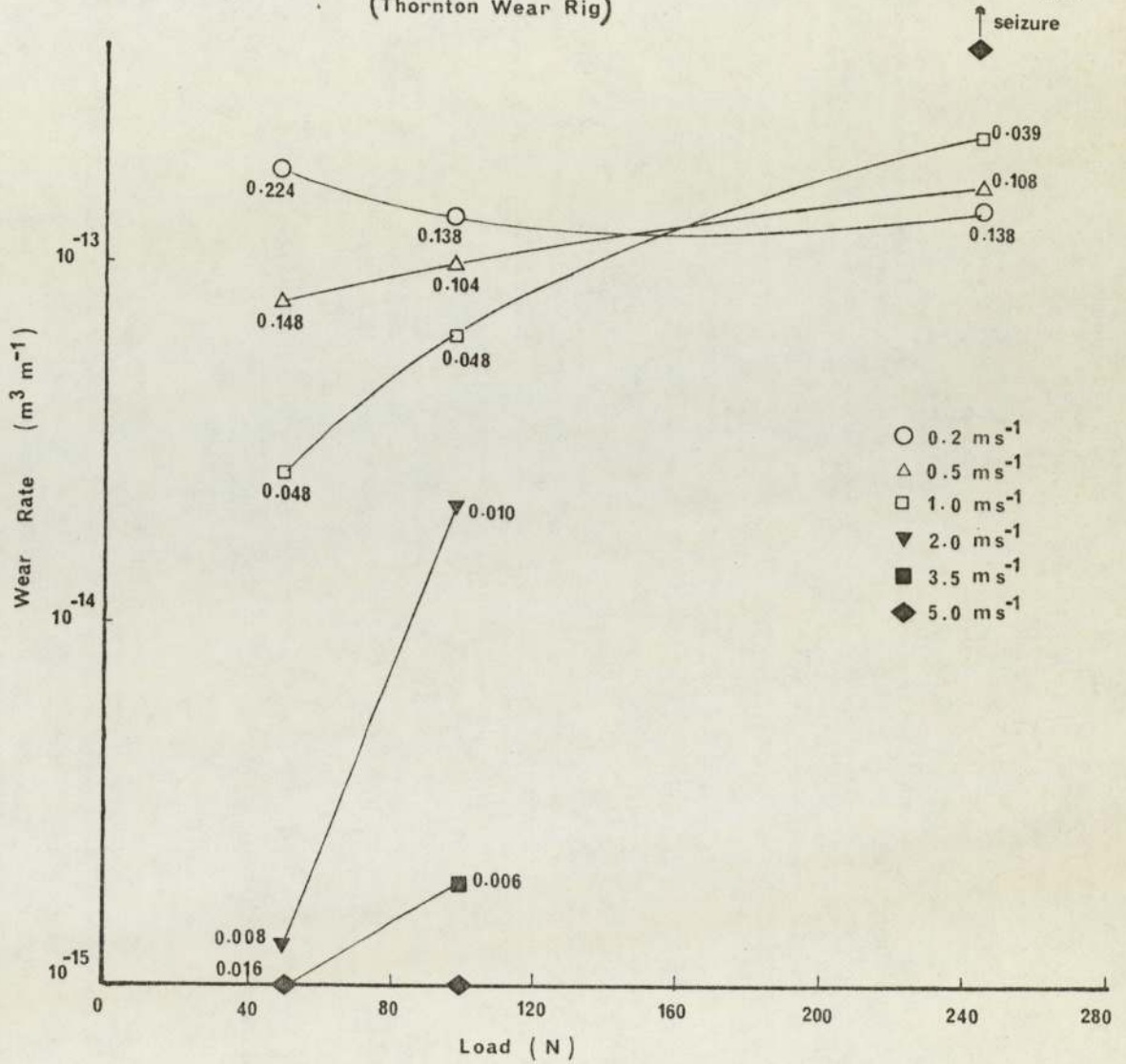
Figure 3.4. Stribeck Curves Showing Three Constant Loads – 3mm diameter Bronze A pins with Hitec E515

(Thornton Wear Rig)

Figure 3.5. Wear Rate Versus Speed – Fuel with Hitec E515

-3 mm φ Bronze A Pins
(Thornton Wear Rig)

Figure 3.6. Wear Rate Versus Load for Different Velocities — 3mm diameter Bronze A pins — Fuel with Hitec E515 (Thornton Wear Rig)
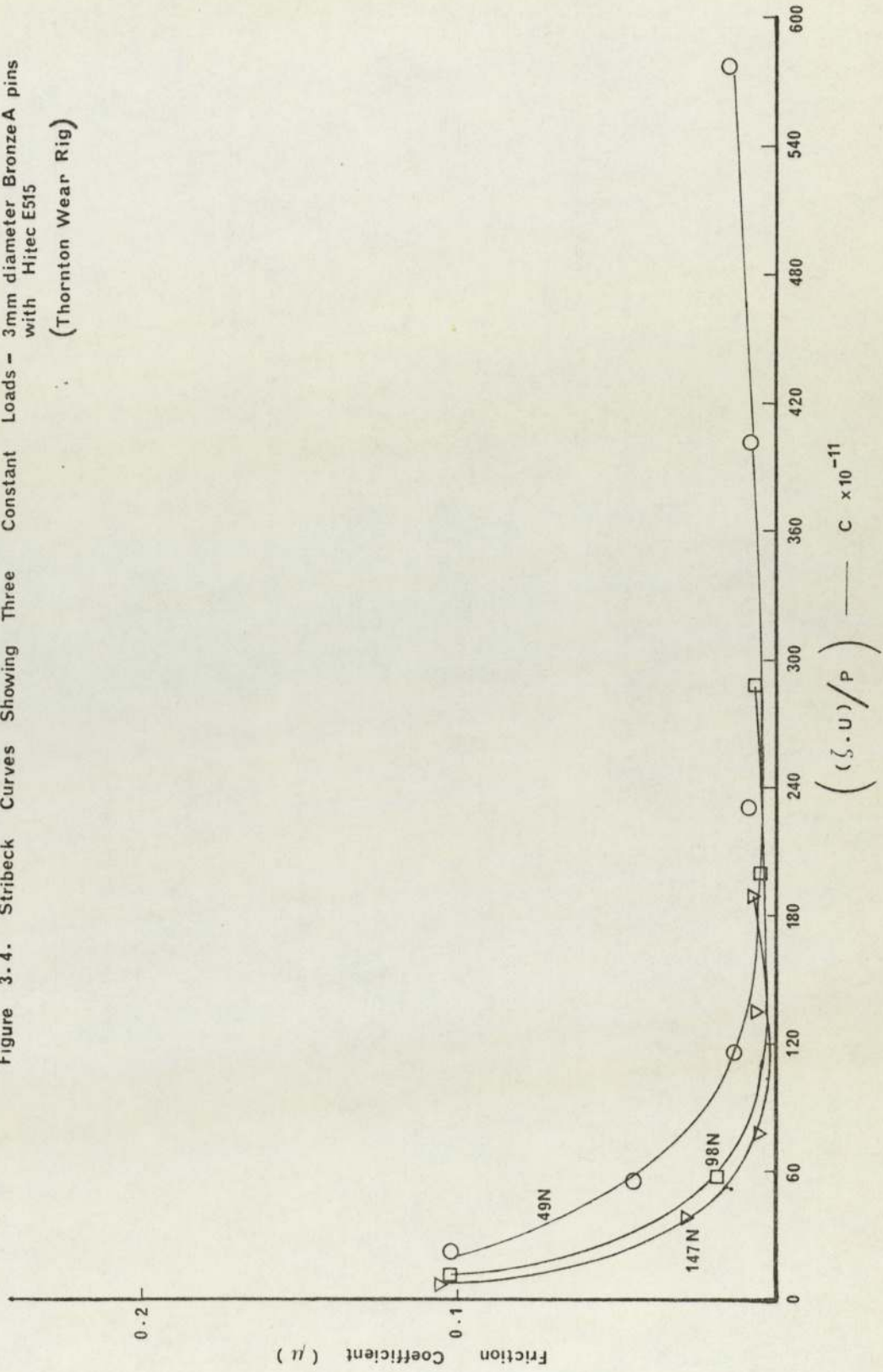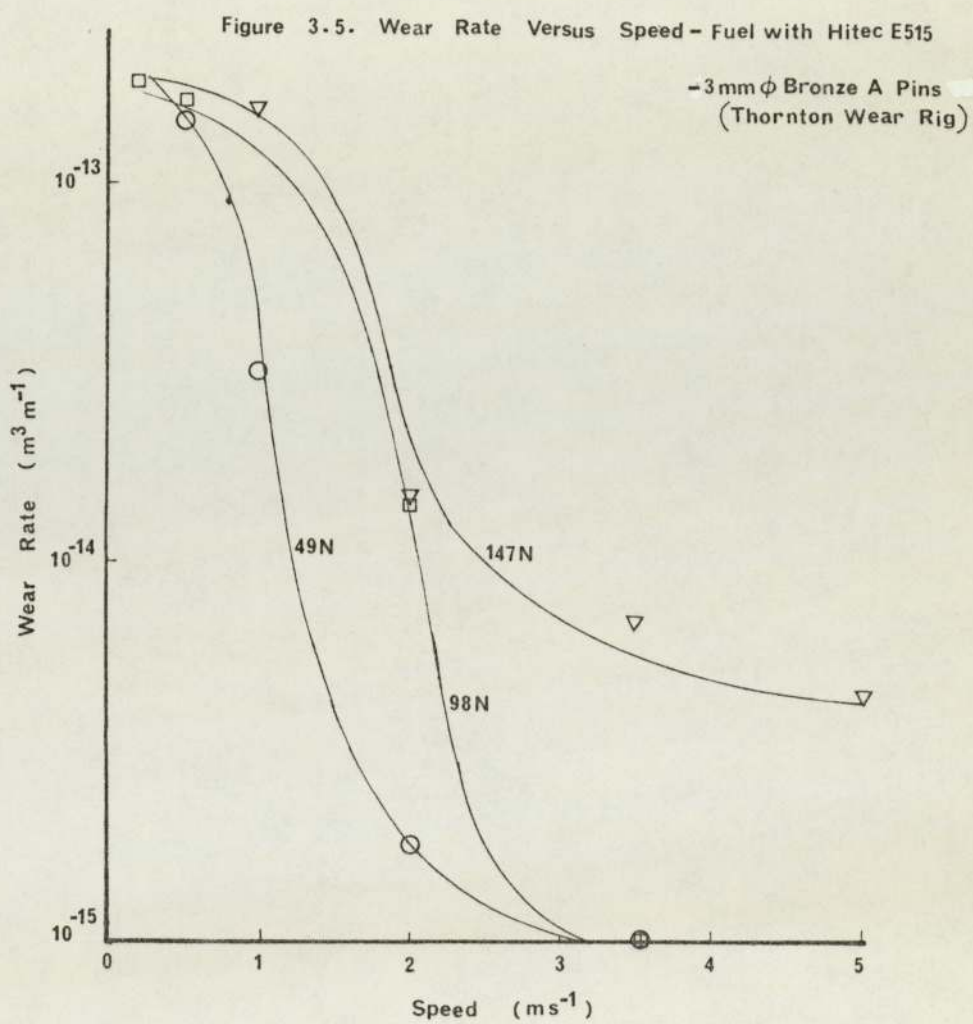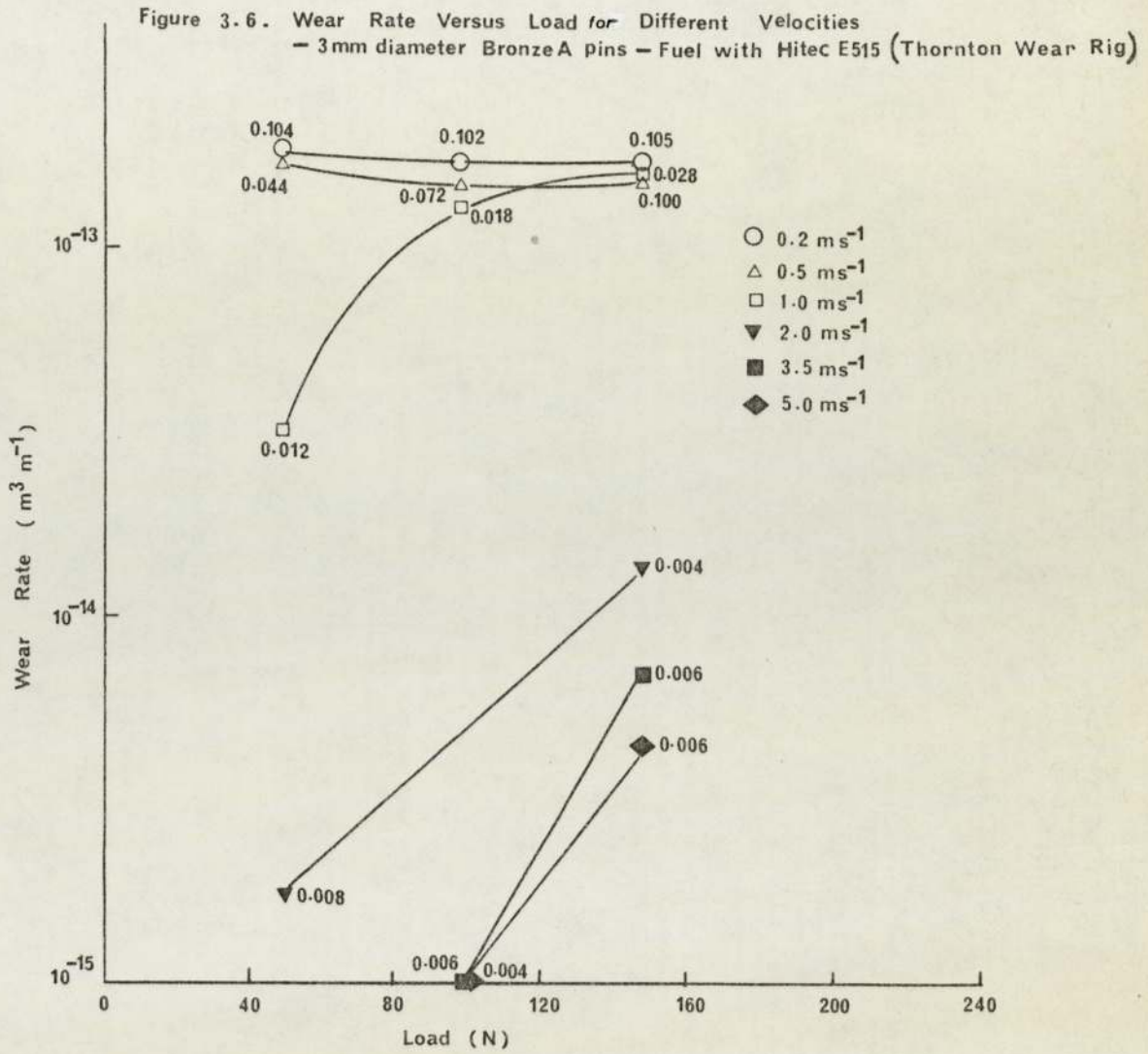
3.3 <u>Denison Wear Mode</u>

It has been suggested that Stribeck curves serve as a guide in order to establish appropriate boundary conditions. The conditions of the Stribeck curves vary from system to system with the parameters of the running systems, types of lubricant, surface roughnesses, metallurgical aspects of the material being used, etc. To take an example, Poole (86) found that for higher surface roughness discs (0.06 μm C.L.A.) the coefficient of friction did not fall to the full fluid film value of those with lower surface roughness (0.0254 μm C.L.A.). Hence, the Stribeck curves established from the Thornton wear tests might not be suitably applied to Denison wear tests. A fact, that was found to be true as the two running systems were different. The Thornton Wear Machine used pins run on the rim of the disc with fuel in a single pass flooded condition, whereas the Denison Wear Machine used pins run on the flat surface of the disc with a starvation fuel flow in an open atmosphere and also had variable diameter wear tracks. The fluid films tended to be of greater thickness towards the outer wear track, especially when sliding at low speeds. Typically for a low surface roughness disc, of say 0.0254 μm C.L.A., the fuel flow rate was one of the important parameters to be considered in obtaining boundary lubrication. Another important parameter was the metallurgical aspects of the materials, it seemed that Bronze E(Delta) had better wear resistance compared to Bronze A(IMI), Bronze B(Poole Type I) and Bronze C(Poole Type II). This will be explained in details in a later section.

The loads used for these experiments were between 24.5N
to 196N inclusive with a surface sliding speeds of $0._{6}$, 2
and 4 ms^{-1} respectively. The fuel flow rate was 20 ml min^{-1},
feeding at a position close to the centre of the rotating
disc in open atmosphere and at ambient temperature. The
results of the wear tests are plotted in Figures 3.7 to 3.9
and the values imprinted are the coefficients of friction
and track radius (within parentheses) respectively. Curve A
(figure 3.7) shows the results using a new pin and a new
track for each test run without running-in. The low wear
rates were due to the tests running in a mixed lubrication
region indicated by the low coefficients of friction. The
wear machine stopped at 147N load due to operating at a low
speed when the machine was unable to overcome the high torque
caused by the high applied load. The low wear rates were
probably due to the wear pins not being run-in, thus creating
a tendency to form a hydrodynamic wedge at the sliding inter-
face, since the machined marks were still clearly visible
on the worn pin surfaces after removal. Curve B (figure 3.7)
shows the results using the same pin and same track for all
test runs with a run-in pin. The wear rates increased with
increase in coefficients of friction. This indicates that
some degree of running-in would bring more metal-to-metal
contact and eliminated the tendency to create a hydrodynamic
wedge. The machine also stopped at 147N load because of
the high applied load at low speed.

Figure 3.8 shows the results of 2 ms^{-1} test runs. Most
of the wear results were very inconsistent with mainly

negligible wear. The reasons for all these inconsistencies were substantial, such as wear pins not being run-in, using different combinations of Al-bronze pins (e.g. Bronze B(Poole Type I), Bronze C(Poole Type II), and Bronze E(Delta)), using different wear tracks (variation of fluid film thickness with radius), high sliding speed and high fuel flow rate (20 ml min^{-1}).

Figure 3.9 shows the results of 4 ms^{-1} test runs. Again, the wear results were widely spread due to the variations of the parameters outlined above.

With an understanding of the problem, all the wear tests from this point were performed only using Bronze E (Delta), sliding with 12 p.p.m. additive Hitec E580 in fuel. Again, most of the wear rates were negligible which gave no meaningful results for wear analysis. At this stage, it is worthwhile to establish a Stribeck curve for the Denison Wear Machine by varying speed and loading conditions, so that effective boundary lubrication can be obtained. Since the wear rig system was already contaminated with the additive from the previous experiments, the same source of fuel with Hitec E580 was used to establish a Stribeck curve. Surprisingly the wear rates were as before, i.e. either giving zero wear or the machine stopped. At this stage, it was not possible to establish the Stribeck curve since no data was available from the coefficients of friction. From the observation obtained, the machine would not stop even at 196N load at low speed (0.6 ms^{-1}) provided that an innermost track (r=25mm) was used. This means that the wear machine was operating in the region of low torque (i.e. using innermost

track) as torque is generally calculated by multiplying together the magnitude of the force and its perpendicular distance from the axis of rotation.

The high flow rate at 20 ml min^{-1} could be one of the factor forming a thick film separating the two rubbing surfaces especially sliding at high speed and hence giving zero wear and zero friction. Using the present fuel supplying system, the fuel pump was operated at its lowest speed with minimum flow rate of about 1.7 ml min^{-1}. The experiments were conducted again. The wear results gave an initial short period of running-in wear and later followed by a sudden large decrease in friction and hence giving zero wear again.

A further reduction in flow rate was carried out by modifying the fuel outlet system. This was achieved by narrowing the bore-diameter of the fuel outlet and a valve was fitted at the outlet to control the flow rate. The maximum and minimum flow rate can be maintained at about 1.7 ml min^{-1} and 0.02 ml min^{-1} respectively. But, the latter series of test runs still had not achieved boundary lubricated wear especially using light load at low and high speeds.

The next stage of the work was to increase the pressure on the pin by machining down the 3 mm diameter pin to 2 mm diameter. Reasonable wear rates were then achieved using 2 mm diameter pin with an appropriate starvation of fuel flow in tests between 0.02 to 1.7 ml min^{-1}. This suggested that the Bronze E had a higher wear resistance to the Bronzes A, B and C.

Figure 3.7 Wear Rate Versus Load – 0.6 ms⁻¹ – 3mm diameter Bronze B pins – Fuel alone (Denison Wear Rig) ,

Curve A : Without running–in (new pin & new track for each test run)

Curve B : Run–in with 49N load at 0.2 ms⁻¹ (same pin & same track for all test runs)

Figure 3·8 Wear Rate Versus Load — $2\,ms^{-1}$ — 3 mm diameter pin — Fuel alone (Denison Wear Rig)

i)   □   Bronzes B/C — Without running-in (new pin & new track for each test run)

ii) ■   Bronze C   — Without running-in (same pin & same track for all test runs)

iii) △   Bronze E   — Run-in with sand-blasted disc & then alumina polished disc with 20N load at $0.5\,ms^{-1}$ (same pin & same track for all test runs)

iv) ▽   Bronze E   — Conditions as iii) above

zero wear after 38 min.

zero wear after 21 min.

zero wear after 7 min.

zero wear after 42 min.

Load (N)

Wear Rate (m^3m^{-1})

Figure 3.9 Wear Rate Versus Load — 4 ms⁻¹ — 3mm diameter pin — Fuel alone (Denison Wear Rig)

i) □ Bronzes B/C — Without running-in (new pin & new track for each test run)

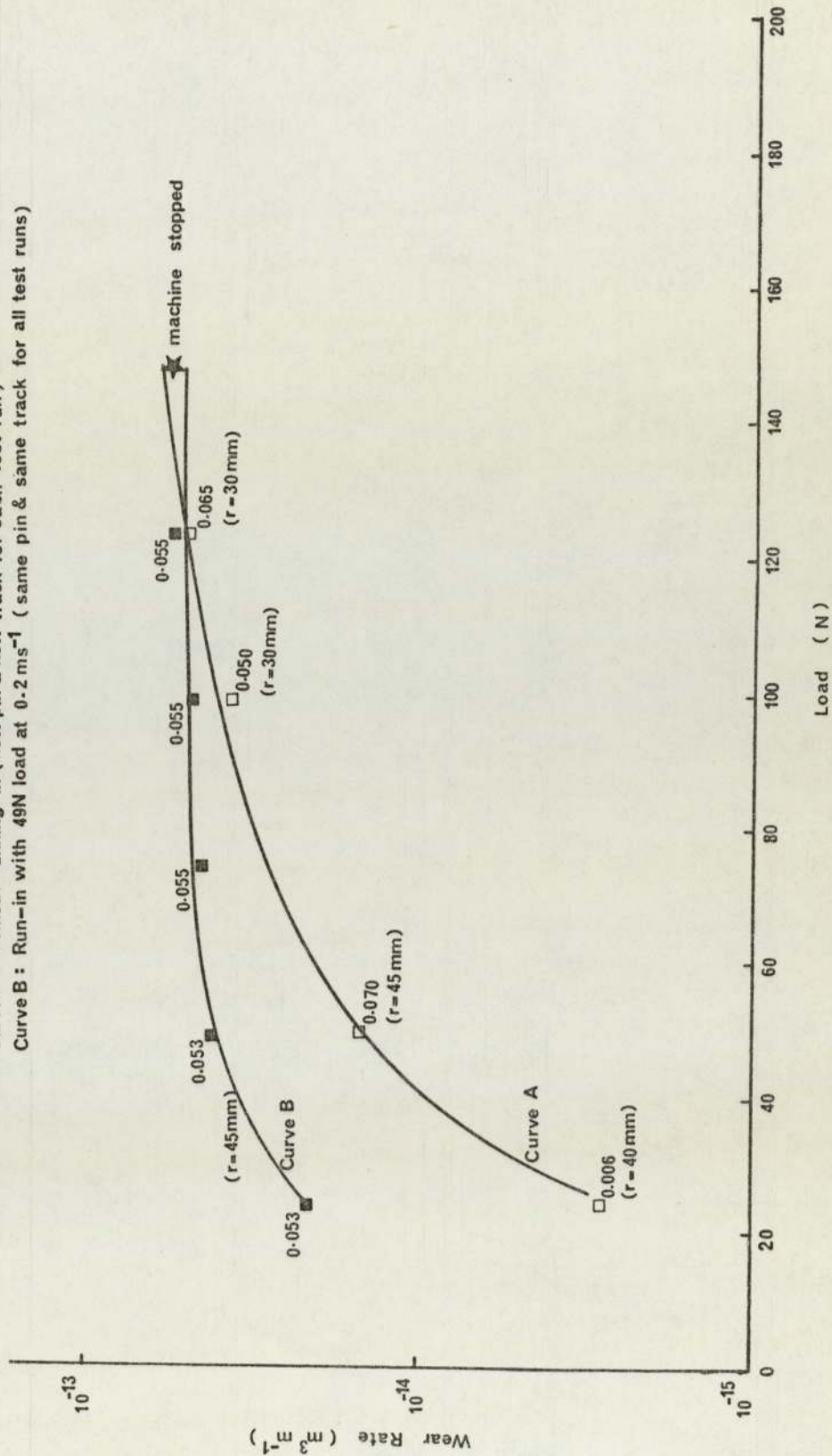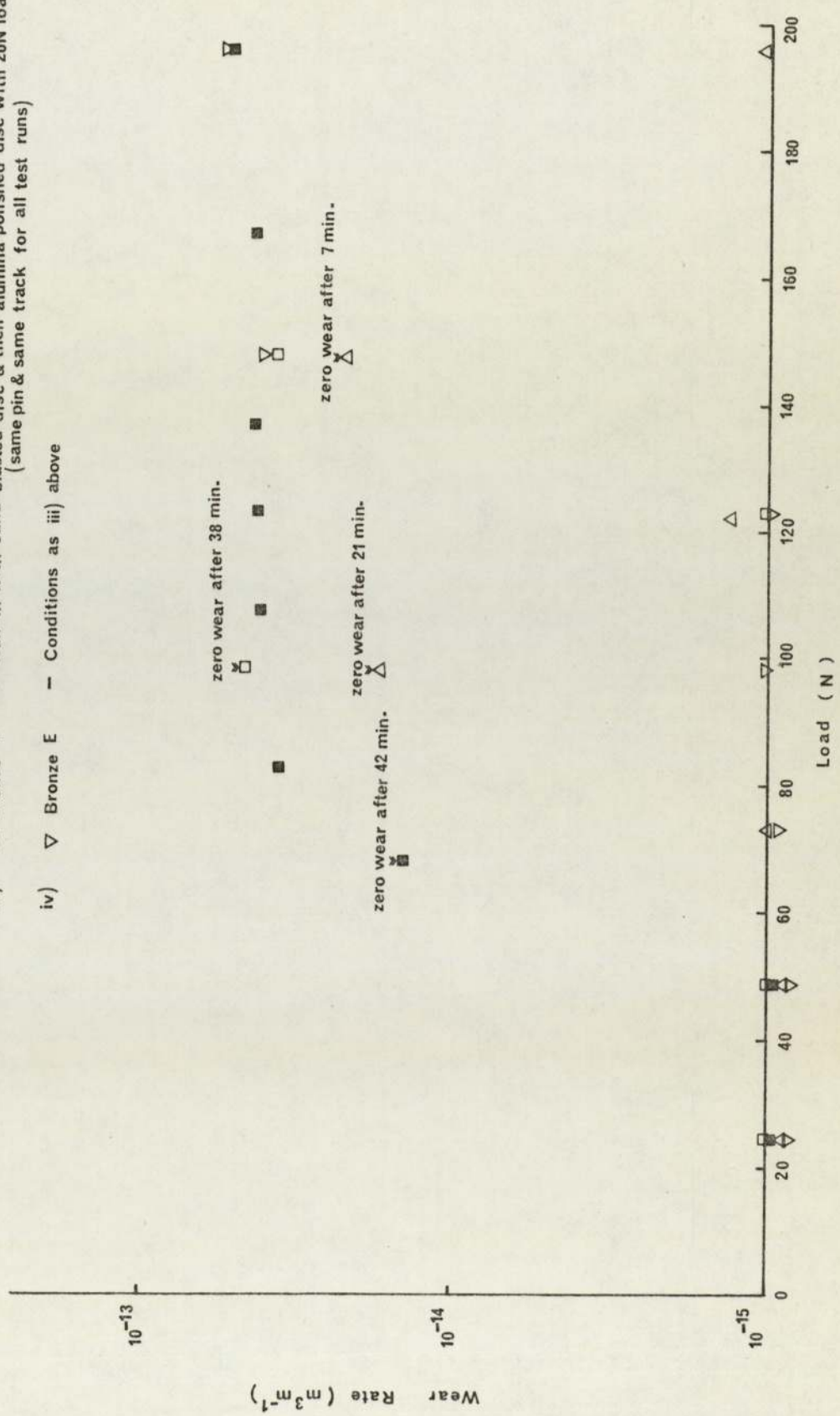ii) ▣ Bronze C — Run-in with 49N load at 0.2 ms⁻¹ (same pin & same track for all test runs)

iii) ▲ Bronze C — Run-in with sand-blasted disc & then alumina polished disc with 20N load at 0.5 ms⁻¹ (same pin & same track for all test runs)

3.3.1 Wear Tests for the 2 mm Diameter Bronze E Pins with Fuel Alone

The wear results described here were all obtained using new pins and new tracks for each test run with all the pins being run-in. Figure 3.10 shows the wear rate against load curves for 0.6, 2.0 and 4.0 ms^{-1}. From the observation of the wear curves' pattern, it suggests that increase in wear rate does not depend on increase in speed without taking into consideration the degree of fluid film support indicated by the coefficient of friction. The low wear rates below 49N load were due to the difficulties in obtaining boundary friction. Hence, starvation of fuel flow was necessary to produce boundary friction. In this case, the surface of the wear pin had been roughened and the hydrodynamic support was eliminated. For instance, the 49N load (4.0 ms^{-1} curve) had a starvation friction $\mu=0.25$. When the flow was supplied at a controlled rate again, the friction value fell to 0.11 maintaining this value throughout the wear process compared to zero friction at the start when flooded conditions prevailed. The same phenomenon was observed for 73.6N load (4.0 ms^{-1} curve) where zero friction and negligible wear were recorded at 1.7 ml min^{-1} flow rate, but by reducing the flow rate, the friction increased to 0.18 and later maintained 0.10 throughout the wear process. High wear rate was associated with less fluid film support indicated by high friction for 98N load. The two friction values noted 0.06 and 0.11, were the steady frictions throughout one hour run. It was extremely difficult to obtain $\mu=0.1$ for 123N load (4.0 ms^{-1} curve) as a slightly reduced flow rate could cause

scuffing wear as shown in one of the test runs where the friction increased from 0.16 and scuffed at 0.24 after 3 minutes run. The wear pins failed at 147N and 196N loads for the speed of 4 ms^{-1}, but operated satisfactorily at speeds of 0.6 and 2.0 ms^{-1} respectively. The above phenomena suggest that friction and hence wear is completely dependent on flow rate.

Figure 3.10   Wear Rate Versus Load — 2 mm diameter Bronze E pins — Fuel alone (Denison Wear Rig)
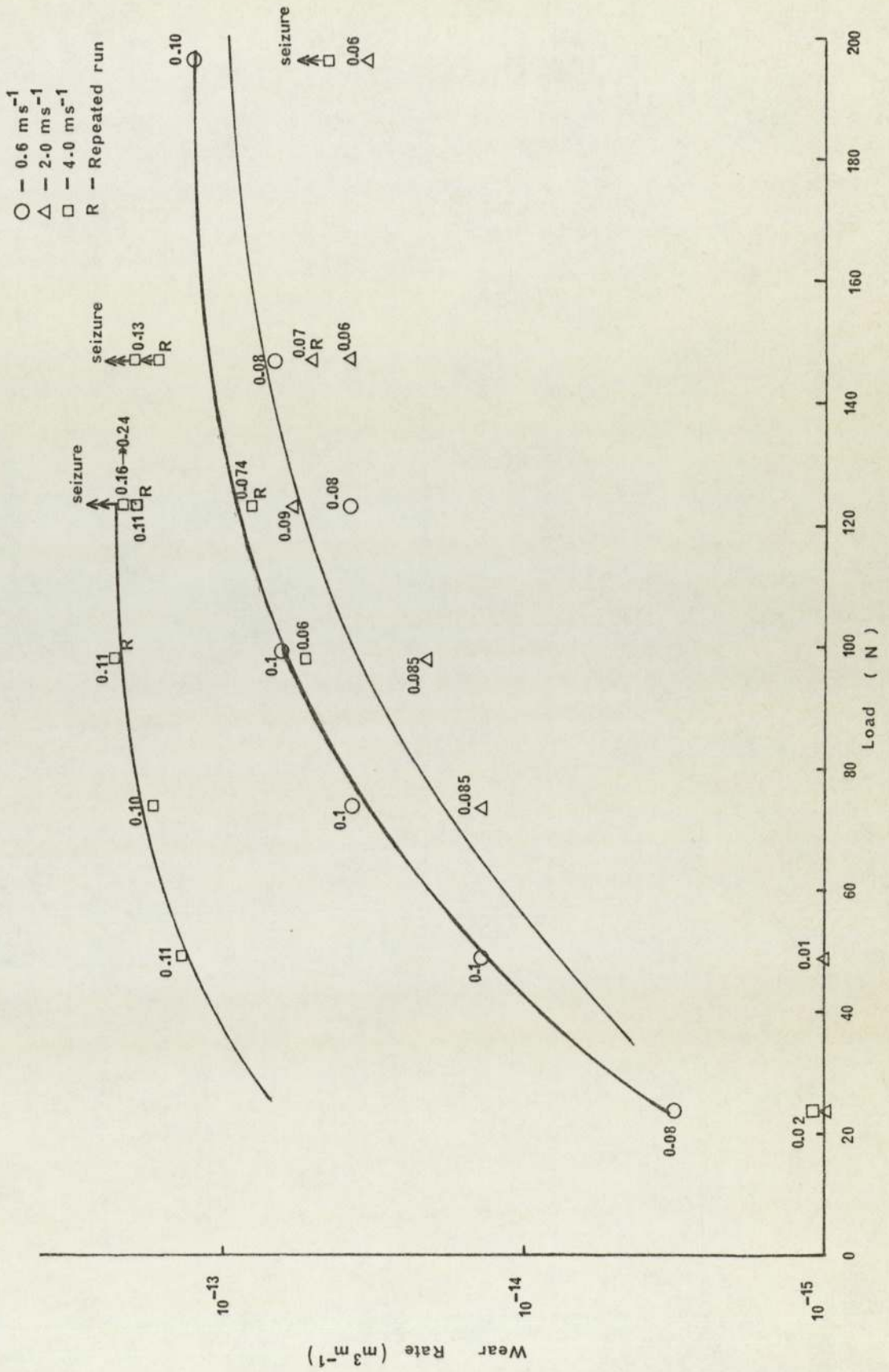
3.3.2 <u>Wear Tests for the 2 mm Diameter Bronze E Pins</u>
       <u>with Additive Hitec E580</u>

The wear tests were conducted with fuel containing 12
p.p.m. Hitec E580. Referring to Figure 3.11, curve (b) shows
an increase in wear rate with load whereas curve (a) shows a
decrease in wear rate above 98N load. The differences in
wear rate was essentially attributed to the degree of fluid
film support indicated by the coefficient of friction. Curve
(a) has much lower associated coefficients of friction than
curve (b) indicating more fluid support and hence less asperity
contacts with consequently less wear. Another similar trend
occurred for 2 ms^{-1} tests where more fluid film support gave
lower wear rate though the applied load was high (figure 3.12).
As before, Figure 3.13 also shows that whenever there was a
sufficient fluid film support, this would produce low wear
rate even though operated at high load and high speed condi-
tions. All these suggested that the wear rate was not depen-
dent on load without taking into consideration the degree
of fluid film support indicated by the coefficient of friction.
No scuffing wear occurred for all the tests with the additives
provided that the fuel flow was kept maximum at 1.7 ml
min^{-1} above 122.6N load (figure 3.14).

Figure 3.11   Wear Rate Versus Load — 0.6 m s⁻¹ — 2 mm diameter Bronze E pins — Fuel with Hitec E580 (Denison Wear Rig)

Curve (a) : same pin & same track for all test runs
Curve (b) : new pin & new track for each test run
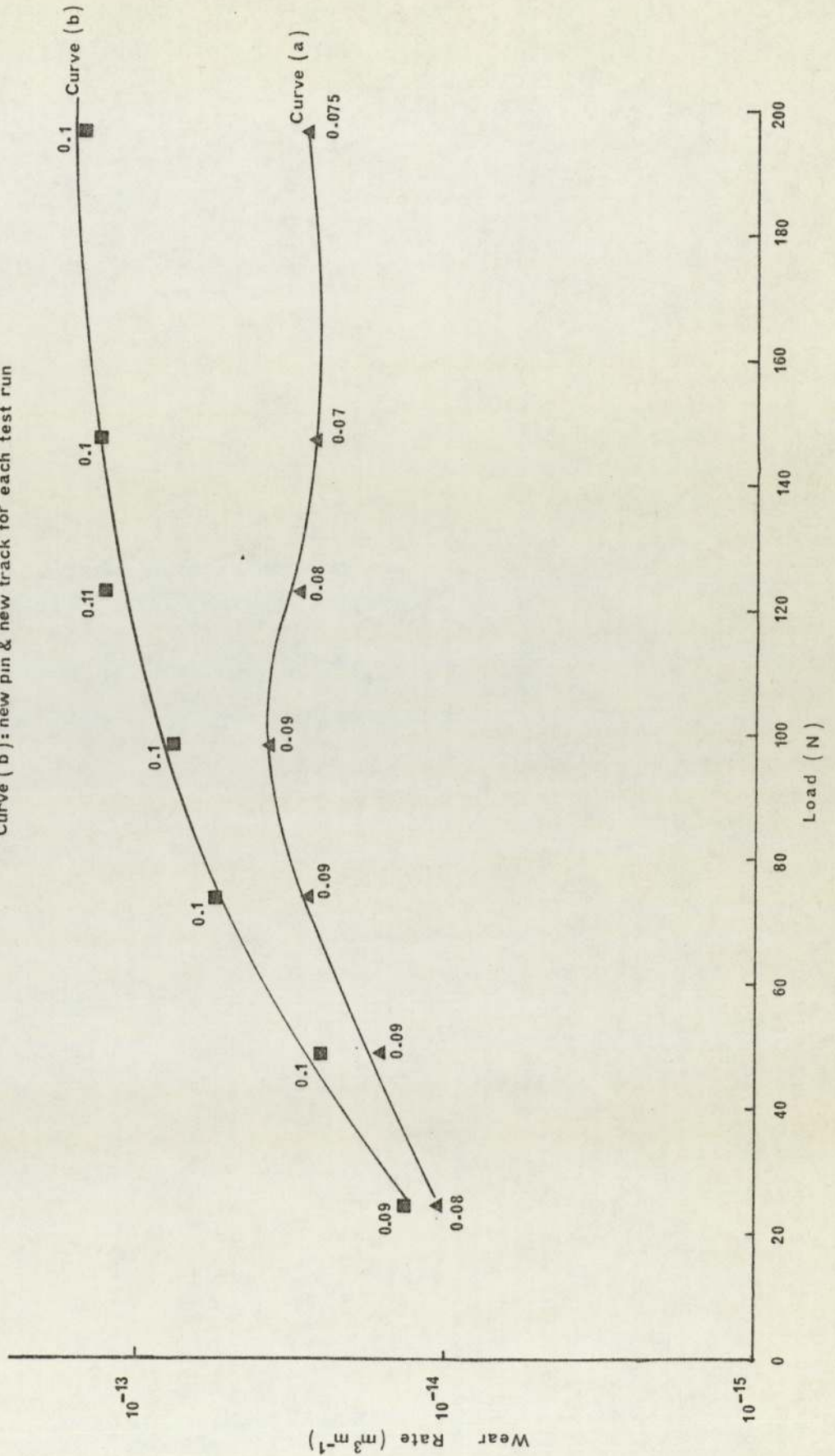
Figure 3.12 Wear Rate Versus Load – 2 m s⁻¹ – 2 mm φ Bronze E pins – Fuel with Hitec E580 (Denison Wear Rig)
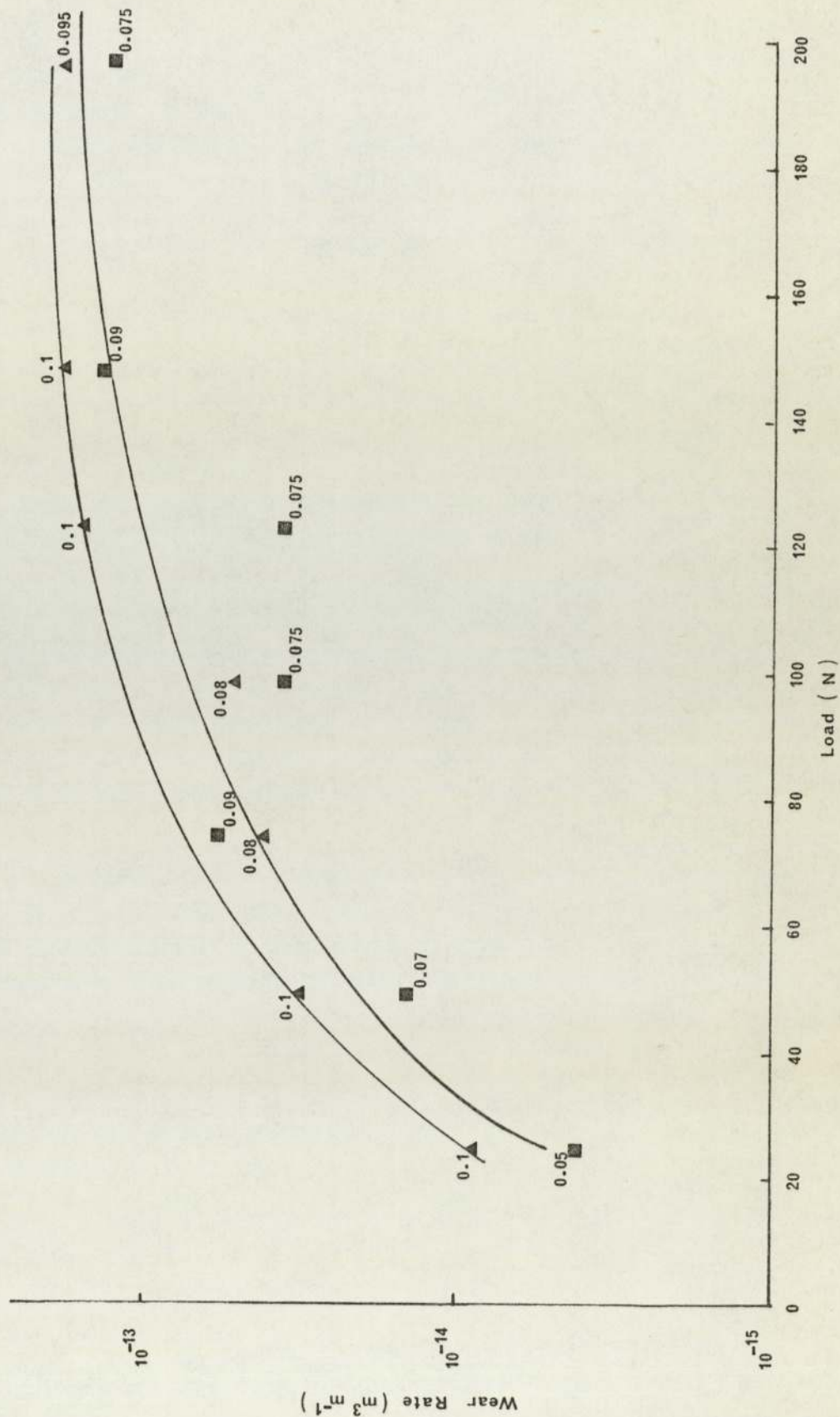
Figure 3.13 Wear Rate Versus Load — 4 ms⁻¹ — 2 mm φ Bronze E pins — Fuel with Hitec E580 (Denison Wear Rig)
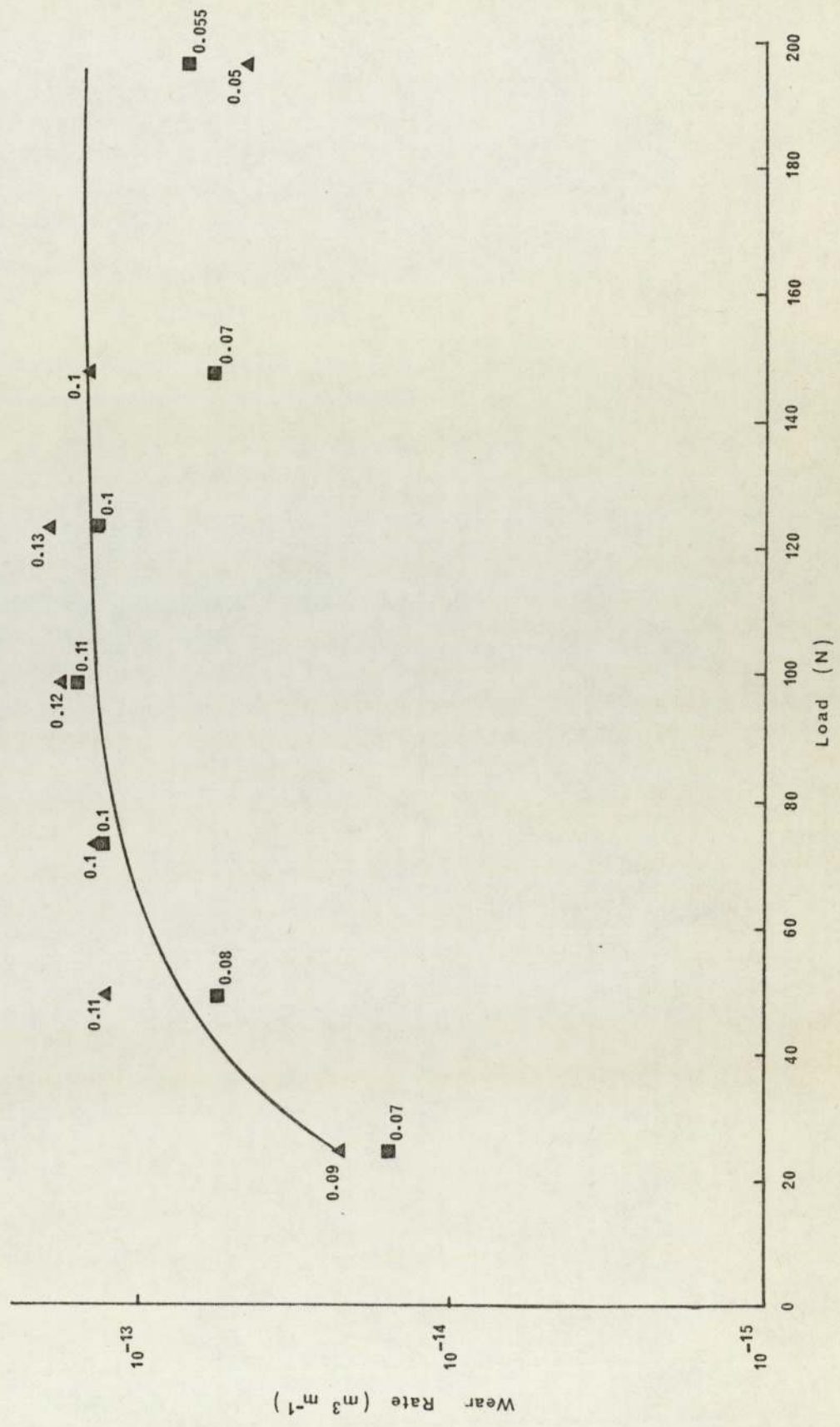
Figure 3.14 Wear Rate Versus Load — 2 mm φ Bronze E pins — Fuel with Hitec E580 (Denison Wear Rig)
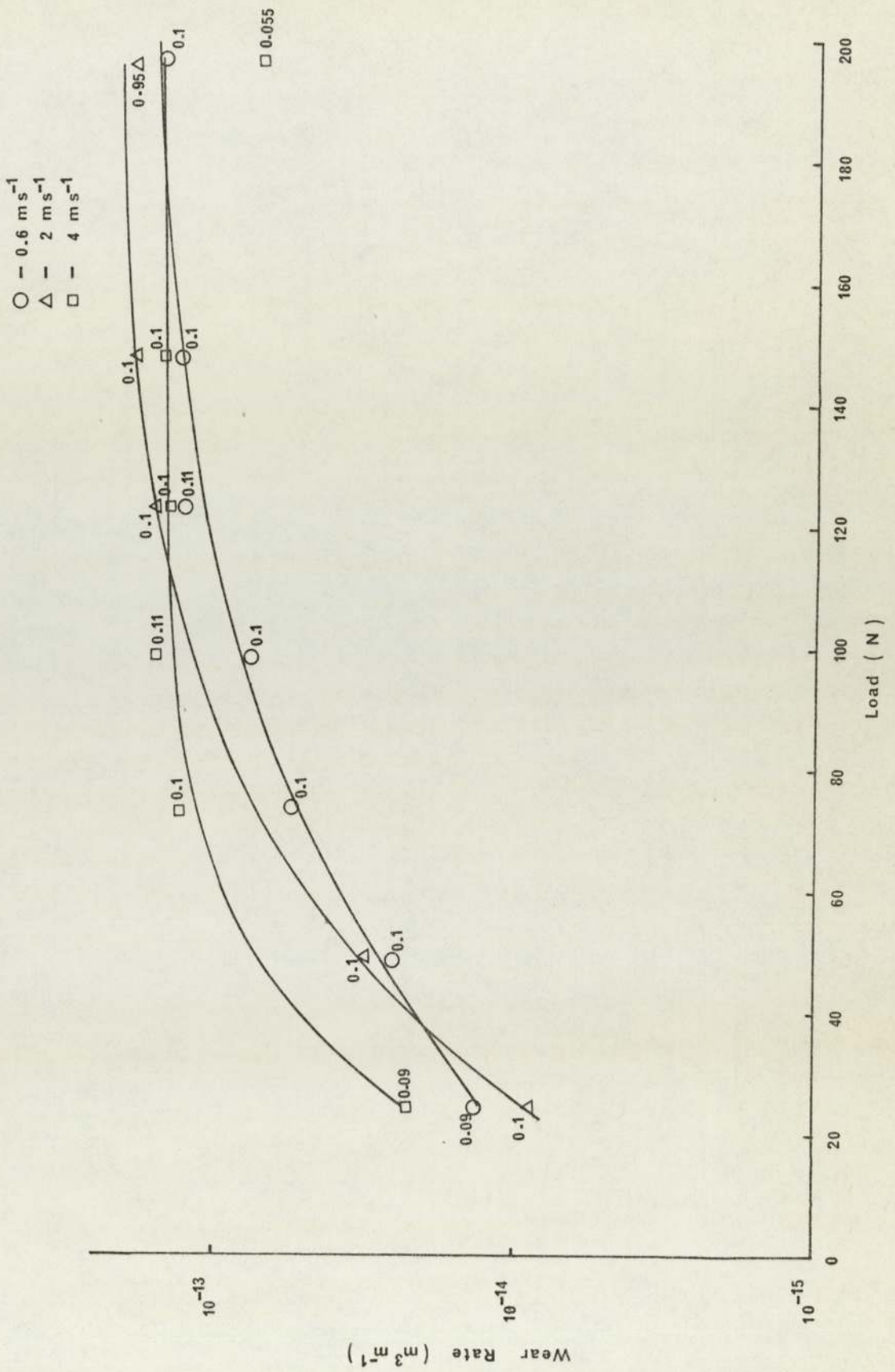
3.3.3   Time-Displacement Curves

Figures 3.15 to 3.17 show the Time-Displacement Curves of the wear experiments for fuel with and without additives. All the Time-Displacement Curves shown were recorded at steady state friction except whenever scuffing occurred, a sudden change in the direction of the displacement representing scuffing wear is marked with arrows. The increased displacement was not due to the increased loads, speeds or even the presence or absence of the additives. It is decided by the regimes of lubrication such as mixed lubrication leading to low friction and hence wear. Also, the formation of oxides on the wear surfaces would give some protection and the presence of additive would only become effective under severe boundary wear conditions.

Figure 3.15 Time – Displacement Curves — 0.6 m s⁻¹ – 2 mm φ Bronze E Pins (Denison Wear Rig)

Figure 3.16 Time–Displacement Curves — 2 ms⁻¹ – 2 mm⌀ Bronze E Pins (Denison Wear Rig)
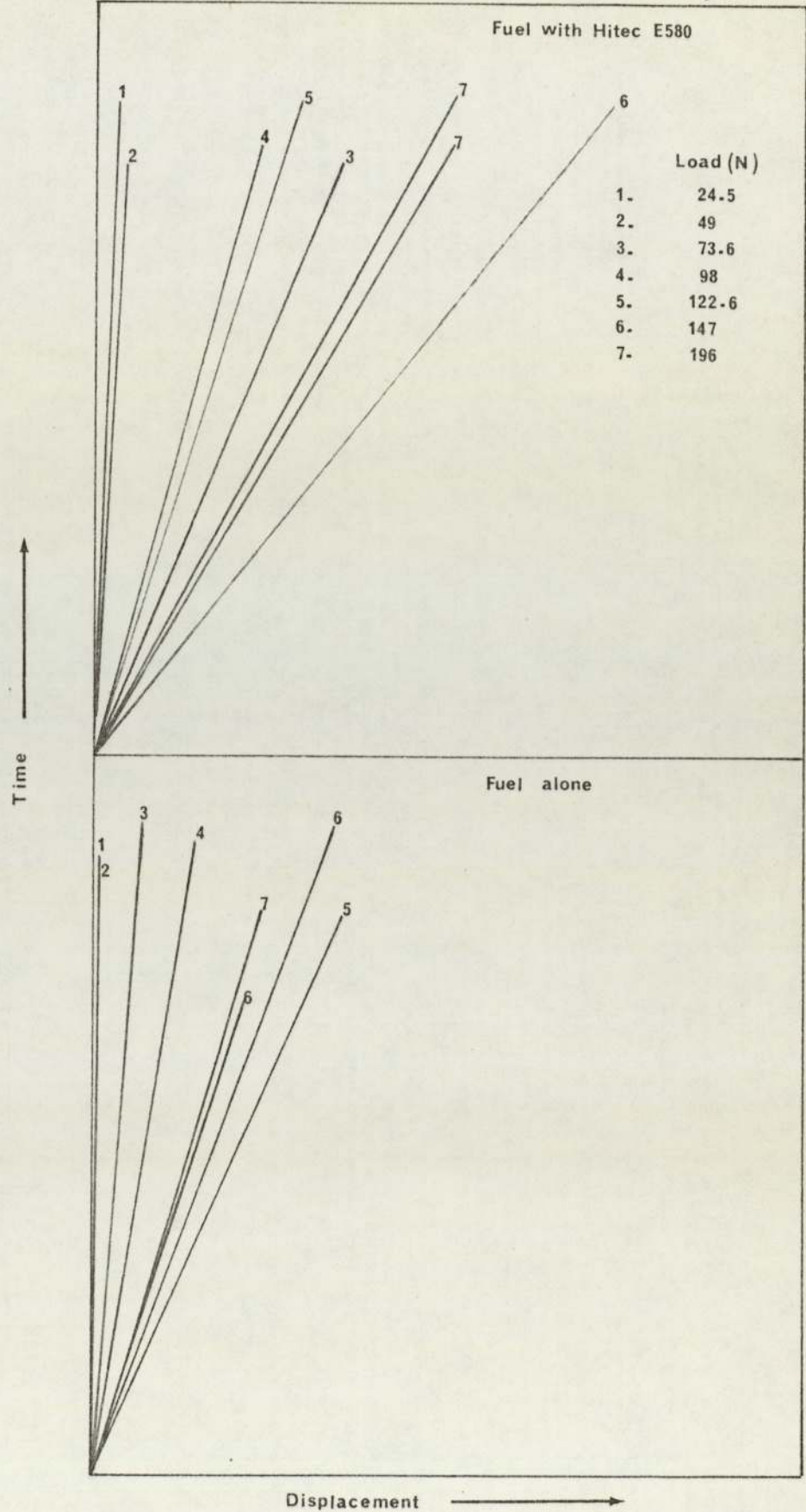
Figure 3.17 Time–Displacement Curves — 4 m s⁻¹ – 2 mm φ Bronze E Pins (Denison Wear Rig)
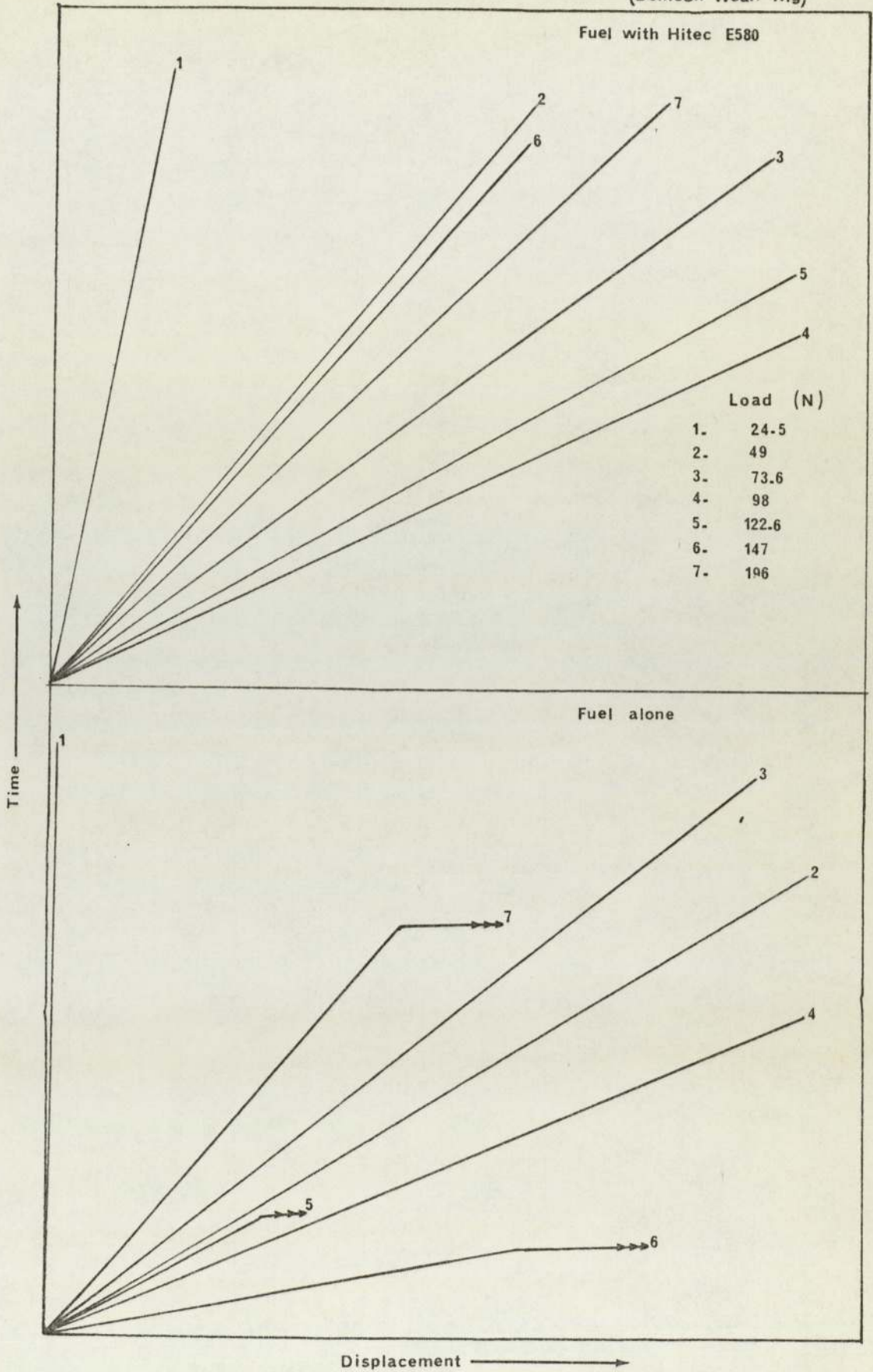
3.4 Vicker's Microhardness on Tapered Section Worn Pins

The degree of strain-hardening on a worn pin surface
varied from one place to the other due to non-uniform wear
rate. Hence the measurement of microhardness below the worn
surface of the bulk material by tapered sectioning served
only as a guide to the degree of material being deformed.
Figure 3.18 shows the microhardness depth positions of the
pins worn at 0.6 ms^{-1}. The unworn or machine finished pin
had an almost constant microhardness throughout the depth,
unlike the other worn pins which had a large increase in
microhardness close to the worn surfaces. The 98N load
specimens had the highest rate of strain-hardening, compared
to those at 24.5N and 49N loads, which reached more than 160
microns depth before approaching bulk microhardness. The
depths at which increases in microhardness were recorded
were lower for the 49N load specimens than the 24.5N load;
the reasons were due to the non uniformity of straining as
mentioned earlier and also the position of selecting micro-
hardness measurement. The degree of increased microhard-
ness on worn surfaces due to the wear process causing straining
can be as high as 50% of its bulk microhardness.

Figure 3.18 Microhardness Versus Depth —— 0.6 m s^{-1} – 3mm φ Bronze B Pins – Fuel Alone
(Denison Wear Rig)
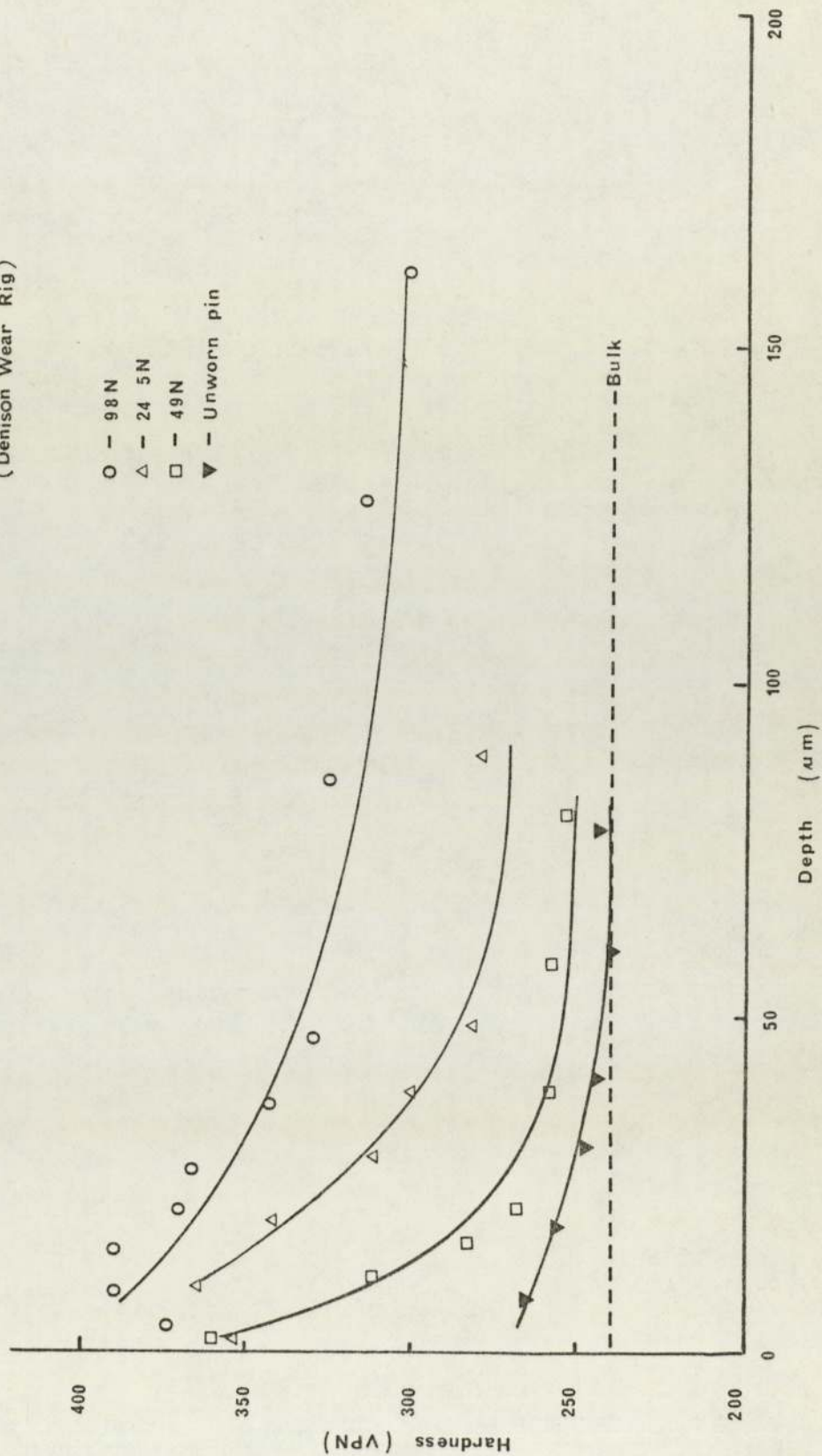
3.5 Optical Microscopy Analysis

The various wear phenomena observed will be discussed
with reference to Figure 3.19 which is a typical, well
established, sequence of sliding surface wear.

Figure 3.19(a) is the surface condition of the unworn
disc. The condition of the pin before sliding is shown in
Figure 3.19(b) with the machine marks clearly visible.
After running-in or wear-in with one micron sand-blasted
disc, the machine marks had been totally removed (figure
3.19(c)). In this system, wear-in duration was short (2 to
3 minutes) compared to the system's total operating time of
more than one hour. The wear-in rate was 3.45×10^{-12} $m^3 m^{-1}$.

Upon observing the bronze sample surfaces after a
wear test, it was found that where wear had occurred, the
surface topography had become smoother. The surface became
increasingly smoother as the loads increased up to 196N for
0.6 and 2.0 ms^{-1} sliding speeds (figure 3.19(d) and (e)).
This type of process in producing a flat surface is called
deformation/smoothening mechanism. Some striation marks
appeared in certain loads, these were due to the starvation
of fuel flow necessary to obtain boundary friction.

In the case of high speed of 4.0 ms^{-1}, the condition
of the surfaces reversed with increasing roughness on high
load, showing the tendency of the surface to failure (figure
3.19(f)).

From the optical point of view, there was no signifi-
cant topographical difference between the two worn surfaces
with fuel alone and fuel with additives. A high degree of

strain apparently can be tolerated by the surface material sliding with fuel plus additives.

Figure 3.20 shows the mating surfaces of the pin and disc being worn under fuel alone and also with additives. In both cases, layers of bronze material had been transferred to the steel counterface. The appearance of bronze colour on the worn disc track was considerably different to the colour of the unworn disc track (figure 3.19(a)).

Figure 3.19. Optical Microscopy of Worn Pins and Discs Surfaces
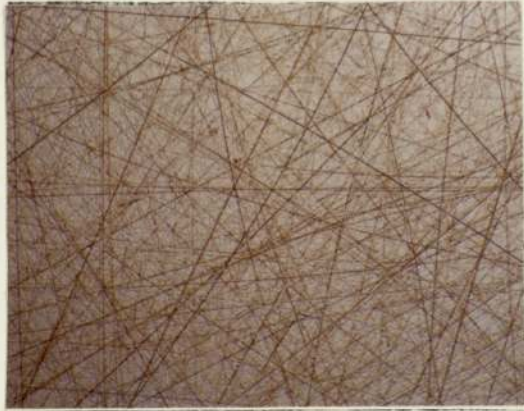
a. 0.025 μ.m. C.L.A. surface finish disc — ×50

b. Pre-running-in pin — ×50
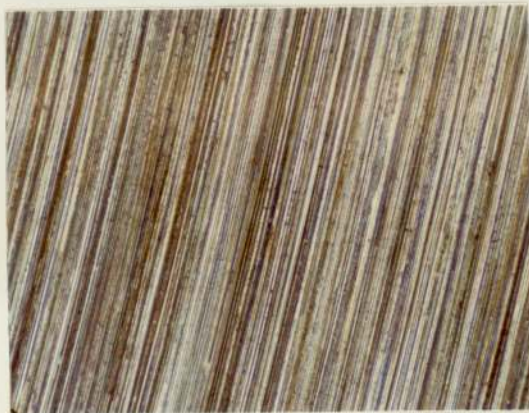
c. After running-in with sand-blast disc at 9.8N — 0.2ms^{-1} — wear rate: 3.45×10^{-12} m^{3}m^{-1} — ×50

d. Worn pins surfaces after sliding at $0.6\,ms^{-1}$ — magnification ×50

Fuel alone   Fuel + Hitec E580

—49 N—

—73.6 N—

—122.6 N—

—147 N—

e. Worn pins surfaces after sliding at $2ms^{-1}$ — magnification ×50

Fuel alone   Fuel + Hitec E580
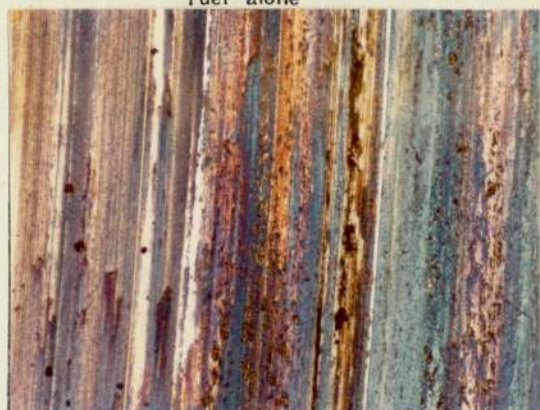
—49N—
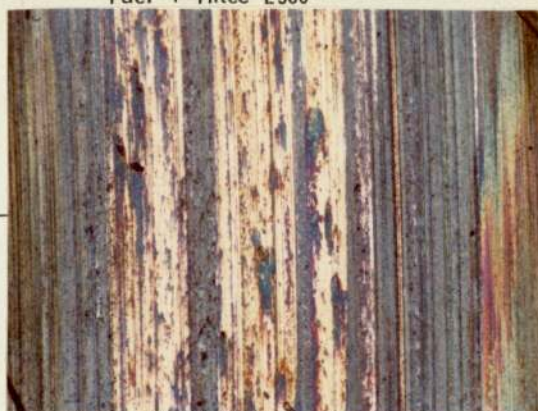
—73.6N—

—122.6N—

—147N—

—196N—

f. Worn pins surfaces after sliding at 4ms^{-1} — magnification ×50

Fuel alone

Fuel + Hitec E580

—49 N—

—98 N—

—122.6 N—

—147 N—

—196 N—

Figure 3.20. Mating Surfaces of Worn Pins and Discs

Fuel alone
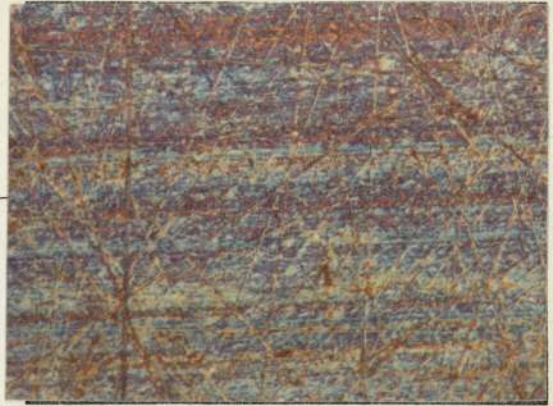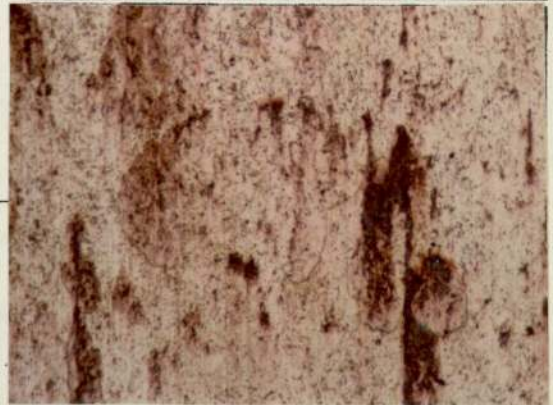
a. 122.6N − 2ms⁻¹ − ×200

b. 147N − 2ms⁻¹ − ×200
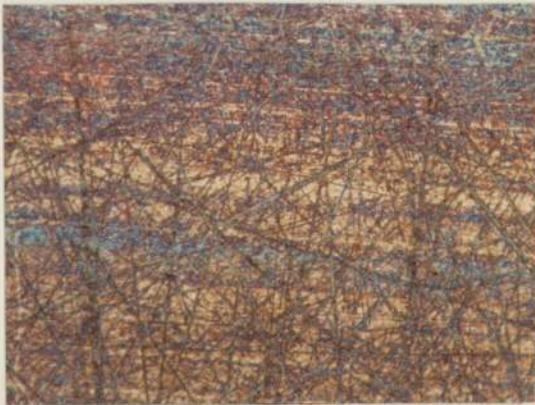
c. 196 N − 2ms⁻¹ − ×200
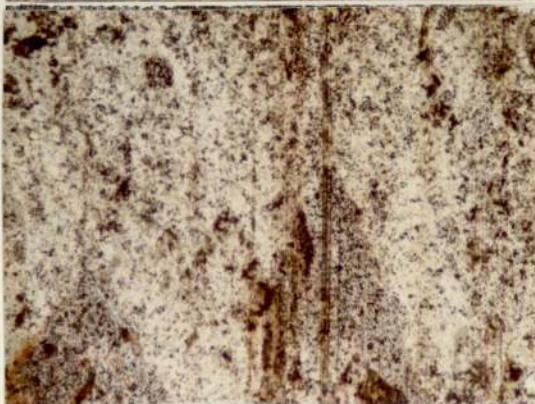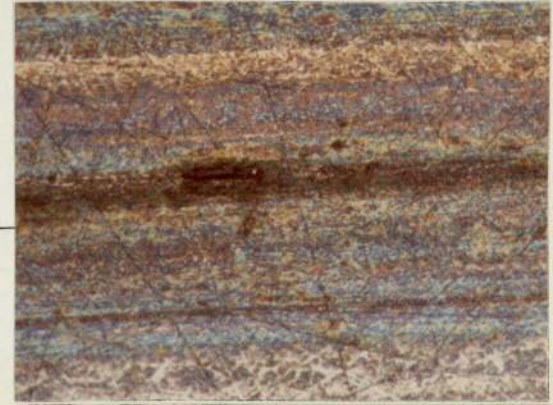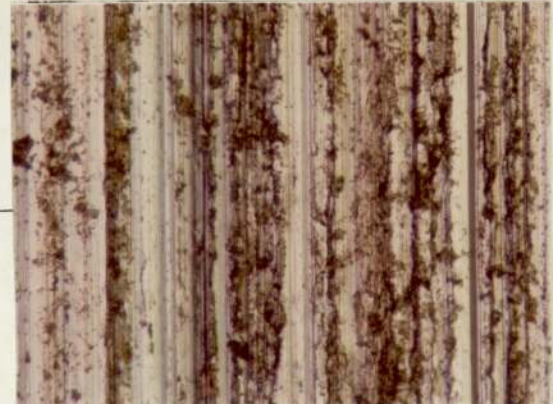
d. 122.6 N − 4ms⁻¹ − ×200

Fuel + Hitec E580
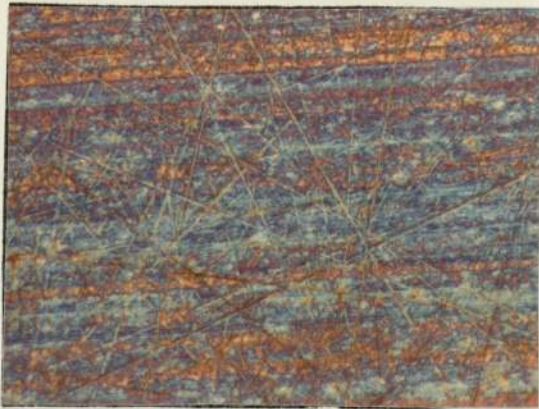
─Disc─
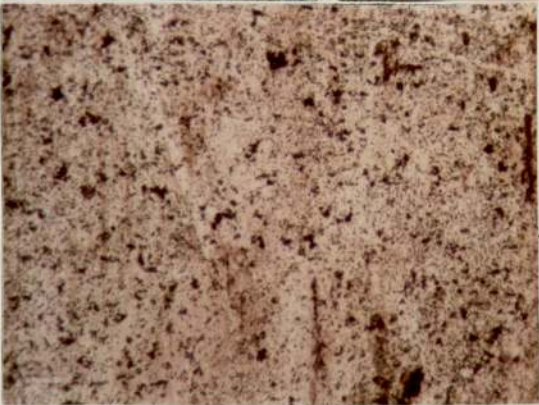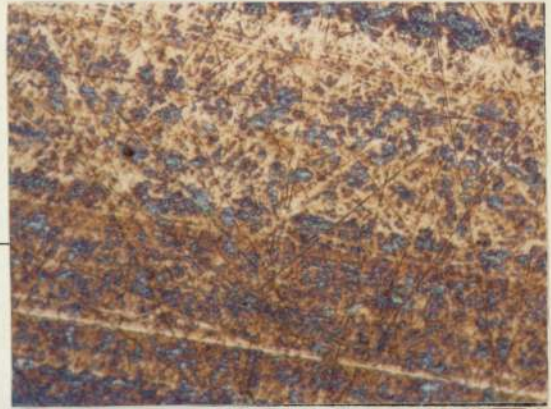
─ Pin ─
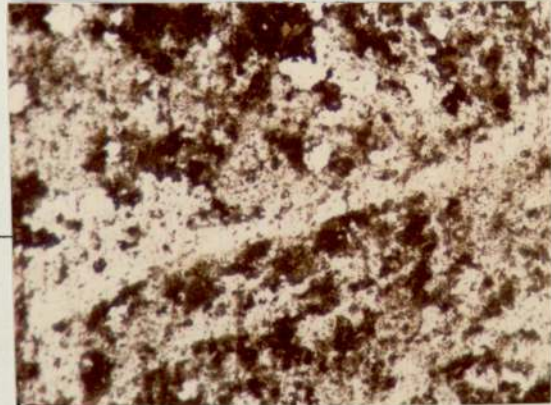
a. 196 N — 2 ms⁻¹ — × 200

b. 196 N — 4 ms⁻¹ — × 200

3.6   The Application of Chemical Etching Techniques to the
      Analysis of the Structure of Aluminium-Bronzes

A chemical etching technique was employed to reveal
the structure of the aluminium-bronzes. All samples were
metallographically polished to 1 μm and etched with ferric
chloride in alcohol.

Judging from the review of cast microstructure of the
kappa phase in Ni-Al bronze (40,45,46), the structures of
the Bronze A(IMI), Bronze B(Poole Type I), Bronze C(Poole
Type II), Bronze D(Original Fuel Pump) and Bronze E(Delta)
could be described with reference to the phase momenclature
based on the phase analyses obtained from SEM and EPMA. It
had been shown from the optical observations that there are
at least four structural differences used in the wear tests
though they all belong to the same category of aluminium-
bronze materials. The present account will draw freely upon
these observations to describe the complexities of each of
the above microstructures of aluminium-bronzes.

3.6.1   Bronze A

The chemical analysis from the Altrincham Laboratories
shows that the chemical compositions of the IMI aluminium-
bronze had 83.9% Cu, 9.3% Al, 3.47% Fe, 2.97% Ni and 0.37%
Mn. That analysis was closely correlated to the compositions
obtained from the EPMA (table 3.2).

Two distinct phases of α and eutectoid phases are
revealed as shown in Figure 3.21(a) with a large amount of
eutectoid phase present. The large volume of eutectoid
α+Ni-K present reflects the larger volume of β present in the

alloy at high temperature at which this transformation occurs. At low temperature, fine faceted particles of Fe-K start to precipitate from the α matrix. From SEM and EPMA spot analyses (table 3.1), the eutectoid region had a higher Ni content than Fe whereas the α matrix had a Ni/Fe ratio with Fe greater than Ni. The finely distributed Fe-K precipitates within α matrix promote a strengthening effect on the α phase. The relatively large volume of eutectoid phase present reduces the tensile strength and toughness of the material.

3.6.2 Bronze B and Bronze C

It was found that Poole (86) had been using two structurally different aluminium-bronzes for his wear tests. The microstructures of these two aluminium-bronze materials are shown in Figure 3.21(b) and (c).

Bronze B consists of a large volume of lamellar Ni-K phase with varying size Fe-K phase morphology. The changes of its morphology can be explained by following its precipitation process. During precipitation reaction, the $\alpha+\beta$ structure existing over a range of temperatures below the solidus contains all the Fe and Ni in solid solution with a partition ratio Fe:Ni>1. As the temperature falls, the solubility of Cu in the β is reduced and new α is formed at the β/α boundary. This continuing process produces a local peripheral enrichment of Ni, Fe and Al at the β surface which increases until the solubility of Fe in β at the α/β interface is exceeded and Fe-K is precipitated forming the large

rosette-shaped phase. Loss of Fe from the shrinkage of the β surface produces a local enrichment of Ni so that this time the ratio Fe:Ni<1 and the eutectoid reaction $\beta \rightarrow \alpha + \text{Ni-K}$ occurs, producing a Ni-rich lamellar fringe around the β phase. On further cooling, small faceted particles of Fe-K start to precipitate from the α matrix and the remaining untransformed β phase decomposes to an optically irresolvable mixture of α and K or α and γ_2. Due to the presence of large volumes of Ni-K phase and uneven distribution of large and small Fe-K precipitates, this aluminium-bronze also has reduced tensile strength and toughness.

Bronze C has a Ni:Fe ratio >1, as a result the solubility of Fe in the β phase is increased. On cooling, the precipitate associated with the large rosette-shaped Fe-K does not appear. Instead, the β volume will reduce by rejection of α. This process is terminated at a high temperature by the complete eutectoidal decomposition $\beta \rightarrow \alpha + \text{Ni-K}$ over a narrow range of temperature. At low temperature, fine faceted particles of Fe-K start to precipitate from the α matrix. As the Ni content exceeds the Fe content, ductility and toughness of this alloy is reduced.

3.6.3 Bronze D

Electron Probe Microanalysis (table 3.2) shows that the Fe and Ni contents exceeded 5% with Ni:Fe>1. Figure 3.21(d) shows the microstructure and the elements distribution. The high level of Fe reflects a large rosette-shaped Fe-K phase present on cooling. As the Ni content exceeds the Fe content,

the Ni-rich K lamellar phase is also present in large amounts. Consequently, the overall high level of Ni makes this alloy less ductile and tough.

3.6.4 Bronze E

This alloy gives the overall best mechanical properties compared to the previous mentioned aluminium-bronzes. The absence of Ni-rich K phase together with the presence of a fairly uniform distribution of fine faceted particles of Fe-K phase around the α grain boundaries makes this alloy higher in strength and toughness than the others examined.

Figure 3.21. Microstructures of Aluminium Bronzes and Distributions of Alloying Elements

a. Bronze A (IMI)

b. Bronze B (Poole Type I)

Microstructures

Copper

Aluminium

Iron

Nickel

c. Bronze C (Poole Type II)   d. Bronze D (Original Fuel Pump)

Microstructures

Copper

Aluminium
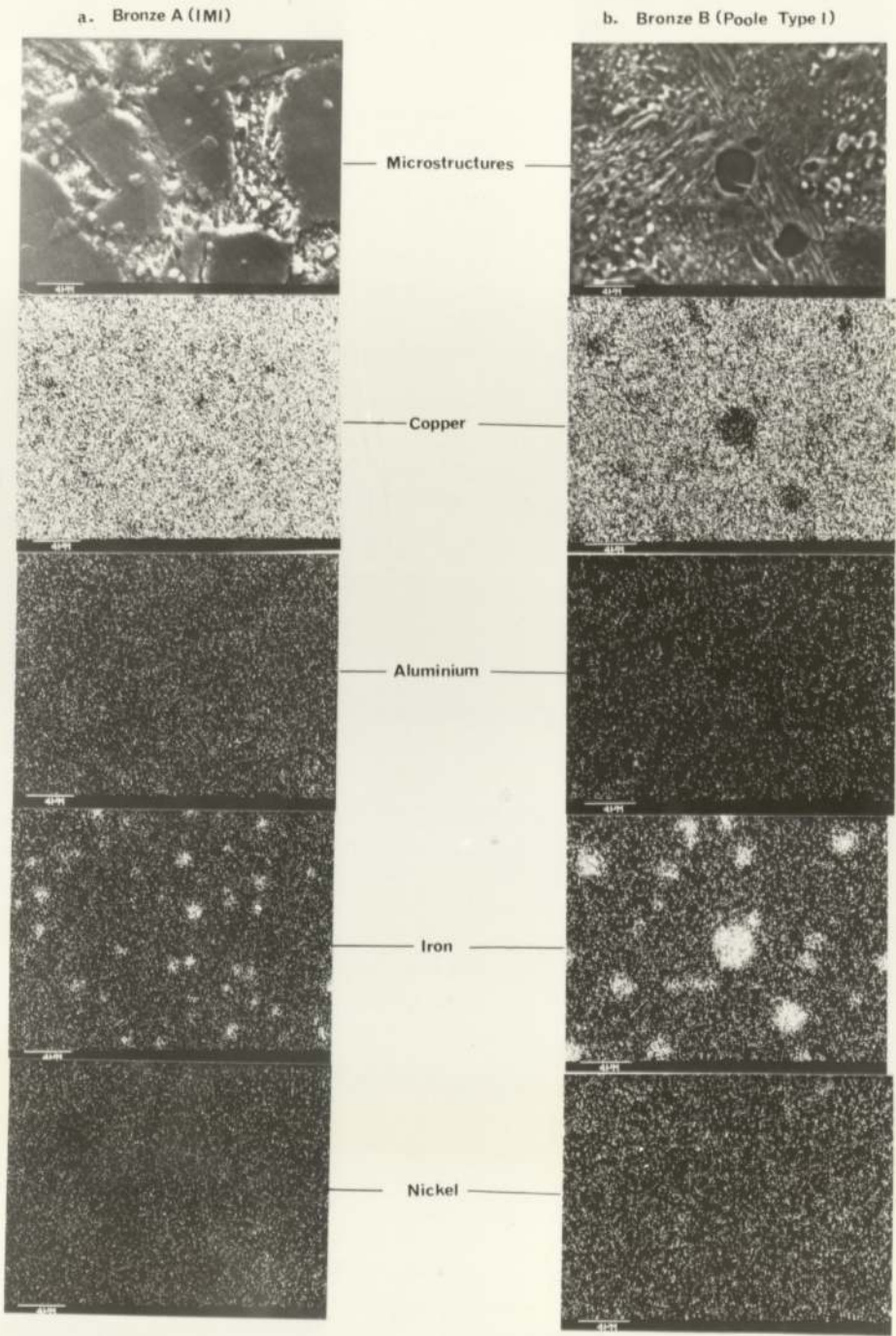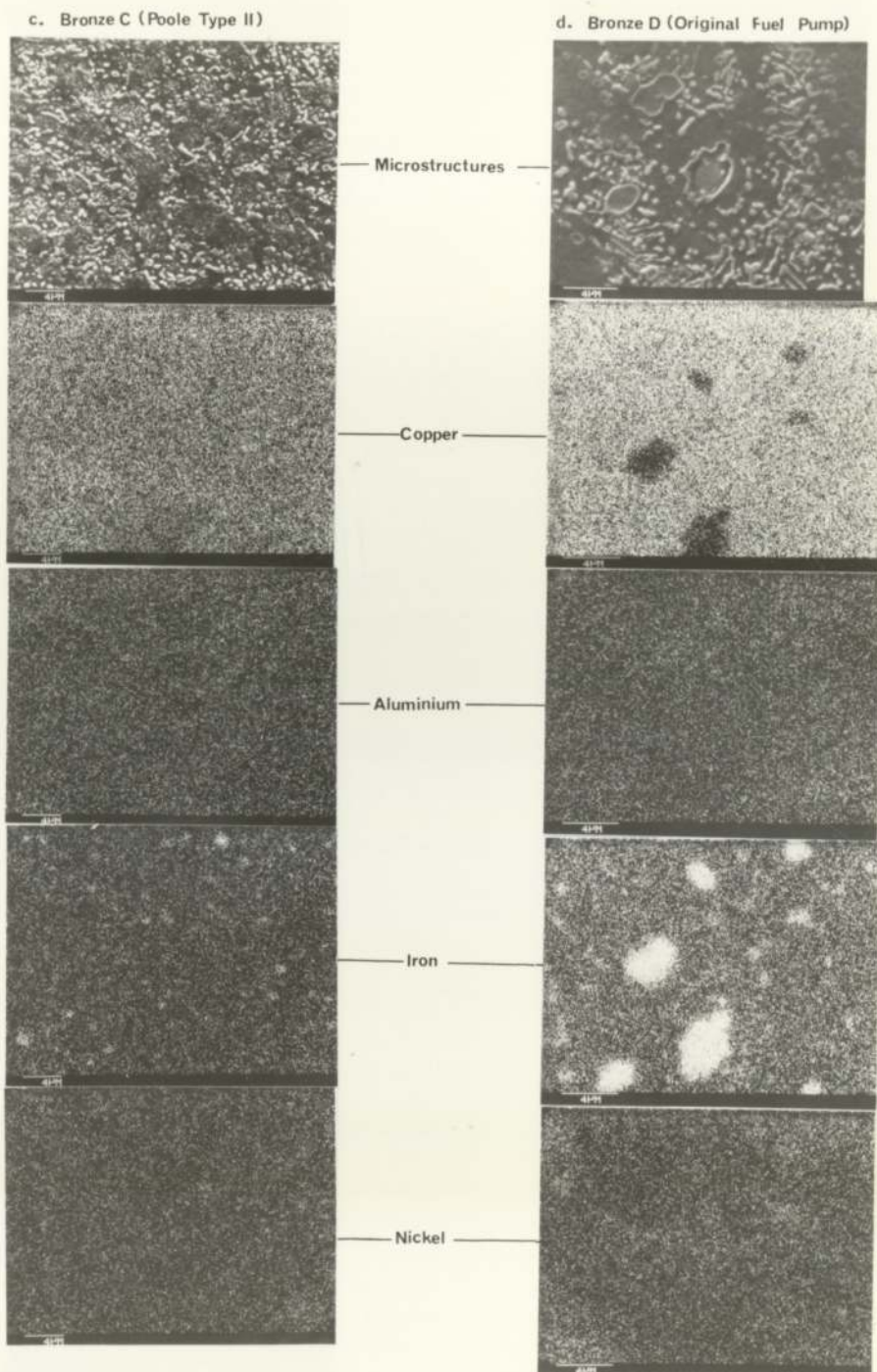
Iron

Nickel

e. Bronze E (Delta)

Microstructure

Copper
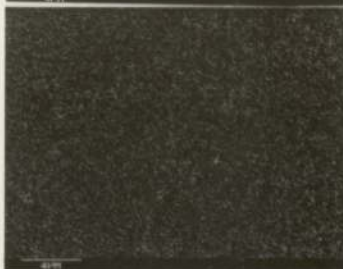
Aluminium
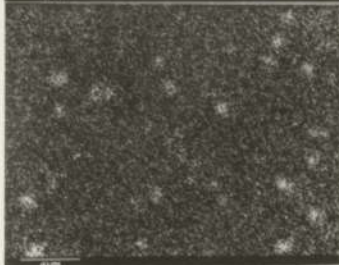
Iron
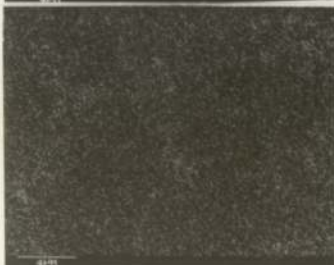
Nickel

3.7   The Application of SEM and EPMA to the Analysis of the Various Phases of Aluminium-Bronzes

The phases present in the aluminium-bronzes were characterized by using SEM and EPMA. The three identified morphologies are α, K and eutectoid phases and the compositions of these three phases was also determined.

When using SEM, X-ray energy dispersive analysis, the peak-heights were measured from the phases to give an overall comparison of elements Cu, Al, Fe and Ni present in each phase. No attempts were made to correct for the effects of atomic number, absorption and fluorescence.

The use of EPMA is advantageous over SEM, because the final compositions of the elements takes account of the effects of atomic number, absorption and fluorescence. Hence, final results are more reliable.
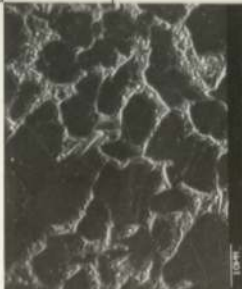
Table 3.1 shows the phase analyses of the Bronze A (IMI), Bronze B(Poole Type I), Bronze C(Poole Type II), Bronze D(Original Fuel Pump) and Bronze E(Delta). The Ni/Fe ratios in the α phases for the Bronze A, Bronze C and Bronze E are less than one, indicating that they have better strength and toughness than the eutectoid phases where the Ni/Fe ratios are greater than one. The overall strength of the above bronzes, except Bronze E, is low due to large volumes of eutectoid phase being present. On the other hand, the Ni/Fe ratios in the α phases, as well as eutedtoid phases, for the Bronze D and Bronze B are greater than one, giving the overall structures less strength and toughness. The high level of nickel present in the α and eutectoid phases for both cases is attributed to the original compositions with the

nickel content higher than the iron (table 3.2). This reflects the large volume of Ni-rich K phases present in both Bronze D and Bronze B.

The conclusion can be made that Bronze E gives overall best strength and toughness over other bronzes used. This bronze has a uniform structure with many faceted particles of Fe-K phase within and surrounding the α phase boundaries.

Table 3.1. Analysis of Phases Present in Aluminium Bronzes

Microstructures	Type	α phase					κ phase					Eutectoid phase				
		Cu	Al	Fe	Ni	Ni:Fe	Cu	Al	Fe	Ni	Ni:Fe	Cu	Al	Fe	Ni	Ni:Fe
Bronze A	SEM	87.52	4.66	5.36	2.46	0.46	36.44	8.24	52.15	3.16	0.06	78.68	10.28	5.40	5.60	1.04
							(Fine precipitates of Fe–K phase dispersed within α grains)									
	EPMA	86.31	7.47	3.38	2.84	0.84	73.35	9.10	13.36 (Fe–K)	4.19	0.31	80.66	10.60	3.33	5.42	1.60
Bronze B	SEM	78.68	8.40	6.85	6.07	0.89	37.68	9.28	45.05	8.00	0.18	84.19	6.42	4.26	5.14	1.20
							(Propeller Fe–K precipitates along lamellar phase)									
							6.98	6.22	83.16	3.65	0.04					
							(Large globule Fe–K precipitates)									
	EPMA	76.93	10.51	5.94	6.62	1.11	26.40	9.69	56.34 (Fe–K)	7.57	0.13	78.45	10.23	4.03	7.29	1.81
Bronze C	SEM	77.48	11.87	6.67	3.97	0.60	15.79	11.21	67.73	5.27	0.08	58.89	18.54	10.73	11.84	1.10
							(Fine Fe–K precipitates)									
	EPMA	81.43	9.21	4.88	4.48	0.92	70.32	8.75	13.74 (Fe–K)	7.19	0.52	74.34	10.88	6.31	8.47	1.34

Microstructures	Type	α phase					κ phase					Eutectoid phase				
		Cu	Al	Fe	Ni	Ni:Fe	Cu	Al	Fe	Ni	Ni:Fe	Cu	Al	Fe	Ni	Ni:Fe
	SEM	82.78	5.57	7.28	4.38	0.60	6.09	1.78	87.26	4.87	0.06	65.99	13.14	9.62	11.25	1.17
Bronze D									(Large globule Fe–K precipitates)							
							77.14	9.69	5.61	7.56	1.34					
									(Fine lamellar Ni–K phase)							
	EPMA	83.06	8.48	4.16	4.30	1.03	41.99	8.40	45.08	4.52	0.10	76.34	11.02	4.54	8.10	1.78
									(Fe–K)							
	SEM	84.64	4.76	7.17	3.44	0.48	59.19	7.96	24.25	8.60	0.35	—	—	—	—	—
Bronze E									(Fine Fe–K precipitates at α grain boundary)							
	EPMA	82.59	8.14	4.95	4.32	0.88	70.66	7.95	17.28	4.11	0.24	74.51	9.84	6.88	8.77	1.27
									(Fe–K)							

continued

TABLE 3.2 ELECTRON PROBE MICROANALYSIS OF ALUMINIUM-BRONZE COMPOSITIONS

Type	Element Content (Atomic %)				
	Cu	Al	Fe	Ni	Mn
Bronze A(IMI)	82.61 ±0.62	9.63 ±0.22	3.99 ±0.21	3.32 ±0.15	0.44 ±0.09
Bronze B(Poole Type I)	78.38 ±0.11	10.58 ±0.31	5.18 ±0.26	5.36 ±0.16	0.50 ±0.05
Bronze C(Poole Type II)	80.21 ±0.09	9.55 ±0.22	4.76 ±0.22	5.00 ±0.38	0.48 ±0.09
Bronze D(Original Fuel Pump)	78.42 ±0.62	9.85 ±0.23	5.33 ±0.18	5.83 ±0.10	0.57 ±0.09
Bronze E(Delta)	80.12 ±0.58	9.69 ±0.34	4.88 ±0.12	4.81 ±0.19	0.50 ±0.06

3.8   Results of the Scanning Electron Microscopy Analysis of Worn Surfaces

Metallographic examination is likely to yield decisive information about the mechanism of wear damage, leading to the development of methods for its control. Hence, Scanning Electron Microscopy was used to image the surface and sub-surface of the worn pins.

3.8.1   Analysis of the Bakelite Compound

The bakelite is essentially used to mount the specimen before examination under SEM. It is advantageous to know what sorts of compounds are present in the bakelite so that the junction between the taper section pin and the bakelite surface can easily be identified during the elemental X-ray scan over the whole surface. Figure 3.22 shows the structure and the elements contained in the bakelite. The principle elements present are silicon, sulphur, aluminium, cadmium and iron.

3.8.2   Analysis of Bronze A Worn Pin - (Fuel Alone)

Figure 3.23 is a unique scuffing failure of the worn pin at a speed of 1 ms^{-1} and 245N load. This failure bears some resemblance to a pitting failure where the worn surface was characterised by the formation of many small pits. Cracks are formed on the surface perpendicular to the wear direction. Cracking and spalling of the worn surface has occurred to form a lump of wear particles. It is believed that the pits were initiated at the eutectoid phases where

Figure 3.22.   Scanning Electron Micrographs of Bakelite Compound and
Distribution of *Impurity* Elements

a. Bakelite structure

d. Aluminium
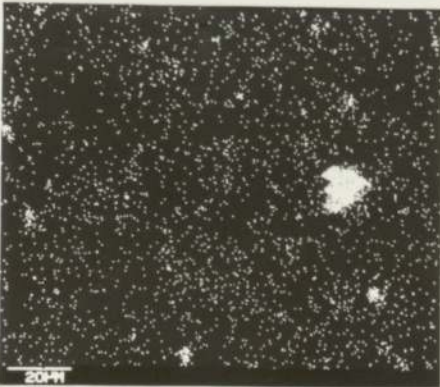
b. Silicon
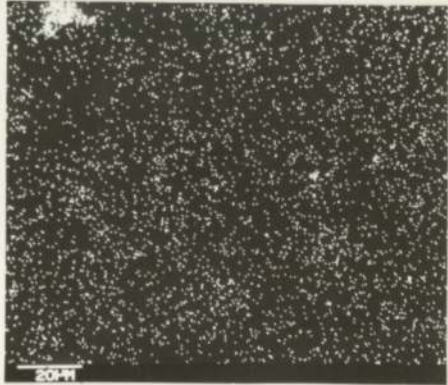
e. Sulphur
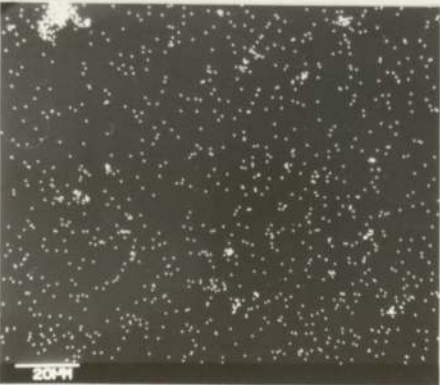
c. Iron
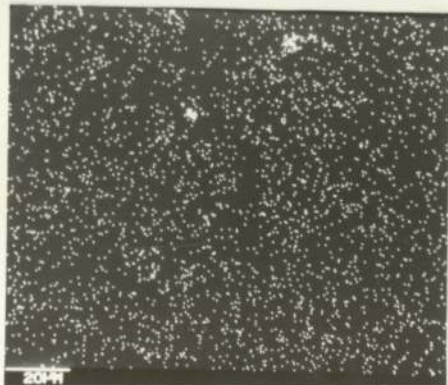
f. Cadmium

Figure 3.23. Scanning Electron Micrographs of Bronze A   Worn Pin

a. Resemblance to pitting failure   245 N — 1ms^{-1}

b. Cracking and spalling to form wear particles

the maximum shear stress occurred. The areas in the region of α phase have better strength and toughness than the areas in the eutectoid phase.

3.8.3 Analysis of Bronze B Worn Pin —— (Fuel Alone)

The surface of a 3 mm diameter pin, worn at 0.6 ms^{-1} and 24.5N load, which had a low wear rate of 4.6 x 10^{-15} m^{3}m^{-1}, is shown in Figure 3.24. The top part of the Figure 3.24(a) is the unetched wear region and the lower part is the region of etched and tapered section pin. In between these two regions is a clear and distinct deformed layer of about 2 μm depth. Though the applied load and speed were low, the aluminium-bronze material showed deformation caused by sliding wear. Figures 3.24(b) to (f) show the elemental distributions of Cu, Ni, Fe, Al and Mn over the worn and tapered surfaces. A distinctive depleted layer of aluminium was found at the deformed layer. Other elements showed uniform distributions across the deformed boundaries.

Figure 3.25 shows a severe wear pin (3 mm diameter pin), worn from 24.5 to 196N load at 4 ms^{-1}. The pin did not fail at the end of the run, but showed many cracks all over the wear surface. The two pins (*i.e. Figs. 3.24 & 3.25*) show opposite ends of the wear spectrum. The first was conducted under low speed low load and the second under high speed high load conditions.

Figure 3.24. Scanning Electron Micrographs of Bronze B Worn Pin and
Distribution of Alloying Elements

a. Electron image
   24.5 N — 0.6 ms⁻¹

b. Copper

c. Nickel

d. Iron

e. Aluminium

f. Manganese
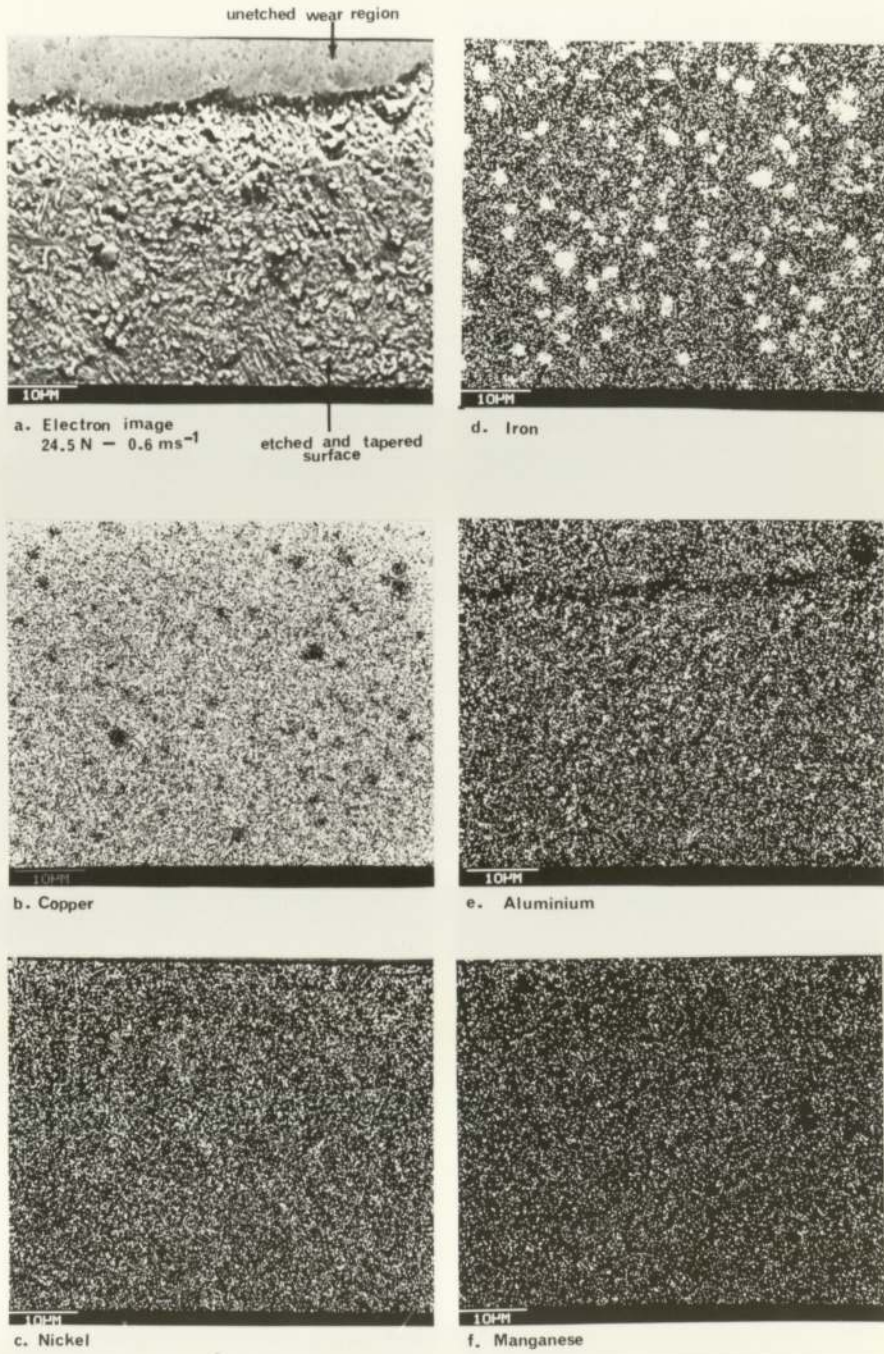
Figure 3.25. Scanning Electron Micrographs of Bronze B Worn Pin

a. Wear from 24.5 to 196 N — 4 ms^{-1}
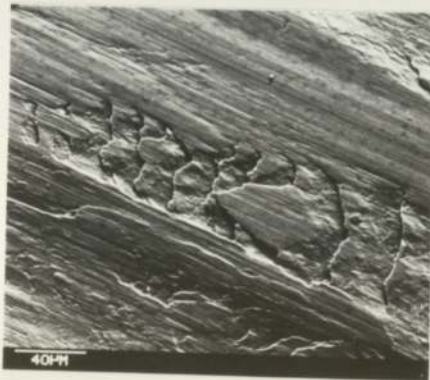
b. Severely worn surface

3.8.4 Analysis of Bronze E Worn Pin

(i) Fuel Alone

Figure 3.26 shows the condition of a 2mm diameter wear pin surface for 98N load at 4 ms^{-1}. The wear surface has been heavily striated. The wear particles were formed by the surface material fracturing or tearing due to the high strain suffered. This mechanism was found where the wear rate was high and a large amount of loose debris was found on the surface. The surface of this pin had almost reached a critical condition, any load higher than this would have caused scuffing failure. Figure 3.27 shows the tapered section of this pin, perpendicular to the wear direction. The upper region of the Figure 3.27(a) is the mounted bakelite whilst the lower region is the tapered surface of the unetched worn pin. There was no distinctive deformed layer shown at the sub-surface of this pin compared to that worn at low load and speed (figure 3.24) which revealed a clear and distinctive deformed layer. A possible reason could be that, due to the high wear rate, the rate of removal of the deformed layer was greater than the rate of formation. Figure 3.27(b) reveals many cavities formed in the sub-surface layer of the pin. The formation of these cavities is probably due to high strain-rate caused by sliding contact. The sizes of the cavities become increasingly larger when approaching the wear surface. Figures 3.27 (c) to (f) show the X-ray scan of Cu, Ni, Fe and Al. A certain degree of aluminium depletion was found in the sub-surface of the pin. Figure 3.28(1→10) shows the metallographic changes from the wear surface towards the bulk of the material.

-142-

Figure 3.26. Scanning Electron Micrographs of Bronze E Worn Pin
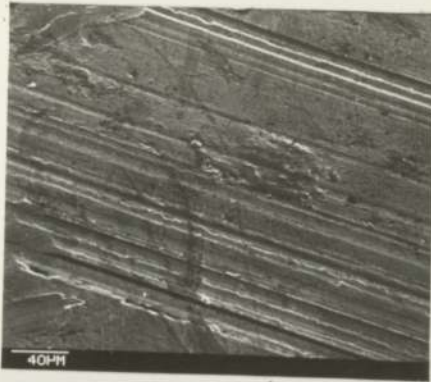
a. Wear at $98N - 4ms^{-1}$.
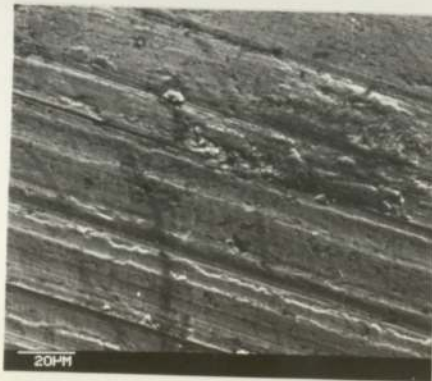
b. Heavily striated surface

Figure 3.27. Taper Section of Bronze E Worn Pin and Distribution of Alloying Elements

Bakelite surface

a. Tapered and unetched surface
98 N — 4 m s⁻¹

b. Showing sub-surface cavities

c. Copper

d. Nickel

e. Iron

f. Aluminium
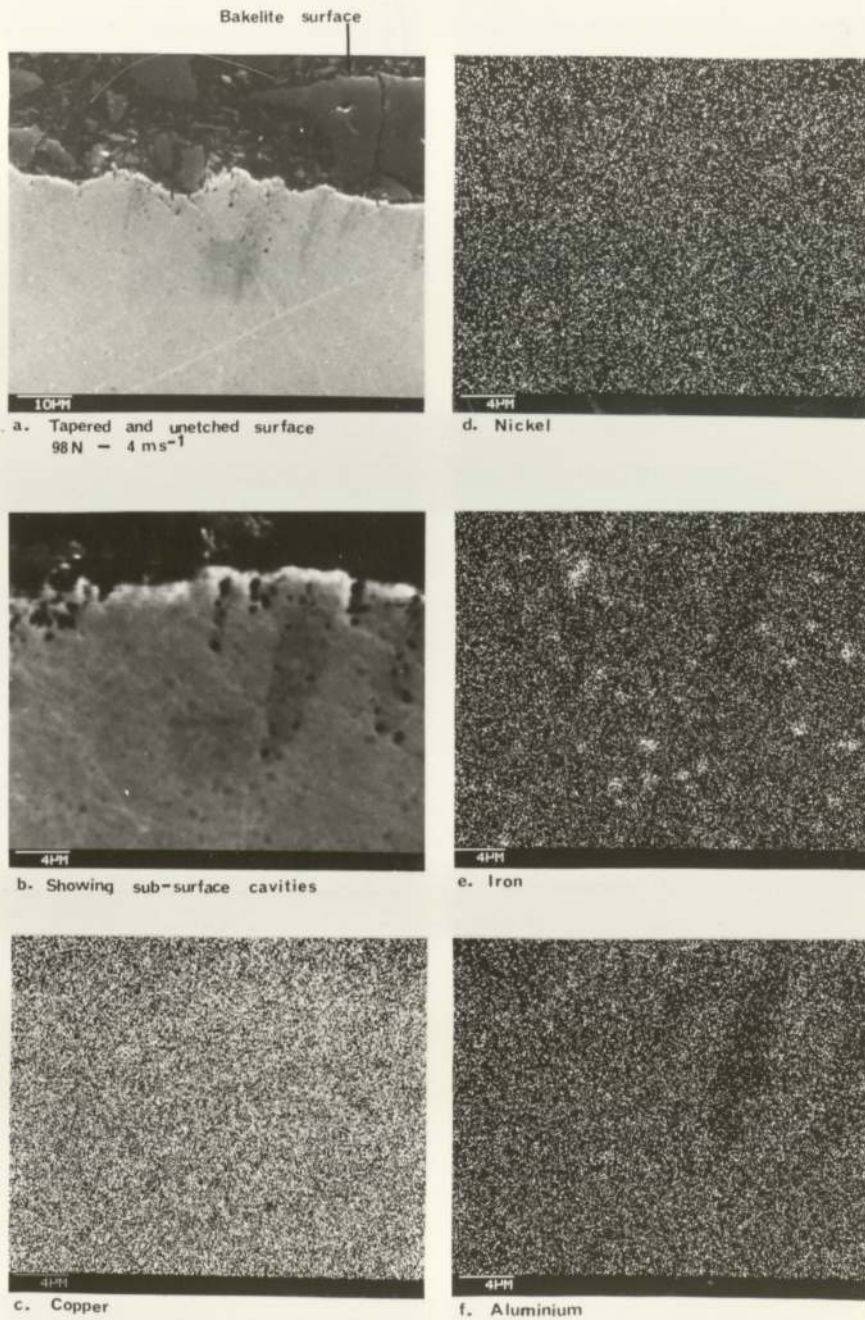
Figure 3.28. Taper Section Showing Metallographic Changes

Heavily deformed sub-surface layer
98 N — 4ms^{-1} — without additive

starting from top layer towards
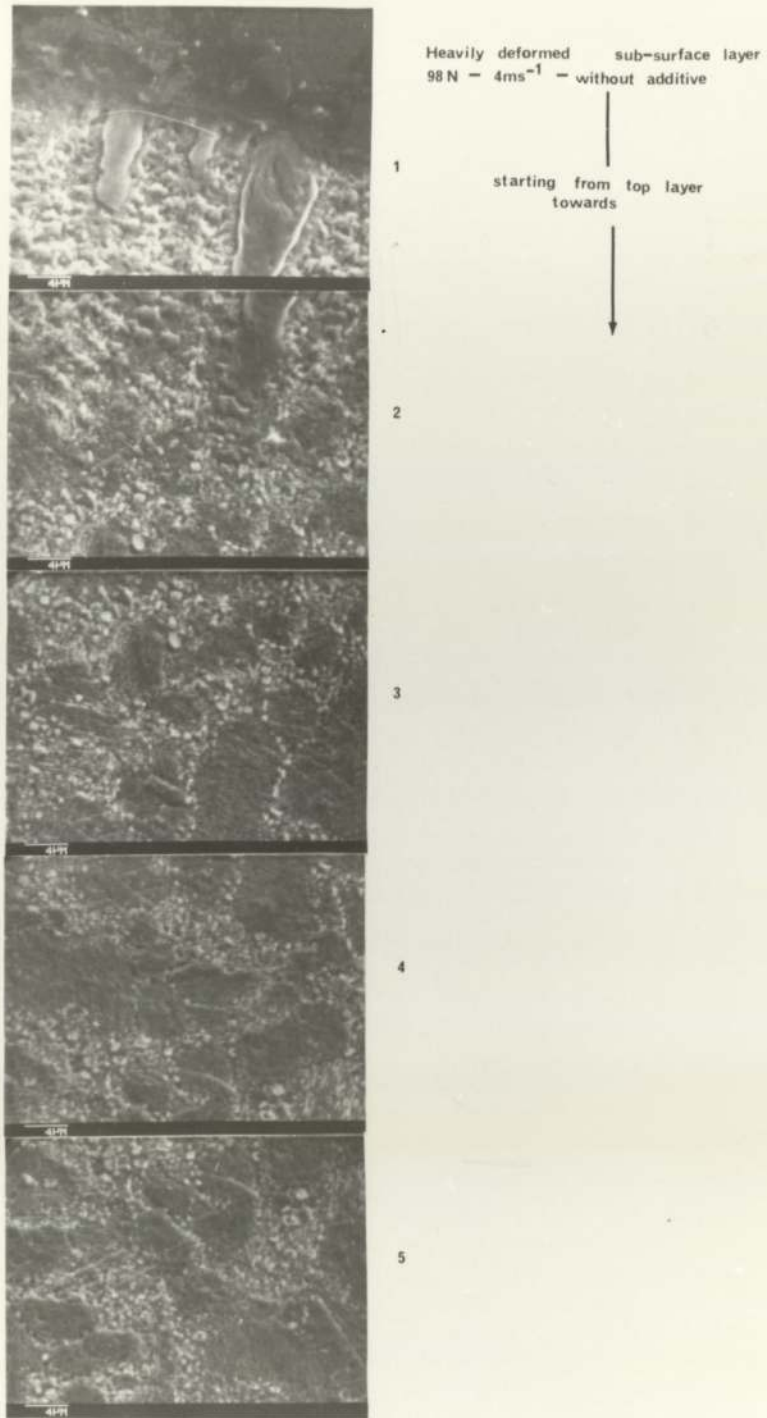
bulk structure

The heavily deformed layer extended to a depth of about
4 μm where the morphologies of various phases were not
capable of identification. The morphologies of the α
phases and its subsequent Fe-K precipitates could only
be recognizable below the deformed layer in the bulk
material.

(ii)Fuel with Hitec E580

A typical example of a tapered and etched surface of
a 2 mm diameter Bronze E(Delta) pin, worn with the additive,
is shown in Figure 3.29. Unlike the Bronze B(Poole Type I)
worn pin (figure 3.24), the degree of surface deformation
was much less severe and extended to a depth of less than
1 μm. The deformed layer was not as pronounced as the
Bronze B(Poole Type I) worn pin (figure 3.24), indicating
that the Bronze E(Delta) has better wear resistance.
Aluminium depletion was also detected at the worn surface
of the Bronze E(Delta) pin (figure 3.29(e)).

The severity of the surface deformation at high load
and high speed (147N - 4 ms^{-1}) was also investigated as shown
in Figure 3.30. The unetched taper section indicates a
mechanism of wear at the region below the worn surface.
Cavities have been observed to form below the rubbing
surface during superplastic shear deformation of the Bronze
E(Delta). Figures 3.31(a) to (e) show the tapered surface
and its elemental distributions. Clearly, the depletion of
aluminium was detected to about 1 μm depth from the worn
surface (figure 3.31(e)). Figure 3.32 shows one of the wear
particles just about to breakdown. This particle had been

-147-

Figure 3.29. Scanning Electron Micrographs of Bronze E Worn Pin and Distribution of Alloying Elements

Bakelite surface

a. Tapered and etched surface
24·5 N — 0·6 ms⁻¹ — Hitec E 580

d. Iron

b. Copper

e. Aluminium

c. Nickel

f. Manganese
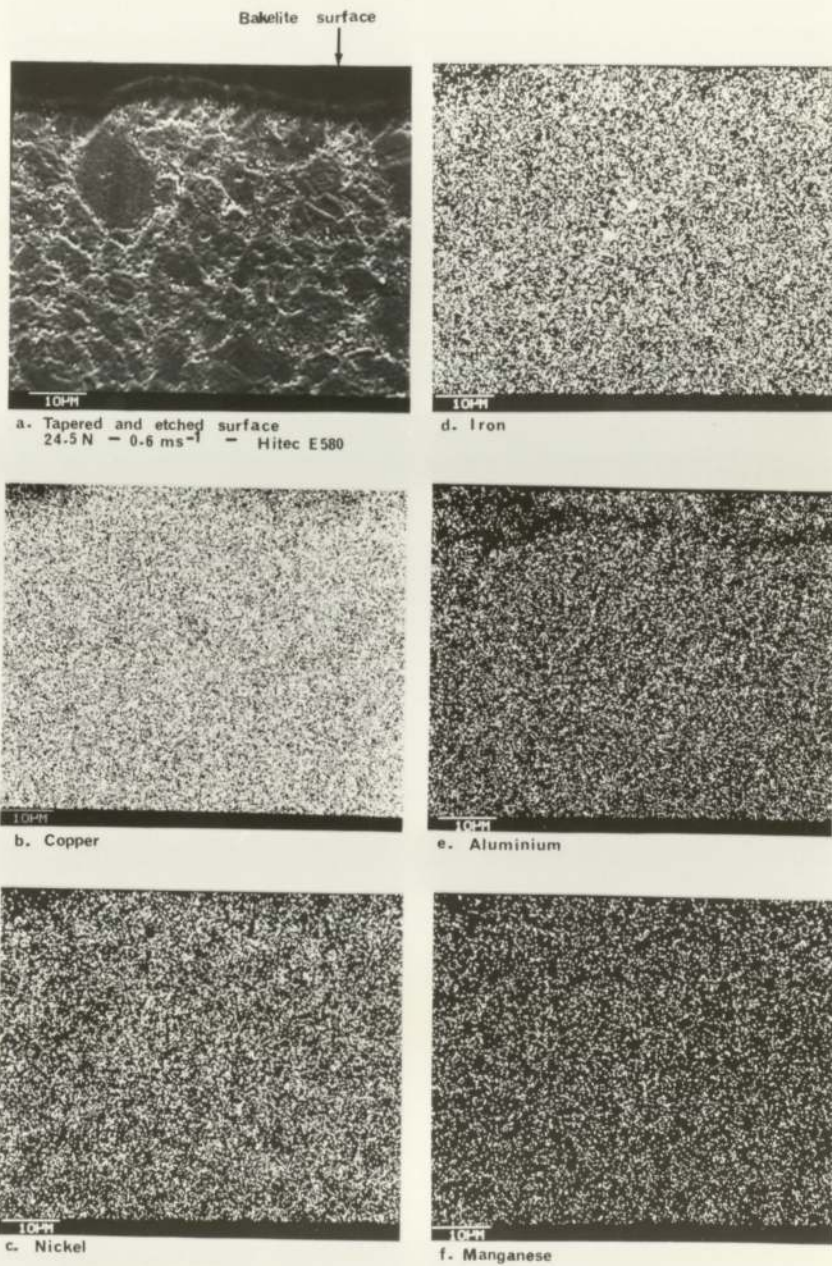
Figure 3-30. Scanning Electron Micrographs of Bronze E Worn Pin at
High Load and High Speed
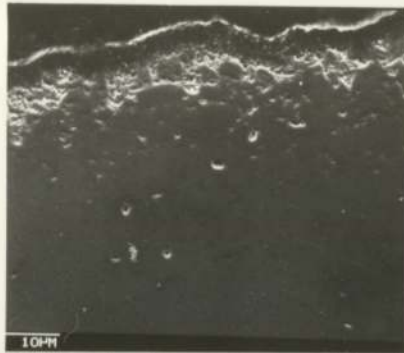
a. Tapered surface showing severe deformation
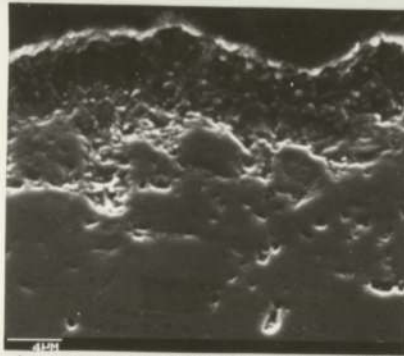
b. Sub-surface deformation with cavities

c. Superplastic shear deformation

—149—

Figure 3.31. Scanning Electron Micrographs of Bronze E Worn Pin and Distribution of Alloying Elements
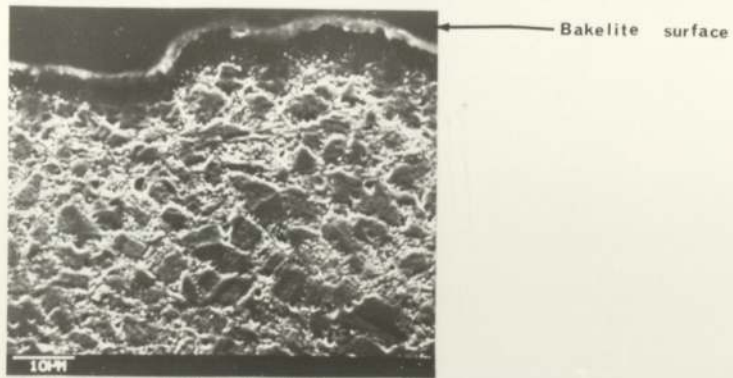
a. Tapered and etched surface
   147 N — 4ms^{-1}

b. Copper

d. Iron

c. Nickel

e. Aluminium

—149—
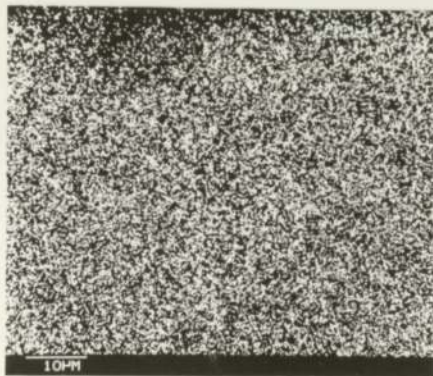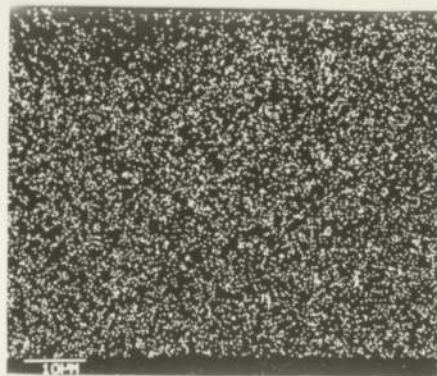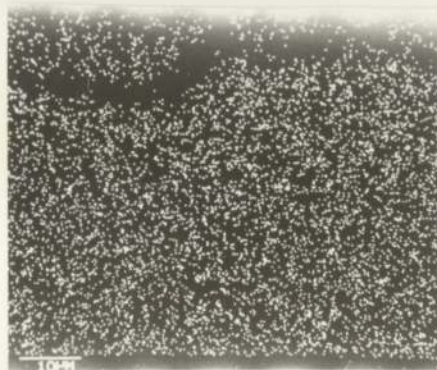
Figure 3.32. Scanning Electron Micrographs of Wear *particle*

← Bakelite surface

10ɥM
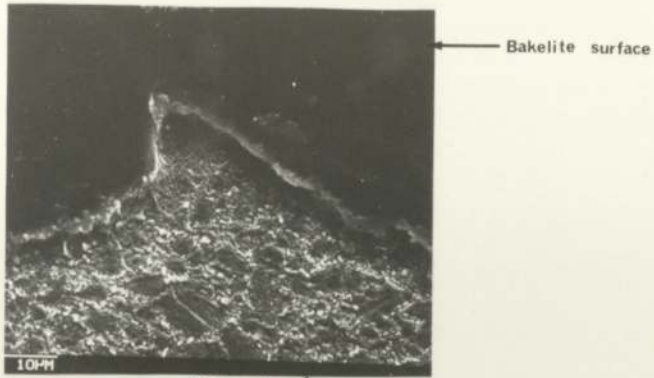
a. Wear *particle* 147N — 4ms⁻¹ — Hitec E580

4ɥM
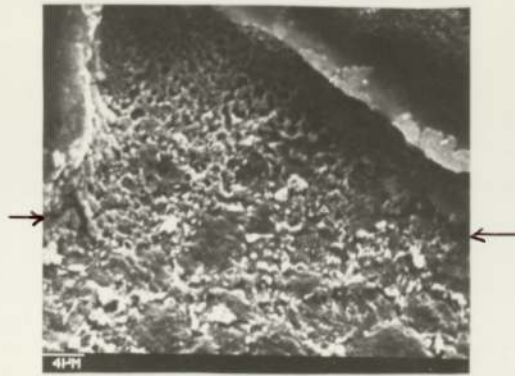
b. Showing a *particle* about to break

2ɥM
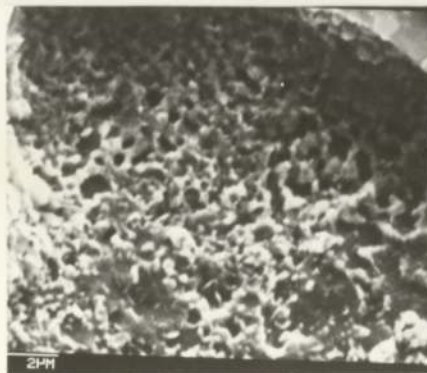
c. *Severe disruption*

Figure 3.33. Taper Section Showing Metallographic Changes

Heavily deformed sub-surface
layer   147 N – 4ms^{-1} – Hitec E580

1

starting from top layer
towards

2

3

4
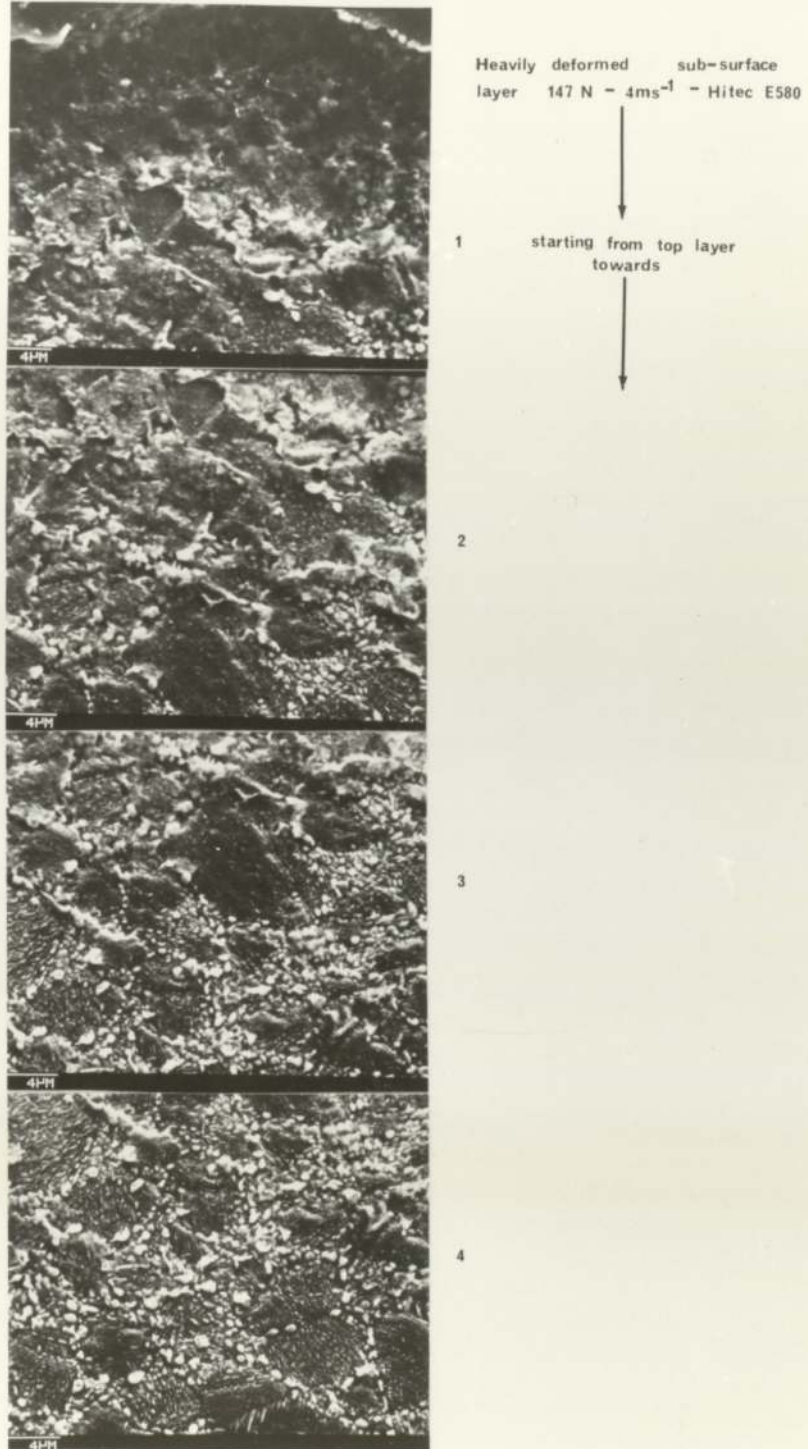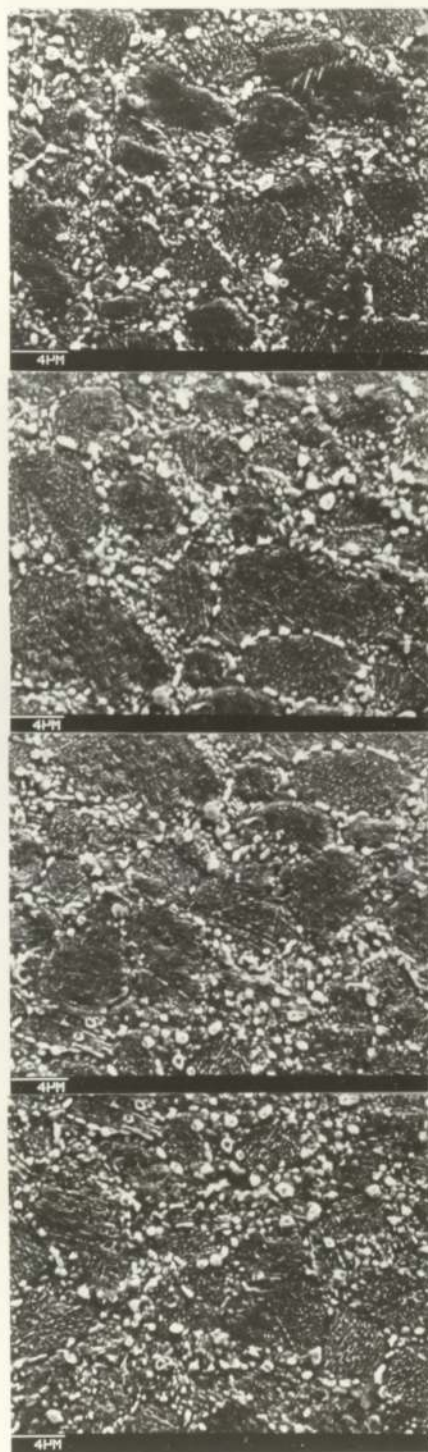
bulk structure

heavily disrupted with the interlinkage of cavities causing the
wear particle to break (figure 3.32(b)). In the case of
high load and high speed boundary lubricated sliding wear,
the degree of surface deformation extended to a
depth of more than 10 μm as shown in Figure 3.33.

3.8.5 Analysis of the Wear Track

The wear track analysis will give important informa-
tion in the determination of material transferred
from the bronze surface to the steel counterface. The condi-
tion of the pre-wear track was described in Section 2.4
showing the principle elemental intensities of iron and
chromium and the background intensities of aluminium, silicon
and sulphur respectively. The wear tracks were analysed
after being worn with fuel alone and with additive.

(i) Wear Track (Fuel Alone)

The wear track after being worn under a load of 196N
at 2 ms^{-1} is shown in Figure 3.34. Two areas of the wear
track were analysed, together showing the principle elemental
scans of iron, chromium, copper, and aluminium. Area A is
much smoother than Area B where most of the lapping marks
on the pre-wear disc surface had been removed or covered
with a thin film or oxide. In both areas, the transfer of
aluminium is high compared to the background aluminium inten-
sity of the pre-wear disc surface (figure 2.4(d)). The
transferred aluminium has a unique pattern of transfer lines
which followed the direction of wear. This heavy aluminium
transfer line probably corresponds to the maximum numbers of

contacts between bronze pin and steel disc surfaces.

Figure 3.35 shows another wear track worn under a load of 122.6N at 4 ms^{-1}. The surface condition of the wear track was very rough showing a great deal of metallic transfer. This heavy metallic transfer corresponded closely to the copper X-ray scan. The aluminium appears to be transferred more to the smoother side of the wear track.

A perpendicular section of the wear track was made to determine the depth of aluminium diffusion and this is shown in Figure 3.36. The depth of aluminium diffusion is difficult to measure between the edge of the wear track and sectioned surface. But a great contrast is apparent between these two faces where there is a great deal of Cu, Al and S on the wear track compared to the unworn sectioned surface.

(ii) Wear Track (Fuel with Hitec E580)

Figure 3.37 shows a typical wear track worn under a load of 196N at 4 ms^{-1}. The additive appears to have increased the load carrying capacity without causing failure and reduced the coefficient of friction. The wear track has a much smoother surface and is without obvious sign of metal transfer. The rate of aluminium transfer has also been reduced as shown in Figure 3.37(e) when compared to those worn under similar conditions with no additive (figure 3.35).

In both cases, whether with or without additive, sulphur was detected on the wear track surface which originates from the base fuel.

Figure 3.34. Scanning Electron Micrographs of Wear Track and Distribution of Alloying and Transferred Elements
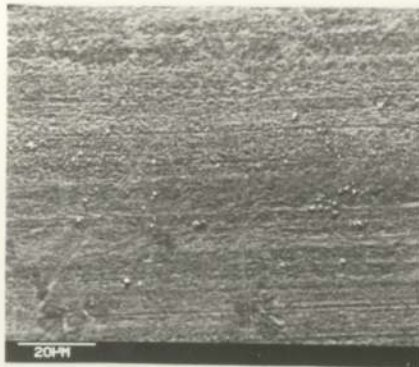
a. Area A   196 N — 2 ms^{-1}

b. Iron
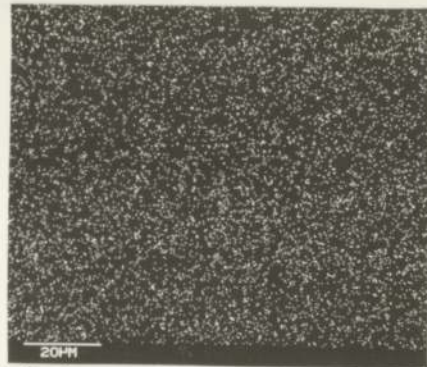
d. Copper
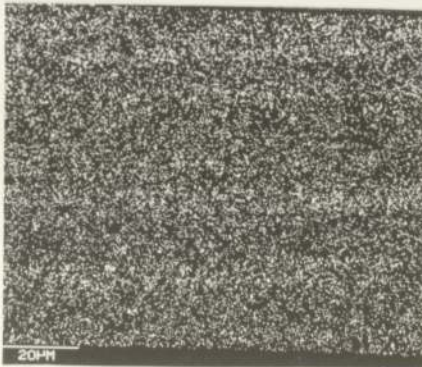
c. Chromium

e. Aluminium

a. Area B
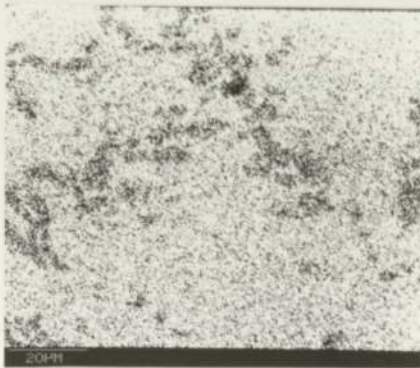
b. Iron
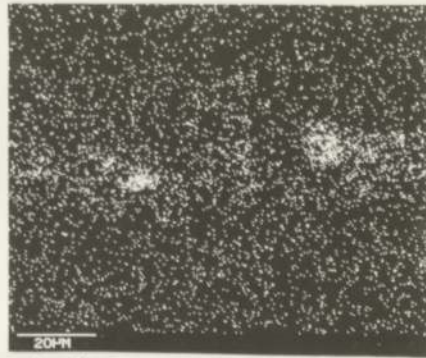
d. Copper

c. Chromium
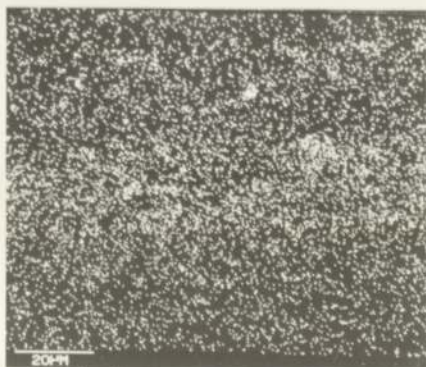
e. Aluminium

Figure 3.35. Scanning Electron Micrographs of Wear Track and Distribution of Alloying and Transferred Elements
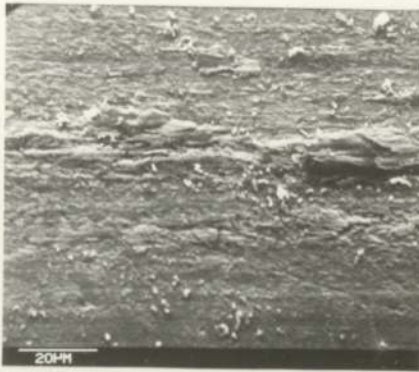
a. Worn track surface 122.6 N — 4ms⁻¹
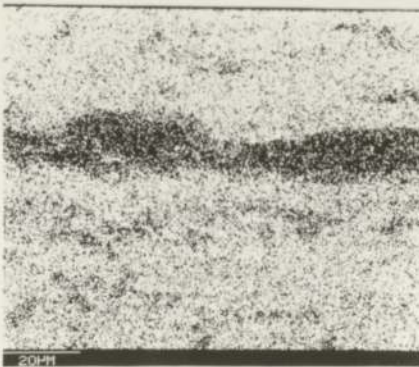
b. Iron
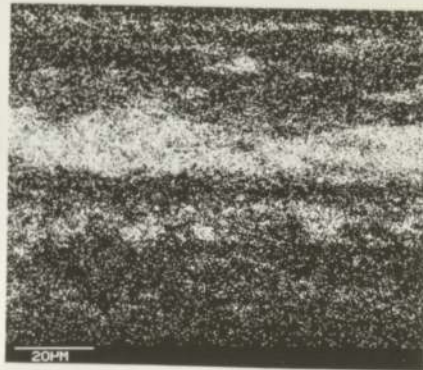
d. Copper
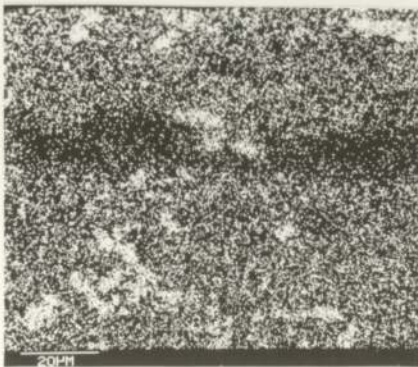
c. Chromium
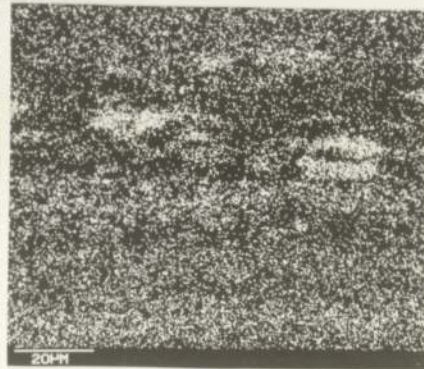
e. Aluminium

Figure 3.36.   Scanning Electron Micrographs of Taper Wear Track   and
Distribution of Alloying and Transferred Elements

a. Perpendicular sectioned along the direction
of wear track   122.6 N — 4ms⁻¹

d. Copper

b. Iron

e. Aluminium

c. Chromium

f. Sulphur
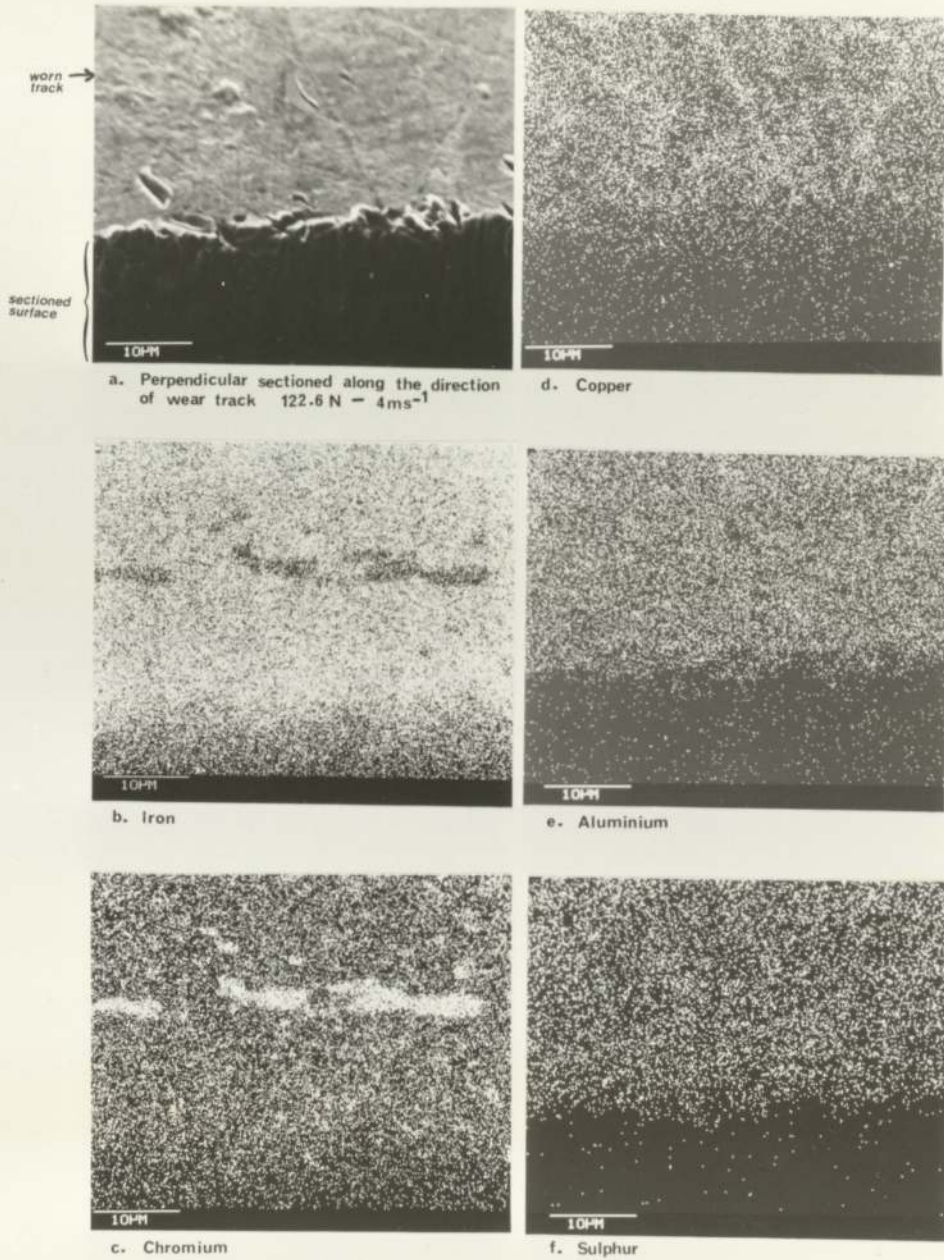
Figure 3.37. Scanning Electron Micrographs of Wear Track and Distribution of Alloying and Transferred Elements

a. Disc surface before wear
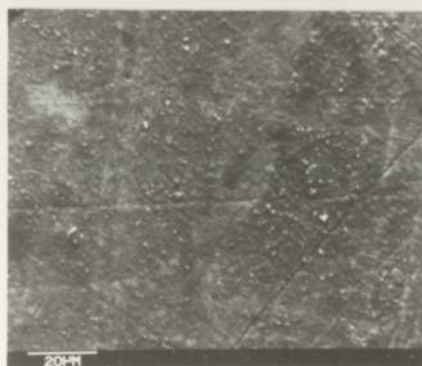
b. After wear 196 N — 4ms⁻¹ — Hitec E580

d. Chromium

c. Iron

e. Aluminium

3.8.6 <u>Analysis of the Wear Debris</u>

The results of the X-ray analysis of the wear debris
are listed as shown in Table 3.3. The measured 'd' spacings
are given in descending order according to the intensities
of the diffraction lines. The resultant diffraction pattern
mainly consisted of six identical lines for both fuel with
and without additives. Irrespective of the speeds and loads,
copper and copper oxide were the two main components detected.
Aluminium and other solute elements of bronze were not
detected in the wear debris due to insufficient quantities
for detection, i.e. ~2%.

The SEM analysis of wear debris is an alternative
method to detect small quantity of solutes present in bronze.
The wear debris was mixed with graphite dispersion so that it
could stick onto the pure nickel plated surface of the
mounting stud. The pure nickel plating was used because
the mounting stud,used in SEM, contained aluminium. Figures
3.38 and 3.39 show the SEM micrographs of the wear debris,
both with and without additive. In both cases, aluminium
was detected, revealing a small quantity present in the
wear debris.

TABLE 3.3   X-RAY ANALYSIS OF WEAR DEBRIS

"d" Spacings

	ASTM File Values			Fuel Alone			Fuel with Hitec E580		
				24.5 to 196N $0.6\ ms^{-1}$	122.6N $4\ ms^{-1}$	196N $4\ ms^{-1}$	196N $2\ ms^{-1}$	24.5N $4\ ms^{-1}$	196N $4\ ms^{-1}$
Aluminium	2.34	2.02	1.22	2.09	2.08	2.08	2.08	2.08	2.08
Aluminium Oxide	2.55	2.09	1.60	1.81	1.80	1.80	1.80	1.80	1.80
Copper	2.09	1.81	1.28	2.48	2.46	2.46	2.46	2.46	2.46
Copper Oxide (Cu_2O)	2.47	2.14	1.51	1.28	1.28	1.28	1.28	1.28	1.28
Iron	2.03	1.71	1.43	1.09	1.09	1.09	1.09	1.09	1.09
Nickel	2.03	1.76	1.25	1.04	1.04	1.04	1.04	1.04	1.04
				3.33					
				3.04					

Figure 3.38. Scanning Electron Micrographs of Wear Debris and Distribution of Elements

a. Wear debris mixed with graphite
122.6 N — 4ms⁻¹

b. Copper

d. Iron

c. Nickel

e. Aluminium

-163-
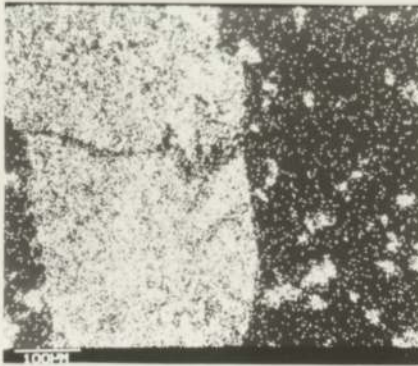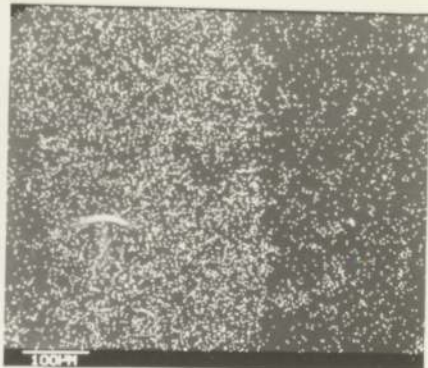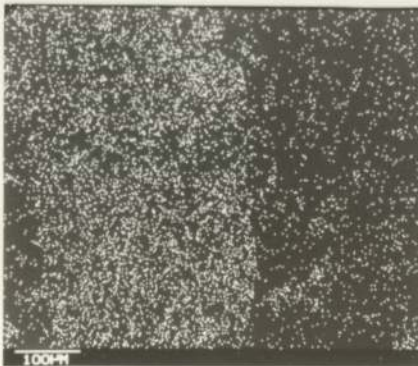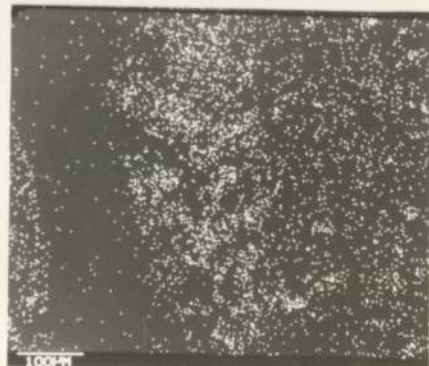
Figure 3.39. Scanning Electron Micrographs of Wear Debris and Distribution of Elements

a. Wear debris mixed with graphite
122.6 N — 4 ms⁻¹ — Hitec E 580
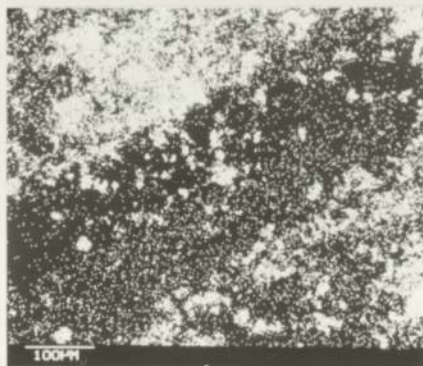
b. Copper
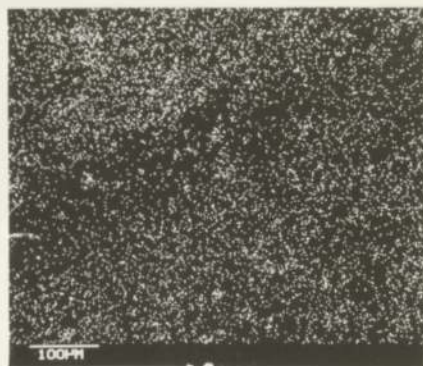
d. Iron

c. Nickel
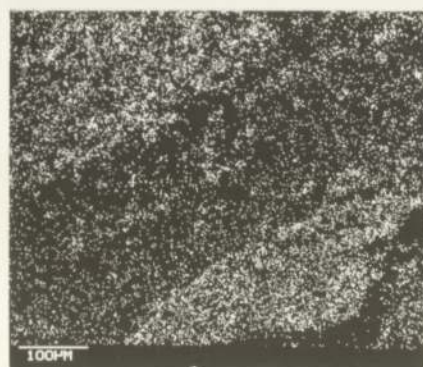
e. Aluminium

3.9 Results of Electron Probe Microanalysis on Worn Surfaces

The worn pins were analysed, using electron spot analysis, to determine the depletion of aluminium on the surfaces. After the corrections for the atomic number effect, absorption and fluorescence effects, a statistical analysis on a true percentage concentration of aluminium was calculated to present the spread of the results. Figures 3.40 to 3.42 are the plots of aluminium concentration on worn pin surfaces versus load for the speeds of 0.6, 2.0 and 4.0 ms^{-1} respectively. In all cases, the degree of aluminium depletion on worn surfaces was generally increased with load with the exception that high wear rates had a tendency to expose the original bulk aluminium concentration. It seemed that the increase in surface temperatures has the effect of escalating aluminium diffusion, thus allowing more aluminium transfer to the steel counterface. Figure 3.42 (Fuel with additive) has shown that the percentage of aluminium concentration could be as low as 2% on the worn surface. For the fuel alone at 4 ms^{-1}, bulk concentrations of aluminium were detected, due to the failures of the pins at 147N and $196N$ loads.

Using electron spot analysis, the pre-wear and worn track surfaces were also scanned so that comparison could be made to detect the bronze transferred to the steel track. Table 3.4 shows the results of the spots analyses for elements Cu, Al, Ni, Fe and Cr, for fuel alone and for fuel with Hitec E580. In both cases, a great deal of Cu and Al had transferred to the steel surface.

Figure 3.40 Aluminium Concentration Versus Load — 0·6 ms⁻¹ –2 mmφ Bronze E Pins
(Denison Wear Rig)
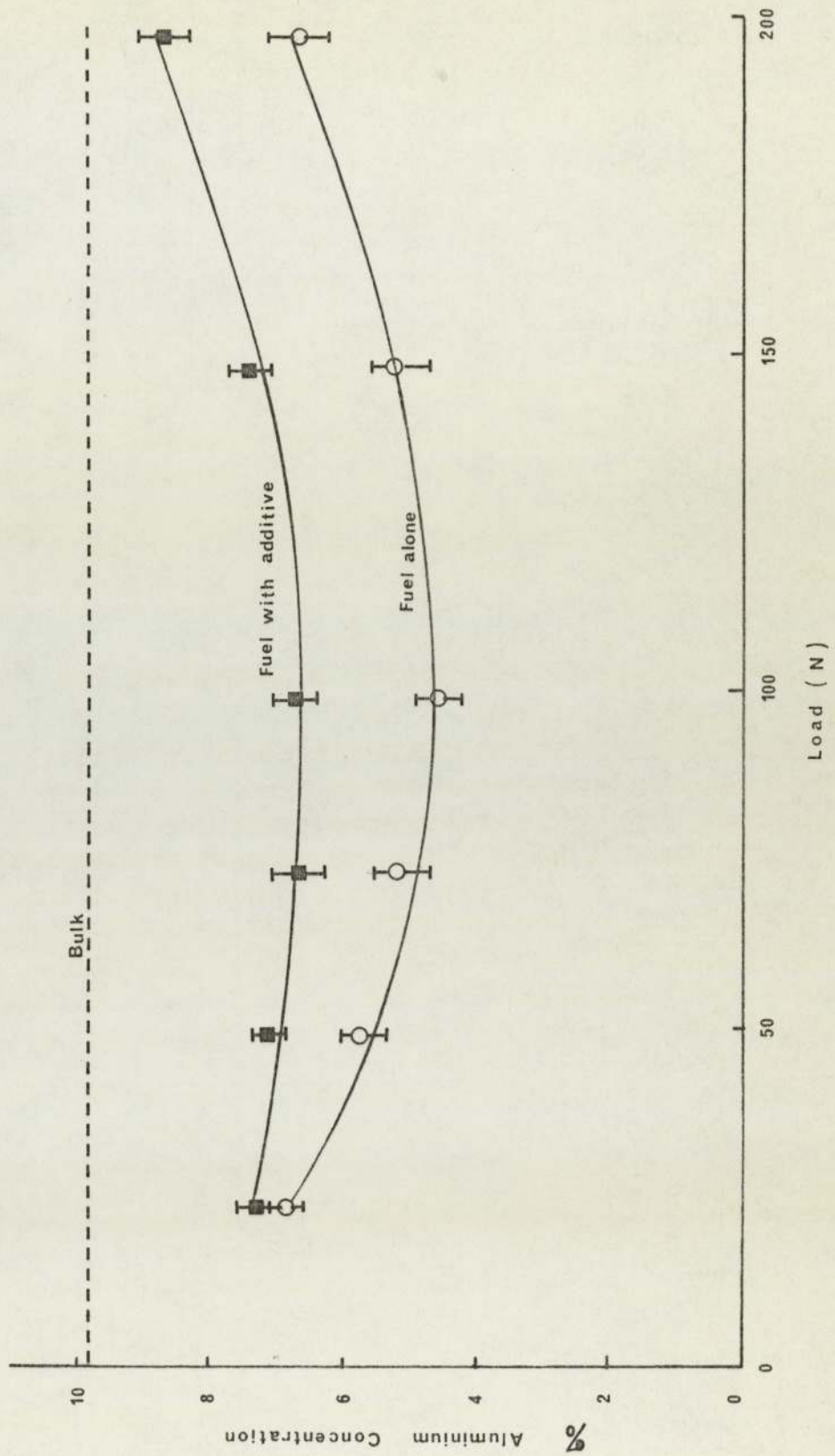
Figure 3.41 Aluminium Concentration Versus Load — 2 m s⁻¹ – 2 mmφ Bronze E Pins (Denison Wear Rig)

Figure 3 42   Aluminium   Concentration   Versus   Load — 4 m s⁻¹ –2 mmφ Bronze E Pins
(Denison Wear Rig)
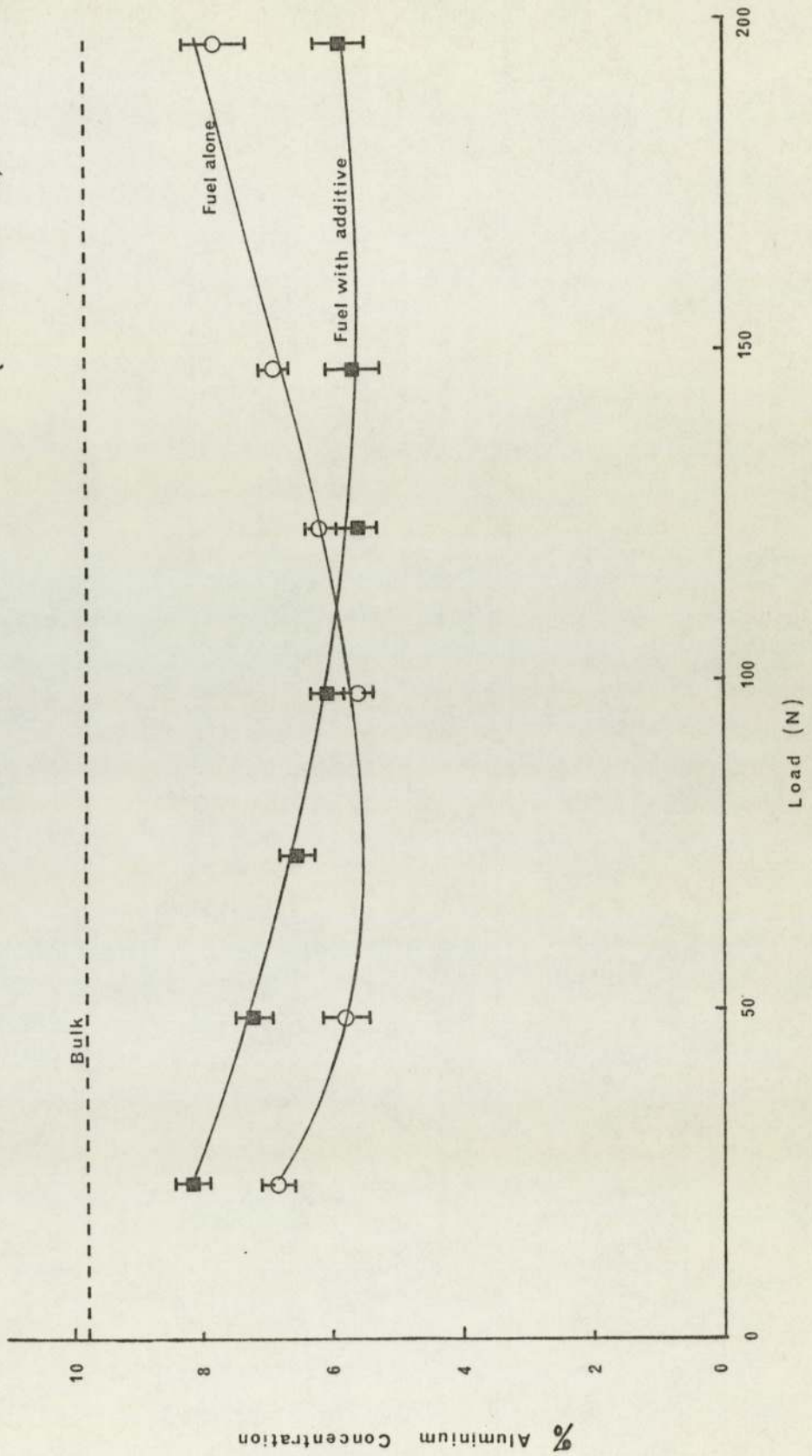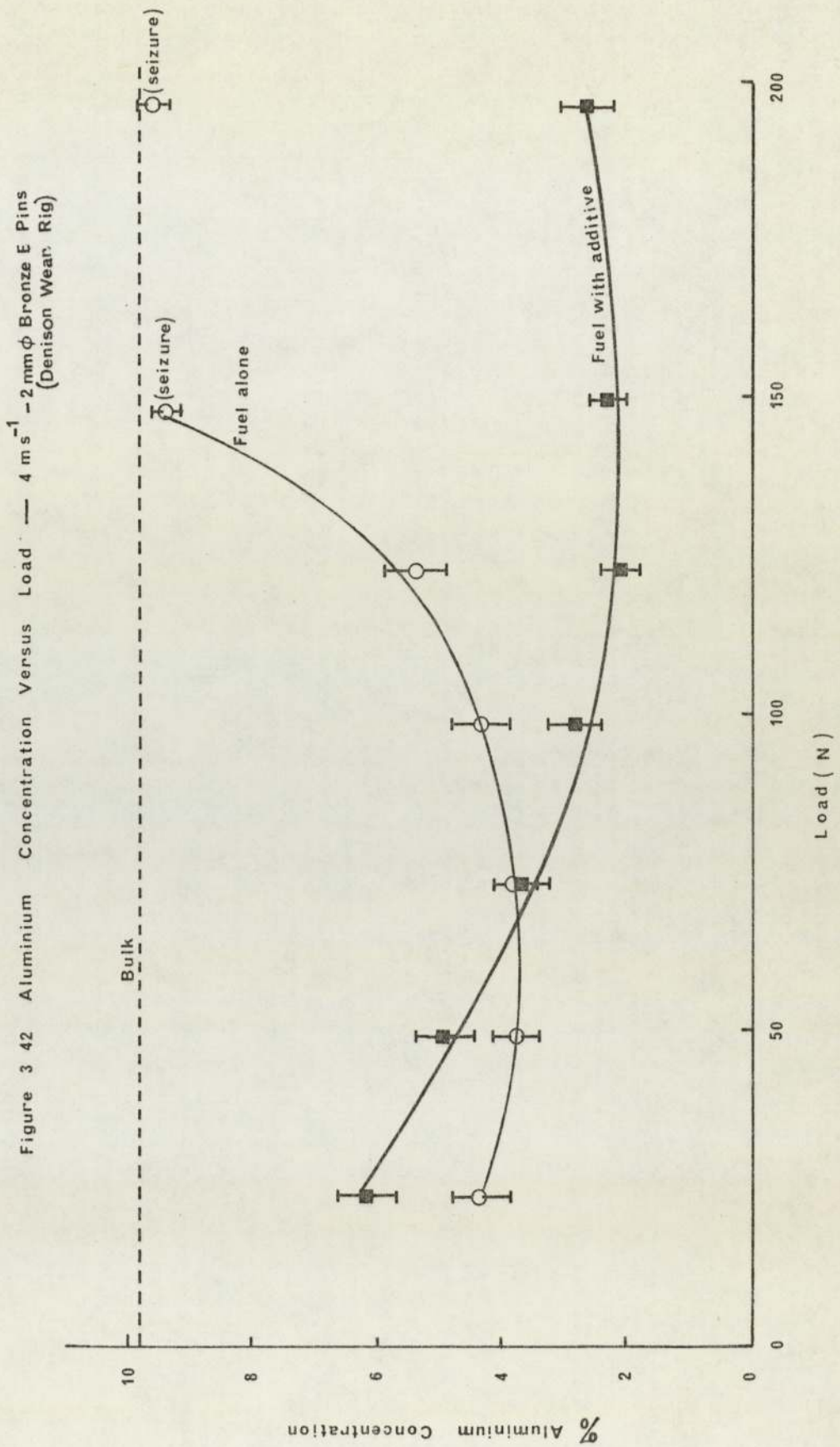
TABLE 3.4   ELECTRON PROBE MICROANALYSIS ON STEEL TRACK
Atomic concentration of elements expressed as percentage

Position	Unworn Disc Surface					Worn Track Surface 196N-2ms^{-1}-Fuel with Hitec E580					Worn Track Surface 196N-2ms^{-1}-Fuel Alone				
	Cu	Al	Ni	Fe	Cr	Cu	Al	Ni	Fe	Cr	Cu	Al	Ni	Fe	Cr
1	0.184	0.246	0.042	81.843	15.378	0.749	0.754	0.302	83.038	12.812	2.262	1.115	0.688	75.894	16.559
2	0.207	0.275	0.042	80.938	15.361	0.782	0.725	0.333	82.617	12.917	4.094	1.049	0.593	76.728	14.127
3	0.163	0.058	0.251	82.710	12.518	0.737	0.753	0.364	82.213	13.799	3.906	1.429	0.613	79.287	11.951
4	0.153	0.072	0.125	76.910	17.844	0.608	0.696	0.323	81.935	13.619	4.897	1.374	0.697	78.282	11.325
5						0.794	0.696	0.385	81.989	12.989	4.124	0.998	0.570	79.482	11.189
6						0.903	0.813	0.407	82.227	12.166	2.543	1.237	0.562	80.995	11.567
7						0.923	0.943	0.427	82.229	13.027	4.707	1.416	0.695	79.367	11.850
8						1.407	0.956	0.428	77.225	15.442	1.957	1.250	0.521	81.284	11.809

3.10 Results of Auger Electron Spectroscopy on Worn Surfaces

(i) Bronze A

The surfaces of the pins worn with and without additives were examined at four different locations, namely location A, B, C and D. In both cases the depth profile analyses were carried out only at location D (i.e., near the centre of the pin), by sputtering their surfaces with 0.5 KV Argon ions whilst monitoring the peak intensities of the elements of interest (i.e. C, O, Cu, Fe, and Al or S).

The spectra recorded for pins worn in the presence of fuel alone are shown in Figure 3.43. The initial spectrum, before sputtering, shows the presence of sulphur, chlorine, carbon, nitrogen, oxygen and copper at all four locations. Only at location B were weak peaks from iron and aluminium detected. After about 8 μA. minutes sputtering at location D, the iron and aluminium began to be resolved and the intensities of iron and aluminium were more clearly resolved after 200 μA. minutes sputtering. The result of depth profiling is shown in Figure 3.44. The intensity of the carbon peak falls very rapidly during the first 12 μA. minutes and then reaches a steady low level after 40 μA. minutes sputtering. The presence of carbon in the spectra at this stage could be due to a knock-on effect caused by the Argon ions. The intensity of oxygen is low, suggesting that very little oxide is present as there has been evidence of severe wear at the final stages of this test. The increase of the copper peak to a maximum and constant intensity is very rapid, probably reaching this level within 16 μA. minutes of

sputtering. However, the aluminium and iron peaks appear to reach a constant but very low intensity level in about 20 μA. minutes.

Figure 3.45 shows the spectra for pin worn with additive Hitec E580. Aluminium was detected at all four locations with the peak being most intense at location A. At this location iron was also detected and the oxygen peak was significantly more intense than at locations B, C and D. Carbon was relatively less intense at A than at B, C or D, suggesting that the overlayer was of variable thickness on the worn surface. The carbon Auger micrograph (figure 3.46) deliberately recorded with high contrast, exaggerates the non-uniformity of the overlayer. The copper and aluminium Auger micrographs show the distribution of these elements in the wear track region. The oxygen Auger micrograph suggests that this element is associated more with aluminium than copper; this tends to suggest that aluminium oxides could be present at the overlayer. X-ray diffraction analysis of debris has not however shown Al_2O_3 to be present in sufficient quantities for detection i.e. ~2%. The result of depth profiling for wear with Hitec E580 is shown in Figure 3.47. After about 8 μA. minutes of sputtering at location D (i.e. near the centre of the pin), the oxygen peak increased significantly and the iron and aluminium peaks also became more intense, but the copper peak increased only slightly. More pronounced intensities of oxygen and aluminium were recorded after about 20 μA. minutes and 12 μA. minutes respectively. The intensity of carbon falls very rapidly during the first 12 μA. minutes, but the rate of fall is more gradual than the rate for fuel alone.

Figure 3.43. Auger spectra for fuel alone – <u>Bronze A</u> worn pin (3 mm φ)
Load up to 294N (Thornton Wear Rig)
– 0.5 m s⁻¹
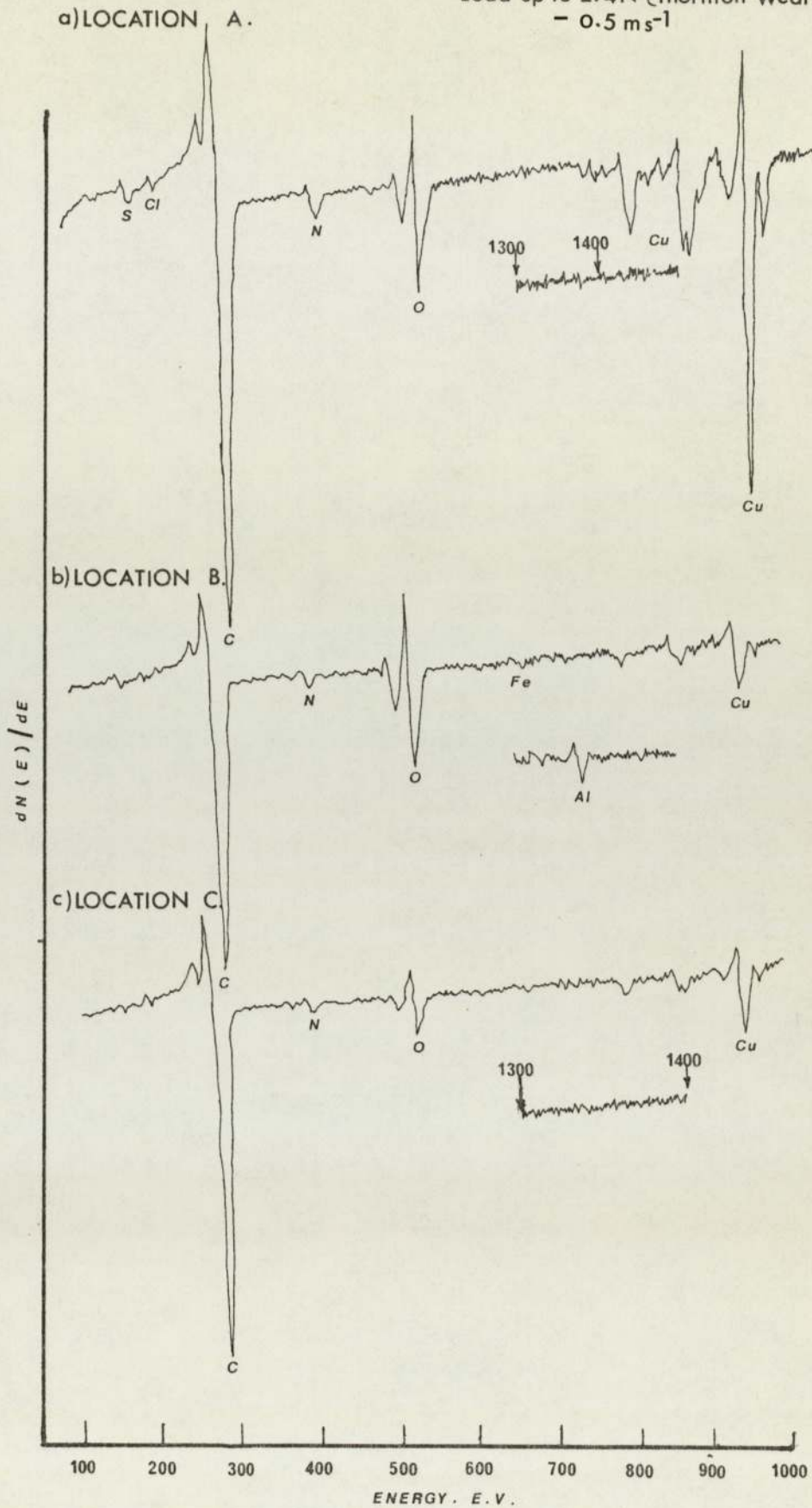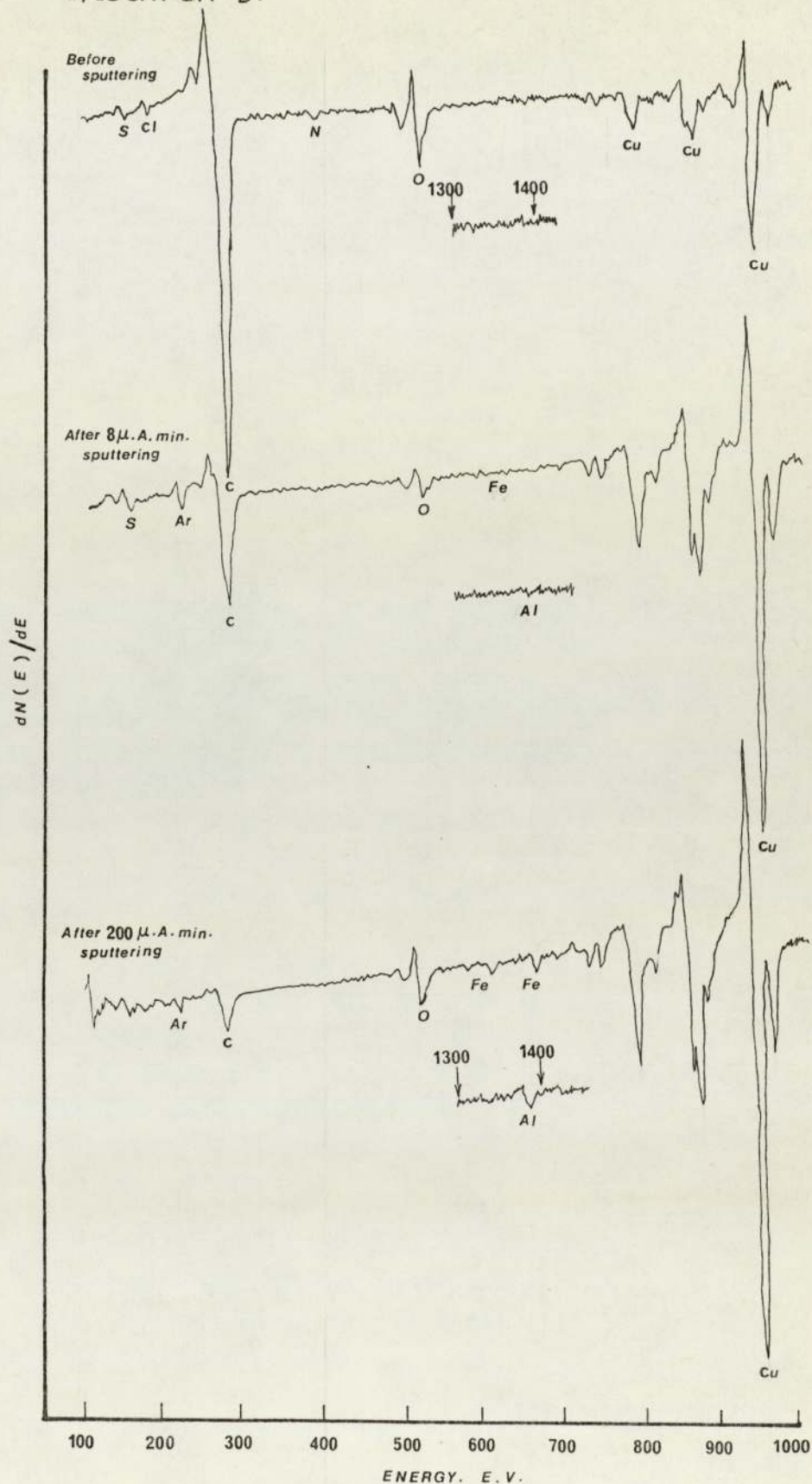
d) LOCATION D.

Figure 3.44   Auger Depth Profile — Bronze A
— Fuel alone
(Thornton Wear Rig)
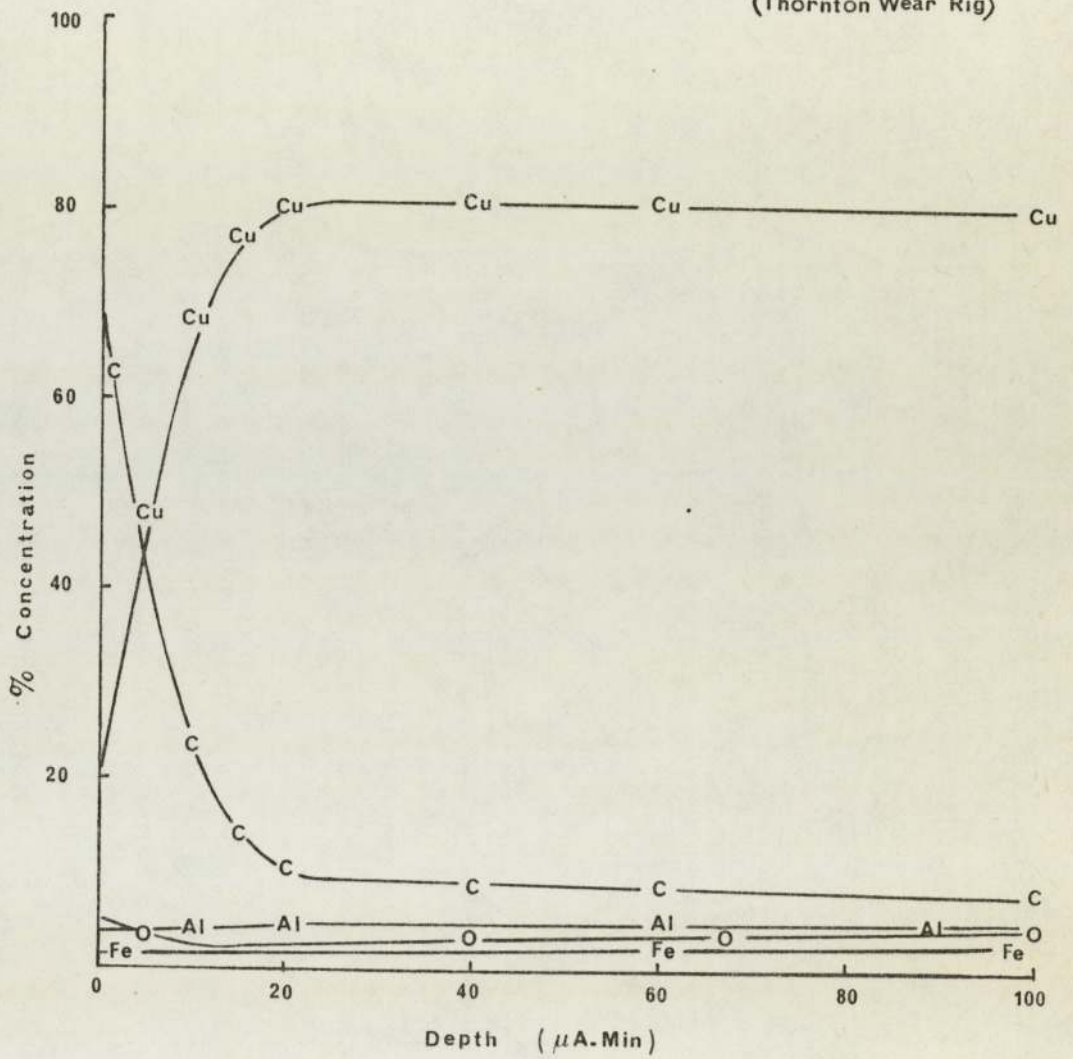
Figure 3.45 . Auger spectra for fuel with additive – <u>Bronze A</u> worn pin(3mmφ)
Load up to 294N (Thornton Wear Rig)
– 0.5m s⁻¹
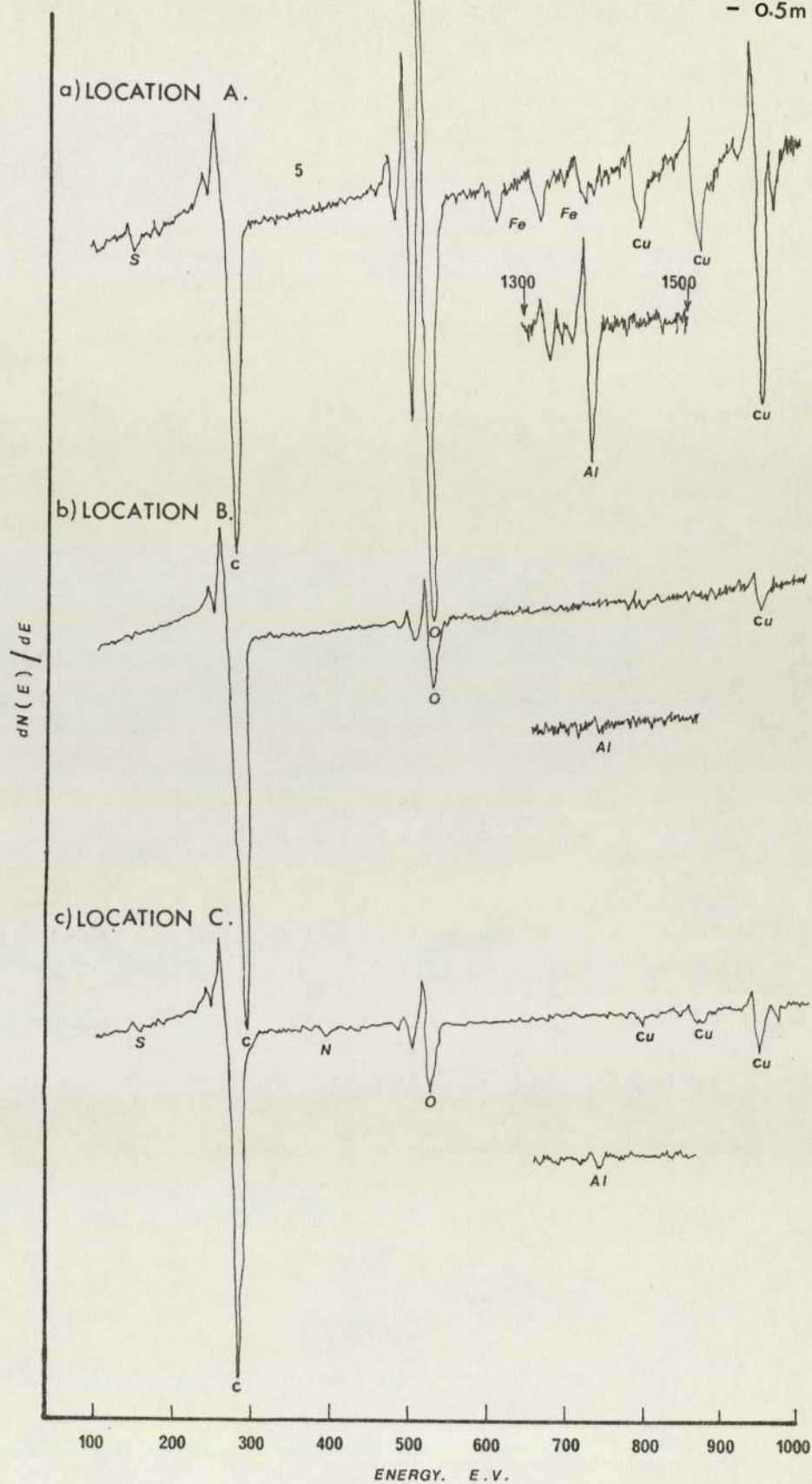
d) LOCATION D.
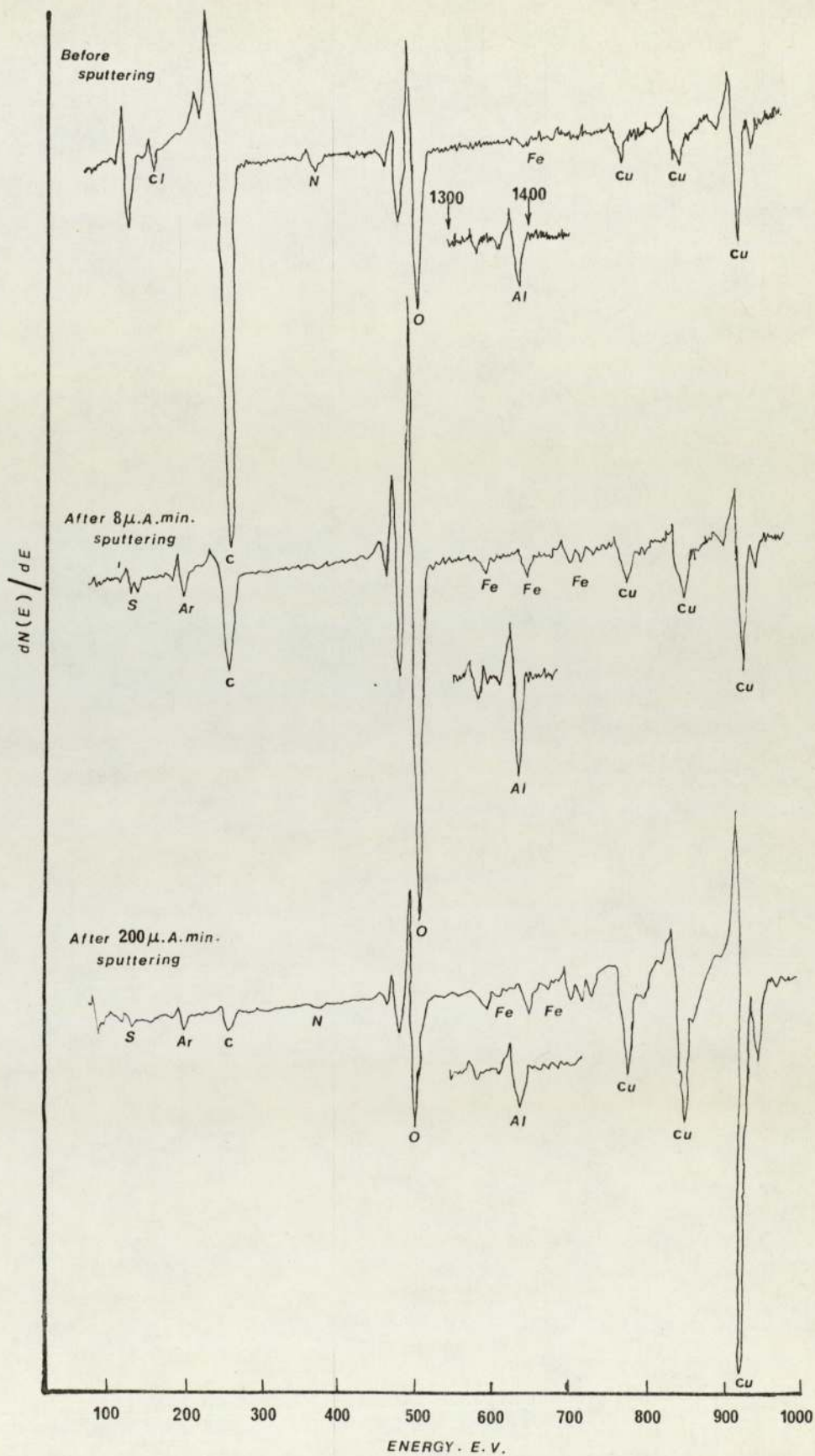
Figure 3·46. Auger micrographs for fuel with additive – <u>Bronze A</u> worn pin
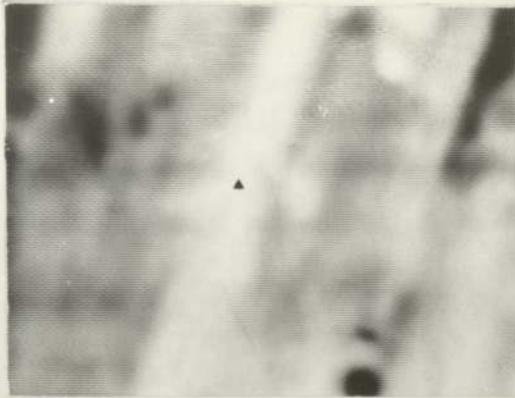
Figure 3.47 Auger Depth Profile — Bronze A
— Fuel with Hitec E580
(Thornton Wear Rig)
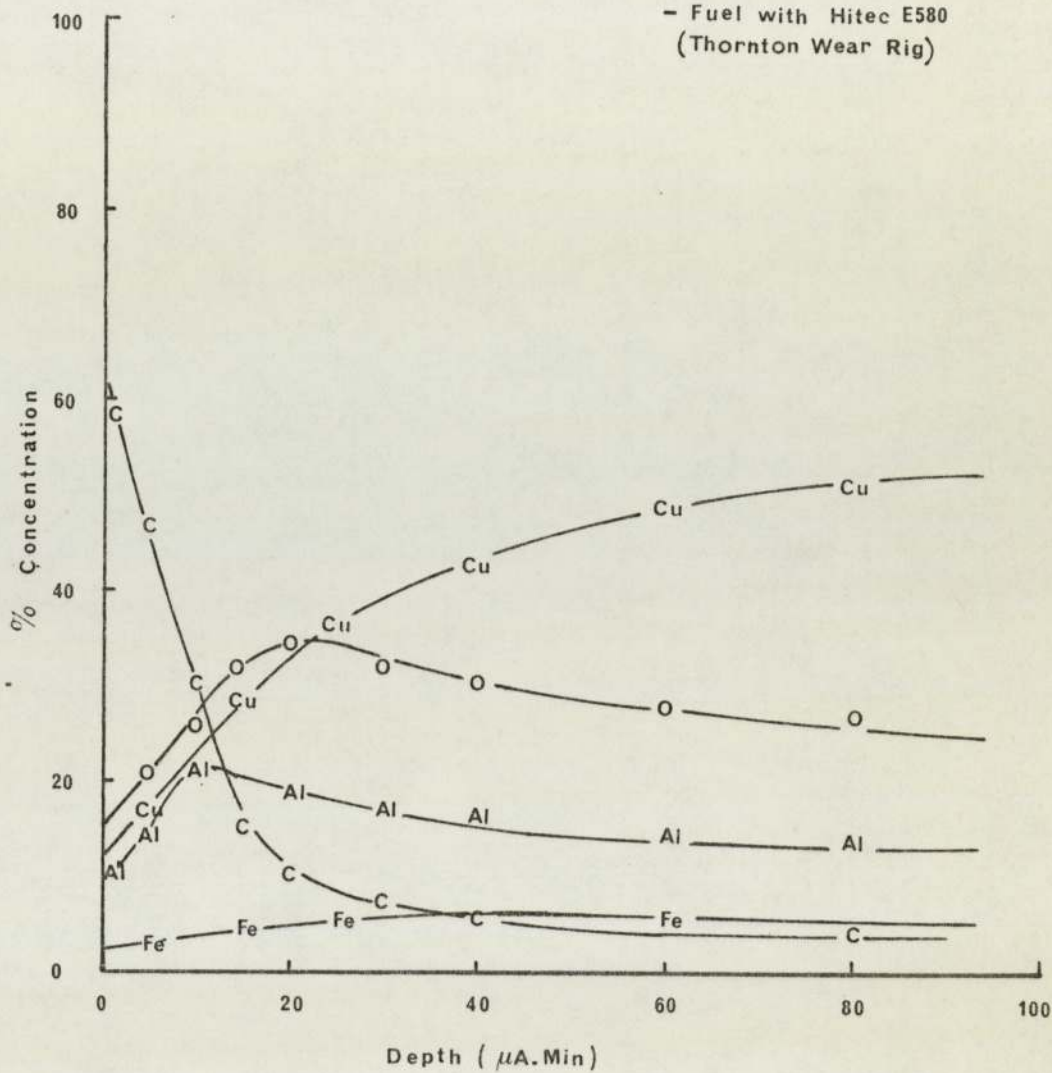
(ii)Bronze E

The spectra recorded for 74N load worn pins, in the presence of fuel alone at different speeds, are shown in Figure 3.48. The initial spectrum, before depth profiling, shows S, Cl, C, N, O, Fe and Cu present. The S and Cl peaks were effectively removed after the end of depth profiling. The iron and copper peaks became more intense for all speeds after depth profiling whilst the intensities of oxygen and carbon were subsequently reduced. Figure 3.49 shows the result of depth profiling for fuel alone. The intensity of sulphur is very low after about 20 μA. minutes sputtering. The presence of sulphur originated from the fuel. The intensity of iron remains at a constant level, i.e. reaching its bulk concentration after over 20 μA. minutes of sputtering. The oxygen profile is generally high, suggesting a thicker or more uniform oxide film formed on the surface. The carbon profile falls very rapidly to its contaminated level after about 12 μA. minutes sputtering.

Figure 3.50 shows another spectra of the same load and speed conditions, with the exception that the fuel contained Hitec E580. The spectra of all elements are generally the same as those without Hitec E580, with the exception that the carbon peaks are more pronounced. The depth profiling (figure 3.51) shows that carbon concentration is higher, suggesting a hydrocarbon layer formed on the surface due to the additive.

Results at other loads and speeds were also recorded and showed very similar trends to those shown in the above Figures.

Figure 3.48.   Auger spectra for fuel alone – Bronze E
(Denison Wear Rig)

2.0 ms^{-1} 74N
b) Before depth profiling
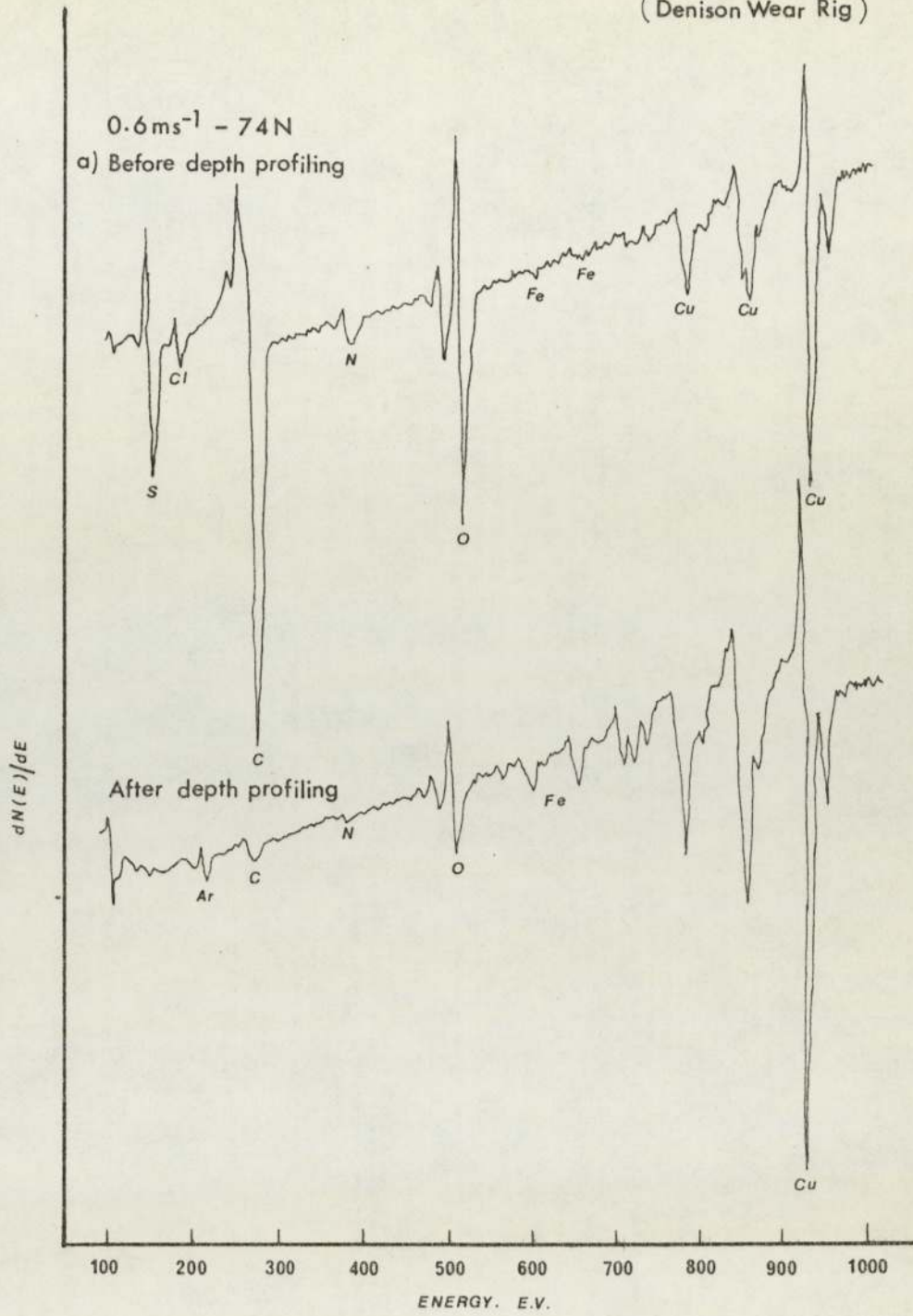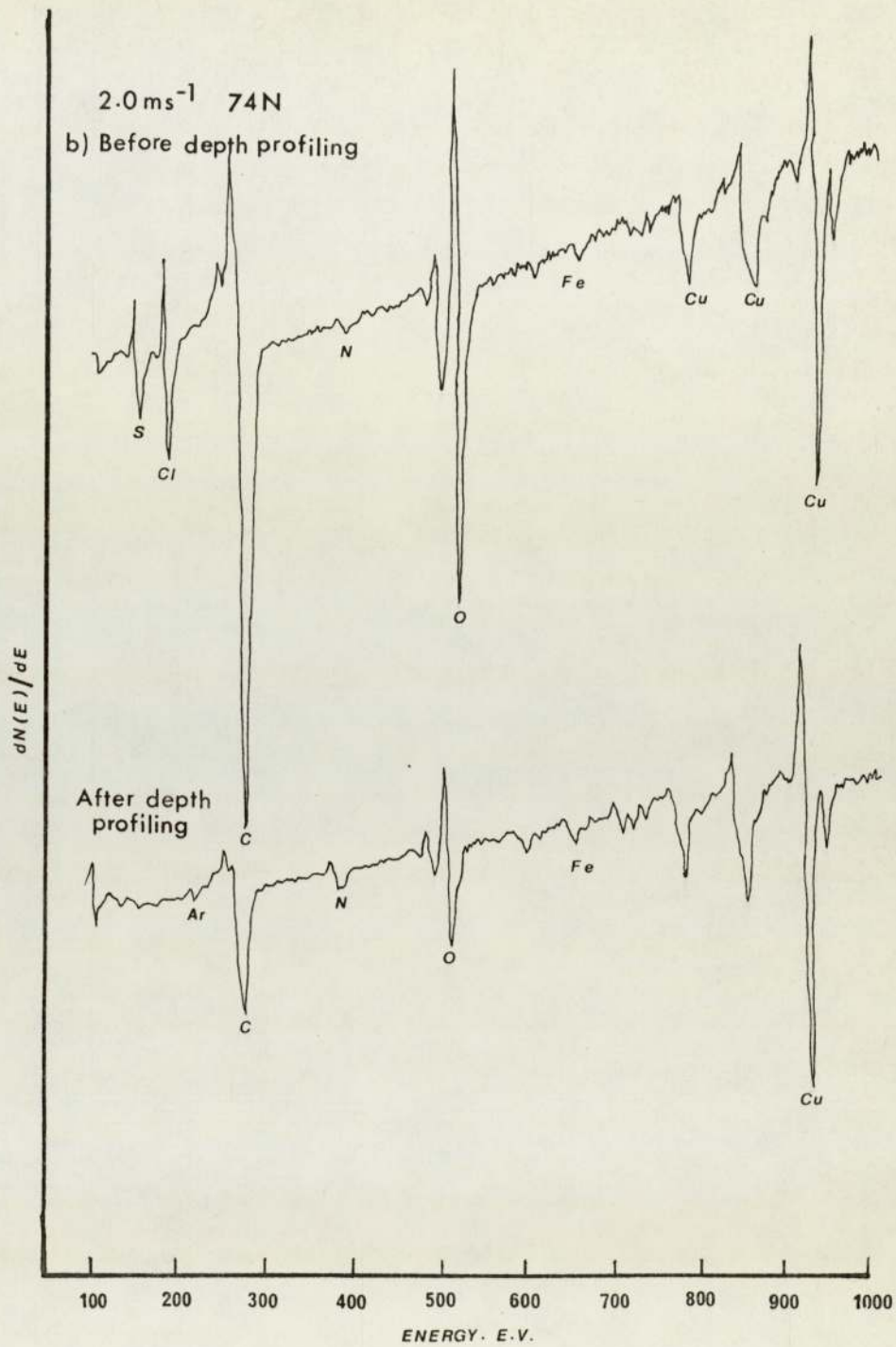
Figure 3.49 Auger Depth Profile — Bronze E
— Fuel alone
(Denison Wear Rig)
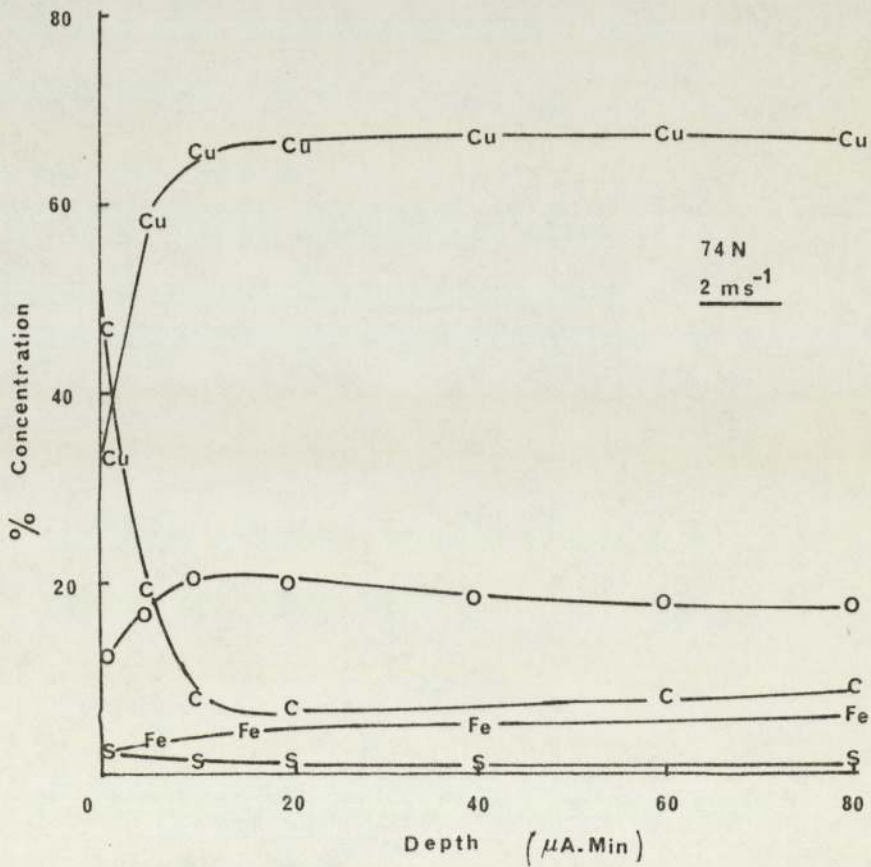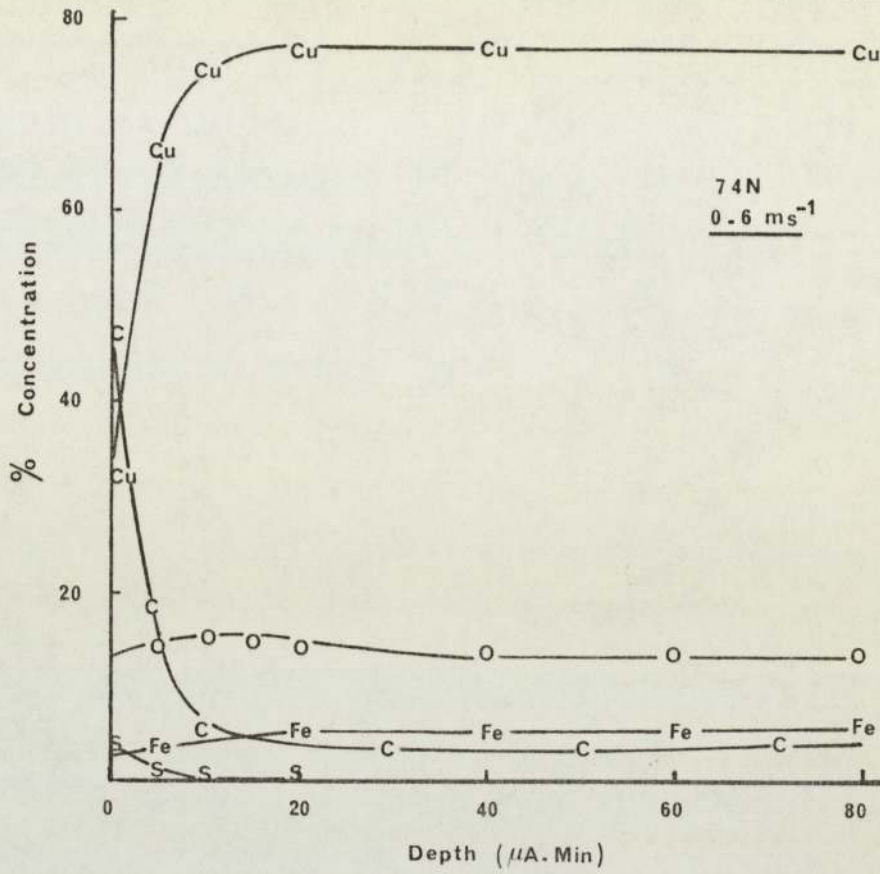
Figure 3.50.   Auger spectra for fuel with additive - Bronze E

(Denison Wear Rig)
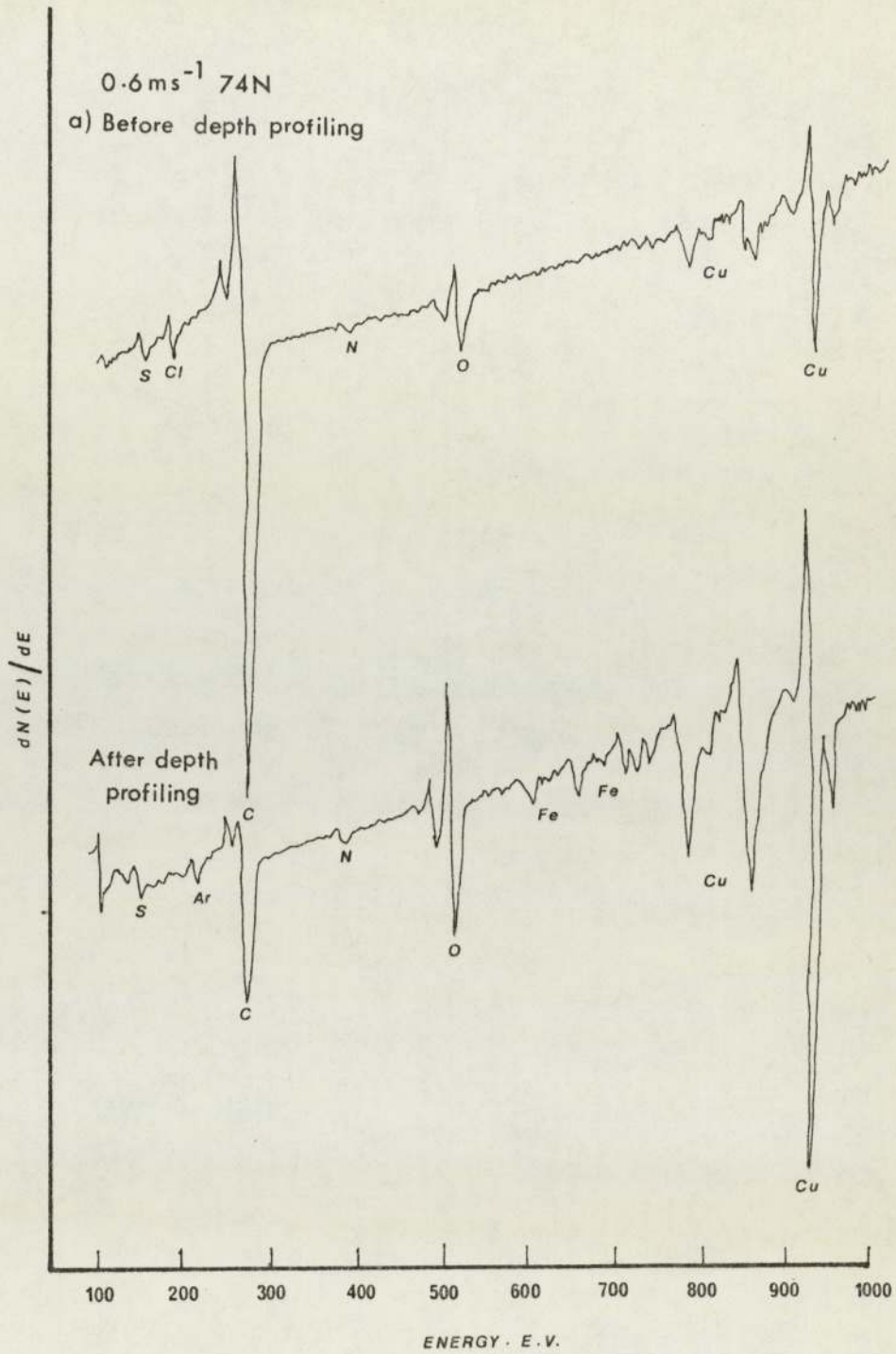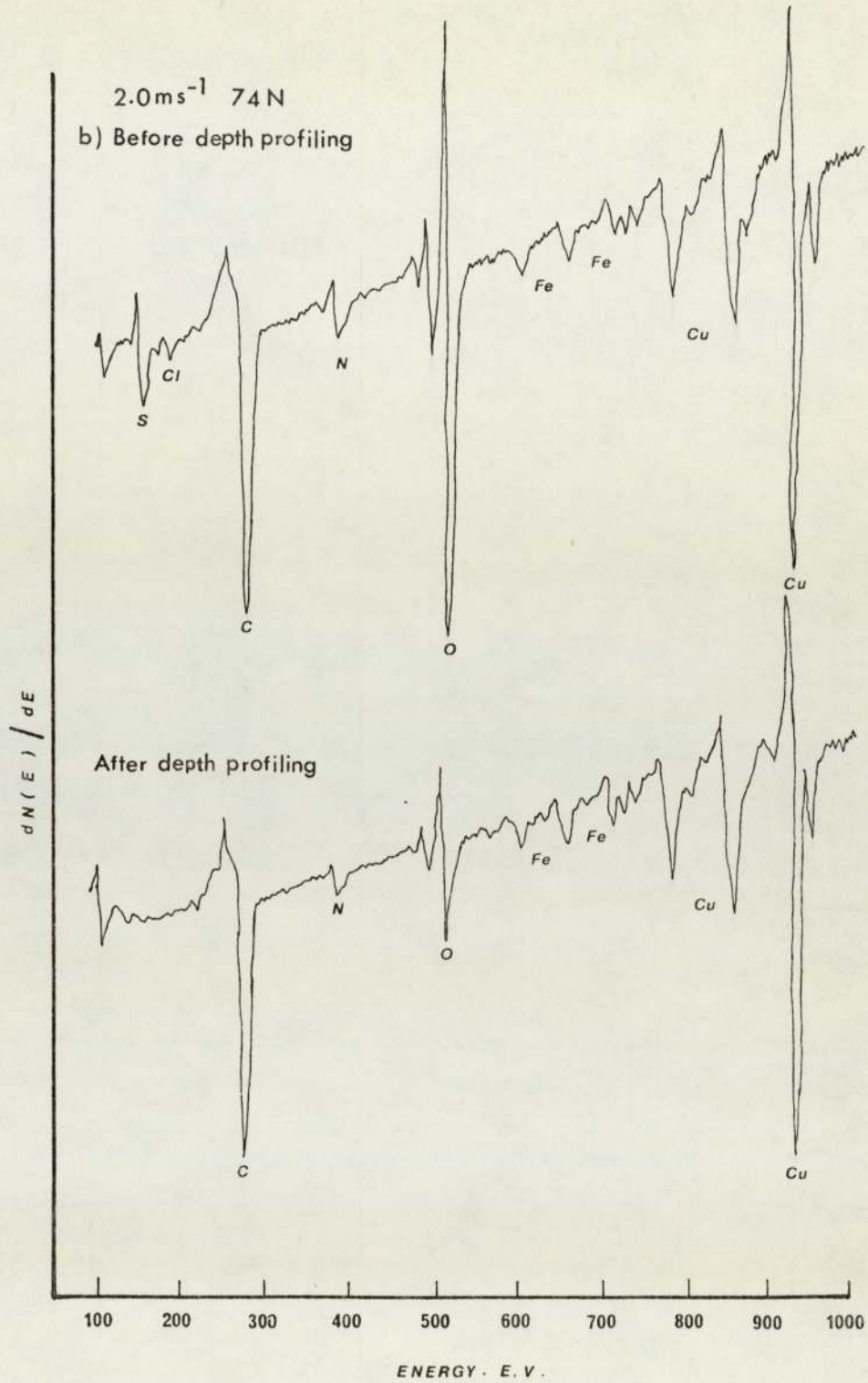
Figure 3.51 Auger Depth Profile — Bronze E
— Fuel with Hitec E580
(Denison Wear Rig)
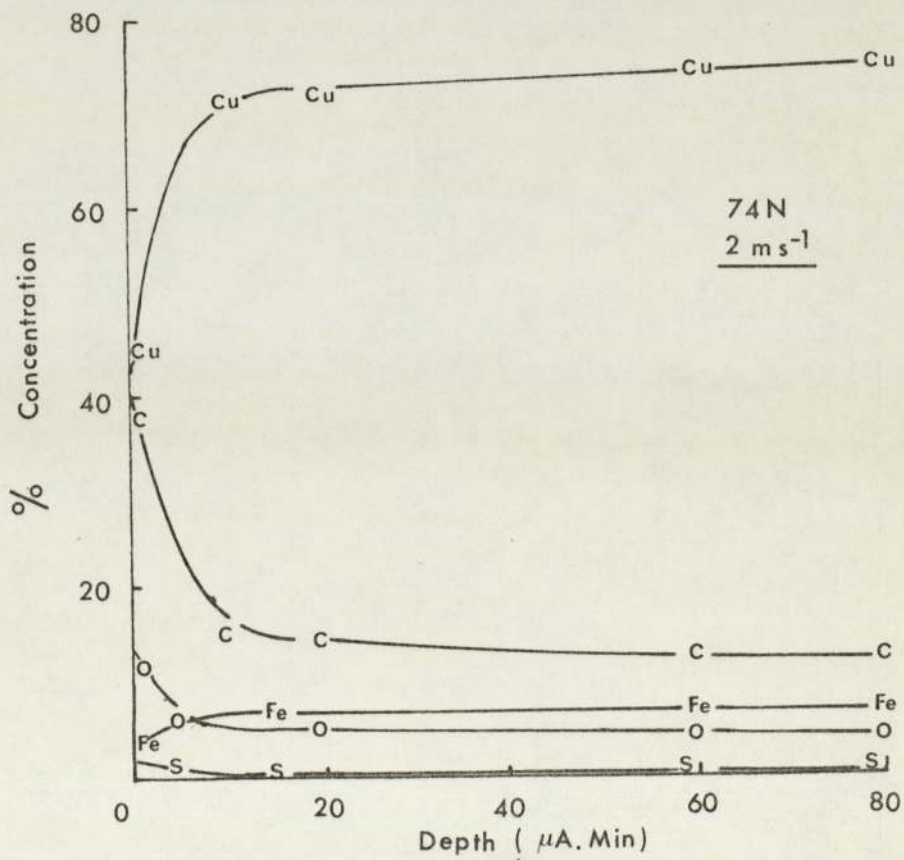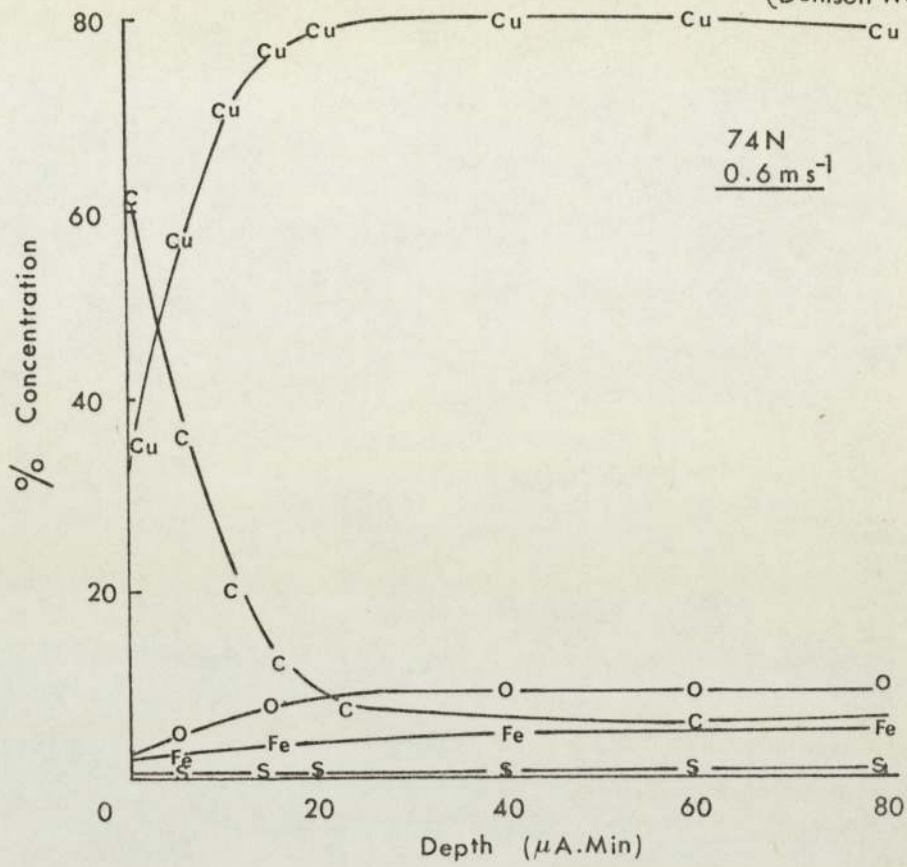
CHAPTER 4

THEORETICAL CONSIDERATIONS

4.1 Introduction

For a dry wear situation, Quinn et al (84,85,97)
developed an oxidational theory of the mild wear of low
alloy steels. The formation of the oxide layer, generated
by frictional heating, acts as a protective film in reducing
the wear rate. Mild wear clearly involves reaction with the
oxygen in the environment. It is not always appreciated
that mild wear can occur even under lubricated conditions
due to the large amounts of dissolved oxygen in the lubri-
cants as well as from the test surroundings.

The results of the experiments with aluminium-bronze
sliding against steel in the presence of kerosene have
shown that an oxide layer exists at the surface of the bronze,
both with and without additive. The additive E580 contains
a dimerised unsaturated fatty acid which acts as a boundary
lubricant in this system.

The effect of a boundary lubricant is to reduce the
number of dry contact asperities by the adsorption of polar
molecules onto the surface. However, it is not always the
case that these contact regions are fully protected especially
sliding in high load, low speed and high temperature condi-
tions. As a result this protective film is broken down so
that at a fraction of the dry contact asperities oxidation
and wear can take place as in the dry wear situation. Also
because of the adsorption-desorption effects of the polar

molecules of the lubricant, it is unlikely for a fluid film to generate a complete protection between the two contacting surfaces.

A theory will now be developed which takes into account the oxidation of the surface and also the thermal adsorption-desorption effects of a boundary lubricant.

4.2 Oxidational Wear

Considering the wear of dry contacts, Archard (73) proposed the equation:

$$\frac{V}{d} = K A_r \qquad \ldots\ldots (1)$$

where V is the volume of material removed, d is the total sliding distance, A_r the total real area of contact and K the dimensionless proportionality constant considered to be the probability of removing a wear particle.

Quinn (84) assumed that K factor is related to the oxide film thickness with time through a parabolic relation. The mass per unit area of oxide growth, Δm, is given by:

$$\Delta m^2 = K_p t \qquad \ldots\ldots (2)$$

where K_p is the parabolic rate constant and t the oxidation time to produce a wear particle. The total oxidation time can be expressed as:

$$t = \frac{a}{U K} \qquad \ldots\ldots (3)$$

where 'a' is a distance of a wearing asperity contact associated with Hertzian diameter, U the sliding speed

and K as defined above.

By substituting equations ... (3) into ... (2) gives,

$$\Delta m^2 = \frac{a\, K_p}{U\, K} \qquad \ldots (4)$$

By definition, $\Delta m = \rho\, g\, h$ $\qquad \ldots (5)$

where g is the fraction of oxide film which is oxygen, ρ the density of the oxide and h the oxide film thickness. Hence, by squaring both sides of equation ... (5) and equating equations ... (4) and ... (5) gives,

$$K = \frac{a\, K_p}{U\, \rho^2\, g^2\, h^2} \qquad \ldots (6)$$

The accepted relationship between the parabolic rate constant K_p, and activation energy for parabolic oxidation, Q_p, is given by the expression:

$$K_p = A_p \exp(-Q_p/(R\, T_s)) \qquad \ldots (7)$$

where A_p is the Arrhenius constant for parabolic oxidation, T_s the temperature at which the surfaces of the sliding interface oxidise and R, the universal gas constant.

By substituting equations ... (7) into ... (6) to give:

$$K = \frac{a\, A_p \exp(-Q_p/(R\, T_s))}{U\, \rho^2\, g^2\, h^2} \qquad \ldots (8)$$

The real area of contact between rubbing surfaces is given by the equation:

$$A_r = \frac{W}{P_m} \qquad \ldots (9)$$

$$\text{or} \quad A_r = \frac{N \pi a^2}{4} \qquad \qquad \cdots \cdots (10)$$

where W is the normal load, P_m the flow hardness of the softer material, N the number of contacting asperities and 'a' as defined before.

Equating ... (9) and ... (10) gives,

$$a = \frac{2 (W/P_m)^{\frac{1}{2}}}{(N \pi)^{\frac{1}{2}}} \qquad \qquad \cdots \cdots (11)$$

Combining equations ... (8), ... (9) and ... (11) and finally substituting into equation ... (1) leads to the oxidational wear equation for the dry wear situation, i.e.:

$$\frac{V}{d} = \frac{2 A_p \exp(-Q_p/(R T_s))}{U g^2 \rho^2 h^2 (N \pi)^{\frac{1}{2}}} \left(\frac{W}{P_m}\right)^{3/2} \qquad \cdots \cdots (12)$$

4.3 Boundary Lubricated Wear

Under conditions of boundary lubrication, a fraction of the real area of contact is prevented from coming into contact by the lubricant. Wear occurs only at the area of metal-metal contact. Hence, the real area of contact can now be expressed as :

$$\text{Real area of contact} = \alpha A_r \qquad \qquad \cdots \cdots (13)$$

where A_r is the total real area of contact under dry wear conditions and α the fractional film defect. The wear equation for boundary lubrication can now be written as:

$$\frac{V}{d} = K \, \alpha \, A_r \qquad \qquad \ldots\ldots (14)$$

Frenkel (98) has shown that the average time, t_r, spent by one molecule in the same site is given by the following expression:

$$t_r = t_0 \, \exp(E/R \, T_s) \qquad \ldots\ldots (15)$$

where t_0 is the time of vibration of the molecule, E the heat of adsorption of the boundary lubricant and T_s is the temperature of the surface film.

Kingsbury (75,76) proposed a relationship between α, the fractional film defect, and the ratio of the time for the asperity to travel a distance equivalent to the diameter of the adsorbed molecule t_x and the average time that a molecule remains at a given surface site t_r:

$$1 - \alpha = \exp(-t_x/t_r) \qquad \ldots\ldots (16)$$

The time required for an asperity to move a distance, x, at a speed U ms^{-1} is given by:

$$t_x = \frac{x}{U} \qquad \qquad \ldots\ldots (17)$$

where x is the metal lattice spacing or the diameter of an adsorbed molecule.

By substituting equations ... (15) and ... (17) into equation ... (16) gives,

$$1 - \alpha = \exp\left(-\frac{x}{U \, t_0 \, \exp(E/R \, T_s)}\right) \ldots\ldots (18)$$

Taking Naperian logarithms on both sides of equation ... (18) gives

$$Ln \ (1 - \alpha) = - \frac{x}{U \ t_0 \ exp(E/R \ T_s)} \qquad \ldots \ldots (19)$$

Equation ... (19) is applicable to the experimental conditions for $U > 0.1 \ ms^{-1}$ and $\alpha \leq 0.01$, even for a poor lubricant. Consequently the term $Ln \ (1 - \alpha)$ is approximately equal to $-\alpha$ and equation ... (19) becomes

$$\alpha = \frac{x}{U \ t_0 \ exp(E/R \ T_s)} \qquad \ldots \ldots (20)$$

By multiplying fractional film defect, α, of equation ... (20) into the right hand side of equation ... (12) results in the desired boundary oxidational lubricated wear equation, i.e.:

$$\frac{V}{d} = \frac{2 \ x \ A_p \ exp(-(Q_p + E)/(R \ T_s))}{U^2 \ t_0 \ g^2 \ \rho^2 \ h^2 \ (N \ \pi)^{\frac{1}{2}}} \left(\frac{W}{P_m}\right)^{3/2} \quad \ldots (21)$$

which is equivalent to boundary lubrication equation ... (14).

The above equation ... (21) has assumed that the temperature of the surface film is equal to the oxidation temperature at the contact. In an actual situation, the oxidation temperature at the sliding surface is likely to be higher than the desorption temperature, T_d, of the boundary lubricant. This will allow the surface molecules to desorb resulting in dry contact to occur. This then allows

the metallic surfaces to interact producing a sharp rise in temperature at the surface and hence escalating the rate of oxidation. As the asperities are removed the lubricant will rapidly cool the surface allowing polar molecules to re-adsorb onto the worn region. By considering the effect of polar molecules protection up to the desorption temperature, the boundary oxidational lubricated wear equation ... (21) can be modified by dividing the exponential term into two components, i.e.:

$$\exp(-Q_p/(R\ T_s))\ \ x\ \ \exp(-E/(R\ T_d))$$

where the first term represents the oxidation term and the second the polar molecules term.

Hence, the final boundary oxidational lubricated wear equation will be written as:

$$\frac{V}{d} = \frac{2\ x\ A_p\ \exp(-Q_p/(R\ T_s))\ \exp(-E/(R\ T_d))}{(U\ g\ \rho\ h)^2\ t_0\ (N\ \pi)^{\frac{1}{2}}}\left(\frac{W}{P_m}\right)^{\frac{1}{2}}\ \ \ldots\ (22)$$

4.3.1 Arrhenius Constant (A_p) and Activation Energy (Q_p)

From the static oxidation experiments of oxygen-free copper in air in the temperature range of 300°C to 550°C, Tylecote (99) quoted that the Arrhenius Constant is of the order of $1.5\ x\ 10^{-3}\ kg^2\ m^{-4}\ s^{-1}$ and the corresponding. Activation Energy is 84 KJmol^{-1}. In a tribological condition, however, the values of Activation Energies (Q_p) and the accompanying Arrhenius Constants (A_p) may be quite different. Sullivan et al (85) have recently illustrated

the changes of the Q_p and A_p in different temperature ranges of the oxidational wear of low alloy steels. The values of A_p and Q_p for oxide growth will depend on surface conditioning, plastic flow, void and dislocation and other factors (100). In lubricated wear of Al-bronze on steel, Poole (86) estimated that the value of A_p was 1.84×10^6 $kg^2 m^{-4} s^{-1}$ for a load of 10 kg and wear rate of 1.35×10^{-12} $m^3 m^{-1}$. In order to predict the boundary oxidational wear rates, correct assignments of A_p and Q_p are essential with relation to the surface contact temperatures.

4.3.2   Lattice Spacing or Molecular Diameter, x

Values of x are not generally available, although limited data of x are available from McClellen and Harnsberger (101), or it can be calculated from the formula proposed by Beerbower (83):

$$ x = \left(\frac{6 \, V_m}{\pi \, N_a} \right)^{\frac{1}{3}} \quad\quad\quad \ldots.. \ (23) $$

where V_m is the molecular volume (m^3) of the lubricant and N_a (mol^{-1}) the Avogadro's number.

Using the above equation ... (23) and taking $V_m = 325 \times 10^{-6} \ m^3$ for the present boundary lubricant and $N_a = 6.02 \times 10^{23} \ mol^{-1}$, the value of x was calculated as 1.5×10^{-9} m.

4.3.3   Time of Vibration, t_0

Lindemann (102) has suggested

$$t_0 = 1.54 \times 10^{-9} \left(\frac{M \, V_m^{2/3}}{T_m} \right)^{1/2} \quad \text{seconds} \quad \ldots \ldots (24)$$

for estimating t_0 in the solid state where M is the molecular weight (kg) of the lubricant, V_m its molecular volume (m^3) and T_m is the absolute melting point ($^{\circ}K$).

In this work, the above equation ... (24) was applied and taking $M = 0.283$ kg, $V_m = 325 \times 10^{-6}$ m^3 and $T_m = 353^{\circ}K$, the time of vibration, t_0 was calculated as 3×10^{-12} second.

4.3.4   Surface Contact Temperature, T_s

The temperature at the surface, T_s, is dependent on both the load and the coefficient of friction. An estimate of the temperature rise due to frictional heating can be made by using the simplified theory of Bowden and Tabor (103):

$$T_s = T_b + 0.438 \, F \, U \, \frac{(W \, P_m)^{1/2}}{(K_1 + K_2)} \quad \ldots \ldots (25)$$

where T_b is the bulk lubricant temperature ($^{\circ}K$), F and U the coefficient of friction and sliding velocity ($m \, s^{-1}$) respectively, W the load (N) and P_m the flow pressure of metal under static loading ($N \, m^{-2}$) and finally, K_1 and K_2 the thermal conductivities of both surfaces ($J/m \, sec \, ^{\circ}C$).

In the case of Al-bronze sliding on steel disc,

K_1 (aluminium-bronze) and K_2 (steel) are given as 46.05 and 75.36 J/m sec $^\circ$C respectively. The measured flow pressure, P_m, of Al-bronze was 2.4×10^9 N m^{-2}.

Hence, for a load of 98N and 0.6 m s^{-1} sliding velocity under boundary lubricated condition and taking the bulk lubricant temperature, T_b, as 295°K, the surface contact temperature, T_s, was estimated as 400°K.

It should be emphasised that the above relationship does not take into account many parameters which will affect the surface temperatures, for example numbers of contacts, thickness of oxide film, thermal conductivities of surface film and thermal diffusivity of the surfaces. As such, therefore, the temperature calculated may only be regarded as a rough guide.

4.3.5 Other Fixed Parameters

Certain parameters in the boundary oxidational lubricated wear equation ... (22) have been assumed to be constants in order to predict the theoretical wear rates. The values of Q_p, x and t_0 have been defined earlier and assumed constants. The fraction of oxide, g, which is oxygen was given as 0.11 for copper oxide. The density of this oxide, ρ, is about 6×10^3 kg m^{-3}. The oxide film thickness, h, was estimated from the scanning electron microscope photographs on tapered surface to be about 3×10^{-6} m and the measured hardness, P_m, immediately beneath the oxide surface was about 2.4×10^9 N m^{-2}.

The value of the heat of adsorption, E, for a dimer

acid is about 54.6 KJmol^{-1} which was given by Allen and Drauglis (104). It has also been assumed that the total number of contacts, N, is about 100. Finally, it leaves only the parameter A_p not fixed as it has been regarded as a variable depending on the surface conditioning. By using the surface contact temperature, T_s, of equation ... (25) and then subsequently applying the boundary oxidational lubricated wear equation ... (22) with the experimental values of wear rates, a range of A_p values can be estimated.

4.3.6 Evaluations of Surface Temperature (T_s) and Arrhenius Constant (A_p)

The estimated values of T_s and A_p are shown in Table 4.1. The value of A_p was shown to be changed by eight orders of magnitude in the temperature range 350° to 1300°K. The Arrhenius constant is seen to be very sensitive to temperature. The experimental wear rates were in the range 1.11 x 10^{-14} to 2.52 x 10^{-13} m^3m^{-1} which is quite low in magnitude by considering the high load and high speed ranges.

It is, therefore, necessary to assign which A_p value should be used in the correct temperature range without jeopardizing the use of oxidational theory of boundary lubricated wear equation ... (22).

TABLE 4.1	VALUES OF T_s AND A_p		
Speed (ms^{-1})	Load (N)	T_s (^{o}K)	A_p ($kg^2m^{-4}s^{-1}$)
0.6	24.5	347	1.54×10^{11}
	49.1	369	1.92×10^{10}
	73.6	386	1.04×10^{10}
	98.1	400	3.10×10^{9}
	122.6	413	1.24×10^{9}
	147.2	424	5.40×10^{8}
	196.2	444	1.50×10^{8}
2.0	24.5	471	3.90×10^{8}
	49.1	543	2.13×10^{7}
	73.6	599	1.07×10^{7}
	98.1	646	1.49×10^{6}
	122.6	688	4.11×10^{5}
	147.2	725	3.72×10^{5}
	196.2	792	5.44×10^{4}
4.0	24.5	646	1.55×10^{7}
	49.1	792	1.27×10^{6}
	73.6	903	2.76×10^{5}
	98.1	998	8.70×10^{4}
	122.6	1080	1.07×10^{4}
	147.2	1155	4.38×10^{3}
	196.2	1288	1.30×10^{3}

CHAPTER 5

DISCUSSION

5.1 Introduction

The conditions necessary to establish boundary lubrica-
ted wear will be discussed in relation to the strength and
toughness properties of the investigated Bronzes A(IMI),
B(Poole Type I), C(Poole Type II), D(Original Fuel Pump) and
E(Delta). The terminology of strength and toughness will
also be defined with regards to the properties of aluminium-
bronzes. Since only bronzes A, B and E were available for
the present wear tests, comparison of strength and toughness
upon wear resistance will be discussed only for these bronzes.

The wear results will be compared to those obtained
by other workers, in particular a comparison was made between
fuel without additive, with Hitec E515 (containing a phosphate
ester component) and with Hitec E580 (without a phosphate
ester component). The role played by surface oxidation and
the ability of the additive to give surface protection will
be discussed. Finally, a theory will be proposed to elucidate
the mechanism of wear in the absence and presence of organic
acid additives.

5.2 Discussion of Experimental Results

It was found that at least five different structures
of aluminium-bronzes have been used by various investigators

(figure 3.21). The compositions of each of the five
investigated bronzes are shown in Table 3.2. Thomson, Cook
and Sarkar (46,49,50) have shown that the best combination
of properties is obtained in alloys containing 10% aluminium,
5% iron and 5% nickel with 1% manganese. With respect to
the composition range of Bronze A, iron and nickel contents
are very much lower than the optimum value of the above
mentioned bronze (i.e. 10/5/5 alloy). The low levels of iron
and nickel present increase a tendency to form γ_2 phase which
is prone to corrode. A large volume of eutectoid phase (i.e.
$\beta \longrightarrow \alpha + K + \gamma_2$) is present and with the existence of large grain
sizes produces a reduction of tensile strength and toughness
in this alloy (figure 3.21(a)). Hence, Bronze A has a lower
strength and toughness than either Bronze B or Bronze E.
Strength properties are defined as the ability of the material
to resist applied forces. The capacity of material to absorb
energy before fracture is described as toughness which is
related to the ductility of the material. The assessment of
toughness is not simply determined from a tensile stress-
strain curve since fracture energy is considerably influenced
by factors such as stress conditions and geometry of material,
velocity of loading, and temperature of test. The above con-
ditions are particularly related to the aluminium-bronze
materials in the wear conditions. For instance, aluminium-
bronzes have an ability to deform superplastically at elevated
temperature when an enhanced strain-rate sensitivity of flow
stress in the material is achieved. This will increase

the fatigue life of the bronze in the wear process. The
degree of superplastic deformation before fracture is
very much dependent on compositions and structures of
aluminium-bronzes. Although the compositions of Bronze B
and Bronze E are approximately within the optimum compo-
sition range of 10/5/5 alloy, they have entirely different
structures (figure 3.21(b) and (e)). Bronze B has a large
volume of lamellar Ni-K phase present which contributes to
better corrosion resistance. The presence of a large
number of Ni-K phase regions reflect the original higher
nickel cotent than iron present in this alloy (table 3.2).
Higher nickel contents than iron in the alloys will reduce
its elongation and hence toughness. If the Ni-Fe ratio
exceeds 1.8, the strength is drastically reduced (41,46).
The presence of an uneven distributions of a large rosette
type of Fe-K phases also contributes to an overall reduction
of the strength of this alloy. The composition and struc-
ture of Bronze E is likely to exhibit the best all round
properties. The absence of the continuity of the embritt-
ling α+Ni-K phase in this alloy results in retaining its
ductility and toughness (figure 3.21(e)). A large number
of finely uniform distributions of Fe-K precipitates within
α grains contribute an increased strength of the structure.
A further contribution is the presence of a large number of
small Fe-K phases around the α grain boundaries which have
the beneficial effect of strengthening the adjacent grains.
A fine uniform microstructure with hardly distinguishable
small grains between the grains and its boundaries makes
this alloy stronger and tougher. One of the necessities

for superplasticity is a small and fine grain structure
which remains stable, without any appreciable growth, during
the deformation process. In this study, Scanning Electron
Microscopy observations on tapered worn surfaces (figure
3.33) of Bronze E showed that there was no appreciable
grain growth. It is also supported by the work of Moon and
Garwood (105) that the existence of iron rich particles
inhibit grain growth during superplastic deformation.
The influence of iron content on ductility of CDA 619 (86.5%
Cu, 9.5%Al, 4.0%Fe) was observed by Dunlop and Taplin (106),
and it was shown that there was more elongation than in
alloy CDA 624 which contains no iron. The effect of grain
size on ductility of Bronze E, compared to Bronze A and
Bronze B, leads to the conclusion that larger grain sizes
lead to lower values of ductility, i.e. its toughness. This
agrees with the explanation by Johnson (107) and Davies et
al (108) which states that if a large proportion of the
strain is to occur by grain boundary sliding, the ductility
will be enhanced at finer grain sizes because of the increase
in the amount of grain boundary area per unit volume.

Providing the metallurgical combinations of the
wearing components, apparatus and operating conditions
remain the same, a plot of Stribeck curve may give a useful
means of determining conditions for boundary lubrication.
A typical plot of friction coefficient versus (speed(U) x
viscosity(ζ)/pressure(P) curve is shown in Figure 3.1. The
shape of this Stribeck curve does not follow the classical
Stribeck shape (figure 1.3) where the boundary region A has
been clearly defined. From the results of wear rate and

friction values shown in Figure 3.3, the correct order of
speed for a boundary wear mode to occur in flooded conditions
was operating below 1 ms^{-1}. Above this speed, the wear
entered in semi-fluid or full fluid lubrication region.
When the additive was present (figures 3.4 and 3.6) the
phenomena was similar to that without additive present,
with the exception that the coefficient of friction is
lower. There seemed to be no reduction in wear rates, on
the contrary, the presence of the additive, in this case
Hitec E515, was found to have a pro-wear effect (figures
3.3 and 3.6). This pro-wear phenomenon of Hitec has also
been reported by many other workers. The reason for this
pro-wear effect of Hitec will be discussed later.

Poole (86) established that, for a 3 mm diameter
Bronze B pin, a speed of about 0.6 ms^{-1} and a load range
from 5 to 200N produced boundary wear under flooded condi-
tions. But in this investigation using Bronze E, it has
been found that wear rates were either very low or negligible
under the same experimental conditions. It was impossible to
reproduce the results of Poole's Bronze B using Bronze E.
The main reason was that Bronze E is tougher than Bronze B
because of its microstructure mentioned earlier. It is
important to keep in mind that the metallurgical differences
will affect the wear process. This was one of the major reasons
contributing to a wide variation of wear results among these
bronzes during the early stage of the experiments without
pre-knowledge of the existence of different types of bronzes.
Another contributing factor was the use of different wear
tracks for the experiments. The experiments have shown that

measurable wear occurred on inner tracks but zero wear on
the outer tracks of the disc under the same load and speed
conditions. This suggests that fluid film thickness increases
from the inner towards the outer wear tracks, thus giving
fluid film support in some regions. This was more notice-
able when Bronze E was used.

It was impossible to establish a wear mode for Bronze
E without changing the boundary lubricated wear conditions,
i.e. by reducing a fuel flow rate to starved conditions
(originally from 20 ml min^{-1} to less than 2 ml min^{-1}). Even
then difficulties still arose with unmeasurable wear rates
when a 3 mm diameter Bronze E pin was used and the author
was forced to reduce the pin diameter to 2 mm in order to
obtain sensible results. Inevitably, a further artificially
controlled flow rate to a minimum of less than 0.5 ml min^{-1}
was necessary to maintain friction coefficients at a level
of about 0.1, especially for those experiments operating at
high speeds. This could lead to large variations in wear rates
if the friction changed slightly (figure 3.10). With an
understanding of these problems, it is now possible to
explain the wear process conducted with 2 mm diameter Bronze
E pins in the presence and absence of a boundary lubricant.

Work carried out by Poole (86) has indicated speed
might be an important factor in film breakdown and seizure.
Hence the present investigation set out to study wear over
a reasonable wide speed range 0.6 to 4 ms^{-1} and over a wide
range of loads. By this means it was possible to observe
details of seizure under the various conditions. Most of
the previous published work has been directly involved with

kerosene lubricity problems. Emphasis has been placed mainly on the chemistry of the fuels with little attention being paid to metallurgical changes occurring during the tests. However, in order to understand the problem entirely and elucidate wear mechanisms, it is pertinent to also consider what happens to the metal surfaces and sub-surfaces rather than to investigate the fuels in isolation. It is particularly true when aluminium-bronzes have been reported to behave superplastically and generate cavities at intermediate strain rate at elevated temperature (47,68).

The results of wear rate and imprinted friction value are reproduced so that comparisons can be made between those obtained with kerosene and those with kerosene plus additive (figure 5.1(a), (b) and (c)). For 0.6 and 2.0 ms^{-1} speeds, both the hydrotreated fuel and fuel with additive produce a steady increase in wear with load when boundary friction was maintained at 0.1. For a 4 ms^{-1} speed, seizure occurred for fuel alone at 123N load. The presence of additive at 4 ms^{-1} speed showed that wear rates were constant between the load range 98 to 196N (figure 5.1(c)). In fact, wear rates showed a slight tendency to fall between these load ranges. This constant wear phenomena can be explained in terms of bronze material being subjected to superplastic deformation in this load range during the wear process. It has been confirmed that superplastic deformation and cavity formation occurred on tapered worn surfaces of 98N and 147N worn pins (figures 3.27 and 3.30). These cavities could only be formed when the material was subjected to superplastic deformation at elevated temperature. If the right conditions prevail,

superplasticity will give an increase in fatigue life of the material without fracture. At low and intermediate speed (0.6 and 2 ms^{-1}), the fuel containing additive produced a pro-wear effect over all the load range. At a high speed (4 ms^{-1}), a reversal occurred showing that the additive has a tendency to promote lower wear and give seizure protection.

It is now appropriate to introduce what is meant by mild and severe boundary conditions. Mild boundary wear we will define as the wear of surfaces which are protected by full boundary films of either oxide, metallic soap or both and where the wear rates are low and scuffing is nonexistant. These conditions were found to apply in those experiments conducted at 0.6 ms^{-1} for all loads and for 2 ms^{-1} for loads below about 100N. Severe boundary wear involved superplastic deformation and cavity formation in the bronze, the formation of incomplete boundary film and some evidence of scuffing surface damage. This mode of wear was apparent in experiments conducted at 2 ms^{-1} at loads above 100N and 4 ms^{-1} for loads above 70N.

The results for the fuel without additive suggest that the formation of copper oxide on the wear surface is responsible for the lower wear rates of bronze in a mild boundary condition. The high toughness of Bronze E made this material more able to resist wear and thus allows more stable and thicker oxides to be produced. When severe boundary conditions become prevalent, i.e. no effective oxide films separating the two rubbing surfaces, high wear rates

remove the surface at a rate greater than the oxide pro-
duction, thus causing seizure to occur (figure 5.1(c)).

The pro-wear effect of Hitec when operating in mild
boundary conditions suggest that the thick hydrocarbon
layer is responsible for the restriction of oxide formation
on the wear surface, thus leading to higher wear rates.
As the boundary conditions become more severe, the adsorp-
tion of the fatty acid on the wear surface gives sufficient
protection to allow some oxidation to take place and thus
prevent seizure. Once the bronze surface has established
an optimum superplastic flow condition, the wearing surfaces
become very stable with a reduction in friction and wear,
and increase in the fatigue life of the bronze. This finding
is supported by the work of Gandhi et al (109). They
investigated the low cycle fatigue behaviour of a super-
plastic aluminium-bronze at elevated temperature and found
that the fatigue life has been increased significantly above
a temperature of $500^{\circ}C$ which corresponded to the enhanced
strain-rate sensitivity of flow stress in the material.

The work of Poole and Sullivan (33) has shown that
aluminium migrating to the surface is corrosively attacked
by the products of the phosphate ester producing mainly
aluminium phosphates. This process leads to higher wear
rates than without Hitec E515. Under more severe conditions,
a chemical breakdown of the ester occurs, i.e. in this case
aluminium phosphides are formed on the surface giving some
extreme pressure protection and thus producing a fall in
wear rate.

The present work has shown that aluminium migration and transfer to steel surfaces was detected both with and without the presence of Hitec E580. The amount of material transferred and the distribution of elements in the transfer film will be different in both cases (figures 3.34(e) and 3.37(e)). The powder X-ray diffraction analysis has shown that the debris is mainly Cu and Cu_2O. The absence of phosphorus compounds in the wear debris was expected because Hitec E580 contains no phosphate ester component. Under mild boundary conditions, there is a competing reaction between the oxygen and the fatty acid with the surface. This leads to a thinner oxide film, less protection and hence higher wear rates than with fuel alone. This has been confirmed by Auger analysis on 74N load, 0.6 ms^{-1} worn pin (figure 3.48(a), before depth profiling), a high oxygen peak suggested that a thicker oxide film was present on the worn surface, thus giving better protection than those with additives, i.e. indicated by low oxygen peak (figure 3.50(a), before depth profiling). A high carbon peak for the fuel with additive (figure 3.50(a), before depth profiling) further confirmed the presence of a thick hydrocarbon layer which prevented the formation of a thick oxide film in the mild boundary region. When the conditions become more severe, the adsorption of the fatty acid gives sufficient protection to allow some oxidation to take place and hence to prevent seizure. This is confirmed by the observations of large oxygen peaks produced at higher speed (figure 3.50(b) before depth profiling) and a thicker oxide layer produced at higher loads and speeds on tapered worn surface for fuel with

additive (figure 3.30). The strain-rate sensitivity of this superplastic material under these severe conditions probably further contributes to reduction in friction and wear. To summarize, both additives (Hitec E515 and E580) are pro-wear under mild boundary conditions bur anti-wear when conditions become more severe.

From the observations of scanning electron micrographs, a scuffing failure of a 3 mm diameter Bronze A pin (figure 3.23) bears some resemblance to the pitting failure where the worn surface was characterised by the formation of many small pits. Previous investigators (86) have found that seizure occurred on a 2 mm diameter Bronze B pin at 123N, 0.6 ms^{-1} under flooded conditions. The present findings have also indicated cracking failure on a 3 mm diameter Bronze B pin (figure 3.25), after being worn from 24.5N to 196N load at 4 ms^{-1}. When a 2 mm diameter Bronze E pin was used, the author found that there was no indication of severe surface damage at all loading and speed conditions. Typical surface condition of a 2 mm diameter Bronze E pin after being worn at 98N load, 4 ms^{-1} is shown in Figure 3.26. It has been mentioned earlier that metallurgical structure differences and compositions play a significant role in determining the optimum properties of the materials. The composition and microstructure of Bronze A (table 3.2 and figure 3.2(a)) does not seem to provide good wear resistance due to the lower iron and nickel contents present and a large, distinguishable grain size. It is believed that the pits were initiated at the weak eutectoid phases as α phases are much stronger. Though the

composition of Bronze B is within the optimum limit, its microstructure does not conform to the better wear resistance structure of Bronze E (figure 3.21(b) and (e)). This is due to the presence of non-uniform structure with a large volume of weak Ni-K phases. Electron Probe Micro-analysis on each of the individual phases has shown that the overall structure of Bronze B had a Ni/Fe ratio greater than one (table 3.1). A higher nickel content than iron was also confirmed by composition analysis (table 3.2). A higher nickel than iron ratio makes this alloy less strong and tough. It has been mentioned earlier that Bronze E provides better wear resistance due to its composition and microstructure (figure 3.21(e)).

The tapered surfaces of Bronze E have shown that many cavities have been formed in the sub-surface layers of worn pins both with and without additive (figure 3.27(b), (c) and figure 3.30). The degree of cavitation increases towards the rubbing surfaces. The process of cavitation is associated with grain boundary sliding and cavity nuclea-tion probably occurs at points of shear stress concentration in the sliding interfaces. The interlinkage of cavities at high shear strains cause the grains and interfacial phases to break. The action of high temperature at the rubbing surfaces causes a further breakdown of grains and phases to form oxides on the rubbing surface. A typical example of one of the asperities being heavily deformed with the interlinkage of cavities to create a wear particle is shown in Figure 3.32.

Scanning Electron Microscopy on a tapered surface of

a 3 mm diameter Bronze B pin has shown a unique layer
(about 1 μm depth) of aluminium depletion just below the
worn surface (figure 3.24(e)). The unetched wear region
(figure 3.24(a)) showed a normal distribution of aluminium
(figure 3.24(e)). This indicates that an aluminium depleted
layer was associated with a diffusion mechanism occurring
at the region of maximum shear stress just below the worn
surface. The depleted layer is not likely to be an oxide
layer, based on the observations of normal aluminium distri-
bution on the unetched smooth wear surface.

X-ray element distributions across tapered surfaces
have revealed a distinctive layer of aluminium depletion
and the depth of depletion depends on the degree of sub-
surface deformation, such as that shown in Figures 3.31(e)
and 3.29(e) where a severely deformed layer produces about
6 μm depth of aluminium depletion compared to 1 μm depth
with less deformation. In severe wear conditions, such as
147N load at 4 ms^{-1} (figures 3.31 and 3.32), an oxide film
was produced on the worn surface. The estimated oxide
thickness, based on an oxidised asperity shown in Figure
3.32, was about 2 μm compared to a 6 μm depth of aluminium
depletion in the deformed layer. It is reasonable to expect
that the oxide film thickness is less than the depth of
aluminium diffusion due to a greater depth of sub-surface
deformation caused by the severe wear process.

Nakajima et al (110) have studied the interaction of
solute atoms with dislocations in surface layers of abraded
Cu-Al alloys and found some increase of the intensity of
the Al-K$_\alpha$ radiation in the rubbed surface layer compared

with that in the initial state. Funamizu et al and
Oikawa et al (111,112) have investigated the interdiffusion
of aluminium in Copper (Rich) system and found that alumi-
nium diffuses more rapidly than copper in this system. The
present finding has also indicated that aluminium diffuses
more rapidly than copper and is transferred to the steel
surface, thus leaving a copper rich layer on the pin sur-
face to be oxidised. This is confirmed by the findings
of aluminium depletion on the pin surface and Cu_2O found
in the wear debris. A typical example of greater aluminium
intensity than copper intensity on the transferred track
surface is shown in Figure 3.34(d) and (e). The copper
and aluminium were scanned at the same condition and speed.
This further suggests that aluminium transferred more
readily than copper to the steel surface. It has also been
observed that the transferred aluminium has a unique pattern
of transfer line which followed the direction of wear
(figure 3.35(e)). This heavy aluminium transfer line
probably corresponds to the maximum numbers of contacts
between bronze pin and steel disc surfaces. There appears
to be more aluminium transfer on the smoother side of the
wear track.

The surfaces of Bronze E worn pins were measured to
determine aluminium concentrations by means of Electron
Probe Microanalysis. Aluminium concentrations versus load
for speeds of 0.6, 2, and 4 ms^{-1} (figures 3.40 to 3.42)
have indicated three important parameters in the wear
mechanism; these are (i) depletion of aluminium, (ii)forma-
tion of oxide, and (iii)additive-surface interactions. The

results for the fuel without additive suggest that the
formation of copper oxide on the wear surface is repon-
sible for the low wear of bronze in mild boundary conditions
since copper oxide has been detected from the wear debris
analysis. Electron Probe Microanalysis on worn pin surfaces
has shown that aluminium depletion was greater in the absence
of additive (figure 3.40). Once aluminium is removed from
the surface, the copper rich layer is free to be oxidised,
hence giving the surface added protection. These protective
oxide films were maintained up to about 98N load at 2 ms^{-1}
(figure 3.41), then a transition occurred showing that the
presence of fuel with additive became more protective at
higher loads. When severe boundary conditions become pre-
valent (i.e. above 98N load at 4 ms^{-1}), the fuel without
additive is no longer protective as a result of the boundary
film being broken down, leading to metal-to-metal contact.
Hence, this leads to surface seizure with aluminium bulk
concentrations being measured (figure 3.42).

The results of higher wear rates for the fuel with
additive in mild boundary conditions suggest that the thick
carbon layer is responsible for restriction of oxide
growth on the wear surface. This is supported by the
observation of a thick carbon layer on the thin oxide
surface on the Auger depth profile (figure 3.50(a), before
depth profiling). It is expected that aluminium depletion
on worn pin surfaces was less than that with fuel alone
(figure 3.40). Consequently, the copper free surface area
has been reduced and this limits the chances of thick oxide

formation. As the boundary conditions become more severe, the adsorption of the fatty acid on the wear surface gives sufficient protection to allow some oxidation to take place and hence provide anti-wear and anti-seizure. It is confirmed by a pronounced depletion of aluminium on bronze surfaces, as low as 2% aluminium detected on depleted surface for 123N load at 4 ms^{-1}, hence allowing large copper free surface areas to be oxidised.

We must now ask what happens to the aluminium when it migrates to the steel surface. Elliott and Wallach (113,114) have carried out a study of the diffusion bonding and friction welding of aluminium to steel. Diffusion bonding involves minutes or hours at temperatures less than 0.7 T_m (where T_m is the melting point in degrees absolute of the lower melting point material). In friction welding, the surfaces to be bonded are rubbed together to render one or both materials plastic in the region of the interface. In both cases, they found that a brittle intermetallics, e.g. of the type $FeAl_3$, Fe_2Al_5 are formed at the joint interface. Polyakov (115) has also carried out an investigation of the transition zone and structure formed during the impulse deposition of aluminium on steel. In the impulse compression of aluminium powder on steel, a diffusion transition zone was formed by movement of Fe, Al and O by the order of several microns. Outside these zones there was no diffusion of Fe→Al and the reverse Al→Fe occurred. In explosive welding conditions, FeAl and Fe_2Al_5 intermetallic compounds were found in the transition zone. The present finding has shown that Al content of the transfer film on

the steel was always higher than in the bulk bronze
ranging from about 20% to 100% of the transfer film (table
3.4). This finding is supported by the work of Dzhevaza
and Lebedev (116). They investigated the welding proper-
ties of aluminium bronze to carbon steel and found that,
on the steel side of the weld, the concentration of alumi-
nium was as high as 14-17 per cent. This implies that the
same mechanism had occurred as friction welding where
aluminium migrates into the steel surface with an $Fe_x Al_y$
type intermetallic compound being formed.

Auger Electron Spectroscopy (AES) was found useful
for detecting thin surface layers on worn samples. The
spectra recorded for Bronze A worn samples with and without
additive are shown in Figures 3.43 and 3.45. From the depth
profile analyses, it would appear that both samples have a
carbon overlayer on their surface of approximately the same
thickness (figures 3.43(d) and 3.45(d), before and after
sputtering). However, the spectra recorded before sputtering
indicate the overlayer for samples without additive is quite
continuous (figure 3.43(a), (b), (c) and (d)) whilst that
for samples with additive is non-uniform, typically for a
large variations of oxygen and aluminium peaks (figure 3.45
(a), (b), (c) and (d)). The Auger micrographs (figure 3.46)
also show that the carbon film for a sample with additive is
of variable thickness. The Auger depth profiles for Bronze
A worn pins are reproduced here (figure 5.2), by combining
fuel and fuel plus Hitec E580, so that a direct comparison
can be made between them. Only the important carbon, oxygen
and aluminium profiles are shown. Clearly, low concentration

of oxygen and normal aluminium profile for fuel alone
suggest that no oxide was present and that aluminium bulk
concentration was present on the worn surface. Once the
carbon overlayer is removed, the aluminium-bronze substrate
is revealed. This is expected because there was evidence
of seizure failure at the final stages of this test, thus
exposing bulk material surface. In the case of fuel plus
Hitec E580, there was no sign of seizure failure at the end
of the tests. The high oxygen profile suggests that copper
oxide and probably aluminium oxide could be present in the
overlayer. Unfortunately, there was no Bronze A type of
wear debris available for X-ray analysis to confirm the
presence of copper and aluminium oxides. However, wear
debris analysis for Bronze E has only shown copper oxide
and no aluminium oxide probably due to the fact that Al_2O_3
concentration was below the limit of detection for this
technique. The high aluminium segregation on Bronze A
surface could probably be explained in terms of the operating
conditions. The flooded fuel flow conditions for Bronze A
tests tend to reduce the chances of aluminium transfer to
the steel surface due to the cooling effect of the fuel
compared to the starved flow conditions of Bronze E tests
where aluminium transferred more readily due to increase
temperature between bronze and steel.

The Auger depth profiles for Bronze E worn pins have
given another useful comparison (figure 5.3). The high
oxygen profile indicates the presence of Cu_2O, which
provides some protection during mild boundary wear condi-
tions when the additive was absent. With the additive present,

as the boundary wear conditions become severe, the formation of thick hydrocarbon layer, due to the fatty acid-surface interaction, allows a sufficiently thick oxide layer to build up providing effective surface protection.

5.3 Wear Mechanisms

5.3.1 Wear Mechanism in the Absence of Hitec E580

During mild boundary wear conditions, the results have shown that when the aluminium-bronze is worn against steel in the presence of a hydrotreated fuel, the wearing surface develops a thick oxide layer which leads to low wear. The worn surface has no boundary lubricant film on it and in all cases depletion of aluminium was detected. This depletion of aluminium on the worn surface is associated with a transfer of the aluminium from the bronze to the steel. The SEM X-ray intensities of copper and aluminium on steel surfaces have shown that aluminium is preferentially transferred from the bronze to the steel. A similar situation has been found by Nakajima and Yamamoto (110) when Cu-Al alloys were abraded by sand paper. They found that a high aluminium concentration migrates towards the rubbed surface compared with that in the initial state. In a study of interdiffusion in the Cu-Al system, Oikawa et al and Funamizu et al (111,112) also showed that aluminium diffuses more rapidly than copper does in this solid solution. When severe boundary wear conditions prevail, the original thick oxide layer on the bronze surface no longer exists due to the rate of removal of the oxide being greater than the rate of formation; thus this leads to metallic wear

and seizure. Though the material at this stage is super-plastically deformed, the high shear rate causes the inter-linkage of cavities to form, thus causing surface fatigue failure.

At present, it may be necessary to recognize the various factors that may affect the diffusivity of alumi-nium. The major factors that have been found to affect diffusion are (a)increase in temperature (117); (b)where an external stress gradient is applied (118,119); (c)where the metal has been plastically deformed (120,121); (d)where an external electric potential is applied (122,123); (e)where prior bombardment by neutrons or other penetrating radiation has modified the atomic configuration (124,125); (f)where an excess of vacancies is introduced by quenching from high temperature (126). Of the above factors, temperature, external stress, and plastic deformation are particularly relevant to the condition of the wearing system. Poole (86) has estimated that the surface temperatures under dry wear conditions are in the range $180^{\circ}C$ to $400^{\circ}C$ which are similar to those measured by Furey (127). Neglecting the cooling effect of the fuel, the same temperature range would be expected in this lubricated situation. The present experi-ments have been conducted under starved fuel flow conditions and with sliding speeds much higher. Hence it is expected, in certain cases, that surface contact temperatures would be higher than the range $180^{\circ}C$ to $400^{\circ}C$, especially under severe boundary wear conditions in conjunction with a super-plastic deformation of the bronze material. Superplastic deformation and cavity formation have been observed in the wear process during severe boundary wear conditions (figure

3.30). These can occur when the surface temperatures reach $300^{\circ}C$ to $500^{\circ}C$ and again above $600^{\circ}C$ with the superplastic deformation process corresponding to the enhanced strain-rate sensitivity of the material. The above superplasticity and cavitation of aluminium-bronzes have been reported by a number of research workers (47,68,109,128). Taking the above factors into account the processes by which wear and seizure occur can now be elucidated.

Consider the two opposing asperities before they approach to each other, there will be some fluid in the space between the two metal surfaces (figure 5.4(a)). As the two opposing asperities get closer, the kerosene is forced out from between the two surfaces. Due to the weakly bound molecules, the two asperities will come into contact (figure 5.4(b)) and during contact frictional heating occurs and the surface contact temperature rises sharply. This increase will depend on the severity of load and speed. If the wear process is mild, transfer of free aluminium to the steel will occur, by the Kirkendall effect (110,111,112), at the interface (figure 5.4(c)). At the same time, the surface contact temperature is high enough to oxidise a free copper rich layer on the bronze surface. The presence of dissolved oxygen in the kerosene will probably allow this process to occur. The formation of a thick copper oxide layer, which is strongly bonded on bronze surface, is sufficient to reduce metal to metal contact and hence produces an anti-wear effect. If the wear process is severe, the frictional heating will further increase the surface contact temperature, thus enhancing the formation of cavities below

the bronze surface and the bronze material is now in a state
of superplasticity. At this stage the rate of removal of
copper oxide is greater than the rate of formation, and as a
result of the interlinkage of cavities, basic fatigue cracking
failure below the bronze surface will occur (figure 5.4(d)).
Finally, this will then leave transferred bronze on the
steel with bronze debris appearing in the fuel. Basically
a metal to metal wear process occurring under these severe
conditions.

5.3.2 Wear Mechanism in the Presence of Hitec E580

Consider two asperities approaching each other with
components of Hitec E580 present on each surface (figure
5.5 (a)). Auger Electron Spectroscopy has shown that a thick
carbon layer exists on the surfaces (figure 5.3), and X-ray
analysis revealed copper oxides in the wear debris, when
Hitec is present. This suggests that the dimeric acid (long
chain polar molecules of dilinoleic acid) and the copper
oxides have an effect on the wear process. As the asperi-
ties approach, the boundary film experiences increased shear
and when contact occurs the surface temperature increases.
If the surface temperature is less than the desorption tem-
perature of boundary lubricant ($<80^{\circ}C$) (129), the fatty acid
molecules will cover the surface in the form of a metallic
soap. This is a competing reaction with surface oxidation.
This soap provides a very low shear stress film which prevents
temperatures rising at many of the asperities. If the surface
temeprature exceeds $80^{\circ}C$ (i.e. desorption temperature of
boundary lubricant), then the dilinoleic acid will desorb from

the surface, and thus allow metal-metal or metal-oxide
contact to occur (figure 5.5(b)). Since the oxide will be
more sparse than in the case where no additive was present,
due to the fact that the acid has inhibited oxidation, this
will mean that at the points where the acid film does break
down more wear will occur. The areas of the surfaces which
are still covered by the acid film will restrict free migra-
tion of aluminium to the steel surface (figure 5.5(c)). This
is confirmed by Electron Probe spot analysis on worn pin
surfaces where depletion of aluminium on the bronze surface is
less with the additive present (figure 3.40). This occurs
in a mild boundary wear condition. The competing reaction
between the dimer acid additive and the oxygen at the bronze
surface results in oxygen having restricted access to sites
on that surface. Thus unless the acid is desorbed oxide
will not readily form. This leads to a thinner oxide being
present on surfaces worn in the presence of fuel plus addi-
tive. This thinner surface oxide film is insufficient to
protect the surface, hence it will give rise to a greater
wear in this condition. As the conditions of wear become
more severe, the adsorption of fatty acid will give limited
protection and allow some oxidation to take place. This
will give some protection on the wearing surfaces, hence
the wear will be very much lower than would be the case for
the fuel alone due to this limited protection. Once the
bronze surface has established its optimum superplastic
flow condition, the wearing surfaces become very stable and
friction and wear tend to be reduced (figure 5.5(d)), due to
increased fatigue life of bronze. This finding is supported
by the work of Gandhi et al (109) on the low cycle fatigue

behaviour of a superplastic aluminium-bronze. They found
that the fatigue life increases significantly at about $500^{\circ}C$
which is related to the enhanced strain-rate sensitivity of
flow stress in the material. Though cavities are still
present at the sub-surface of bronze, the ductility is not
markedly impaired by the cavities because the enhanced
strain-rate sensitivity of the material inhibits the inter-
linkage of cavities at high strains.

Figure 5.1 Wear Rate Versus Load — 2 mm φ Bronze E Pins (Denison Wear Rig)

a: 0.6 m s⁻¹

b: 2 m s⁻¹

Fuel with Hitec E580

Fuel alone

Fuel with Hitec E580

seizure

Fuel alone

c : 4 m s⁻¹

Load {N}

Wear Rate {m³ m⁻¹}

Figure 5.2 Auger Depth Profile -3mm φ Bronze A Pins
Load up to 294N — 0.5 ms^{-1}
(Thornton Wear Rig)

- - - - - Fuel alone
———— Fuel with Hitec E580

% Concentration

Depth {μA.Min}
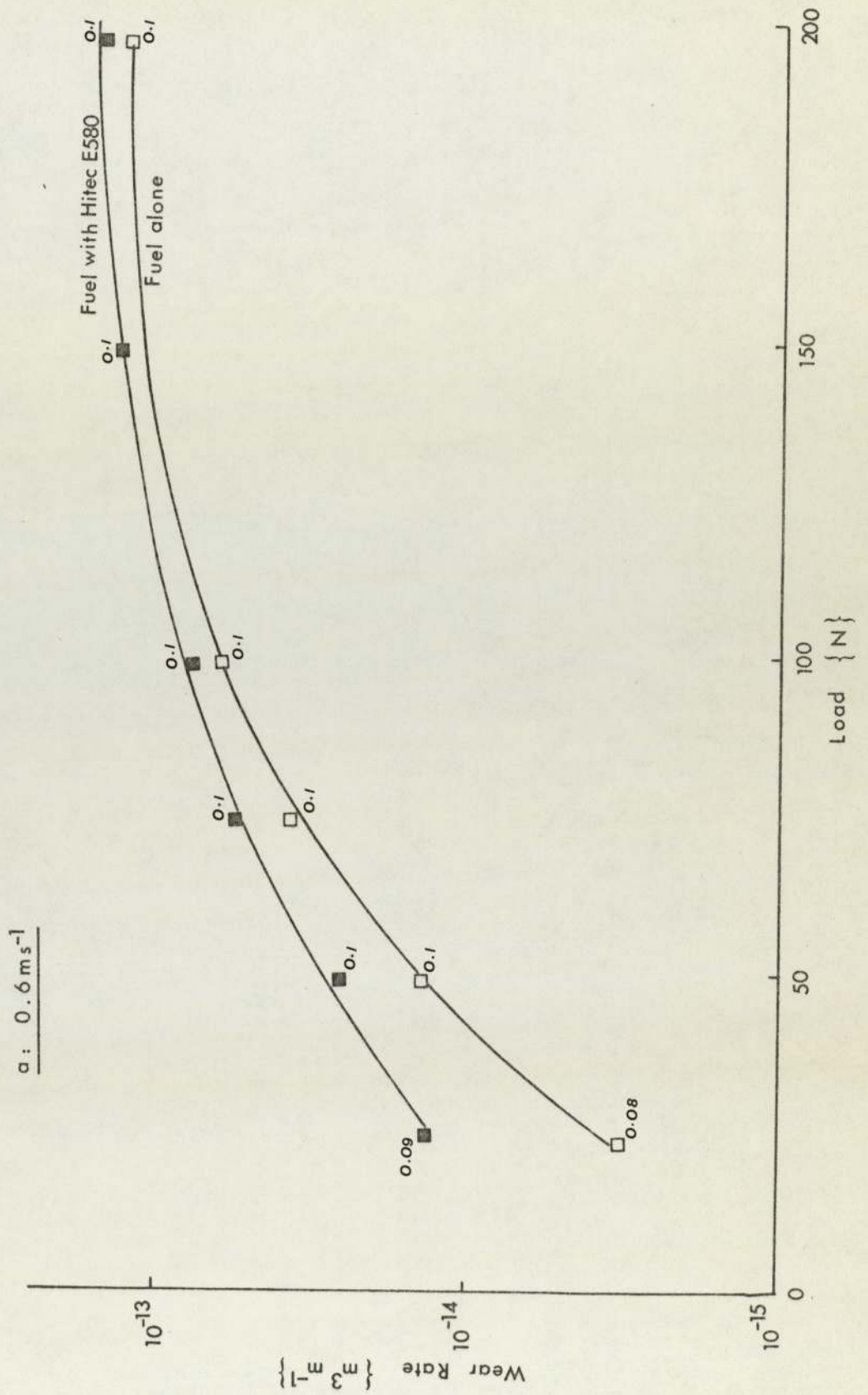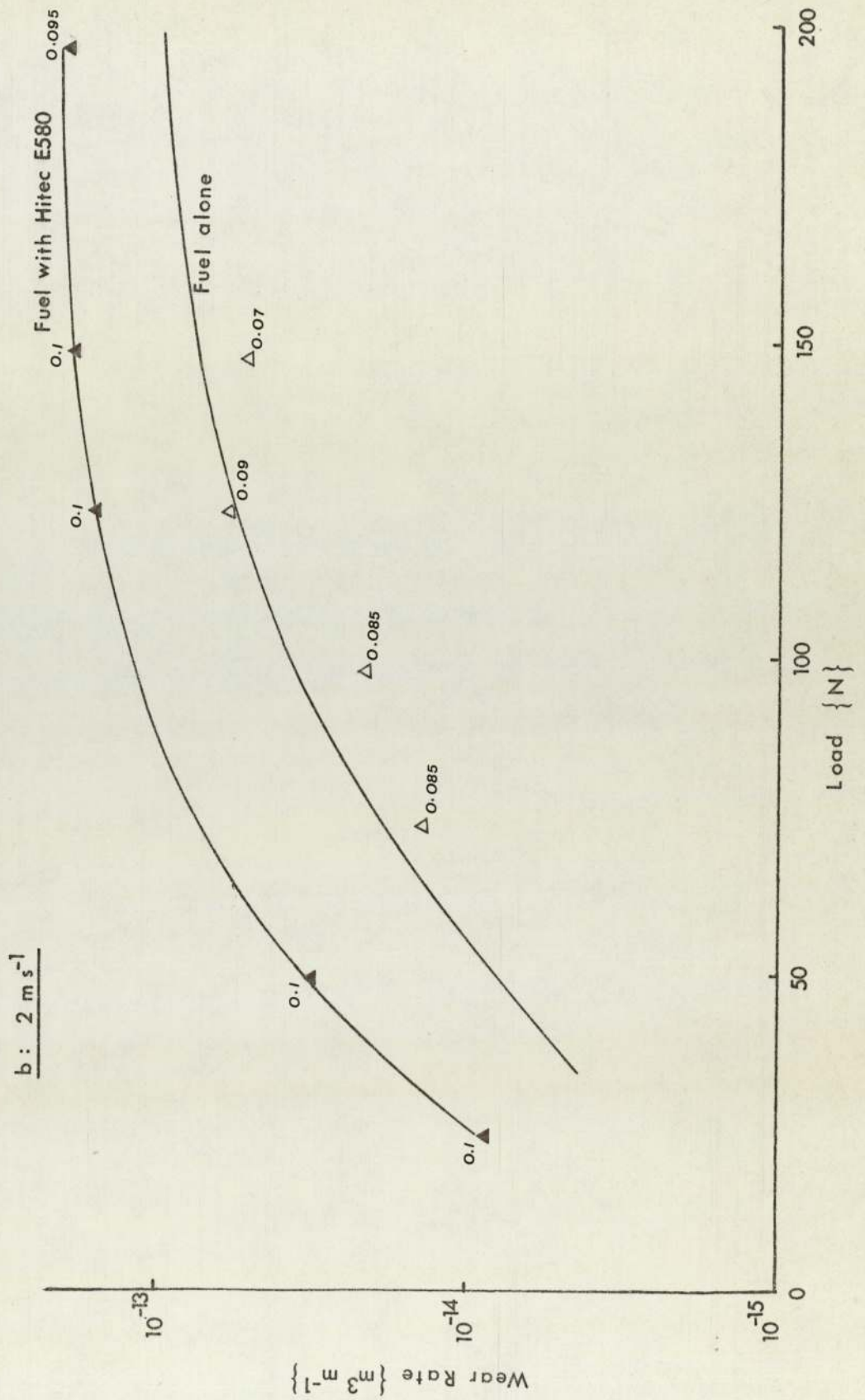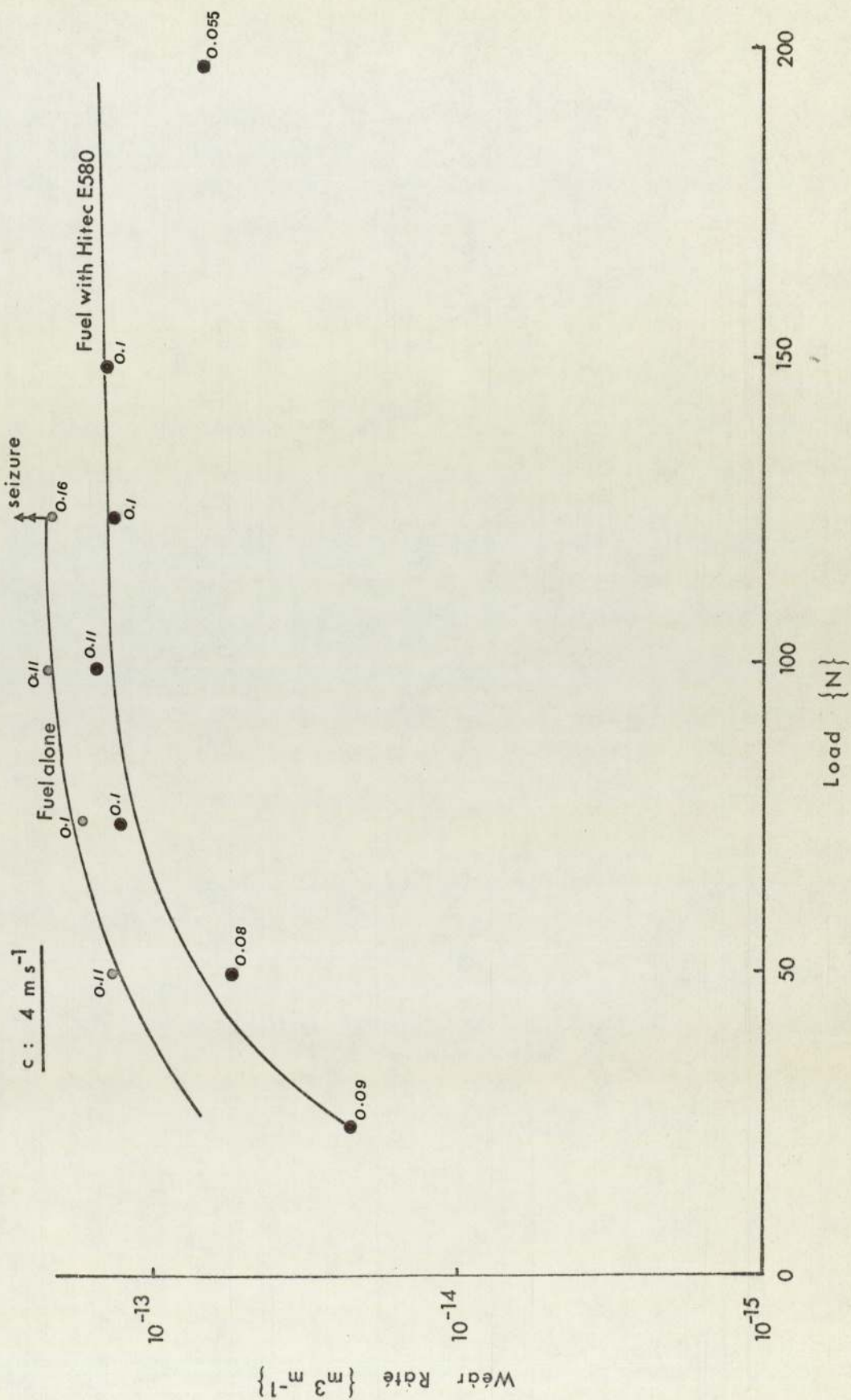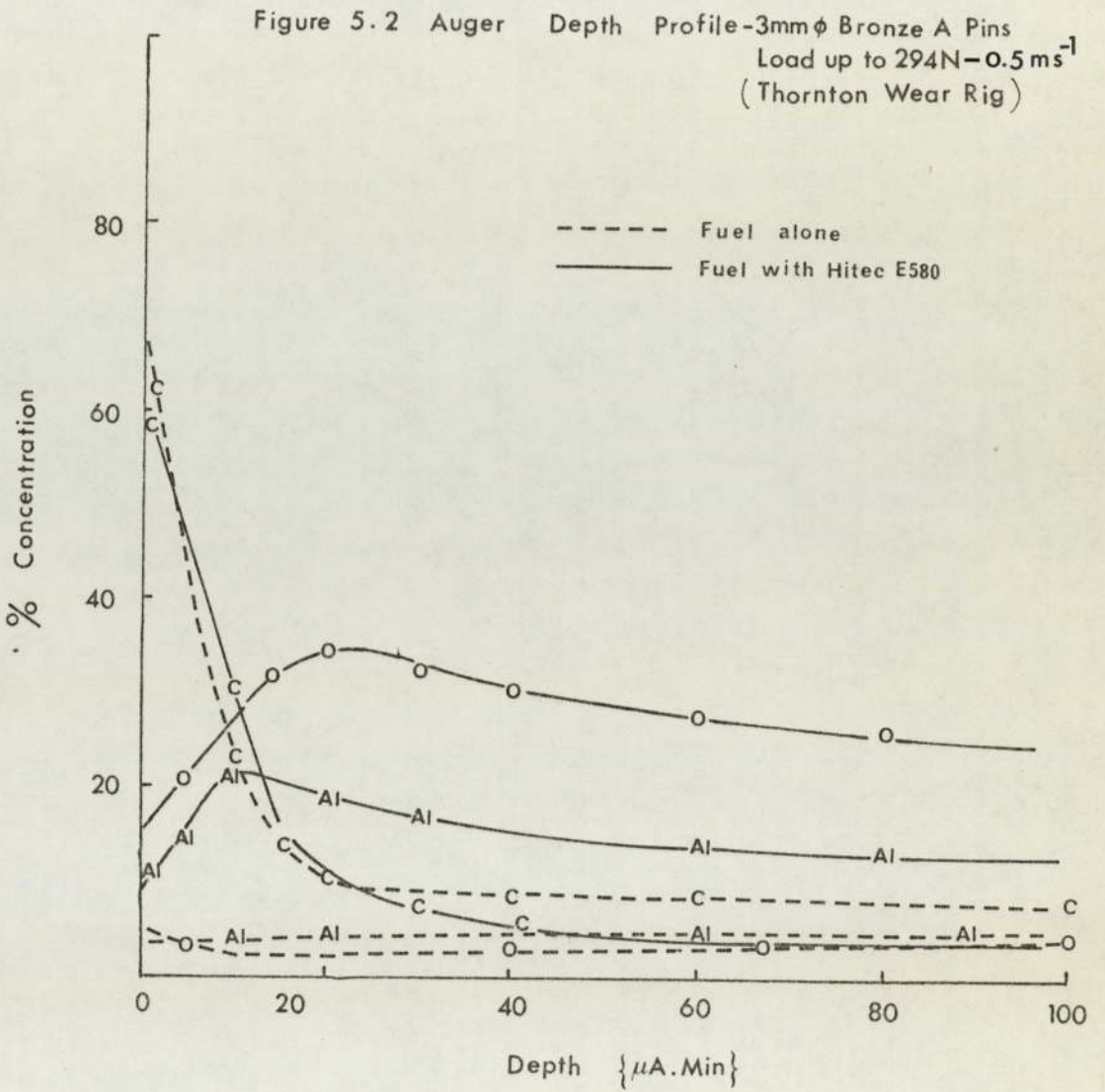
Figure 5. 3 Auger Depth Profile ——Bronze E (2mm φ pins)
(Denison Wear Rig)

a : Approaching Asperities

b : Contact Occuring

e : Aluminium Diffusion , Followed by Cu_2O Formation

d : Fatigue Cracking Failure
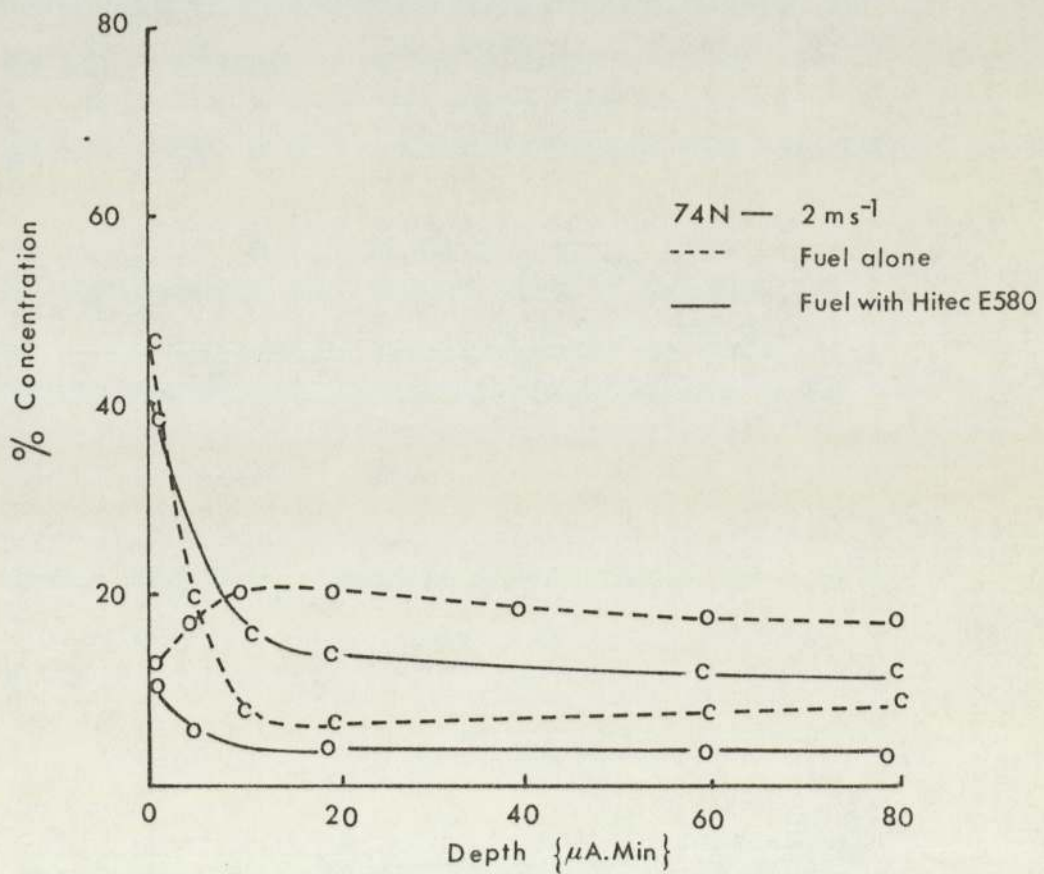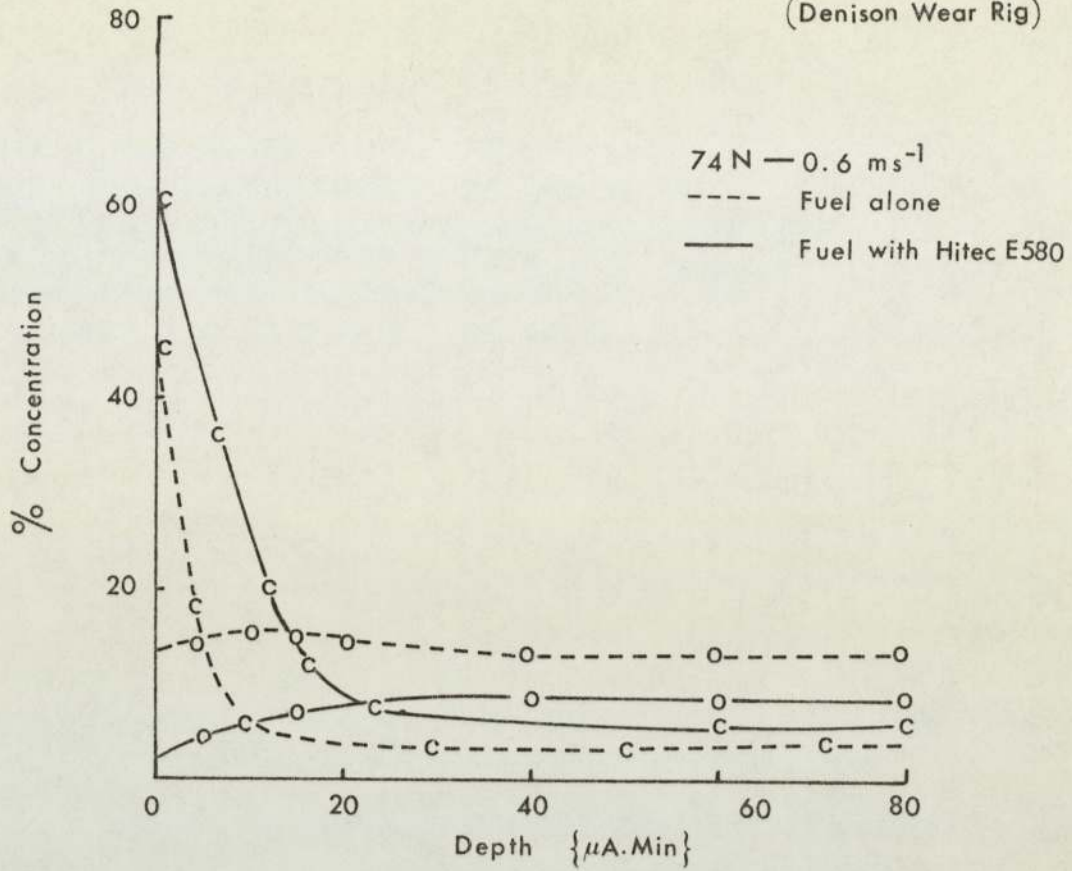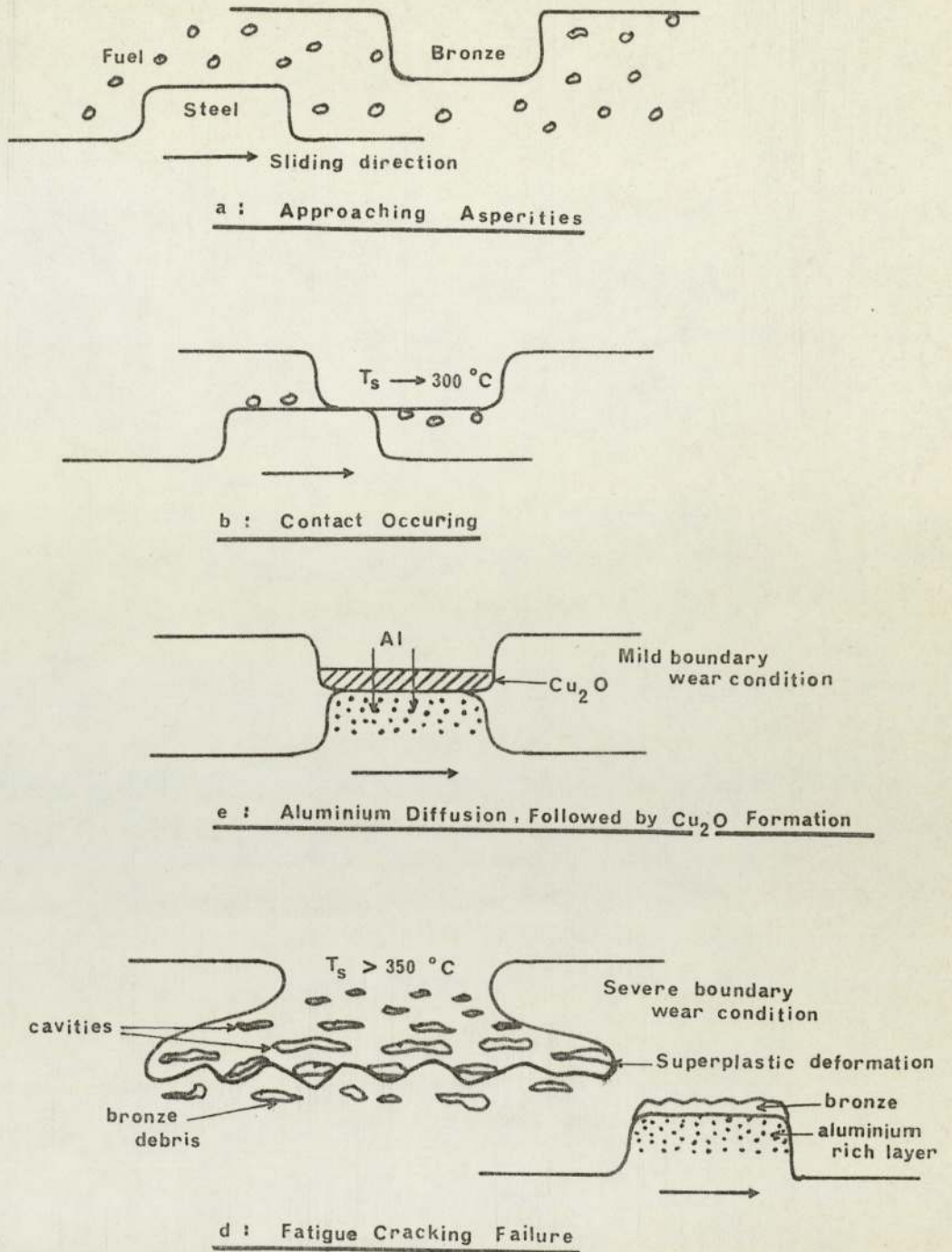
Figure 5.4   Wear with Hydrotreated Fuel
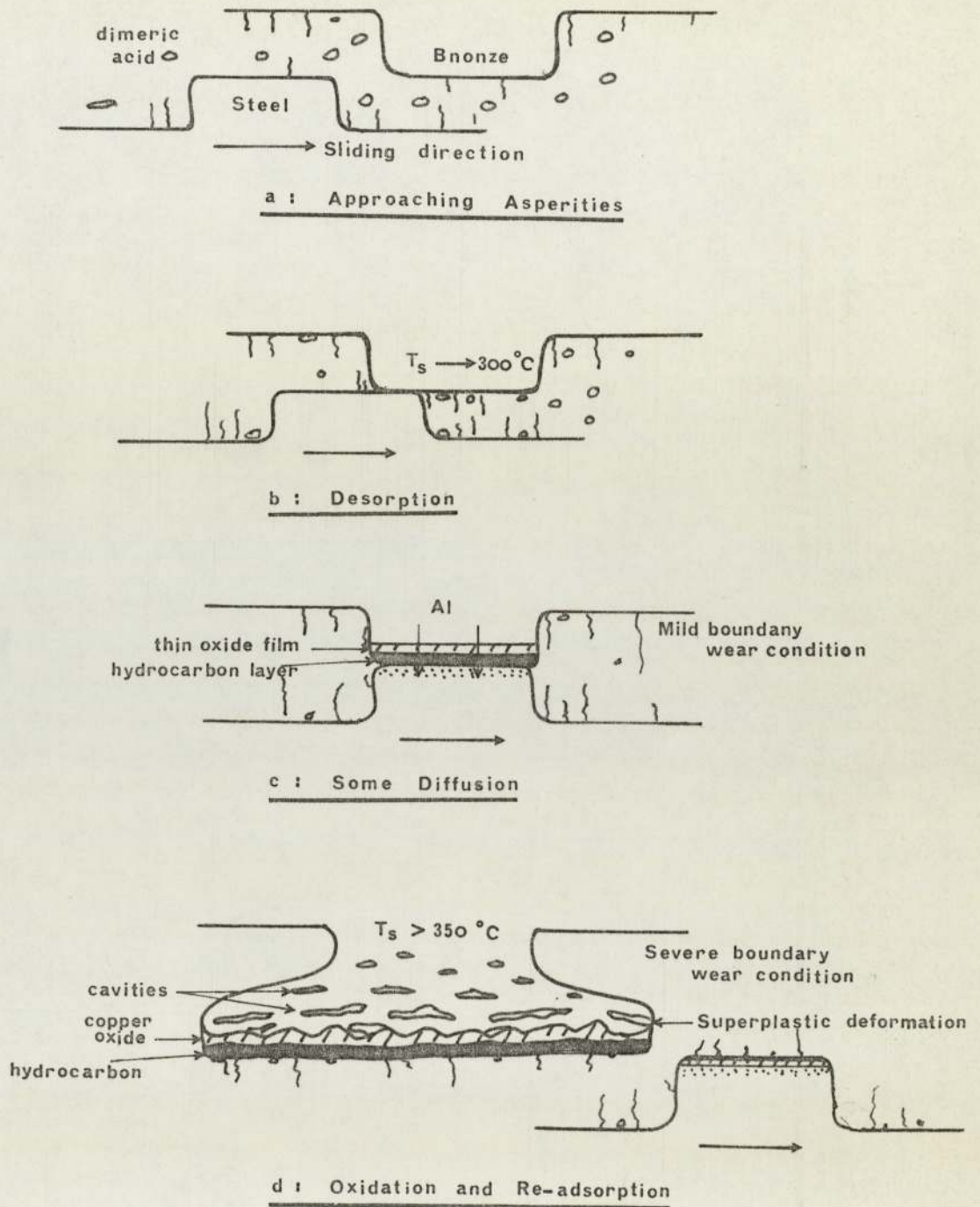
Figure 5.5 Wear with Hydrotreated Fuel plus Hitec E580

5.4 Application of Theory

The use of X-ray Diffraction, Scanning Electron
Microscopy, Electron Probe Microanalysis, Auger Electron
Spectroscopy together with the extensive study of sub-
surfaces of worn pins by Taper Sectioning enabled surface
models for the wear of aluminium-bronze, in the presence
of fuel with and without Hitec, to be proposed. Thus, the
present boundary lubricated wear theory, based on the sur-
face model, has taken into account factors such as desorp-
tion of boundary molecules followed by oxidation, in the
derivation of the thoery.

Since a large number of variables are incorporated
into the wear equation ... (22), assumptions had to be
made about a number of parameters, assigned to be constants,
so that the wear equation is manageable. Oxide film thick-
ness was one of the parameters assumed to be constant and
the average thickness used was obtained from electron
micrographs estimation. The lattice spacing or molecular
diameter was calculated from equation ... (23), proposed by
Beerbower (83), which was found to be 1.5×10^{-9} m. The
time of vibration of a molecule on the surface was estimated
using equation ... (24), being suggested by Lindemann (102).
The activation energy for parabolic oxidation was assumed
constant and the value taken was for pure copper, this may
not be correct for aluminium-bronze material because alumi-
nium bronze has better oxidation resistance. The surface
temperature can be estimated by using the simplified theory
of Bowden and Tabor (103) of equation ... (25). Other
parameters could be more easily assigned values. If the

values of parameters are correct and using the experimental wear rates in conjunction with surface temperature of equation ... (25) and wear equation ... (22), the values of Arrhenius constant (A_p) can be estimated (table 4.1).

An important feature of the table is the value of A_p which varies by six orders of magnitude. This suggests that A_p is likely to vary over a given oxide range, or even over a single oxide range, due to the rate of oxidation affected by the dynamic nature of the wearing system. The rate constant will be determined by the time for which any two wearing asperities are in contact, the temperature and the oxygen pressure. It is also known that where fresh metal is continuously being exposed that the oxidation rate is extremely fast. Sullivan, Quinn and Rowson (85) suggest that the activation energies (Q_p) for static and sliding conditions are likely to be the same, but the accompanying Arrhenius constants (A_p) will be very different, leading to very different oxide growth rates. They proposed that A_p and Q_p have three sets of values, in the case for low alloy steels, in different temperature ranges based on the types of oxide being formed. Kubaschewski and Hopkins (100) show that the value of the Arrhenius constant is influenced by many factors such as the number of voids and dislocations present, surface conditioning and partial oxygen pressure. This is, particularly true when aluminium-bronze has been detected under superplastic deformation and cavity formation in the present sliding system. We may say, therefore, that the Arrhenius constants, unlike the activation energies,

will be very different in the tribological situation due
to the greater degree of surface disruption which occurs
during sliding. Unfortunately, there is no relevant work
being done to measure the Arrhenius constant and Activation
energy of aluminium-bronze in static and dynamic conditions.
If the correct values of A_p and Q_p were known, then improved
solutions could be found for this wear equation.

The theory as developed so far can be criticised in
that it takes no account of the depletion of aluminium-
bronze from the bronze surface or of the sub-surface cavity
growth due to superplastic flow of bronze material under
sliding wear conditions. It is difficult to incorporate
these effects at this stage in view of the problems of
solving the present equation. An attempt to do so would
make the equation more unmanageable. However, the theore-
tical and practical approaches are so far in the right
direction. Further work is required to understand the
dynamic influence of the present existing variable parameters,
such as how different materials behave at elevated tempera-
tures under tribological conditions. Conditions are
changing at all times with change of load, temperature,
superplastic deformation, cavity growth, etc. which may,
therefore, lead to the possibilities of changing Arrhenius
constants and hence Activation energies and other parameters.

CHAPTER 6

CONCLUSIONS AND SUGGESTIONS FOR FURTHER WORK

The main conclusions that can be drawn from the work described in this thesis concern (i) the metallographic aspects of wear, (ii) the wear tests, (iii) the analytical tests based on the results obtained from the worn surfaces and (iv) the development of new oxidational wear theory under boundary lubricated conditions.

6.1 Metallographic Aspects of Wear

The present work has found that at least five different structures of aluminium bronzes have been used by various investigators. The differences in compositions and structures of aluminium bronzes have resulted in a wide variation of wear rates. The majority of the work described used Bronze E, i.e. Delta-bronze CA2 (or DTD 197A) which gave the best wear resistance compared to other bronzes investigated. The good wear resistance of this Delta alloy is attributed to the optimum composition range (i.e. Cu 10%Al 5%Fe 5%Ni) and the structure which has fine and uniform small grains with uniform distribution of Fe-K precipitates within α grains which contribute an increased strength and toughness. The presence of a large number of small Fe-K phases surrounding the α grain boundaries has the further beneficial effect of strengthening the adjacent grains. A high ductility characteristic at elevated temperature makes this alloy less prone to wear. This was one of the major reason contributing to the change of experimental conditions

required when using Delta-bronze, i.e. by reducing a fuel
flow rate so that starved conditions prevailed and reducing
the pin diameter from 3 mm to 2 mm in order to produce
sensible wear results.

6.2 Wear Tests

Plotting of Stribeck curves is useful for determining
the conditions of boundary lubrication provided the metallur-
gical combinations of the wearing components, machine system
and operating conditions remain the same. It is not suitable
just to use for ranking fuels without further investigating
the chemical and metallurgical changes that will occur in
the fuel and wearing components during the tests. For instance,
the Stribeck curves which were obtained from the Thornton Wear
Rig would not be suitable if used in Denison Wear Rig due to
the differences in the machine and operating systems and also
the structures of aluminium bronzes were different. The
Thornton wear experiments were conducted using 3 mm diameter
Bronze A pins (figure 3.21) running on the rim of a disc under
flooded conditions, whereas the Denison wear experiments used
2 mm diameter Bronze E pins running on the flat surface of
the disc under starved flow conditions.

The use of different pin-on-disc configurations has some
unforeseen effects in the wear process. Some workers use pins
running on the rim of the disc and others use pins running on
the flat surface of a disc in order to be able to conduct more
experiments. The author has found that the latter pin-on-disc
configuration, i.e. pin running on flat surface of the disc,
is likely to generate a variable distributions of fluid film

thickness across the flat surface of the various wear tracks, thus creating different lubrication regimes in different regions. Consequently, it will produce misleading analyses of wear results due to the use of different wear tracks under the pre-set lubricated wear conditions.

The plotting of wear rate against load curves serves a useful purpose in comparing the differences between wear results for fuels with and without additive. It also serves as a guide in selecting a suitable number of samples for detailed analysis, particularly if there is an interesting transition period on the wear curve, such as transition from high to low wear rates. Although, in certain tests, the scatter of wear results is quite large, constant monitoring and recording of frictional forces serves as an indication of what types of boundary lubrication regimes are encountered. For example when low wear rates occur at low recorded friction values. The low coefficients of friction indicate the transition from boundary to mixed or hydrodynamic lubrication and hence increased fluid film support.

6.3 Worn Surface Analysis

The technique used in measuring the microhardness on tapered surfaces was found to be useful in the study of the changes of mechanical properties on the deformed surface. It was found that the sub-surface hardness of the worn pin, due to strain-hardening, had increased to values 50% above its bulk microhardness. It was also found that very important physical changes had occurred on the sub-surface layer of worn pin surfaces. This could only be detected by using techniques,

such as taper sectioning, to obtain a better understanding
of the mechanism involved during the wear process. It was
observed that aluminium bronzes underwent superplastic
deformation with the formation of many cavities at the sub-
surface of the worn pin during severe wear conditions. The
above superplasticity was related to the enhanced strain-
rate sensitivity of the material at elevated temperatures.
The superplastic deformation of material has a great effect
in reducing wear.

The chemical etching technique has proved to be useful
in revealing various phases of aluminium bronzes. Composi-
tion of each individual phases can be obtained by Scanning
Electron Microscopy and Electron Probe Microanalysis. Any
selective phase attack by a dealuminification process can
be identified by using the above techniques. Chemical
etching revealed the depth of structural deformation from the
worn surfaces to the bulk material. It was noticed that
metallurgical changes occurred on etched tapered worn surface
which reached a depth of about 20 μm into the bulk structure
(figure 3.33). The depth of aluminium depletion on sub-
surface deformed layers could be easily measured and was
found to be about 6 μm.

The applications of Scanning Electron Microscopy (SEM)
and Electron Probe Microanalysis (EPMA) give a better under-
standing of aluminium depletion on bronze surfaces and
aluminium transfer to steel counterfaces. SEM micrographs
show a distinctive depleted layer of aluminium at the region
where maximum stresses occurred in the sub-surface layer of
the worn pins (figures 3.24 and 3.31), or in the region where
superplastic deformation had occurred indicated by the

appearance of many cavities (figure 3.30). The use of EPMA has further contributed in measuring the atomic percentage of aluminium depletion on the worn pin surfaces for different loads and speeds conditions (figures 3.40 to 3.42). The amount of aluminium measured on the worn track surfaces indicated that aluminium had transferred from bronze surface to steel counterface (table 3.4).

Auger Electron Spectroscopy (AES) in conjunction with Argon ion sputtering is particularly useful in the analysis of thin films on worn surfaces. Elemental concentrations can be derived from an Auger spectrum, while peak shape or peak shift give information on the chemical bond. Auger depth profiles show that more surface carbon was observed for experiments conducted where the additive was present in the fuel than for the fuel alone (figure 5.2 and 5.3). The formation of thick oxide layers played a significant role in reducing wear both with and without additive.

The use of X-ray analysis of wear debris shows that oxides were present which further confirmed the existence of oxide layer on worn pin surfaces indicated by high oxygen Auger depth profiles. Consequently it is suggested that it is always beneficial to use as many techniques as are available in any investigation.

6.4 Surface Models

The collection of data obtained from surface analytical techniques enabled surface models for the wear of the bronze sliding on steel surfaces, in the presence of aviation fuel with and without Hitec E580, to be proposed.

The presence of hydrotreated fuel allows oxidation to take place on the bronze surfaces due to starved fuel flow conditions. This leads to higher surface temperatures than those experiments conducted under flooded conditions. These high temperatures coupled with contact pressures lead to aluminium diffusion (Kirkendall effect) at high stresses and then preferential transfer to the steel surface. As a result, the remaining free copper rich area on the bronze surface is allowed to form protective oxide layers, during mild boundary wear conditions, which have the effects of reducing wear and giving seizure protection. If conditions become severe, i.e. high loads and/or speeds, the fact that there are no polar molecules present in the fuel alone to form a boundary layer leads to the increase in metal-to-metal contact. Wear occurs at this stage rapidly enough to prevent the formation of protective oxide layers and thus seizure may occur.

The presence of the fatty acid (additive) leads to higher wear rates due to a thinner less protective oxide film on the surface under mild boundary conditions. The adsorbed boundary films restrict the access of oxygen to the surface and this results in a thinner oxide film being formed on the surface. If conditions become severe, the adsorption of the fatty acid gives some protection and at the same time allows some oxidation to take place. Consequently this leads to lower wear than would have occurred with the fuel alone and reduces the probability of seizure. The superplastic characteristic of this bronze at this stage tends to further reduce wear due to the toughness of this alloy at elevated temperature.

6.5 Suggestions for Further Work

Overwhelming difficulties have been encountered during the initial stage of the experiments without first knowing the existence of different types of structural aluminium bronzes being used. This hindered the value of early Stribeck curves in establishing boundary lubricated wear conditions. Therefore, it is suggested that a pre-history of the materials used for wear tests should be well understood in terms of its mechanical properties, corrosion resistance, effect at elevated temperatures, etc. To this end, the following forms a concise list of some of the more important points of this work which may be fruitfully extended.

(a) The material first received from delivery has to be examined prior to the wear tests, in terms of its strength, hardness and microstructure, so as to ensure it has the same properties of the original fuel pump metallurgy. Thus, in order to simulate the same wear conditions as that experienced by the aviation fuel pump, it is pertinent to use the same metallurgy designated for manufacture of the aviation piston fuel pump system.

(b) Since the wear results are very inconsistent under the same load and speed conditions when conducted on different wear tracks, it is suggested, for lubricated experiments, that one wear track only should be used, i.e. the inner-most track of a disc should be used for all experiments to avoid uneven distributions of fluid film on the wear tracks. In that connection, constant monitoring and recording of frictional forces should be carried out in each experiment.

(c) The present work has been carried out over a load range from 25 to 200N inclusive, at speed 0.6, 2 and 4 ms^{-1}. In the presence of the additive no seizure failure occurred for all the above loads and speeds range. More information may be obtained if the range is extended to higher loads and speeds particularly in the case where the additive is present. The above suggestion is based on the results obtained from the Bronze E type of material being used.

(d) Consideration of the temperature effect is important in view of the superplastic deformation and cavity formation that occurred in the sub-surface layer of bronze. Attempts should be made to measure surface temperature during wear so that estimation could be made of the temperature at which the bronze material underwent superplastic deformation and cavity formation. An investigation of superplasticity and cavitation can be undertaken on an Instron machine at elevated temperatures *and it would be* useful to conduct some Instron tests on the present investigated Bronze E type material at temperatures about 450°C and 800°C respectively. These are the temperatures at which aluminium bronzes to specification D.T.D. 197 have been superplastically deformed. It would also be interesting to determine at what temperature protection from the additive film breaks down under wearing conditions.

(e) The use of a number of physical methods of analysis have proved to provide useful information for building up a model of the wearing surface. The techniques

which have been employed so far by the author should not be ignored because accumulation of data from each technique would provide a more complete picture of the wearing surface towards the end. Any new inventive instrumentation which proves to be invaluable for tribological purpose should be used.

(f) The use of different material combinations are worth considering, particularly for those materials where no diffusion mechanism occurs. It is also worthwhile to consider using Laser Surface Melting technique on aluminium bronze. The Laser Surface Melting technique has proved to provide enhanced corrosion resistance and reduction in dealuminification (130).

6.6 Theory

Difficulties have been encountered in developing a theory for boundary lubricated wear which covers all the variable parameters. A broad qualitative and quantitative understanding of the ways in which these variable parameters change to affect wear would be fruitful. It is possible to predict wear rates if the various parameters in the wear equation are known. The present work should be incorporated with the work of Sullivan, Quinn and Rowson where they have indicated the possibilities of obtaining various unknown parameters, such as the number and size of asperities, the thickness of the oxide film formed, the oxidation temperature and the oxidational constants appropriate to the conditions of oxidation during wear. The above will provide invaluable information to improve the solutions of the oxidational boundary lubricated wear equation.

APPENDIX 1

Calculation of the Speed Relative to the Selective Track
Radius

One revolution is equivalent to $2\pi r$ metre(m) on the track,
where r is the selective track radius.

$$\therefore \quad 1 \text{ m min}^{-1} \equiv \frac{1}{2\pi r} \text{ rev. min}^{-1}$$

$$\therefore \quad 1 \text{ m sec}^{-1} \equiv \frac{60}{2\pi r} \text{ rev. min}^{-1}$$

For a 25×10^{-3} m track radius and 2 ms^{-1} speed, the
required r.p.m. setting is $\dfrac{60 \times 2}{2\pi \times 25 \times 10^{-3}} = 764$ r.p.m.

Track radius $r \times 10^{-3}$ m	speed ms^{-1} R.P.M. SETTING						
	0.5	0.6	1	2	3.5	4	5
25	191	229	382	764	1337	1528	1910
27.5	174	208	347	694	1215	1389	1736
30	159	191	318	637	1114	1273	1592
32.5	149	176	294	588	1028	1175	1469
35	136	164	273	546	955	1091	1364
37.5	127	153	255	509	891	1019	1273
40	119	143	239	477	836	955	1194
42.5	112	135	225	449	786	899	1123
45	106	127	212	424	743	849	1061
47.5	101	121	201	402	704	804	1005
50	95	115	191	382	668	764	955

REFERENCES

1.   Droegemueller,E.A.,"Fuel requirements for supersonic
        transport",World Petroleum Congress 6th,1963 June,
        Frankfurt REQNO 11842,pp.1-13.

2.   Appeldoorn,J.K.,and Dukek,W.G.,"Lubricity of jet fuels",
        SAE Transactions,1967,Vol.75,pp.428-440.

3.   Aird,R.T.,and Forgham,S.L.,"The lubricating quality of
        aviation fuels",Wear,1971,Vol.18,pp.361-380.

4.   Vere,R.A.,"Aviation fuel lubricity",Report to AGARD
        Meeting,The Hague,May 1971.

5.   Furey,M.J.,and Appeldoorn,J.K.,"The effect of lubricant
        viscosity on metallic contact and friction in a sliding
        system",ASLE Transactions,1962,Vol.5,pp.149-159.

6.   Grubin,A.N.,Central Scientific Research Institute for
        Technology and Mechanical Engineering,Moscow(1949),
        DSIR Trans. No 337.

7.   Klaus,E.E.,and Bieber,H.E.,"Effect of some physical
        and chemical properties of lubricants on boundary
        lubrication",ASLE Transactions,1964,Vol.7,pp.1-10.

8.   Fein,R.S.,"Effect of lubricants on transition temper-
        tures",ASLE Transactions,1965,Vol.8,pp.59-68.

9.   Sablina,Z.A.,and Gureyer,A.A.,Khim. Tekh Top Masel,
        7 (1960),33.

10.   Rounds,F.G.,"Effects of additives on the friction of
        steel on steel. 1. Surface topography and film compo-
        sition studies",ASLE Transactions,1964,Vol.7,pp.11-23.

11.   Feng,I-M.,and Chalk,H.,"Effects of gases and liquids
        in the lubricating fluids on lubrication and surface
        damage",Wear,1961,Vol.4,pp.257-268.

12.   Fein,R.S.,and Kreuz,K.L.,"Chemistry of boundary lubri-
        cation of steel by hydrocarbons",ASLE Transactions,
        1965,Vol.8,pp.29-38.

13.   O.E.C.D. Research Group on Wear of Engineering Materials,
        "Glossary of terms and definitions in the field of
        Friction, Wear and Lubrication.- Tribology", Paris,1969.

14.   Archard,J.F.,and Hirst,W.,"The wear of metals under
      unlubricated conditions",Proc.Roy.Soc.(London),Series A,
      1956,Vol.236,pp.397-410.

15.   Landheer,D.,and Zaat,J.H.,"The mechanism of metal trans-
      fer in sliding friction",Wear,1974,Vol.27,pp.129-145.

16.   Burwell,J.T.,"Survey of possible wear mechanisms",
      Wear,1957/58,Vol.1,pp.119-141.

17.   Khruschov,M.M.,"Principles of abrasive wear",Wear,1974,
      Vol.28,pp.69-88.

18.   Wellinger,K.,Uetz,H.,and Guerleyik,M.,"Gleitveschleiss-
      untersungen an metallen und nicht-metallischen Hartsto-
      ffen unter wirkunqkorniger stoffe",Wear,1968,Vol.11,
      pp.173-199.

19.   Mulhearn,T.O.,and Samuels,L.E.,"The abrasion of metals:
      A model of the process",Wear,1962,Vol.5,pp.478-498.

20.   Sedriks,A.J.,and Mulhearn,T.O.,"Mechanics of cutting
      and rubbing in simulated abrasive processes",Wear,1963,
      Vol.6,pp.457-466.

21.   Wilman,H.,"Abrasion and surface structure",Wear,1969,
      Vol.14,pp.249-254.

22.   Davies,R.M.,"The determination of static and dynamic
      yield stresses using a steel ball",Proc.Roy.Soc.(London),
      Series A,1949,Vol.197,pp.416-432.

23.   Quinn,T.F.J.,"The classification,Laws,Mechanisms and
      Theories of wear",Fundamentals of Tribology,Edited by
      Suh,N.P.,and Saka,N.,The MIT Press, June 1978,pp.477-492.

24.   Dowson,D.,"Transition to boundary lubrication from
      elastohydrodynamic lubrication",Boundary Lubrication-
      An Appraisal of World Literature,Ed.Ling,F.F.,Klaus,E.E.,
      and Fein,R.S.,A.S.M.E.,1969,pp.229-240.

25.   Ling,F.F.,and Fein,R.S.,"Boundary Lubrication-An Apprai-
      sal of World Literature",A.S.M.E.,1969.

26.   Procurement Executive Ministry of Defence,Directorate
      General of Engines, "Lubricity of Aviation Turbine Fuels",
      Second Report of the work and findings of the MOD/PE/
      Fuel Lubricity Panel,Edited by Vere,R.A.,Askwith,T.C.,
      and Hardy,P.J.,January 1976,Ref:AX/395/014.

27.   "Specification D.Eng.R.D.2494",(P.E.) M.O.D., Sept.1974
        REF AX/403/02 (for example).

28.   Chrtkov,V.B.,and Piskunov,V.A.,"Polyfunctional Additives
        for Jet Fuels",Chem.&Tech.of Fuel Oils(USA),1969,
        No.5/6,pp.377-380.

29.   Edwin Cooper and Company Ltd., Technical Report No.193,
        "A pipeline corrosion inhibitor/lubricity improving
        additive",August 1978,Private Communication-Patent
        Specification 1 501 868.

30.   Dacre,B.,Savory,B.,and Wheeler,P.A.,"Adsorption of
        Lubricity Additives",Part 1,Technical Report AC/R/13
        Royal Military College of Science,Shrivingham,M.O.D.
        Contact AT/2160/025,ENG.,D.,(1977).

31.   Misra,A.K.,Mehrotra,A.K.,and Srivastava,R.D.,"Anti-
        wear Characteristics of Additives:Synergistic and
        Adverse effects",Wear,1975.Vol.31,pp.345-357.

32.   Poole,W.,and Sullivan,J.L.,"The wear of aluminium-bronze
        on steel in the presence of aviation fuel",ASLE Tran-
        sactions,1979,Vol.22,No.2,pp.154-161.

33.   Poole,W.,and Sullivan,J.L.,"The role of aluminium
        segregation in the wear of aluminium/bronze-steel
        interfaces under conditions of boundary lubrication",
        ASLE Transactions,1980,Vol.23,No.4,pp.401-408.

34.   Willey,L.,Aluminium Vol.1.ASM,1967.

35.   Yutaka,A.,Nippon.Kinzoku.Gakkai-Si,1941,Vol.5,p.136.

36.   Pearson,W.,Handbook of Lattice Spacings and Structures
        of Metals.,Pergamon,Vol.2,1967.

37.   Cook,M.,Fentimen,W.P.,and Davis,E.,"Observations on
        the structure and properties of wrought copper-aluminium
        -nickel-iron alloys",J.Inst.Met.,1951,Vol.80,pp419-429.

38.   West,D.R.F.,and Thomas,D.L.,"The constitution of copper-
        rich alloys of the copper-manganese-aluminium system",
        J.Inst.Met.,1938,Vol.85,pp.97-104.

39.   Alexander,W.O.,"Copper-rich nickel-aluminium-copper
        alloys.Part II.-The constitution of the copper-nickel-
        rich alloys",J.Inst.Met.,1938,Vol.63,pp.163-189.

40. Belkin,E.,"Cast Nickel Containing Aluminium Bronze
    Properties and Microstructure",AFS Transactions,1961,
    Vol.69,pp.383-393.

41. Crofts,W.L.,Townsend,D.W.,and Bates,A.P.,"Soundness
    and Reproducibility of Properties of Sand-cast Complex
    Aluminium Bronzes (BS 1400-AB2)",The British Foundry-
    man,1964.Vol.57,No.2,pp.89-103.

42. Zanis,C.A.,and Ferrara,R.J.,"An investigation into de-
    alloying of cast nickel-aluminium bronze",AFS Transac-
    tions,1972,Vol.80,pp.259-268.

43. Zanis,C.A.,and Ferrara,R.J.,"Sea water corrosion of
    nickel-aluminium bronze",AFS Transactions,1974,Vol.82,
    pp.71-78.

44. Goldspiel,S.,and Fosters,M.L.,Modern Castings,1961,
    Vol.39,No.3,pp.78-95.

45. Thomson,R.,"Charpy impact properties of bronze propeller
    alloys",ASF Transactions,1968,Vol.76,pp.99-109.

46. Thomson,R.,and Edwards,J.O.,"Effect of compositional
    and process variables on the tensil properties of cast
    nickel-aluminium bronze",AFS Transactions,1977,Vol.85,
    pp.13-18.

47. Tyler,D.E.,and Goodwin,R.J.,"The effect of temperature
    upon the mechanical properties of selected Cu-Al-Fe-Ni
    Aluminium Bronzes",J.Inst.Met.,1968,Vol.96,pp.314-319.

48. Cottrell,A.H.,"Structure processes in creep",(Special
    Report No.70),P.1,1961:London(Iron Steel Inst.).

49. Cook,M.,Fentiman,W.P.,and Davies,E.,"Observations on
    the Structure and Properties of Wrought Copper-Aluminium
    -Nickel-Iron Alloys",J.Inst.Met.,1951-52,Vol.80,pp.419
    -429.

50. Sarkar,S.,and Bates,A.P.,"Impact resistance of sand
    cast aluminium bronze (BS1400:AB2)",The British Foundry-
    man,February 1967,pp.38-43.

51. Private Communication,"High tensil brasses welding
    alloys and aluminium bronzes",Delta(Manganese Bronze)
    Ltd.,Handford Works,P.O.Box No.22,Hadleigh Road,Ipswich,
    1P2 0EG,U.K.

52. Sury,P.,and Oswald,H.R.,"On the corrosion behaviour of
    individual phases present in aluminium bronzes",
    Corr.Sci.,1972,Vol.12,pp.77-90.

53. Upton,B.,"Corrosion resistance in sea water of medium
strength aluminium bronzes",Corrosion,1963.Vol.19.
pp.204t-209t.

54. Klement,J.F.,Maersch,R.E.,and Tully,P.A.,"Use of alloy
additions to prevent intergranular stress corrosion
cracking in aluminium bronze",Corrosion,1960,Vol.16,
pp.519t-522t.

55. Rowlands,J.C.,"Electrochemical aspects of preferential
phase corrosion in complex alloys",Corr.Sci.,1962,
Vol.2,pp.89-94.

56. Bradley,J.N.,"Recent developments in copper-base alloys
for naval marine applications",Int.Met.Rev.,1972,
Vol.162,pp.81-99.

57. Niederberger,R.B.,"Composition and heat treatment effect
on dealuminization of aluminium bronzes",Modern Castings,
1964,Vol.45,No.3,pp.115-128.

58. Williams,W.L.,"Aluminium bronzes for marine applications",
J.American Society of Naval Engineers,August 1957,
Vol.69,p.453.

59. Stead,D.D.,"Some notes on the aluminium bronzes",
Australasian Engineer,March 7,1951,Vol.44,p.44.

60. Schussler,M.,and Napolitan,D.S.,"Dealuminization of
aluminium bronze",Corrosion,March 1956,Vol.12,pp.25-30.

61. Arnaud,D.,Paton,R.,Wigy,S.,and Masere,C.,"Contribution
to the study of the dealuminization of cast aluminium
bronze",Centre Technique Des Industries De La Fonderie
Report(August 1964).

62. Belkin,E.,"Cast nickel containing aluminium bronze
properties and microstructures",Modern Castings,
August 1961,p.87.

63. Heidersbach,R.,"Classification of the mechanism of the
dealloying phenomenon",Corrosion,February 1968,Vol.24,
No.2,pp.38-44.

64. Hull,D.,and Rimmer.D.E.,"The growth of grain-boundary
voids under stress",Philos.Mag.,1959,Vol.4,pp.673-687.

65. Hancock,J.W.,"Creep cavitation without a vacancy flux",
Met.Sci.,1976,Vol.10,pp.319-325.

66.   Beere,W.,and Speight,M.V.,"Creep cavitation by vacancy
       diffusion in plastically deforming solid",Met.Sci.,1978,
       Vol.12,pp.172-176.

67.   Dunlop,G.L.,Reid,J.D.,and Taplin,D.M.R.,"Anisotropic
       ductility of a superplastic aluminium bronze",
       Met.Transactions,August 1971,Vol.2,pp.2308-2310.

68.   Shapiro,E.,Dunlop,V.L.,Taplin,D.M.R.,and Crane,J.,
       "Cavitation at grain and phase boundaries during super-
       plastic flow of an aluminium bronze",Met.Transactions,
       September 1973,Vol.4,pp.2039-2044.

69.   Sagat,S.,Blenkinsop,P.,and Taplin,D.M.R.,"A metallogra-
       hic study of superplasticity and cavitation in micro-
       duplex Cu-40%Zn",J.Inst.Met.,1972,Vol.100,pp.268-274.

70.   Holm,R.,Electric Contacts Handbook,@th Edition,Springer-
       Verlag(Berlin),pp.199,ff.(1967).

71.   Burwell,J.T.,and Strang,C.D.,"On the emperical law of
       adhesive wear",J.Appl.Phys.,1952,Vol.23,pp.18-28.

72.   Archard,J.F.,"Single contacts and multiple encounters",
       J.Appl.Phys.,1961,Vol.32,pp.1420-1425.

73.   Archard,J.F.,"Contact and rubbing of flat surfaces",
       J.Appl.Phys.,1953,Vol.24,pp.981-988.

74.   Archard,J.F.,"The wear of metals",New Scientist,Vol.5,
       1959,pp.1299-1301.

75.   Kingsbury,E.P.,"Some aspect of thermal desorption of
       a boundary lubricant",J.Appl.Phys.,1958,Vol.29,No.6,
       pp.888-891.

76.   Kingsbury,E.P.,"The heat of adsorption of a boundary
       lubricant",ASLE Transactions,1960,Vol.3,pp.30-33.

77.   Rowe,C.N.,"Some aspects of the heat of adsorption in
       the function of a boundary lubricant",ASLE Transactions,
       1966,Vol.9,pp.101-111.

78.   Thompson,R.A.,and Bocchi,W.,"A model for asperity load
       sharing in lubricated contacts",ASLE Transactions,1972,
       Vol.15,pp.67-79.

79.   Stolarski,T.A.,"Adhesive wear of lubricated contacts",
       Tribology International,August 1979,pp.169-179.

80.   Stolarski,T.A.,"A contribution to the theory of lubri-
       cated wear",Wear,1980,Vol.59,pp.309-322.

81.   Johnson,K.L.,Greenwood,J.A.,and Poon,S.Y.,"A simple
       theory of asperity contact in elastohydrodynamic
       lubrication",Wear,1972,Vol.19,pp.91-108.

82.   Kregelskii,J.V.,Friction and Wear,Butterworths,Washing-
       ton,1965.

83.   Beerbower,A.,"A critical survey of mathematical models
       for boundary lubrication",ASLE Transactions,1971,Vol.14,
       pp.90-104.

84.   Quinn,T.F.J.,"The effect of 'hot-spot' temperatures on
       the unlubricated wear of steel",ASLE Transactions,1967,
       Vol.10,pp.158-168.

85.   Sullivan,J.L.,Quinn,T.F.J.,and Rowson,D.M.,"Application
       of the oxidational theory of mild wear to the sliding
       wear of low alloy steel",Wear,1980,Vol.65,pp.1-20.

86.   Poole,W.,Thesis: The Wear of Aluminium Bronze on Steel
       in Aviation Kerosene,Department of Physics,The Universi-
       ty of Aston in Birmingham,1979.

87.   Recchuite,A.D.,and Newingham,T.D.,"Effect of zinc
       dithiophosphates on axial piston pump performance",
       J. American Society of Lubrication Engineering,1976,
       Vol.32,No.9,pp.481-488.

88.   Godfrey,D.,"Review of usefulness of new surface analysis
       instruments in understanding boundary lubrication",
       Fundamental of Tribology,Edited by Nam P.Suh,and N.Saka,
       The MIT Press,June 1978,pp.945-947.

89.   John,V.B.,Introduction to Engineering Materials,Published
       by The Macmillan Press Ltd.,1972.

90.   Duncumb,P.,"The design of electron probe microanalysers",
       J.Inst.Met.,1961-62,Vol.90,pp.154-159.

91.   Melford,D.A.,"The use of electron probe microanalysis
       in physical metallurgy",J.Inst.Met.,1961-62,Vol.90,
       pp.217-223.

92..   Belk,J.A., Electron Microscopy and Microanalysis of
       Crystalline Materials,Applied Science Publishers Ltd.,
       1979.

93.   Coy,R.C.,and Quinn,T.F.J.,"The use of physical methods
       of analysis to identify surface layers formed by
       organosulfur compounds in wear tests",ASLE Transactions,
       1975,Vol.18,No.3,pp.163-174.

94.   Chang,C.C.,"Analytical Auger Spectroscopy",Ch.20,pp.509-561,Characterization of Solid Surfaces,Published by Plenum Press,New york(1974).

95.   (a).   Siegbahn,K.,Nordling,C.,and Fahlman,A,et al.,in Atomic,Molecular and Solid State Structure Studied by Means of Electron Spectroscopy,ESCA(Electron Spectroscopy for Chemical Analysis),Almquist and Wiksell Boktryckeri AB.,Uppsala(1967).

        (b).   Bearden,J.A.,and Burr,A.F.,Rev.Mod.Phys.Vol.39. p.125,(1967).

        (c).   Wiech,G,and Zopf,E.,Physik,Vol.244,94(1971).

96.   Sim,J.M.,"The lubricating quality of aviation fuels", Thornton Research Centre,Shell Research Limited,U.K., October,1974 Report.

97.   Sullivan,J.L.,Quinn,T.F.J.,and Rowson,D.M.,"Developments in the oxidational theory of mild wear",Tribology International,August 1980,pp.153-158.

98.   Frenkel,J.,"Theorie der Adsorption und Verwandter Ersheinungen",Z.Physik,1924,Vol.26.pp.117-138.

99.   Tylecote,R.F.,"Review of Published Information on the Oxidation and Scaling of Copper Base Alloys",J.Inst. Met.,1950-51,Vol.78,pp.259-300.

100.   Kubaschewki,O.,and Hopkins,B.E.,Oxidation of Metals and Alloys,Butterworths,London,1962.

101.   McClellan,A.L.,and Harnsberger,H.F.,"Cross-sectional areas of molecules adsorbed on solid surfaces",J.Coll. and Inter.Sci.,1967,Vol.23,pp.577-599.

102.   Lindemann,F.A.,"The calculation of molecular vibration frequencies",Z.Physik,1910,Vol.11,pp.609-612.

103.   Bowden,F.P.,and Tabor,D.,"The friction and lubrication of solids",Oxford University Press,London,1954.

104.   Allen,C.M.,and Drauolis,E.,"Boundary layer Lubrication: Monolayer or Multilayer",Wear,1969,Vol.14,pp.363-384.

105.   Moon,J.R.,and Garwood,R.D.,"Transformation during continuous cooling of the beta phase in copper-aluminium alloys",J.Inst.Met.,1968,Vol.96,pp.1909-1933.

106.   Dunlop,G.L.,and Taplin,D.M.R.,"Textures and anisotropic flow of a superplastic aluminium bronze",J.Aust.Inst.Met., 1971,Vol.16,pp.195-203.

107. Johnson,R.H.,"Superplasticity",Met.Rev.,1970,Vol.15,
      pp.115-134.

108. Davies,G.J.,Edington,J.W.,Cutler,C.P.,and Padmanabhan,
      K.A.,J.Mater.Sci.,1970,Vol.5,p.1091.

109. Gandhi,C.,Rama Rao,P.,Taplin,D.M.R.,"Low cycle fatigue
      behaviour of a superplastic aluminium-bronze",Met.Sci.,
      January 1978,pp.30-34.

110. Nakajima,K.,Yamamoto,N.,and Isonai,A.,"Interaction of
      solute atoms with dislocation in surface layer of abraded
      Cu-Al alloys",JIM Transactions,1969,Vol.10,pp.223-226.

111. Funamizu,Y.,Watanabe,K.,"Interdiffusion in the Al-Cu
      system",JIM Transactions,1971,Vol.12,pp.147-152.

112. Oikawa,H.,and Karashima,S.,"On the self-diffusion co-
      efficients od aluminium in copper(rich)-aluminium solid
      solutions",JIM Transactions,1970,Vol.11,pp.431-433.

113. Elliott,S.,Wallach,E.R.,"Joining aluminium to steel
      Part I-Diffusion bonding",Met.Constr.,March 1981,
      pp.167-171.

114. Elliott,S.,Wallach,E.R.,"Joining aluminium to steel
      Part 2 - Friction welding",Met.Constr.,April 1981,
      pp.221-225.

115. Polyakov,V.N.,"The transition zone and structure formed
      during the impulse deposition of aluminium on steel",
      Korroz.Zashch.,1980,Vol.6,pp.14-17.(in Russian).

116. Dzhevaga,I.I.,Lebedev,Y.M.,"Research into the fusion
      zones of welded joints between carbon steel and aluminium
      bronze",Avt.Svarka,1970,No.8,pp.10-14.

117. Bishop,M.,and Fletcher,K.E.,"Diffusion in aluminium",
      Inter.Met.Rev.,1972,Vol.17,pp.203-225.

118. Shewmon,P.G.,"Diffusion in solids",1963:New York and
      London (McGraw Hill): (a) p.23.

119. Hirsi,A.M.,Mem.Sci.Rev.Met.,1967,Vol.64,(7/8),p.683.

120. Dienes,G.J.,"Enhanced Diffusion",J.Met.,April 1959,
      Vol.11,p.281.

121. Brown,A.F.,and Blackburn,D.A.,"Apparent enchancement
      of diffusion coefficients in plastically deformed metals",
      Acta Met.,1963.Vol.11,pp1017-1021.

122. Kuzmenko,P.P.,and Ostrovsky,L.F.,Ukrain.Fiz.Zhur.,1961,
      Vol.6,p.525, AERE Translation 979.

123. Kuzmenko,P.P.,and Kharkov,Y.I.,ibid.,1958,3,528.

124.   Damask,A.C.,"Radiation damage in solids",1962,p.163,
       New York and London (academic Press).

125.   Lenchenko,V.M.,and Pugacheva,T.S.,"Radiatsionnye
       Effekty v Tverdykh Telakh"(Edited by Yu.N.Talanin),p.78.
       1963:Tashkent(Publishing House of Academy of Sciences).

126.   Federighi,T.,"Proceedings of Internal School of Physics,
       Enrico Fermi,1960",1962,18,801.

127.   Furey,M.J.,"Surface temperatures in sliding contact",
       ASLE Transactions,1964,Vol.7,pp.133-146.

128.   Taplin,D.M.R.,and Sagat,S.,"The tensile characteristics
       of a superplastic aluminium bronze",Mater.Sci.Eng.,1972,
       Vol.9,pp.53-55.

129.   Bradley,G.,Edwin Cooper Report NO. EC314-September 1973,
       (Prepared under contact to Ministry of Defence).

130.   Draper,C.W.,Woods,R.E.,and Meyer,L.S.,"Enhanced Corrosion
       Resistance of Laser Melted Aluminium Bronze D (CDA-614)",
       Corrosion-Nace,August 1980,Vol.36,No.8,pp.405-408.